UNDERSTANDING THE SOURCES, ATMOSPHERIC PROCESSES, HEALTH ASSOCIATIONS, AND SIZE DISTRIBUTION OF AEROSOL OXIDATIVE POTENTIAL

A Dissertation
Presented to
The Academic Faculty

by

Ting Fang

In Partial Fulfillment
of the Requirements for the Degree
Doctorate of Philosophy in the
School of Earth & Atmospheric Sciences

Georgia Institute of Technology
August 2017

COPYRIGHT © 2017 BY TING FANG

UNDERSTANDING THE SOURCES, ATMOSPHERIC PROCESSES, HEALTH ASSOCIATIONS, AND SIZE DISTRIBUTION OF AEROSOL OXIDATIVE POTENTIAL

Approved by:

Dr. Rodney J. Weber, Advisor
School of Earth and Atmospheric Sciences
Georgia Institute of Technology

Dr. Nga Lee (Sally) Ng
School of Chemical and Biomolecular Engineering
Georgia Institute of Technology

Dr. Gregory L. Huey
School of Earth and Atmospheric Sciences
Georgia Institute of Technology

Dr. James A. Mulholland
School of Civil and Environmental Engineering
Georgia Institute of Technology

Dr. Armistead G. Russell
School of Civil and Environmental Engineering
Georgia Institute of Technology

Date Approved:

ACKNOWLEDGEMENTS

The last five years has been an incredible life time experience to me. This experience has helped me grow both individually and professionally: From learning how to live in a foreign country to gaining valuable communication and research skills, and to setting career goals. I am thankful to everyone who supported me in gaining all of them: my advisor Rodney Weber, who is truly an inspiration to me. He was more than just an advisor whose scientific insights are incredible but was also extremely supportive. Thank you for giving enough freedom to me but sometimes push me little into the right path whenever I got lost; Dr. Vishal Verma, who worked as a postdoc when I joined the group in 2012. Without his help, my research would have been very difficult. Thank you for always keeping your door open and your patience in answering all my questions no matter how trivial they were. I was privileged to work with several experts, Dr. Athanasios Nenes, Dr. Armistead Russell, Dr. Rick Peltier, Dr. Aleksandr Stefaniak, and folks from Emory University whose critical input improved the quality of our papers. I would also like to thank my committee members, Dr. Armistead Russell, Dr. Nga Lee Ng, Dr. Gregory Huey, and Dr. Jim Mulholland for taking the time to review my thesis. I am grateful to my past and current group mates, Dr. Jiumeng Liu, Laura King, Neel Kotra, Gabby Agostini, Dong Gao, Hongyu Guo, Linghan Zeng, Qian Zhang, Dr. Theo Nah, Dr. Jenny Wong, and Dr. Yuzhong Zhang. Special thanks to Hongyu. My smooth transition into this new life in U.S. would not have been possible without your help. I am also thankful to my parents and my brothers who believed in me and love me unconditionally. Thank you for not only celebrating every achievement I made but also lifting me up whenever I was down.

TABLE OF CONTENTS

LIST OF TABLES

LIST OF FIGURES

LIST OF SYMBOLS AND ABBREVIATIONS

AA	Ascorbic Acid
AAm	AA activity per PM mass
AAv	AA activity per air volume
AMBSLF	Ammonium bisulfate
AMNITR	Ambient nitrate
AMSULF	Ambient sulfate
ANOVA	Analysis of Variace
As	Arsenic
Ba	Barium
Br	Bromine
BrC	Brown carbon
BURN	Biomass burning
Ca	Calcium
CAPS	Concentrated ambient particles
CHF	Congestive heart failure
CMB-E	Chemical Mass Balance Method with ensemble-averaged source impact profiles
COD	Coefficient of Divergence
Cu	Copper
CV	Coefficient of Variation
DCM	Dichloromethane
DI	Deionized water

DTNB	5,5’-dithiobis-(2-nitrobenzoic acid)
DTT	dithiothreitol
DTTm	DTT activity per PM mass, mass-normalized DTT activity
DTTv	DTT activity per air volume, volume-normalized DTT activity
EC	Elemental carbon
ED	emergency department
EDTA	ethylenediaminetetraacetate
EPFRs	Environmentally persistent free radicals
Fe	Iron
GMD	Geometric mean diameters
GSH	Glutathione
HDDV	Heavy-duty diesel vehicles
HULIS	HUmic-LIke Substances
K	Potassium
LDGV	Light-duty gasoline vehicles
LOD	Limit of detection
LWCC	Liquid Wave-guide Capillary Cell
Mn	Manganese
MOUDI	Micro-Orifice Uniform Deposit Impactor
O_2	Oxygen
$O_2^{\cdot}$	Superoxide anion
OC	Organic carbon
OP	Oxidative potential
OP^{AA}	Dithiothreitol Activity

OP^{DTT}	Ascorbic acid activity
OTHER_OC	Not otherwise apportioned organic carbon
PAHs	Polycyclic aromatic hydrocarbons
Pb	Lead
PM	Particulate Matter
PMF	Positive Matrix Factorization
PQN	9,10-phenanthraquinone
ROS	reactive oxygen species
RTLF	Synthetic respiratory tract lining fluid model
S	Sulfur
Se	Selenium
Sr	Strontium
Sr	Scandium
TCA	Trichloroacetic acid
Ti	Titanium
TNB	2-nitro-5-thiobenzoic acid
WSOC	Water-soluble organic carbon
XRF	X-ray fluorescence
Zn	Zinc
OP_{ws}^{DTT}	Water-soluble DTT activity per air volume
OP_{ws}^{AA}	Water-soluble AA activity per air volume
OP_{wi}^{DTT}	Water-insoluble DTT activity per air volume
OP_{total}^{DTT}	total DTT activity per air volume

DTT_v^e Estimated DTT per air volume activity from CMB-E identified sources

AA_v^e Estimated AA per air volume activity from CMB-E identified sources

SUMMARY

This dissertation aims to connect aerosol oxidative potential (OP) to toxic chemical components and support oxidative stress as a potential mechanism for ambient particle (or its components) toxicity. Aerosol OP, the ability of particulate matter (PM) to deplete antioxidants and generate reactive oxygen species (ROS) *in vivo*, plays an important role in upsetting redox homeostasis, causing oxidative stress, and leading to adverse health effects. This dissertation presents the sources, atmospheric processes, health associations, and lung deposition of atmospheric aerosol OP, and suggests OP as the health indicator of various chemical toxic components. A semi-automated system was first developed based on two widely used acellular OP measures, the dithiothreitol (DTT) and ascorbic acid (AA) assays, to provide the first extensive daily measures of OP of the water-soluble $PM_{2.5}$ (with an aerodynamic diameter smaller than 2.5 μm) fraction from contrasting environments in the southeast U.S. over a 2-year period. It enables strong statistical assessment on the spatiotemporal distributions, sources, and the first large-population based health studies of $PM_{2.5}$ water-soluble OP^{DTT} and OP^{AA}. The data show that $PM_{2.5}$ water-soluble OP^{DTT} on a per air volume basis was spatially uniform and had higher levels in winter than in summer ($winter_{avg}/summer_{avg}$ = 1.5). In contrast, water-soluble OP^{AA} was heterogeneously distributed, with highest levels near traffic, and higher in summer compared to winter ($summer_{avg}/winter_{avg}$ = 1.9). Correlation analysis and source apportionment models suggest a strong contribution from secondary processes and traffic emissions to both water-soluble OP^{DTT} and OP^{AA} in urban Atlanta. Biomass burning was a large source for water-soluble OP^{DTT}, but not for OP^{AA}. $PM_{2.5}$ water-soluble OP^{DTT} was generally well correlated with

$PM_{2.5}$ mass (r=0.49-0.88), while water-soluble OP^{AA} did not co-vary with mass. Strong associations with respiratory and cardiovascular related emergency department visits were observed based on time series epidemiological analyses using reconstructed OP^{DTT} based on the past 10-year source impacts, while water-soluble OP^{AA} was not linked to any investigated health outcomes. The lack of correlation of water-soluble OP^{AA} with $PM_{2.5}$ and health outcomes may be explained by the greater chemical selectivity of AA assay (specific to Cu), whereas the DTT assay is sensitive to both organic species and transition metal ions. Ambient size distributions of OP of samples collected from an urban and road-side site in Atlanta were consistent with the spatial variation, chemical selectivity, and source apportionment results. Both water-soluble OP showed a mono-modal distribution. Water-soluble OP^{AA} had a much narrower distribution (also attributable to narrow chemical sensitivity) and peaked at a larger size than that for water-soluble OP^{DTT}. Water-soluble OP^{AA} was mainly attributed by soluble transition metal ions from secondary processing of sulfate resulting in highly acidic aerosol (pH<2), while water-soluble OP^{DTT} size distribution was a result of a combination of organic species (e.g. quinones from ozone oxidation of PAHs) and acid-processed transition metal ions. Water-insoluble OP^{DTT} was driven by the same chemical players as the water-soluble OP^{DTT}, except that for water-insoluble OP^{DTT}, organic species were absorbed on fine-mode soot surfaces and transition metal ions on coarse-mode dust surfaces, resulting in a bimodal distribution with the minimum at PM_1. Estimated lung deposition showed that although OP per mass (toxicity) was highest for ultrafine particles, estimated lung deposition was mainly from accumulation and coarse particles. The two important chemical players for OP^{DTT} were largely externally mixed and deposited in the different regions in the respiratory system;

transition metal ions predominately in the upper regions, and organic species deeper in the lung. Contrasts in the phases of these forms of OP^{DTT} deposited in the respiratory system may have differing health impacts. The role of sulfate (linked to "strong acidity"), soot, and dust in shaping OP^{DTT} distribution suggests that OP^{DTT} and oxidative stress might provide a link between these PM components and adverse health effects observed in past studies.

CHAPTER 1. INTRODUCTION

1.1 Importance of Atmospheric Aerosols

Air pollution is rising at an alarming rate in cites. World Health Organization (WHO) data shows that outdoor pollution has risen 8% globally in the 2008-2013 periods. Ambient air pollution comprises high concentrations of aerosols, solid or liquid particles that suspended in and are transported through the atmosphere. Aerosols can be directly emitted from primary anthropogenic or biogenic sources, or formed through secondary processes in the atmosphere. Atmospheric aerosols play important roles in climate change and are one of the greatest environmental risks to public health.

1.2 Health Effects of Particulate Matter

The aerosol (or particulate matter) with aerodynamic diameters smaller than 2.5 μm ($PM_{2.5}$) contributes to more than 4.3 million premature deaths worldwide in 2015 (Cohen et al., 2017). $PM_{2.5}$ has been positively associated with cardiovascular (Zanobetti et al., 2014; Sun et al., 2010; Pope et al., 2004; Samet et al., 2000) and respiratory (Harkema et al., 2004; Schaumann et al., 2004; Aust et al., 2002; Norris et al., 1999) diseases. The most recent Global Burden of Disease project (Cohen et al., 2017) ranked $PM_{2.5}$ the 5^{th} out of 79 risk factors attributed to burden of disease globally.

PM_{10} (with aerodynamic diameters smaller than 10 μm) and $PM_{2.5}$ are currently regulated on a mass basis, which is widely used in epidemiological studies to study the health effects of PM. However, PM consists of a wide range of chemical components with potentially varying toxicity, such as transition metal ions (Akhtar et al., 2010; Gasser et al., 2009;

Kodavanti et al., 2005), black carbon (or elemental carbon and associated species) (Kleinman et al., 2007; Brunekreef et al., 1997), polycyclic aromatic hydrocarbons (PAHs) (Lundstedt et al., 2007; Burchiel et al., 2005), and other specific organics species (Nel et al., 2001). Other than chemical components, some studies (Kelly and Fussell, 2012; Nel, 2005) have suggested that size, sources, or surface areas have important implications on PM toxicity. This suggests that mass concentration is not an ideal air quality metric for assessing health impacts. There is, therefore, a need for a more biological relevant metric to represent the integrated effects of PM, motivating continued research on this subject. The mechanisms underlying the health associations of PM are not entirely clear but oxidative stress induced by particles after inhalation, deposition, and translocation has been suggested as a plausible explanation for PM toxicity (Xia et al., 2006; Nel, 2005; Valavanidis et al., 2008).

1.3 Reactive Oxygen Species, Oxidative Stress, and Oxidative Potential

1.3.1 Reactive Oxygen Species

Reactive Oxygen Species (ROS) is a phrase used to describe a number of reactive molecules and free radicals (chemical species with one unpaired electron) derived from molecular oxygen (O_2) (Turrens, 2003). In its "triplet" O(3P) ground state, molecular oxygen has eight electrons but two are unpaired. The two unpaired electrons have the same spin in a chemical bond thus molecular oxygen is not very reactive. However, when molecular oxygen is reduced by one electron (univalent reduction), it produces superoxide anion or superoxide ($O_2^{-}\cdot$). $O_2^{-}\cdot$ poses a variety of treats to human body; 1) direct oxidation of reductants; 2) inactivation of a select group of enzymes; 3) addition of a second electron

gives rise to a more potent oxidant, hydrogen peroxide (H_2O_2), which in turn may be reduced to one of the strongest oxidants in nature, hydroxyl radical (OH·), through the Fenton reaction (Liochev and Fridovich, 2002; Stohs and Bagchi, 1995); 4) $O_2^{-}\cdot$ can directly produce OH· via the Haber-Weiss reaction by reacting with H_2O_2 (Kehrer, 2000), and 5) reaction with other radicals such as nitric oxide (NO·) and produce peroxynitrite, which is also a powerful oxidant (Radi et al., 2002) and a member of the Reactive Nitrogen Species (RNS). $O_2^{-}\cdot$ and its metabolites or "more aged" reactive intermediates are collectively termed ROS or RNS, and the first crucial step to produce ROS or RNS is the univalent reduction of molecular oxygen.

1.3.1.1 Biological sources of ROS

The primary biological source of ROS is $O_2^{-}\cdot$ generation from the mitochondrial electron transport chain (Hayyan et al., 2016; Davies, 1995). Approximately 1-2% of the total daily O_2 consumption goes to mitochondrial superoxide generation. With this estimate, a 60 kg woman would produce 160 to 320 mmol of $O_2^{-}\cdot$ each day from mitochondrial respiration alone (based on an O_2 consumption of 6.41 kg^{-1} day^{-1}) and an 80 kg man would produce 215 to 430 mmol of $O_2^{-}\cdot$ per day (Davies, 1995). In terms of total ROS ($O_2^{-}\cdot$ and H_2O_2 are the two primary products), a human body generates approximately 5 g of ROS per day (Stein, 2002; Halliwell, 1997). Another important biological source of ROS is $O_2^{-}\cdot$ generation from phagocytic cells (Davies, 1995). These cells such as polymorphonuclear leucocytes (neutrophils), monocytes and macrophages, when invaded by micro-organisms, utilize nicotinamide adenine dinucleotide phosphate oxidase (NADPH oxidase) to generate ROS directly as part of the immune defense activities (Bylund et al., 2010). Therefore,

ROS generated in the human body are byproducts of respiration and immune defense activities, and the generation of $O_2^{\cdot-}$ from O_2 is an important step to generate ROS.

1.3.1.2 Ambient sources of ROS

Ambient ROS appears both in gas and particle phases. Most ROS originate from the photolysis of ozone and subsequent radical reactions (Pöschl and Shiraiwa, 2015). They have different lifetimes ranging from seconds to days in the atmosphere depending on their sources and reactivity (Seinfeld and Pandis, 2006). Those with short lifetimes are less of a concern to health. Long-lived ROS can be inhaled into the human body and cause oxidative stress (see section 1.3.2 for introduction), cellular damage and disease (Pöschl and Shiraiwa, 2015; Ayres et al., 2008). An example of "long-lived" ROS is a group of radicals that are formed during combustion and other thermal processes, so-called environmentally persistent free radicals (EPFRs) (Dellinger et al., 2007). EPFRs are formed when chlorine- and hydroxyl-substituted aromatics chemisorb onto metal oxide surfaces (Vejerano et al., 2012; Lomnicki et al., 2008), then are adsorbed on the surface of particles, allowing them to persist in the environment. Several recent studies show that the heterogeneous reaction between ozone and PAHs can also generate EPFRs (Borrowman et al., 2016; Shiraiwa et al., 2011). Some EPFRs, e.g. semiquinones, can undergo redox cycling and ultimately produce more ROS (Dellinger et al., 2001).

1.3.2 Oxidative Stress

The earliest use of the term "oxidative stress" was not associated with cells or organs but happened in rubber research in 1956 (Ore, 1956). Not until 1985 was the term used to refer to oxidative damage to cells and organs (Sies et al., 1985). Nowadays, oxidative stress is

an expression used to describe various deleterious processes resulting from an imbalance between the excessive formation of ROS and/or RNS and limited antioxidant defenses (Turrens, 2003). Under conditions of abundant ROS production, such as during PM exposure, the antioxidant defences may be overwhelmed, leading to a disruption of redox signaling (transmission of a redox signal via an essential redox element from a source to a target) and control and/or molecular damage (Li et al., 2003a). In recent years, oxidative stress has been implicated as a mechanistic explanation for a wide variety of diseases and syndromes, for example, heart failure (Tsutsui et al., 2011), Parkinson's (Dias et al., 2013) and Alzheimer's (Kanti Das et al., 2015) Diseases, ischaemic stroke (Allen and Bayraktutan, 2009), cataract (Spector, 1995), chronic inflammatory diseases (Nemat et al., 2009), asthma (Walsh, 2006; Li et al., 2003a), and cancer (Reuter et al., 2010).

1.3.3 Oxidative Potential

Oxidative potential (OP), defined as the capability of particles to generate ROS by consumption of antioxidants and/or generation of oxidants, has been proposed as a more relevant air quality exposure metric than PM mass concentration, or concentrations of specific aerosol chemical components, when attempting to link aerosols and health endpoints (Ayres et al., 2008). Many studies have linked OP with adverse health effects (Weichenthal et al., 2016b; Weichenthal et al., 2016a; Bates et al., 2015; Øvrevik et al., 2015; Donaldson et al., 2005; Nel, 2005; Shi et al., 2003; Zielinski et al., 1999).

To measure aerosol OP, both cellular (Xia et al., 2006; Kubátová et al., 2006; Bonvallot et al., 2001; Hiura et al., 1999; Antonini et al., 1998) and acellular methods (Zomer et al., 2011; Mudway et al., 2011; Jung et al., 2006; Venkatachari et al., 2005; Cho et al., 2005;

Frampton et al., 1999) have been developed. Both types of methods have advantages and disadvantages. Acellular methods require less controlled environments and provide faster readouts of PM oxidative potential. Acellular assays generally involve measuring the 1) depletion of antioxidants, such as ascorbic acid, urate, and reduced glutathione in a synthetic respiratory tract lining fluid model (RTLF) (Mudway et al., 2004; Zielinski et al., 1999); 2) consumption of cellular reductant surrogate, such as the dithiothreitol (DTT) assay (Cho et al., 2005); 3) formation of OH· using electron paramagnetic/spin resonance (EPR/ESR) (Shi et al., 2003) or high-performance liquid chromatography (HPLC) (Jung et al., 2006); 4) ROS concentration using fluorescent probes, such as dichlorofluorescin (DCFH) probe based on non-fluorescent DCFH which becomes fluorescent in the presence of ROS (Venkatachari et al., 2005; Hung and Wang, 2001), and chemiluminescent reductive acridinium triggering (CRAT) probe based on chemiluminescence emitted from acridinium compounds to quantify the amount of H_2O_2 (Zomer et al., 2011).

1.4 DTT and AA assay

Among the various available methods for measuring aerosol OP, the dithiothreitol (DTT) and ascorbic acid (AA) assays are widely used. Both methods involve incubating DTT or AA with filter aqueous extracts of PM samples at a biologically relevant temperature (37 °C) and pH (7.4), and monitoring the depletion of DTT or AA over time. The quantification of DTT is achieved by adding 5,5'-dithiobis-(2-nitrobenzoic acid (DTNB) to form a color species and measuring the light absorbance at 412 nm wavelength, whereas AA itself absorbs light at 265 nm wavelength. The depletion of DTT happens when PM extracts catalytically transfer one electron from DTT to molecular oxygen and generate superoxide anion (Kumagai et al., 2002), mimicking the crucial initial step of producing ROS *in vivo*

– the univalent reduction of molecular oxygen. AA is one of the physiological antioxidants in lung lining fluid, which prevents the oxidation of lung cells (Valko et al., 2005). Therefore, OP measured by the *in vitro* depletion of DTT and AA by PM (OP^{DTT} and OP^{AA}) might represent the *in vivo* rate of ROS generation and direct antioxidant oxidation, respectively. Both can lead to oxidative stress. This, in theory, provides a mechanistic link between aerosol OP^{DTT} or OP^{AA} and the ability of particles to induce oxidative stress and cause adverse health effects.

Another advantage of the DTT and AA assays is that they are relatively straightforward and reproducible, allowing method automation, largely reducing labor and time, thus making high-throughput routine measurements possible. At the onset of this study, although sufficient studies have associated particle OP with PM toxicity, large population-based epidemiologic studies of aerosol OP have not been possible. The automation of DTT and AA assays allow the generation of large data sets for studying the links between OP and adverse health effects through epidemiology. As potential health indicators, it is important to understand the spatiotemporal variations, sources, major chemical players, and size-dependent characteristics of these OP. In many cases, when implementing the DTT or AA assay, particles are extracted in water followed by liquid filtration to remove solid or insoluble fractions, but studies show that OP^{DTT} can also be associated with insoluble components (Yang et al., 2014; McWhinney et al., 2013a; Li et al., 2013; Verma et al., 2012; Daher et al., 2011). Therefore, it is also important to assess the contribution of insoluble species to aerosol OP^{DTT}.

1.5 Overview

The aims of this thesis were to understand the sources and atmospheric processes of OP^{DTT} and OP^{AA} and assess the value of OP as a PM toxicity indicator.

Within this framework, the thesis has the following structure**: Chapter 2** (Fang et al., 2015b) presents a semi-automated syringe pump system for measuring the OP^{DTT} from water extracts of $PM_{2.5}$ samples. The semi-automation system was used to generate large data set of water-soluble $PM_{2.5}$ OP^{DTT} at urban, rural, and road-side sites in the southeast United States, and later adapted to AA assay (**chapter 4**) (Fang et al., 2016) and was used to measure water-soluble $PM_{2.5}$ OP^{AA} on the same samples as OP^{DTT}. Then we assessed the spatial and temporal variations, and sources of water-soluble transition metal ions in **chapter 3** (Fang et al., 2015a), since transition metal ions, especially copper (Cu), are important contributors to both OP^{DTT} and OP^{AA} and are potentially toxic due to the ability to catalytically generate ROS *in vivo*. **Chapter 4** (Fang et al., 2016) presents a comparison of water-soluble $PM_{2.5}$ OP^{DTT} with OP^{AA} on the spatiotemporal distributions, sources, and health associations using hospital data from Atlanta metropolitan area. In **chapter 5 and 6** (Fang et al., 2017a; Fang et al., 2017b), we investigated the ambient size distributions of water-soluble OP^{DTT} and OP^{AA}, and water-insoluble OP^{DTT} at an urban and road-side site, Atlanta. Through comparing the results, we studied the key chemical players and atmospheric processes of all OP. The size distributions of OP^{DTT} were also used to assess the deposition of both forms of OP^{DTT} in the human respiratory system.

CHAPTER 2. A SEMI-AUTOMATED SYSTEM FOR QUANTIFYING THE OXIDATIVE POTENTIAL OF AMBIENT PARTICLES IN AQUEOUS EXTRACTS USING THE DITHIOTHREITOL (DTT) ASSAY: RESULTS FROM THE SOUTHEASTERN CENTER FOR AIR POLLUTION AND EPIDEMIOLOGY (SCAPE)

Ting Fang
Vishal Verma
Hongyu Guo
Laura E. King
Eric S. Edgerton
Rodney J. Weber

Atmos. Meas. Tech., 8, 471–482, 2015
doi:10.5194/amt-8-471-2015

2.1 Abstract

A variety of methods are used to measure the capability of particulate matter (PM) to catalytically generate reactive oxygen species (ROS) in vivo, also defined as the aerosol oxidative potential. A widely used measure of aerosol oxidative potential is the dithiothreitol (DTT) assay, which monitors the depletion of DTT (a surrogate for cellular antioxidants) as catalyzed by the redox-active species in PM. However, a major constraint in the routine use of the DTT assay for integrating it with the large-scale health studies is its labor-intensive and time-consuming protocol. To specifically address this concern, we have developed a semi-automated system for quantifying the oxidative potential of aerosol liquid extracts using the DTT assay. The system, capable of unattended analysis at one sample per hour, has a high analytical precision (Coefficient of Variation of 12% for standards, 4% for ambient samples), and reasonably low limit of detection (0.31 nmol/min). Comparison of the automated approach with the manual method conducted on ambient samples yielded good agreement (slope = 1.08 ± 0.12, r^2= 0.92, N= 9). The system was utilized for the Southeastern Center for Air Pollution & Epidemiology (SCAPE) to generate an extensive data set on DTT activity of ambient particles collected from contrasting environments (urban, road-side, and rural) in the southeastern US. We find that water-soluble $PM_{2.5}$ DTT activity on a per air volume basis was spatially uniform and often well correlated with $PM_{2.5}$ mass (r = 0.49 to 0.88), suggesting regional sources contributing to the PM oxidative potential in the southeast US. However, the greater heterogeneity in the intrinsic DTT activity (per PM mass basis) across seasons indicates variability in the DTT activity associated with aerosols from sources that vary with season. Although

developed for the DTT assay, the instrument can also be used to determine oxidative potential with other acellular assays.

2.2 Introduction

Epidemiological studies have associated increases in particulate matter (PM) levels with exacerbation of cardiovascular diseases (Zanobetti et al., 2014; Sun et al., 2010; Pope et al., 2004; Samet et al., 2000) and elevated incidence of respiratory disorders such as airway inflammation, bronchial muscle contraction, and asthma (Harkema et al., 2004; Schaumann et al., 2004; Aust et al., 2002; Norris et al., 1999). The mechanisms underlying these associations are not entirely clear but reactive oxygen species (ROS), either adsorbed on inhaled particles or generated in vivo, have been identified as signaling molecules that induce oxidative stress, causing cell damage (Nel, 2005; Gurgueira et al., 2002). These findings imply that aerosol oxidative potential, i.e. the ability of ambient particles to generate ROS, may be a more relevant measurement than PM mass concentration, or concentrations of specific aerosol chemical components when attempting to link aerosols and health endpoints.

Both cellular (Xia et al., 2006; Kubátová et al., 2006; Bonvallot et al., 2001; Hiura et al., 1999; Antonini et al., 1998) and acellular methods (Zomer et al., 2011; Mudway et al., 2011; Jung et al., 2006; Cho et al., 2005; Venkatachari et al., 2005; Frampton et al., 1999) have been developed to measure the oxidative potential of PM. Both types of methods have advantages and disadvantages. Acellular methods require less controlled environments and provide faster readouts of PM oxidative potential. One of the most widely used cell-free measures of particles oxidative potential is the DTT (dithiothreitol,

$HSCH_2(CH(OH))_2CH_2SH$)) assay (Charrier and Anastasio, 2012; Verma et al., 2012; Verma et al., 2009a; Cho et al., 2005; Kumagai et al., 2002; Delfino et al., 2013). Typically, ROS in vivo are mainly produced in mitochondria and endoplasmic reticulum (ER) where molecular oxygen (O_2) are reduced to superoxide anion (O_2^-) by accepting electrons from cellular reductants, such as NADPH, or during ER protein folding process (Alfadda and Sallam, 2012). The DTT assay simulates this electron-transfer mechanism based on the catalytic ability of redox-active species to transfer elections from DTT to oxygen, and thus can be considered a surrogate measure of the in-vivo capacity of PM to induce ROS. The rate of the reaction, commonly called DTT activity, is determined by measuring the consumption of DTT over time, which is proportional to the concentration of redox-active species in PM extracts. Researchers have identified various chemical components that may participate in the reaction, including polycyclic aromatic hydrocarbons (PAHs) (Li et al., 2003b), quinones (Chung et al., 2006; Kumagai et al., 2002), transition metals (Charrier and Anastasio, 2012), water soluble organic carbon (WSOC) (Verma et al., 2009a; Cho et al., 2005), and HUmic-LIke Substances (HULIS) (Verma et al., 2012; Lin and Yu, 2011). However, a consensus on the relative contributions of these species in the overall DTT activity of ambient particles is currently lacking.

Studies have also reported the association between DTT activity of ambient particles and cellular biomarkers such as fractional exhaled nitric oxide (FE_{NO}) - a marker of airway inflammation (Delfino et al., 2013), hemeoxygenase (HO-1) - an enzyme responsive to oxidative stress (Li et al., 2003b), and 3-(4,5-Dimethylthiazol-2-yl)-2,5-Diphenyltetrazolium Bromide (MTT)-reduction activity (Steenhof et al., 2011). These studies suggest a plausible mechanistic link between DTT-assessed oxidative potential and

adverse health effects of ambient particles. Routine DTT analysis as part of large-scale toxicological and health studies involving aerosol exposure is needed to further establish the health relevance of the DTT assay (and other chemical assays in general).

One major limitation in conducting the DTT assay on a large scale is its laborious and time-intensive analytical protocol, which requires precise handling practices at each step of the reaction for an accurate determination of the rate of DTT oxidation. Researchers have also developed alternative approaches to conduct the DTT assay other than the traditional protocol (Cho et al., 2005) for new applications. For example, a paper-based analytical device (μPAD) DTT assay was developed for personal exposure studies (Sameenoi et al., 2012b) and a microfluidic electrochemical sensor coupled with a particle-into-liquid-sampler (PILS) was developed for real-time measurement of aerosol DTT activity (Koehler et al., 2014; Sameenoi et al., 2012a). We have developed a semi-automated system using programmable syringe pumps with selector valves for conducting the DTT assay on various extracts. The system is based on a simplified protocol in which the aerosol extract oxidizes DTT in a single vial. A small aliquot is withdrawn at various time intervals to determine the remaining DTT concentration and calculate the rate of DTT consumption. Particulate samples are extracted to an aqueous state and analyzed in batches using an auto-sampler, at roughly one hour per sample. Extraction liquids can be either deionized water or organic solvents, in the latter case the solvent is evaporated and reconstituted in deionized water. The system was validated against the manual protocol using both standards and ambient filter samples. The DTT activity of more than 500 samples collected from the southeastern United States as part of the Southeastern Center for Air Pollution & Epidemiology (SCAPE) were analyzed for this study. Here we provide a detailed

description and characterization of the automated system and an overview of aerosol oxidative potential in the southeastern United States. Sources and components of $PM_{2.5}$ that produce the DTT activity are presented in other papers.

2.3 Methods

2.3.1 Chemicals

Dithiothreitol (DTT), Tris base, dimethyl sulfoxide (DMSO), 5,5'-dithiobis-(2-nitrobenzoic acid) (DTNB) and 9,10-phenanthraquinone (PQN) were obtained from Sigma Aldrich (St. Louis, MO, USA). Trichloroacetic acid (TCA, 10% w/v) was obtained from LabChem Inc. (Pittsburgh, PA, USA). Monopotassium phosphate (KH_2PO_4), dipotassium phosphate (K_2HPO_4), and ethylenediaminetetraacetate (EDTA) were obtained from VWR International LLC (West Chester, PA, USA). Details of the chemical preparation and storage are provided in the Appendix A.1 Chemical preparation and storage information.

2.3.2 Automated DTT assay system development

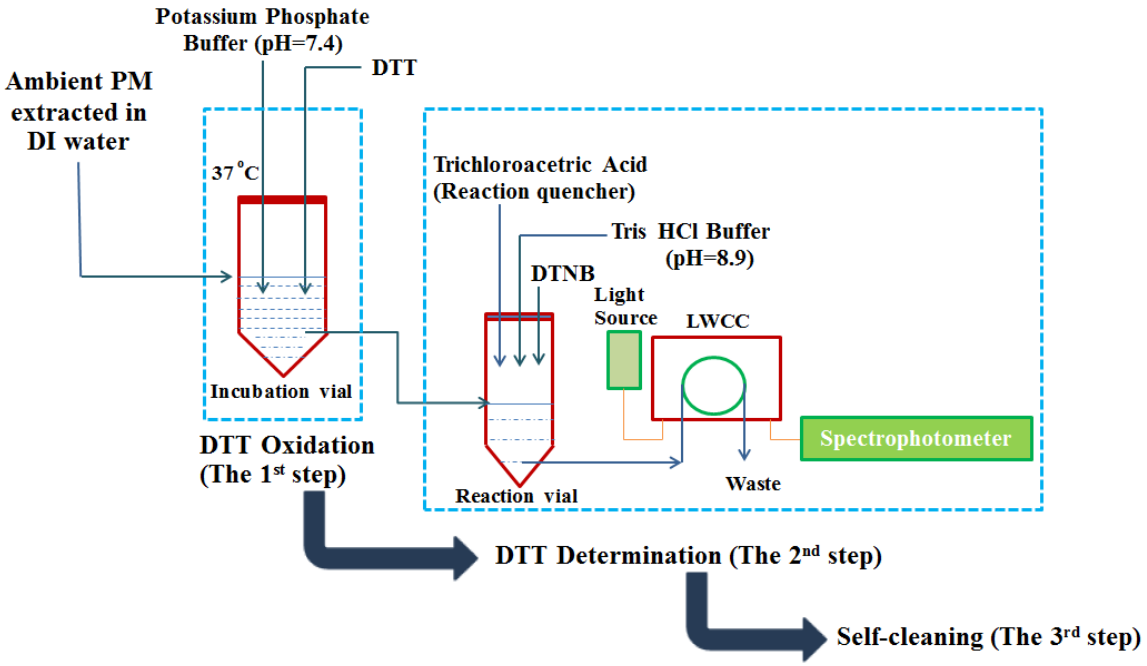

Figure 2-1. Automated system protocol.

Illustrated protocol and setup schematic of the semi-automated DTT assay system are shown in Figure 2-1 and Figure 2-2, respectively. There are three steps in the automated DTT method. In the first step (DTT oxidation step), 3.5 mL of the aerosol extract sample and 1 mL potassium phosphate buffer (0.5 mM) are loaded into an incubation vial (Figure 2-1 & 2-2) (sterile polypropylene centrifuge tube, VWR International LLC, Suwanee, GA, USA) using a programmable syringe pump (A) (Figure 2-2) (Kloehn, Inc., Las Vegas, NV, USA). 0.5 mL of DTT (1 mM) is then added to the incubation vial using another programmable syringe pump (B) (Figure 2-2). The DTT-buffer-sample mixture is incubated at 37 °C and continuously shaken at a rotational frequency of 400 rpm via a ThermoMixer (incubating accuracy: ±0.5 °C, Eppendorf North America, Inc., Hauppauge,

NY, USA). DTT in the mixture is consumed over time in the incubation vial due to catalytic reaction of DTT-active components of the aerosol extract.

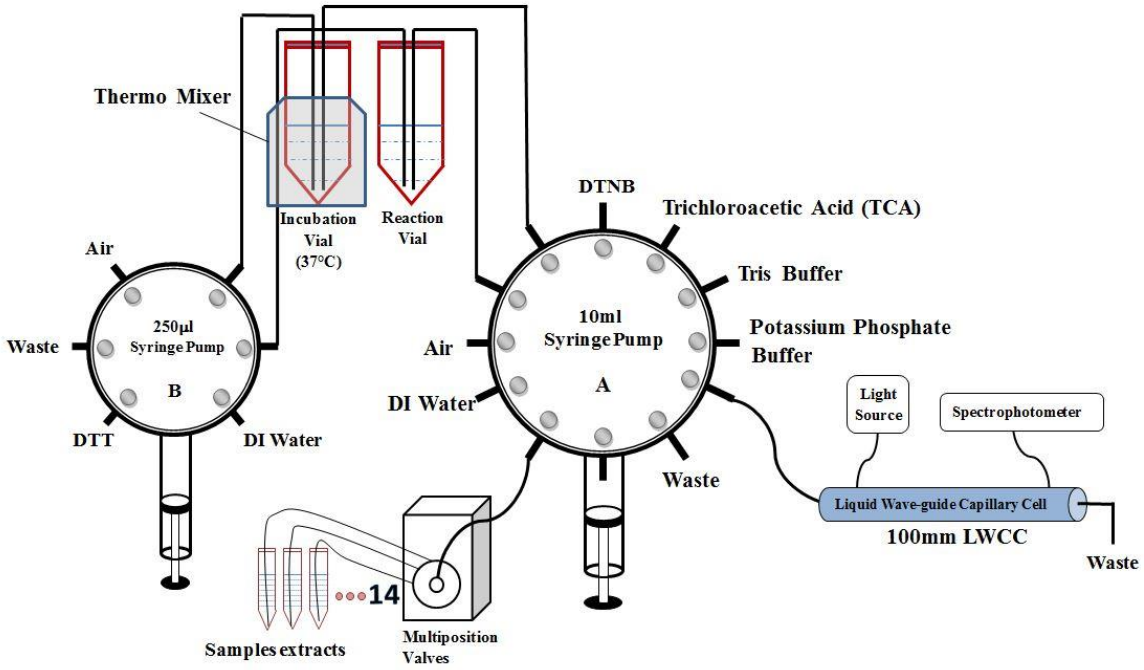

Figure 2-2. Automated system setup.

In the second step (DTT determination step), at a specified time (4 minutes) following the completion of step one, a small aliquot (100 µl) of the incubated mixture is withdrawn and transferred to another centrifuge tube (referred to as, reaction vial), wrapped in aluminum foil to prevent possible light interference, using Pump B. This is mixed with 1 mL TCA (1% w/v; the quenching agent), which had previously been added to the reaction vial by pump A. The quenched mixture with residual DTT is further mixed with 2 mL of Tris buffer (0.08 M with 4 mM EDTA) and 0.5 mL DTNB (0.2 mM) added by pump A. Reaction between the residual DTT and DTNB forms a light absorbing product, 2-nitro-5-

thiobenzoic acid (TNB), which has a high extinction coefficient of 14,150 M^{-1} cm^{-1} at 412 nm wavelength. Pump A then withdraws the final mixture from the reaction vial and pushes it through a Liquid Wave-guide Capillary Cell (LWCC-M-100; World Precision Instruments, Inc., FL, USA) with an optical path length of 100 mm. The waveguide is coupled to an online spectrophotometer (Ocean Optics, Inc., Dunedin, FL, USA), which included a UV-VIS light source (Ocean Optics DT-Mini-2), and a multi-wavelength light detector (USB4000 Miniature Fiber Optic Spectrometer). Absorbance intensity at 412 nm and 700 nm (chosen as the baseline absorbance for TNB) are recorded every 2 seconds using data acquisition software (SpectraSuite). The system then performs a self-cleaning using deionized water (DI water, >18 MΩ cm^{-1}) to eliminate any residual liquid in the reaction vial, tubing, syringes and LWCC. This second step is repeated four more times, at specific time intervals (13, 23, 30 and 41 minutes), generating a total of 5 data points of remaining DTT concentration with time. Following this, the automated system again performs a self-cleaning routine (third step) to ensure no carry-over in the incubation vial, tubing, syringes, and LWCC, before analyzing the next aerosol sample. A 14-port Multi-position Valve (VICI® Valco Instrument Co. Inc., USA) is used to consecutively select individual aerosol samples for analysis. The Kloehn control program code written for conducting the DTT assay, including hardware and software details are included in the SI. The automated system is cleaned periodically (about every 15 days) by flushing at least 3 times with methanol, followed by 6 times with DI water.

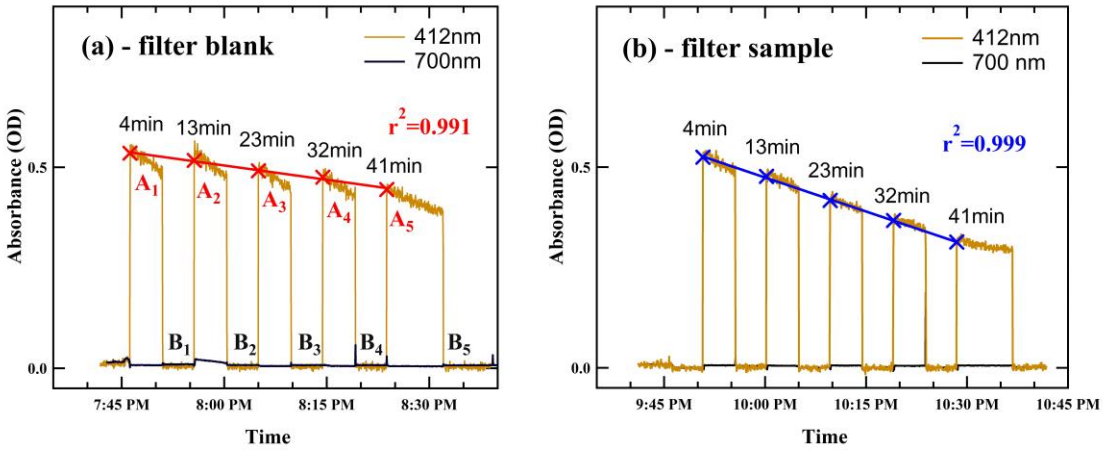

Figure 2-3. Example of an absorbance plot for a filter blank (a) and an ambient aerosol sample (b).

DTT activity determination: Figure 2-3 shows an example of the absorbance intensity plot measured over time for a filter blank (a) and sample (b), obtained from the data acquisition software. The time intervals (4, 13, 23, 30 and 41 min) represent the incubation duration of DTT and sample in potassium phosphate buffer for each measurement. Withdrawal of the mixture containing TNB and pushing it through the LWCC (DTT determination step) causes the corresponding jumps in light absorbance at 412 nm [A_1, A_2, A_3, A_4, A_5 in Figure 2-3 (a)]. After the absorbance measurement, pump A pushes DI water through the LWCC, which returns the absorbance back to the baseline value [i.e. absorbance at 412 nm equals absorbance at 700 nm; B_1, B_2, B_3, B_4, B_5 in Figure 2-3 (a)], thus generating a series of roughly square bars. A decreasing absorption intensity between successive measurements ($A_1>A_2>A_3>A_4>A_5$) for a sample reflects the DTT oxidation over time. During each specified DTT measurement time interval, absorbance decreases (angled top of the square

wave in Figure 2-3); the average of the initial five absorbance data is taken as characteristic absorption for each interval. The rate of DTT consumption (σDTT, nmol/min) was determined from the slope and intercept of the linear regression of measured absorbance versus time as follows:

$$\boldsymbol{\sigma DTT = -\sigma Abs * \frac{N_0\ nmol}{Abs_0}} \qquad \textbf{(Equation 1),}$$

where σAbs is the slope of absorbance versus time; Abs_0 is the initial absorbance calculated from the intercept of the linear regression of absorbance versus time; and N_0 is the initial moles of DTT added to the reaction vial. A steeper slope corresponds to a higher rate of DTT consumption. The final DTT activity for a sample was calculated by subtracting a blank value from the sample and normalized by sample air volume or particle overall mass (or mass of a specific component) represented by the sample in the incubation vial, expressed in the units of nmol/min/m^3 for volume normalized DTT activity (DTTv), or nmol/min/μg for mass normalized DTT activity (DTTm). DTTm represents the intrinsic property of particles linked to sources, while DTTv accounts for the emission rate, dilution, etc., and characterizes exposure to the aerosol. Thus,

$$\boldsymbol{DTT\ activity = \frac{\sigma DTT_{\ sample} - \sigma DTT_{\ blank}}{V_{air}\ (\text{or}\ M_{particle})}} \qquad \textbf{(Equation 2),}$$

where V_{air} and $M_{particle}$ are the ambient air volume (m^3) and total PM mass (μg) represented by the sample in the incubation vial, respectively. For example, a 3.5 mL sample of concentration 40 μg/mL would represent a total PM mass of 140 μg (3.5 × 40) in the incubation vial.

2.3.3 Ambient samples collection and preparation

2.3.3.1 Sampling

For this study, ambient $PM_{2.5}$ samples were collected over 23 hours on pre-baked quartz filters (Pallflex® Tissuquartz™, 8×10 inches) using high-volume (Hi-Vol) samplers (Thermo Anderson, flow rate normally 1.13 m^3/min) as part of SCAPE. One sampler was fixed at a stationary site, Jefferson Street (JST), a central site representative of the Atlanta urban environment, while the other sampler (Trailer) was rotated among a road-side (RS), a near-road (Georgia Tech - GT), and a rural site (Yorkville - YRK), sampling in parallel with the fixed monitoring station (JST). Site characteristics are:

1) RS site was situated within 5 m distance from the interstate highway (I75/85) in Midtown Atlanta and was chosen for capturing immediate traffic emissions;
2) GT site was located on the rooftop of the Ford Environmental Science and Technology Building at Georgia Tech, Atlanta, roughly 30 m above ground level, 840 m from the RS site, providing an intermediate location between RS and the central urban site (JST);
3) YRK site is situated in an agricultural region located approximately 70 km west of JST, representative of a rural environment.

Other sites also include an urban site in Birmingham (BHM), Alabama and its paired rural site, Centerville (CTR), Alabama. JST, YRK, BHM, and CTR are all part of the Southeastern Aerosol Research and Characterization Study (SEARCH) network sites (Hansen et al., 2003). A map of sampling sites is provided in the section 2.6 Figure 2-10. Ambient particles were collected from June 2012 to September 2013. For two periods (November 2012 and April 2013), the trailer was located at the stationary JST site for side-by-side comparisons. **Table 2-1** provides the sampling schedule and number of filters collected at each site. In total, 503 Hi-Vol filters were collected over 15 months. Three

seasons are defined based on the temperature profile throughout sampling period (see section 2.6 Figure 2-11) - summer, fall, and winter, as shown in **Table 2-1**. Collected samples were immediately wrapped in pre-baked aluminum foil and stored at -18 °C until analyzed.

Table 2-1. Sampling schedule and number of Hi-Vol filters collected at each site from June 2012 to September 2013.

Year. Month Season	Stationary site	Sample size	Trailer site	Sample size
2012.6-7 Summer	JST	31	YRK	33
2012.7-8 Summer	JST	37	GT	38
2012.9-10 Fall	JST	26	RS	29
2012.11	JST	13	JST	14
2012.12 Winter	JST	22	YRK	22
2013.1-2 Winter	JST	30	RS	31
2013.3 Winter	JST	23	GT	22
2013.4	JST	14	JST	14
2013.6-7 Summer	CTR	30	BHM	31
2013.9-10 Fall	GT	23	RS	20
Total number of filters				**503**

2.3.3.2 Extraction of PM filters

All filters extracted in DI water via the following method were also extracted with methanol, dried and reconstituted in DI water for DTT analysis. Both water and methanol extracts were separated by solid phase extraction (C-18 resin). DTT activity was analyzed with this system in order to explore the oxidative potential of chemical sub-fractions of the ambient aerosol. Thus, not including blanks and standards, for this project on the order of 2,000 extracts were analyzed for DTT activity. For the water extraction procedure, portions of the filters (about 1/28 area of the Hi-Vol filter, three one-inch diameter punches) were

punched and extracted in 15 mL of DI water in sterile polypropylene centrifuge tubes (VWR International LLC, Suwanee, GA, USA) by sonication for 30 minutes. Extracts were then filtered using PTFE 0.45 μm syringe filters (Fisherbrand^{TM}, Fisher Scientific, PA, USA) to remove insoluble components, and divided into two fractions. One fraction of at least 5 mL was analyzed for DTT activity using the automated system. The other fraction was reserved for other chemical analysis. Here we focus only on the discussion of DTT analysis of only the direct water extracts.

2.3.4 $PM_{2.5}$ mass concentration

$PM_{2.5}$ mass concentration was measured by a Tapered Element Oscillating Microbalance (TEOM) at the SEARCH sites, i.e. JST, YRK, BHM and CTR by Atmospheric Research Analysis (ARA, Inc.) and retrieved from the data archive. For the RS and GT sites, the PM mass concentrations were estimated from the sum of chemical components analyzed on the Hi-Vol filters and the summation method was calibrated with ARA TEOM at the JST site (slope = 1.34 ± 0.06, intercept = - 2.46 ± 0.59 μg/m^3, r^2 = 0.72, N = 162, see section 2.6, Figure 2-12). The measured components include EC (Sunset Laboratory OCEC analyzer), organic mass [OC*1.6 (Turpin and Lim, 2001)], water soluble metals [measured by X-ray fluorescence method (XRF)], and ammonium sulfate [assuming sulfate and ammonium are all $(NH_4)_2SO_4$ (Zhang et al., 2010), where sulfate was calculated from sulfur measured by XRF]. Further description of the analytical procedure for each method will be reported in subsequent publications on the chemical data (Fang et al., 2015a; Verma et al., 2014).

2.4 Results and discussion

2.4.1 Automated system performance

The performance of the automated system was assessed by conducting tests to determine instrument response, limit of detection (LOD), precision and accuracy using both standards and ambient particles.

2.4.1.1 Automated system response to individual compound

9,10-phenanthraquinone (PQN) has been shown to be capable of catalyzing the oxidation of DTT (Li et al., 2009; Kumagai et al., 2002), although it is not highly water-soluble. The automated system was assessed for linearity with PQN (Figure 2-4). The x-axis intercept (0.11 nmol/mL in the incubation vial) represents the minimum concentration of PQN required to produce a measurable signal on the system, pure water with blank subtracted. As shown, the response of the system to PQN is highly linear with a correlation coefficient (r^2) of 0.98. At least one PQN per ambient sample batch (typically 12 samples) is used as a positive control to ensure the consistency of the system.

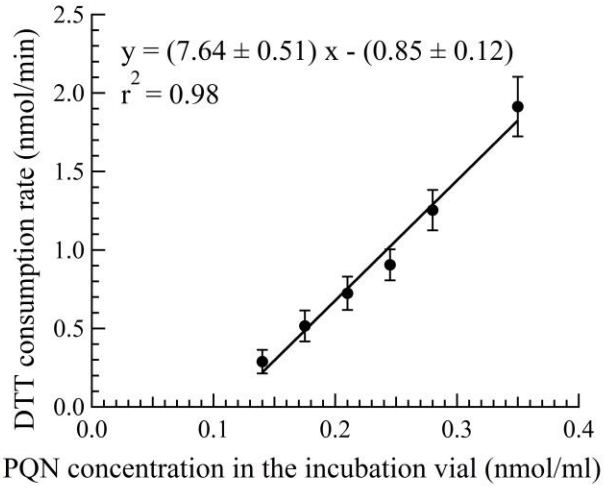

Figure 2-4. Blank corrected DTT consumption rate as a function of PQN (9,10-phenanthraquinone) used as a positive control. Each error bar represents the standard deviation of three independent DTT measurements on each concentration.

2.4.1.2 Limit of detection

The limit of detection (LOD) of the system, defined as three times the standard deviation of DI water-blanks (N = 37), is 0.31 nmol/min. Expressing the LOD in terms of the PM concentration of the sample extract (µg/mL) is not straightforward as it depends on many factors, including extraction efficiency and the relative fractions of DTT active components in ambient particles. Based on the analysis of 503 Hi-Vol samples in the present study from different sites (urban, rural and roadside), approximately 100 µg of $PM_{2.5}$ mass loading on the filter, extracted in 5 mL of DI water was sufficient to have reliable results above LOD. The upper limit of the PM concentration is also constrained such that the DTT consumption remains less than 50% of the initial concentration to ensure the pseudo-1st-order reaction of the DTT oxidation. For most of the PM samples collected, roughly 1/28th area (typical $PM_{2.5}$ mass loading = 0.2-1 mg) of a Hi-Vol filter, extracted in 15mL of DI water, yielded

a DTT consumption rate within these limits (0.8-2.6 nmol/min). In rare cases (<10 %) when the DTT consumption exceeds 50 %, only the initial consumption data points (at least 3) were used for the rate calculation.

2.4.1.3 Precision

The precision of the automated system for ambient samples was assessed by separately extracting seven different equal sections (1/28th each) of the same Hi-Vol filter in 15 mL of DI water and analyzed for DTT activity. A low standard deviation of 0.081 nmol/min [Coefficient of Variation (CV) = 4 %] indicates sufficiently high precision of the system for ambient samples.

2.4.1.4 Accuracy

The system was validated for accuracy by comparing the DTT activity of both standards and ambient PM samples obtained from the automated approach with that from the same experimental protocol performed manually.

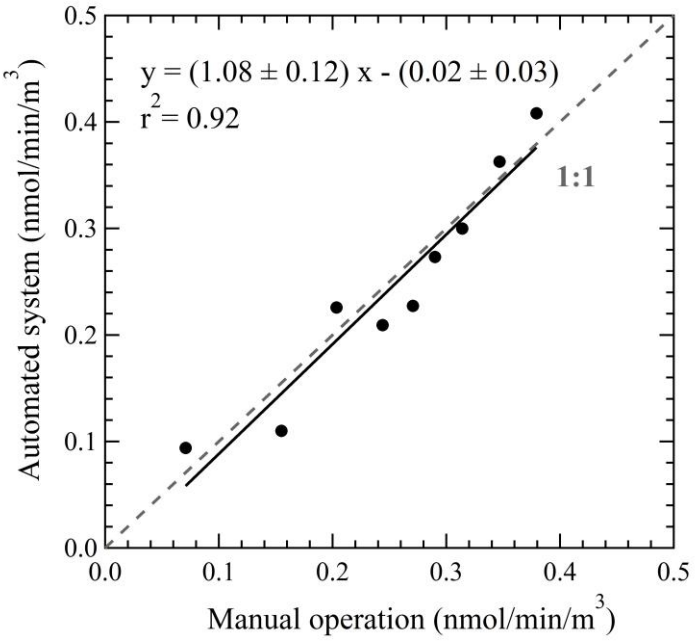

Figure 2-5. Comparison of the automated system with manual operation using ambient aerosol extracts ($PM_{2.5}$ samples collected from JST site, Atlanta, in Dec 2012) (Regression analysis was done by orthogonal regression. The dotted line is 1:1).

Five replicates of the PQN standard (0.21 nmol/mL in the incubation vial) were run both on the automated system and manually. The DTT consumption rate obtained from the automated system (mean ± stdev of 0.77 ± 0.03 nmol/min, CV= 4.24%) was very close to that from the manual operation (0.74 ± 0.03 nmol/min, CV= 3.97 %). As further validation, nine ambient PM samples were analyzed for DTT activity by both manual and automated approach. As shown in Figure 2-5, an orthogonal fit yielded a slope (automated/manual) of 1.08 ± 0.12, intercept close to zero (-0.02 ± 0.03 nmol/min/m^3), and correlation coefficient (r^2) of 0.92. Further, a paired t-test shows no significant difference between the results obtained by two methods [$t(8)<t_{critical}$, p=0.05].

These tests demonstrate the robustness of the instrument as a viable alternative of the manual DTT assay making it useful for rapid and high throughput sample analysis for large-scale studies.

2.4.2 Field evaluation of the automated system

Table 2-2. Performance of the automated system as assessed by consistency of DTT consumption rate for blanks and standard.

Sample	Sample Size	Standard Deviation, nmol/min	%CV
DI Blank	37	0.10	28.1
Field Blank extracted in DI water	63	0.11	31.1
Standard (9,10-Phenanthrenequinone)	55	0.19	15.0

Coefficient of Variation (%CV) = StdDev/Avg*100

The Southeastern Center for Air Pollution & Epidemiology (SCAPE) was a coordinated multi-investigator effort to characterize ambient gas/particle mixtures in southeastern U.S., to elucidate their sources and to assess their impacts on human health. The automated system was used to measure DTT activity on the set of samples (N = 503) collected from multiple sites during SCAPE. Multiple DI water blanks (N = 37), PQN standards (N = 55), in addition to field blanks (N = 63) collected during the sampling were analyzed along with the PM samples. This project provided an ideal opportunity for the field evaluation of the semi-automated DTT assay instrument. Table 2-2 summarizes the performance of the system as evaluated by the stability of the results from both standards and blanks. The system remained fairly consistent throughout the analysis with reasonably small variability

for both standards (CV = 15%) and blanks (DI blanks: CV = 28.1%; field blanks: CV = 26.7%).

2.4.2.1 Overall method precision

The overall precision of the paired ambient sampling method utilized in this study was further assessed by comparing the DTT activity of $PM_{2.5}$ samples collected simultaneously at JST using two Hi-Vols in November 2012 and April 2013 (shown in Figure 2-6). The orthogonal regression yields a slope of 1.03 ± 0.05, with an intercept of 0.02 ± 0.01 nmol/min/m^3, and r^2 = 0.96. Considering the combined uncertainties from sample collection, pretreatment, and extraction, the good agreement between the two sampling systems demonstrates a high overall precision of DTT measurement for ambient samples.

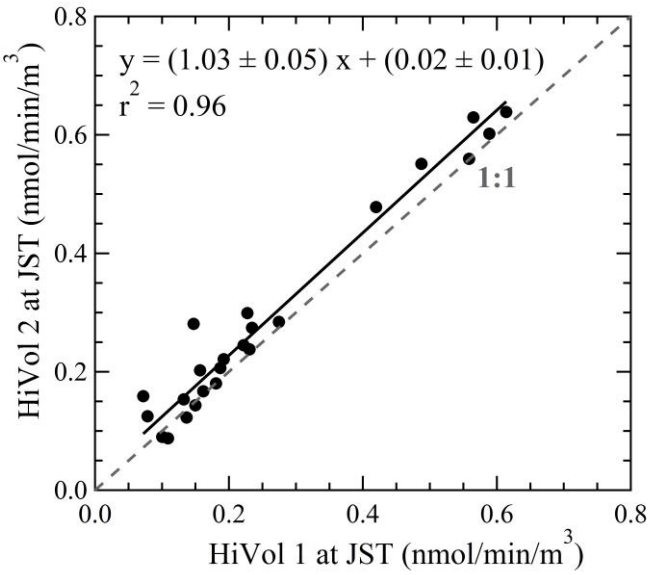

Figure 2-6. Overall method precision of the automated system precision assessed by PM2.5 filter samples (N = 24) collected simultaneously using two Hi-Vol samplers deployed side-by-side at JST during November 2012 and April 2013 (Regression analysis was done by orthogonal regression. The dotted line is 1:1).

2.4.2.2 DTT activity of ambient samples

The time series of both water-soluble volume-normalized (DTTv) and mass-normalized (DTTm) DTT activity are shown in Figure 2-7 (a) and (b), respectively. Comparing the time series of DTTv [Figure 2-7 (a)] between paired sites shows that there is generally little divergence between sites, with the exception of the JST-YRK (urban-rural) pair in winter. Some of this uniformity is due to the 23-hour integrated sampling time of the Hi-Vol filters, which dampens any diurnal variability in the emission sources contributing to PM oxidative potential. Figure 2-8 shows the distribution of water-soluble DTTv and DTTm data of ambient $PM_{2.5}$ obtained in our study in comparison with those from other studies (Charrier and Anastasio, 2012; Verma et al., 2009b; Hu et al., 2008; Ntziachristos et al., 2007; Cho et al., 2005). Our DTTv data [Figure 2-8(a)] are in the range reported in other studies, with an exception for RS (measurements made adjacent to a high-traffic highway), which is lower in the present study. However, comparing the DTTm levels, RS DTTm are well within the typical range of other studies and thus our lower DTTv levels are most probably attributed to higher $PM_{2.5}$ concentrations reported in other studies sampling by roadways. Our study generally shows a broader span for urban and rural sites than reported previously, which is likely due to the much larger dataset collected over a yearlong period that captured a wider range of sources and ambient conditions. Overall, these results show the utility of the automated system for providing a comprehensive assessment of the aerosol oxidative properties.

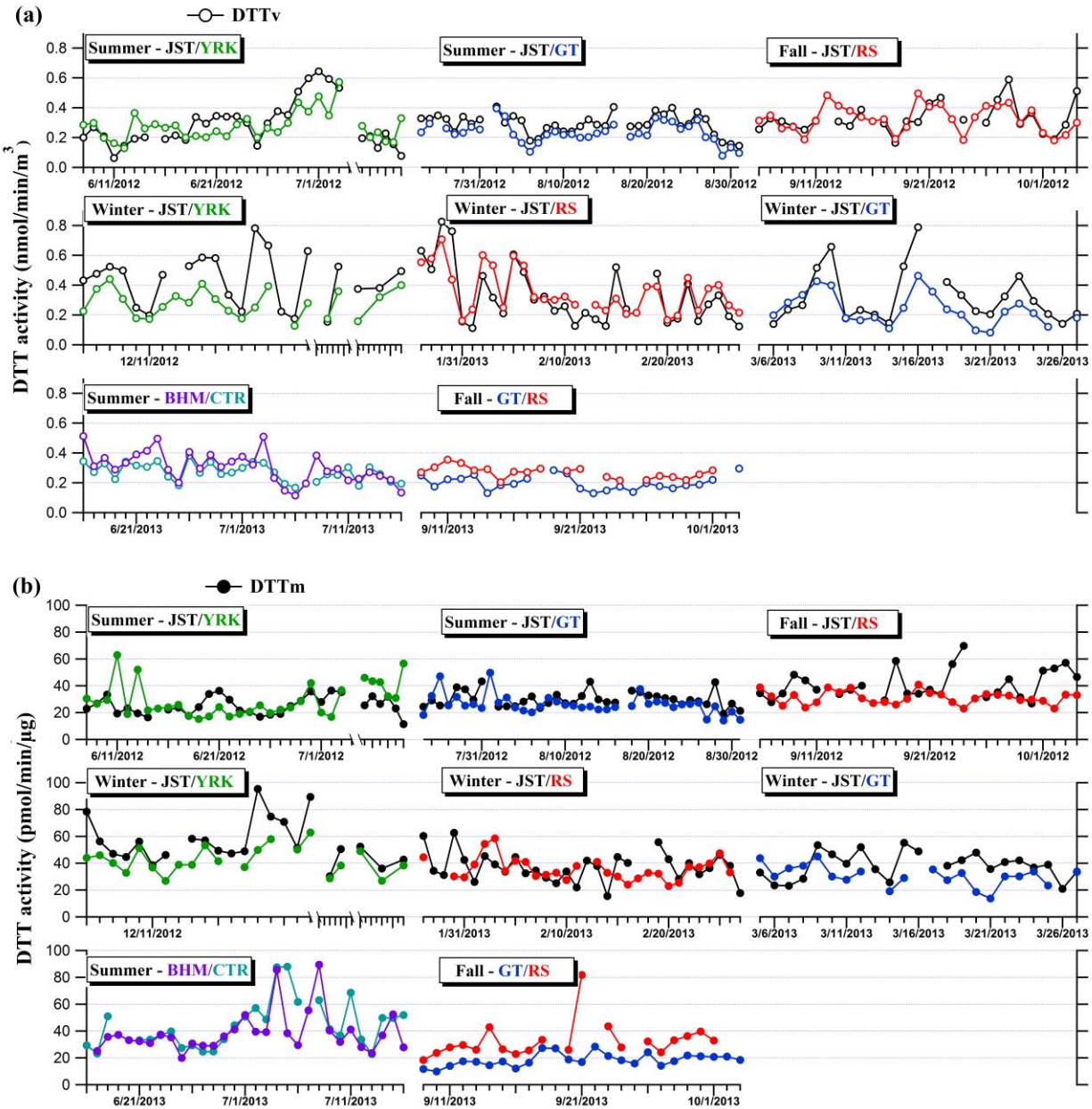

Figure 2-7. Water-soluble DTT activity of the ambient particles collected in paired sampling sites. The plots show (a) volume-normalized (DTTv) and (b) mass-normalized (DTTm) DTT activity at JST (urban, black) paired with YRK (rural, green), RS (roadside, red), GT (near-road, blue). Also included is the CTR (rural, cyan) - BHM (urban, purple) pair, and the GT-RS pair.

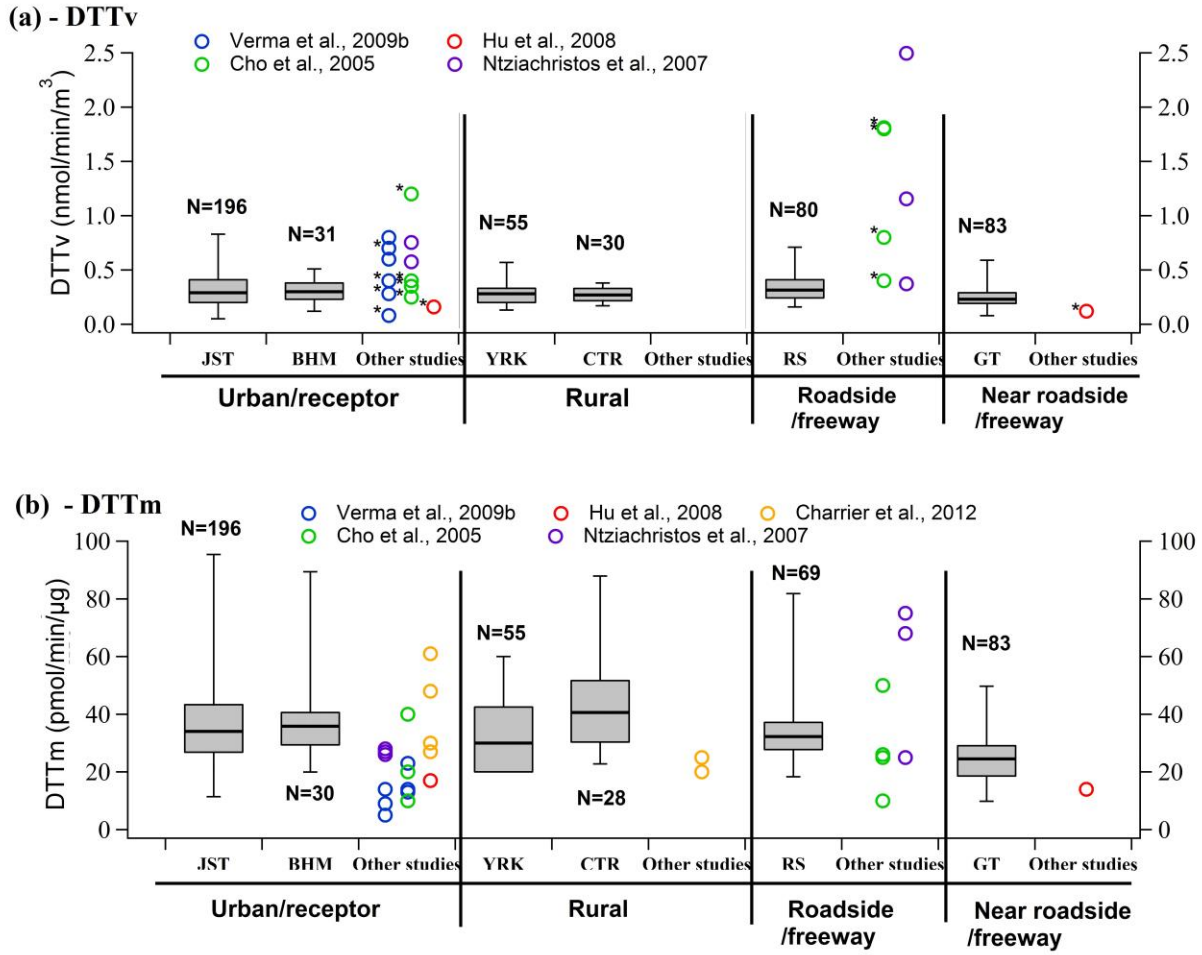

Figure 2-8. Distribution of water-soluble volume-normalized (a) and mass-normalized (b) DTT activity (oxidative potential) of ambient PM2.5 in our study compared with other studies. Data from this study are expressed as median, maximal, minimal, percentile 25 and 75. Roadside/freeway - sampling sites are located adjacent to road/highway; Near roadside/freeway - sampling sites are further away but less than 1km from road/freeway. *- numbers not presented in the paper, thus estimated from graphs.

2.4.2.3 Seasonal and spatial variability

Seasonal and spatial variability of aerosol oxidative potential (both DTTv and DTTm) in the southeast US were assessed by Analysis of Variance (ANOVA) tests and Coefficient of Divergence (COD), respectively. The ANOVA tests were used to assess differences

between seasons at a given site (section 2.6 Table 2-4 and Table 2-5), and the COD (Wilson et al., 2005) was calculated to assess spatial variability (See section 2.6 Table 2-6). The COD is calculated as follows:

$$\boldsymbol{COD} = \sqrt{\frac{\mathbf{1}}{\boldsymbol{N}}\sum_{\boldsymbol{i}=\mathbf{1}}^{\boldsymbol{N}}\left[\frac{\boldsymbol{c_{ij}}-\boldsymbol{c_{ik}}}{\boldsymbol{c_{ij}}+\boldsymbol{c_{ik}}}\right]^{\mathbf{2}}} \qquad \textbf{(Equation 3)}$$

where c_{ij} and c_{ik} are the 23-hour averaged DTT activity (nmol/min/m^3) measured at site j and k, respectively, and N is the sample size. COD ranges from 0 to 1, with values close to 0 representing a homogenous distribution and those near 1 indicating heterogeneity.

Based on ANOVA tests, there was high heterogeneity across seasons for DTTv at JST ($p = 0.01$, see section 2.6 Table 2-5) with the highest DTTv in winter [December (winter) /June (summer) = 1.51], while there was no significant seasonal variation observed at YRK, GT and the RS site ($p>0.01$). In comparison to DTTv, there are greater seasonal variations in DTTm, for example, average DTTm at most sites showed much higher levels in winter than summer and fall (winter/summer = 1.4, 1.2, and 2.2 for YRK, GT, and JST, respectively). ANOVA tests also validated the pronounced seasonal differences for DTTv and DTTm at JST and DTTm at other sites ($p <0.01$, see section 2.6, Table 2-5 and Table 2-6). The higher seasonal differences in DTTm may suggest that the specific chemical components that contribute to the oxidative potential of particles varies between seasons and originate from different sources.

Relatively low levels of the CODs (<0.25) (**Table 2-3**) found for both DTTv and DTTm at paired-sites indicate spatial homogeneity of water-soluble aerosol oxidative potential in the region, suggesting dominant DTT activity sources are regional in nature. Note that JST/RS and GT/RS pairs, in both fall seasons, show slightly lower CODs (more uniformity) in

DTTv than in DTTm (COD for DTTv = 0.13 and 0.18 compared to COD for DTTm = 0.23 and 0.31 for JST/RS and GT/RS, respectively). This indicates that although there may be unique local sources at the RS site, for example, primary vehicle emissions and re-suspended dust, their overall contribution was not substantial compared to the regional DTT signal and so was not clearly resolved.

Table 2-3. Spatial heterogeneity of DTTv and DTTm assessed by Coefficient of Divergence (COD)

Season	Paired sites	CODv (DTTv)	CODm (DTTm)
Summer	JST/YRK	0.21	0.23
Summer	JST/GT	0.15	0.15
Fall	JST/RS	0.13	0.23
Winter	JST/YRK	0.25	0.15
Winter	JST/RS	0.17	0.18
Winter	JST/GT	0.23	0.22
Summer 2013	BHM/CTR	0.12	0.15
Fall 2013	GT/RS	0.18	0.31

2.4.2.4 Oxidative potential and $PM_{2.5}$ mass

Figure 2-9 shows the correlation between DTT activity (DTTv) and $PM_{2.5}$ mass concentrations for all the sites and seasons. DTTv correlates with PM concentration in various degrees (Pearson's r = 0.49-0.88), but generally, the correlations are high for most

sites. For JST, the representative urban site, Pearson's r is particularly high (r = 0.76-0.82) in all seasons. Lowest DTTv - $PM_{2.5}$ mass correlations were at the road-side site, probably due to the influence of unique RS sources that contributed to mass but not significantly to DTT activity (average $PM_{2.5}$ concentrations are 8.7 and 8.2 μg/m^3 at JST compared to 10.4 and 9.5 μg/m^3 at RS in fall and winter, respectively). It is important to note that despite the significant correlation, the slope for DTT activity versus $PM_{2.5}$ mass varies among different sites and seasons. Overall, we attribute the variation in the degree of association between DTT activity and $PM_{2.5}$ mass to the varying PM chemical composition. This is also supported by the spatial and seasonal variability in intrinsic DTT activity (per mass) as discussed above. This analysis suggests that DTT activity in the southeast is likely, to a significant extent, related to regional sources and not dominated by a single source or a limited number of species. Further investigation on identifying the specific sources and aerosol chemical components linked to PM oxidative potential will be discussed in subsequent publications (Verma et al., 2014).

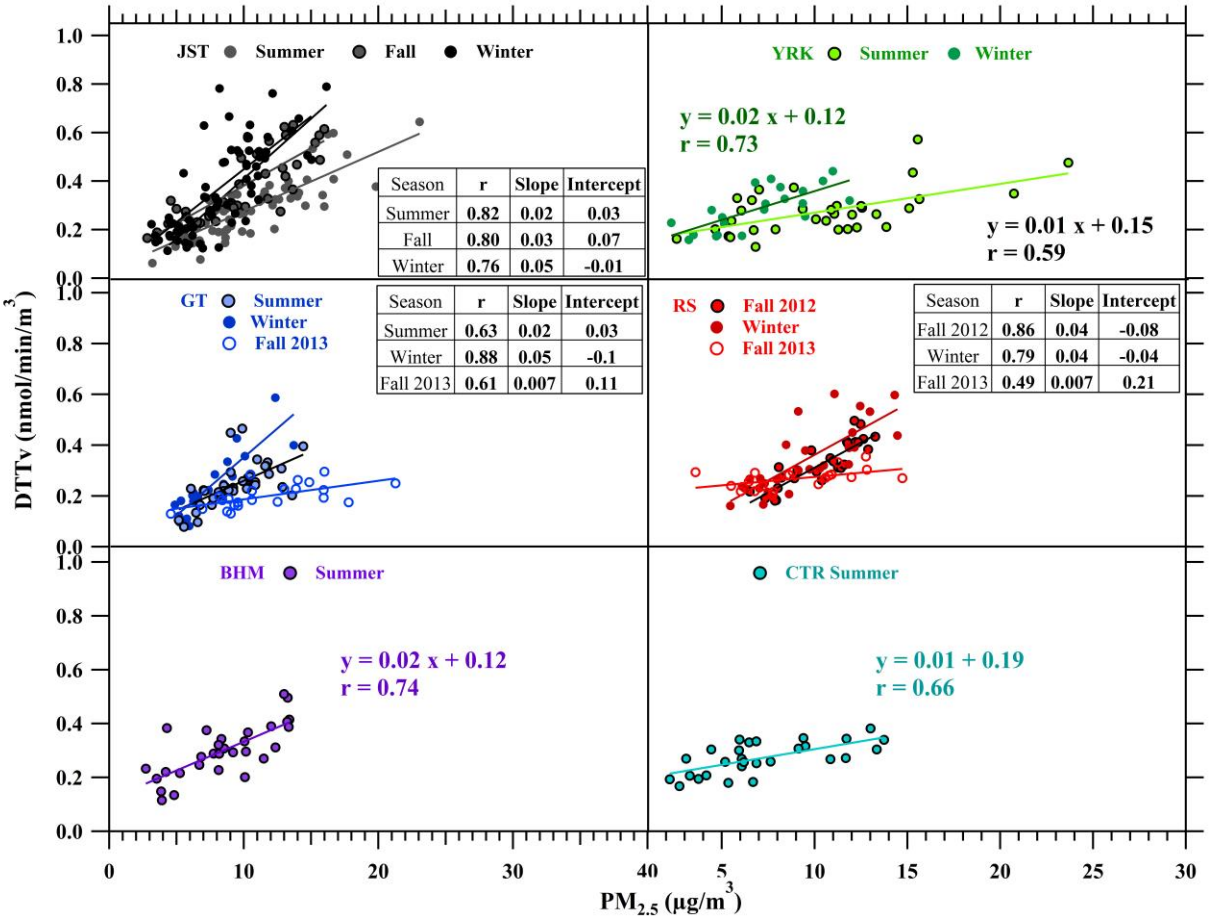

Figure 2-9. Correlation (Pearson's r) between water-soluble DTT activity (DTTv) and PM2.5 mass concentration at JST (urban), YRK (rural), RS (roadside), GT (near-road), CTR (rural), BHM (urban) sites.

Studies have shown a correlation between health end-points and $PM_{2.5}$ mass (Gholampour et al., 2014; Tong et al., 2012; Peter and Steffen, 2010). The overall correlation between water-soluble DTT activity and $PM_{2.5}$ mass concentration observed in this study may help explain, at least in part, some of these associations. However, the varying degree of correlation between DTT activity and $PM_{2.5}$ mass at different sites and seasons suggests that there might be additional advantages of including PM oxidative potential in health studies, rather than relying on PM mass alone. More work is required to identify specific

compounds that are most sensitive in the DTT probe and test how they may contribute to the observed ambient DTT activity. Application of the DTT probe and other acellular and cellular assays in different regions that have a different mix of emission sources is also needed to better understand the possible links between aerosol oxidative potential and health endpoints. The automated DTT assay analytical instrument described here would facilitate these types of future studies. Finally, although the analytical system described here can provide new insight on aerosol oxidative properties from large data sets, it does not solve limitations associated with filter-based particle collection approaches, which entail artifacts due to losses of semi-volatile DTT-active species during sampling and handling procedures. Adapting the DTT assay to an online system could limit sampling artifacts and provide new insights into DTT sources and atmospheric processing that more highly time-resolved data can provide.

2.5 Conclusions

An automated analytical system for quantifying the oxidative potential of aerosol liquid extracts using the DTT assay was developed. The system follows the analytical approach developed by Cho et al., (2005) and is capable of one DTT activity measurement per hour. The system response was assessed by 9,10-phenanthraquinone (PQN), which was used as a positive control when running a series of ambient samples. The method LOD was 0.31 nmol/min. Analytical precision based on both PQN (CV = 15 %) and ambient samples (CV= 4%) was high. The instrument was further validated for accuracy by comparing with the manual procedure using ambient PM samples (r^2 = 0.92, slope = 1.08 ± 0.12). The suitability of the system for large-scale application was assessed by analyzing more than 500 filters collected in the southeastern US as part of SCAPE, the joint Emory/Georgia

Tech Clean Air Research Center. The data shows that water-soluble $PM_{2.5}$ DTT activity on a per volume of air basis was spatially uniform and generally correlated with $PM_{2.5}$ mass ($r = 0.49$ to 0.88), indicating regional sources for aerosol oxidative potential. However, the higher seasonal heterogeneity in the intrinsic water-soluble DTT activity (per PM mass basis) may indicate that the dominant regional sources change with season. More in-depth analysis of the extensive data set generated with the instrument will be forthcoming. Finally, it is noted that the method can be altered to run smaller sample volumes, for situations involving samples of lower mass loadings. It has also been modified for ROS analysis using other assays (e.g., ascorbate depletion assay). The automated system presents a useful new tool for rapid and high throughput measurement of the DTT activity of ambient particle extracts. Its application can facilitate routine use of PM oxidative potential in toxicological, panel exposures, and epidemiological studies.

2.6 Supporting materials

Table 2-4 Comparison of semi-automated DTT assay system to the traditional manual method.

	Traditional manual method	**Semi-automated method**
Labor involved	Yes	No
Numbers of samples analyzed daily	5-8	24
Time for each sample, h	1	1
Remote control	No	Yes
Reaction Volume, mL	1	5
Reaction Vial	Multiple vials	Single vial
Limit of Detection, nmol/min	0.26 (N=5)	0.31 (N=37)

Table 2-5 The seasonal variation on volume-normalized water-soluble DTT activity assessed by ANOVA tests

Site	Season	Average ± variance (nmol/min/m^3)		N	F	P-value	$F_{critical}$
YRK	Summer	0.28	0.01	33	0.01	0.91	7.14
	Winter	0.28	0.01	22			
RS	Fall	0.33	0.01	29	3.87	0.03	4.89
	Winter	0.36	0.02	31			
	Fall 2013	0.27	0.00	20			
GT	Summer	0.24	0.01	38	2.42	0.10	4.88
	Winter	0.25	0.02	22			
	Fall 2013	0.20	0.00	23			
JST	Summer	0.29	0.02	31	3.15	0.01	3.13
	Summer	0.29	0.00	37			
	Fall	0.34	0.01	26			
	Winter	0.43	0.03	22			
	Winter	0.33	0.04	30			
	Spring 2013	0.32	0.03	22			

Table 2-6 The seasonal variation on mass-normalized water-soluble DTT activity assessed by ANOVA tests

Site	Season	Mean ± variance (pmol/min/μg)		N	F	P-value	$F_{critical}$
YRK	Summer	29.76	0.16	33	15.01	3.01E-04	7.15
	Winter	42.38	0.10	21			
RS	Fall	31.15	0.02	29	1.84	0.17	3.12
	Winter	35.65	0.07	28			
	Fall 2013	32.71	0.18	20			
GT	Summer	26.16	0.05	38	19.89	1.05E-07	3.11
	Winter	30.60	0.06	20			
	Fall 2013	18.06	0.02	23			
JST	Summer	25.35	0.05	31	25.17	9.33E-19	3.13
	Summer	29.86	0.03	37			
	Fall	41.06	0.12	26			
	Winter	55.54	0.28	22			
	Winter	37.17	0.12	30			
	Winter	36.82	0.15	23			

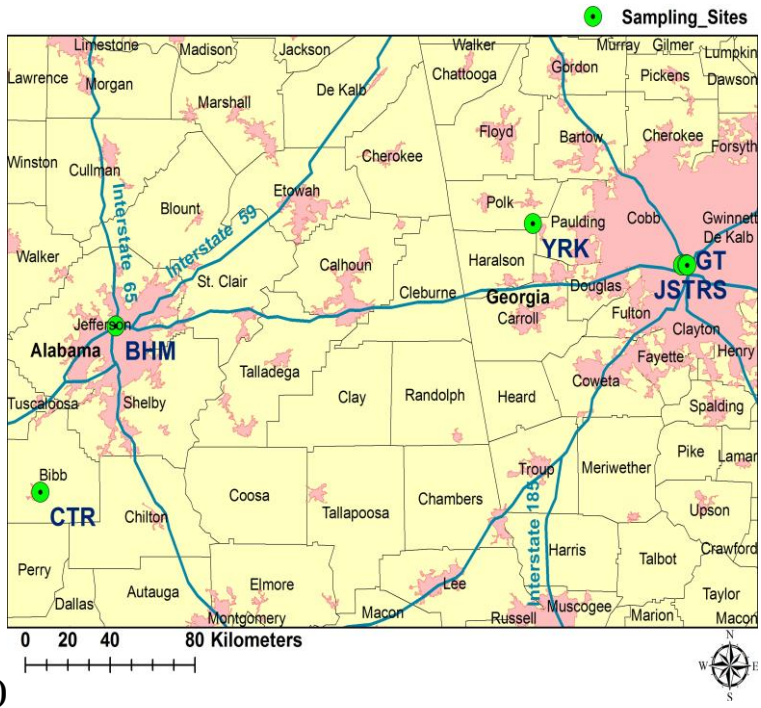

(a)

(b)

Figure 2-10 Map of sampling sites (a) and a picture of trailer at Yorkville (b)

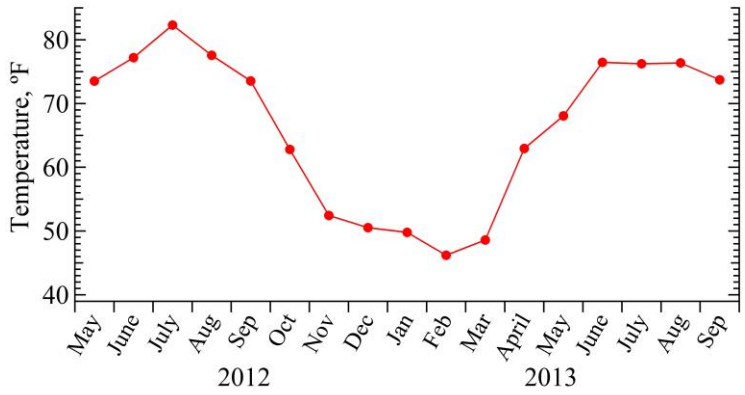

Figure 2-11 Temperature profile from May 2012 to September 2013 in Atlanta, GA

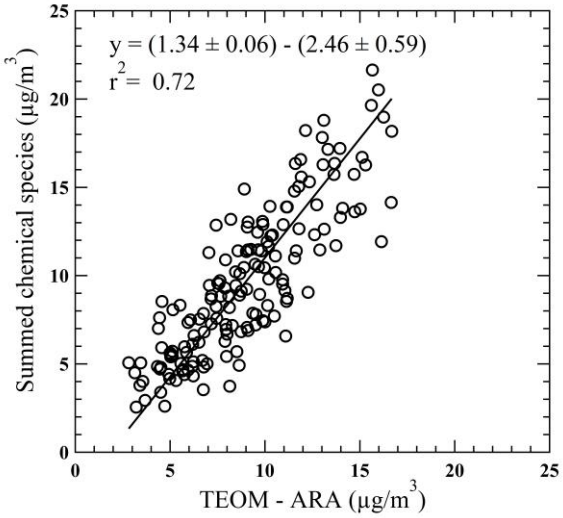

Figure 2-12 Comparison of estimated $PM_{2.5}$ concentration from the sum of components determined from the High Volume filters, which included: EC, organic mass (OC*1.6), ammonium sulfate and water soluble metals concentration with the $PM_{2.5}$ measured by TEOM from Atmospheric Research Analysis data archive at the SEARCH JST site. EC/OC - Sunset Laboratory TOT analyzer; water soluble metals - X-ray fluorescence instrument, XRF, Xact™ 625 Monitoring System; $[(NH_4)_2SO_4] = \frac{MW_{(NH_4)_2SO_4}}{MW_S} \times$ [S], assuming sulfate and ammonium are all $(NH_4)_2SO_4$ and [S] (sulfur) were obtained from XRF metals analysis. (The equation was obtained by orthogonal regression.)

CHAPTER 3. WATER-SOLUBLE ELEMENTS IN THE SOUTHEASTERN UNITED STATES: AUTOMATED ANALYTICAL METHOD DEVELOPMENT, SPATIOTEMPORAL DISTRIBUTIONS, SOURCE APPORTIONMENT, AND IMPLICATIONS FOR HEATH STUDIES

Ting Fang
Hongyu Guo
Vishal Verma
Richard E. Peltier
Rodney J. Weber

Atmos. Chem. Phys., 15, 11667–11682, 2015
doi:10.5194/acp-15-11667-2015

3.1 Abstract

Water-soluble redox-active metals are potentially toxic due to the ability to catalytically generate reactive oxygen species (ROS) *in vivo*, leading to oxidative stress. As part of the Southeastern Center for Air Pollution and Epidemiology (SCAPE), we developed a method to quantify water-soluble elements, including redox-active metals, from a large number of filter samples (N = 530) in support of the Center's health studies. $PM_{2.5}$ samples were collected during 2012-2013 at various sites (three urban, two rural, a near-road, and a road-side site) in the Southeastern United States, using high-volume samplers. Water-soluble elements (S, K, Ca, Ti, Mn, Fe, Cu, Zn, As, Se, Br, Sr, Ba, and Pb) were determined by extracting filters in deionized water and re-aerosolized for analyses by X-ray fluorescence (XRF) using an online aerosol element analyzer (Xact, Cooper Environmental). Concentrations ranged from detection limits (nominally 0.1 to 30 ng/m^3) to 1.2 $\mu g/m^3$, with S as the most abundant element, followed by Ca, K, Fe, Cu, Zn, and Ba. Positive Matrix Factorization (PMF) identified four factors that were associated with specific sources based on relative loadings of various tracers. These include brake/tire wear (with tracers Ba and Cu); biomass burning (K); secondary formation (S, Se, and WSOC); and mineral dust (Ca). Of the four potentially toxic and relatively abundant metals (redox active Cu, Mn, Fe, and redox-inactive Zn), 51% of Cu, 32% of Fe, 17% of Mn, and 45% of Zn, were associated with the brake/tire factor. Mn was mostly associated with the mineral dust factor (45%). Zn was found in a mixture of factors, with 26% associated with mineral dust, 14% biomass burning, and 13% secondary formation. Roughly 50% of Fe and 40% of Cu was apportioned to the secondary formation factor, likely through increases in the soluble fraction of these elements by sulfur-driven aerosol water and acidity. Linkages between

sulfate and water-soluble Fe and Cu may account for some of the past observed associations between sulfate/sulfur oxide and health outcomes. For Cu, Mn, Fe, and Zn, only Fe was correlated with $PM_{2.5}$ mass (r = 0.73-0.80). Overall, mobile source emissions generated through mechanical processes (re-entrained road dust, tire and break wear) and processing by secondary sulfate were major contributors to water-soluble metals known to be capable of generating ROS.

3.2 Introduction

Many fine particle ($PM_{2.5}$) chemical components have been reported as potential contributors to particle toxicity that can lead to various adverse health endpoints, including secondary sulfates (Atkinson et al., 2010; Maynard et al., 2007; Pope et al., 2002), elemental carbon (Kleinman et al., 2007; Brunekreef et al., 1997), metals (Gasser et al., 2009; Burchiel et al., 2005; Pope et al., 2002; Burnett et al., 2000), organic carbon (Kleinman et al., 2007; Nel et al., 2001), semi-volatile organic species (Seagrave et al., 2005; Seagrave et al., 2002), and polycyclic aromatic hydrocarbons (PAHs) (Lundstedt et al., 2007; Burchiel et al., 2005). Identifying the components of aerosols that are responsible for health effects provides a means for effective air quality mitigation by controlling specific sources.

Metals are known to exert pro-oxidant and pro-inflammatory effect in the respiratory system (Cho et al., 2011; Li et al., 2010), and the water-soluble fraction of metals are of special interest as they are more bioavailable (Heal et al., 2005; Shi et al., 2003) and may have higher risk potential. For example, a study with concentrated ambient particles (CAPS) associated inflammatory endpoints (pulmonary and hematological responses) to

water-soluble Fe/Se/S and Cu/Zn/V factors (Huang et al., 2003). Another CAPS study found that the plasma fibrinogen levels (a coronary risk indicator) in spontaneously hypertensive rats were better correlated with water-soluble metals (especially Zn) than total PM mass (Kodavanti et al., 2005). $PM_{2.5}$ water-soluble metals were found to be significantly associated with small reductions in birth weight (Darrow et al., 2011) and daily preterm birth rates (Darrow et al., 2009) in an Atlanta, GA, study.

Water-soluble transition metals toxicity may be due to their ability to generate free radicals, for example, via redox cycling with biological reductants (Chevion, 1988; Stohs and Bagchi, 1995). Transition metals have varying oxidation states, thus metals, especially Fe and Cu, can act as a catalyst for the reactions, e.g. Fenton reaction that converts hydrogen peroxide to the more toxic hydroxyl radicals (Liochev and Fridovich, 2002; Stohs and Bagchi, 1995). Metal-mediated formation of free radicals may lead to DNA modifications, enhanced lipid peroxidation, and altered calcium and sulfhydryl homeostasis (Valko et al., 2005). Water-soluble transition metals have been identified as the potential contributors to reactive oxygen species (ROS) production by different ROS probes such as the DTT (dithiothreitol) (Charrier and Anastasio, 2012), AA (Ascorbate Acid) (Strak et al., 2012; Fang et al., 2016), and macrophage (Saffari et al., 2014b; Verma et al., 2010) assays.

Since most metals in PM have low' solubilities (e.g., Zn ~50%; Cu and Mn 10-40%; Fe <10%) (Birmili et al., 2006; Espinosa et al., 2002), total element concentrations may not represent the roles of redox-active metals' potential effects on human health. The objective of this work, within the framework of the Southeastern Center for Air Pollution & Epidemiology (SCAPE) study, was to provide a reliable measurement of $PM_{2.5}$ water-soluble element concentrations from filter samples collected at seven sites in the

Southeastern U.S. that represent different degrees of anthropogenic and traffic influence. A cost-effective and automated method was required since over 500 filters were available for analyses. The resulting unique large and comprehensive dataset allowed for robust statistical analyses and has informed studies on particle ROS-generating activities based on the DTT (Verma et al., 2015a; Verma et al., 2014) and AA assays (Fang et al., 2016). The data have provided new insights into the health effects of particulate water-soluble metals. This work focuses on a description of the measurement techniques, discussion on the spatiotemporal distribution, and source apportionment of water-soluble elements, with a specific focus on four important health-related water-soluble metals (Fe, Cu, Mn, and Zn).

3.3 Methods

The present work involves measuring water-soluble elements from filter extracts by re-aerosolizing the extract and sampling with an online X-ray fluorescence (XRF) instrument. The ambient mass concentrations of the following water-soluble elements were quantified: S (Sulfur), Ca (Calcium), K (Potassium), Fe (Iron), Cu (Copper), Zn (Zinc), Ba (Barium), Pb (Lead), As (Arsenic), Sr (Strontium), Se (Selenium), Br (Bromine), Mn (Manganese), and Ti (Titanium). S is also included in the discussion since it is a source indicator for secondary processing.

3.3.1 Sampling sites and filter preparation

3.3.1.1 Sampling sites

As part of the SCAPE study, 23-h integrated $PM_{2.5}$ samples were collected on pre-baked (max temperature: 550 °C, time ramp: 3.5 h) quartz filters (Pallflex® Tissuquartz™, 8 × 10 inches) from noon to 11am the following day with high-volume samplers (Hi-Vol) (Thermo Anderson, flow rate normally 1.13 m^3 min^{-1}) in Atlanta, GA, Birmingham and Centerville, AL, and East St. Louis, IL. The sites were:

1) Jefferson Street, GA (JST), a central site representative of the Atlanta urban environment, also a stationary site in this study where one Hi-Vol sampler was operated for most of the study period;
2) Yorkville, GA (YRK), a rural environment, situated in an agricultural region located approximately 70 km west of JST;
3) Roadside, GA (RS), adjacent to an interstate highway (I75/85) in midtown Atlanta;
4) Georgia Tech, GA (GT), a rooftop site on Georgia Tech campus, roughly 30 m above ground level, 840 m from the RS site, providing an intermediate location between RS and the central urban site (JST);
5) Birmingham, AL (BHM), an urban site within a few kilometers of significant transportation and industrial sources;
6) Centerville, AL (CTR), the rural pair of BHM, surrounded by forests and a lightly traveled rural road;
7) East St. Louis, IL (Sauvain et al., 2008), an urban residential/light commercial area approximately 3 km east of the central business district of St. Louis, MO.

JST, YRK, BHM, and CTR are all part of the Southeastern Aerosol Research and Characterization Study (SEARCH) network sites (Hansen et al., 2003). The sampling

approach involved paired simultaneous measurements: one high-volume sampler always at JST and the other sampler moved among RS, GT and YRK on a monthly basis, during different seasons. Paired sampling at BHM and CTR was also undertaken for a month and coincided with the Southern Oxidant and Aerosol Study (SOAS). Detailed sampling schedule and map can be found in the section 3.6 (Table 3-2 & Figure 3-9). Samples were collected from June 2012 to September 2013. In November 2012, two Hi-Vol samplers were co-located at JST for side-by-side comparisons. A total of 530 filters were collected as part of the study. In all cases, collected filter samples were immediately wrapped in prebaked aluminum foil and stored at -18 °C until analyzed.

3.3.1.2 Filter preparation

Four punches of the Hi-Vol filter (5.07 cm^2 each) were extracted in 15 mL of deionized (DI) water (> 18 MΩ cm^{-1}) in a sterile polypropylene centrifuge tube (VWR International LLC, Suwanee, GA, USA) by sonication (Ultrasonic Cleanser, VWR International LLC, West Chester, PA, USA) for half an hour. Extracts were then filtered using PTFE 0.45 µm syringe filters (Fisherbrand™) to remove insoluble material. 120 µL of high purity HNO_3 (OmniTrace® Ultra Nitric Acid, 67 - 70%, EMD Millipore Corporation, Billerica, MA, USA) was then added to 6 mL of the extract (resulting pH ≈ 0.7) to ensure the suspension of all dissolved metals, and were then transferred to a 5 mL DIONEX auto-sampler vial (PolyVial™, Thermo Scientific). Some insoluble elements that are smaller than 0.45 µm diameter can be included in the water-soluble fractions defined by this method. It is also noted that water-soluble element concentrations are operationally defined by the extraction method, and may differ from how elements are dissolved *in vivo*.

3.3.2 Methods for measuring water-soluble element concentration

A Xact^{TM} 625 automated multi-metals monitor (Cooper Environmental, OR, USA) was used to measure the concentration of elements in the liquid samples. The Xact collects particles on a reel-to-reel (RTR) Teflon filter tape, sampling at 16.7 L min^{-1} for a user selected time interval (30 minutes in this case), resulting in a concentrated PM spot on the tape. After the preset sampling interval, the tape is automatically advanced, positioning the PM spot for nondestructive X-ray fluorescence (XRF) analyses to quantify the mass of multiple elements. At the same time, the next sampling is initiated on a fresh tape spot. XRF response is calibrated using a series of metal film standards on B36 mount nucleopore membranes (Nano XRF, Fort Worth, TX, USA), including appropriate interference element analytes. With each sample, the Xact also includes a measurement of pure palladium as an internal standard to automatically adjust the detector energy gain.

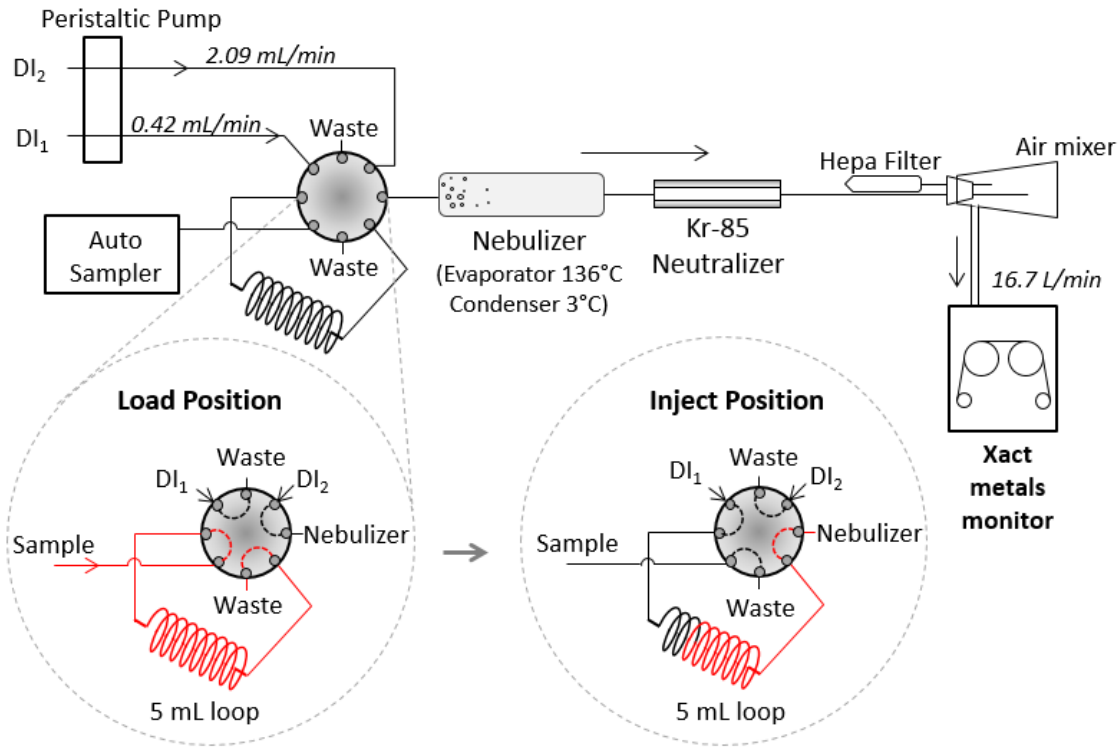

Figure 3-1 Schematic of the automated system developed to measure elements in the water-soluble aerosol extracts using an online XRF element analyzer (Xact™ 625).

To introduce water-soluble metals from filter extracts in Xact, a computer-controlled auto-sampling system was set up using a Dionex autosampler, a multiport injection valve and a continuous flow nebulizer so that sampling and analysis could be performed continuously, except during daily automated quality assurance checks (~1 hour). A schematic diagram of the overall system is shown in Figure 3-1. At "Load" position, liquid sample (at least 6 mL) was loaded by a DIONEX automated sampler (AS40, DIONEX Corporation, Sunnyvale, CA, USA) through a SelectPro two-position fluid processor valve (Alltech, Deerfield, IL, USA) to a 5 mL PEEK sample loop (Upchurch Scientific, Inc., Oak Harbor, WA). After 2.5 minutes, at which point the sample loop had been completely filled with

extract liquid from the Dionex autosampler, the valve was switched to the "Inject" position and all 5 mL of sample injected to an ultrasonic nebulizer (CETAC U5000 AT+, CETAC Technologies, Omaha, NE, USA) via a carrier DI flow of 0.42 mL min^{-1} (DI_1, Fig.1) propelled by a peristaltic pump (Ismatec, Cole-Parmer Instrument Company, Vernon Hills, IL, USA). In the continuous flow ultrasonic nebulizer, liquid sample was converted to a fine aerosol spray and directed by filtered carrier room air of 1.62 L min^{-1} through an evaporator at 136 °C followed by a condenser at 3°C. The dry aerosolized sample was neutralized by a Kr-85 (Model 3077A, TSI) ion source and then mixed with clean filtered (Pall HEPA Capsule) make-up air drawn into the Xact and through the filter tape by the Xact's flow control system. After 14 minutes, at which point all sample in the sample loop had been transferred to the Xact filter tape, the system switched to "Load" position again, and DI water with HNO_3 (final concentration = 2%) was loaded onto the sample loop (2.5 min), after which the system switched to "Inject" position again, and the 2% HNO_3 was directed to the nebulizer and the Xact. This cycle was performed to wash off any metal residuals in the liquid system. After 11 minutes, the filter tape was automatically advanced to a position where total mass for each element from the sample was measured by XRF analysis. At the same time, the system repeated the process for measuring the next sample (i.e., load sample-inject sample-load 2% HNO_3-inject 2% HNO_3, 2.5min-14min-2.5min-11min cycle). To further ensure no carry-over between samples, a faster DI flow (DI_2, 2.09 mL min^{-1}, Figure 3-1) was used for flushing while the SelectPro valve was at the "Load" position. Inserting 2% HNO_3 between samples was found to be an effective method to eliminate carry-over between samples (Figure 3-10).

The final ambient concentration of each element was calculated as follows:

$$C_a = \frac{(C_{sample}V_{sample} - C_{blank}V_{blank})}{m} \times \frac{15mL \frac{A_{filter}}{A_{punches}}}{5mL \times Q\ t}$$ **(Equation 4),**

where C_a is the specific element ambient concentration (ng m^{-3}); C_{sample} (C_{blank}) and V_{sample} (V_{blank}) are the concentration of element (ng m^{-3}) and volume of air (m^3) drawn through the filter tape for sample (blank), respectively, both reported by the XRF in the 30-min sampling time. 15 mL is the volume of DI water used for the filter extraction and 5 mL is the sample liquid volume loaded to the Xact. A_{filter} is the total particle collection area of the Hi-Vol filter (m^2) and $A_{punches}$ is the area used for this analysis (m^2). Q is the Hi-Vol sampling flow rate (~1.13 m^3 min^{-1}) and t is the sampling duration (min). m is the calibration factor determined by multiple external element standard solutions, discussed below (section 3.3.3).

A similar automated system with the DIONEX sampler, SelectPro valve, and a peristaltic pump was also used to measure water-soluble organic carbon (WSOC) on the extracts from the same Hi-vol filters. Filter extracts (~6mL) that had been loaded into a 5 mL sample loop, were first passed through a 1 m Liquid Wave-guide Capillary Cell (LWCC-M-100; World Precision Instruments, Inc., FL, USA), where absorbance at 365 nm wavelength (BrC) was measured (not included in this work). The extracts then entered a TOC analyzer (Sievers Model 900, GE Analytical Instruments, Boulder, CO, USA) for determining WSOC concentration (Sullivan et al., 2006).

3.3.3 Calibration

Multiple element-ion standard stock solutions [$(NH_4)_2SO_4$, $CaCl_2$, $(NH_4)_2Fe(SO_4)_2$, $CuSO_4$, $ZnCl_2$, and $MnCl_2$] were prepared by dissolving powders in DI water with HNO_3 (2% final concentration) and stored in a refrigerator (T = 4°C). $CuSO_4$ and $(NH_4)_2Fe(SO_4)_2$

were obtained from Sigma-Aldrich; $CaCl_2$, $MnCl_2$, and $ZnCl_2$ were obtained from Alfa Aesar; $(NH_4)_2SO_4$ was from Fisher Scientific. Final standard solutions were diluted from stock (20-200 times dilution), 2% HNO_3 added, transferred to DIONEX vials, and ran through the same system as described above.

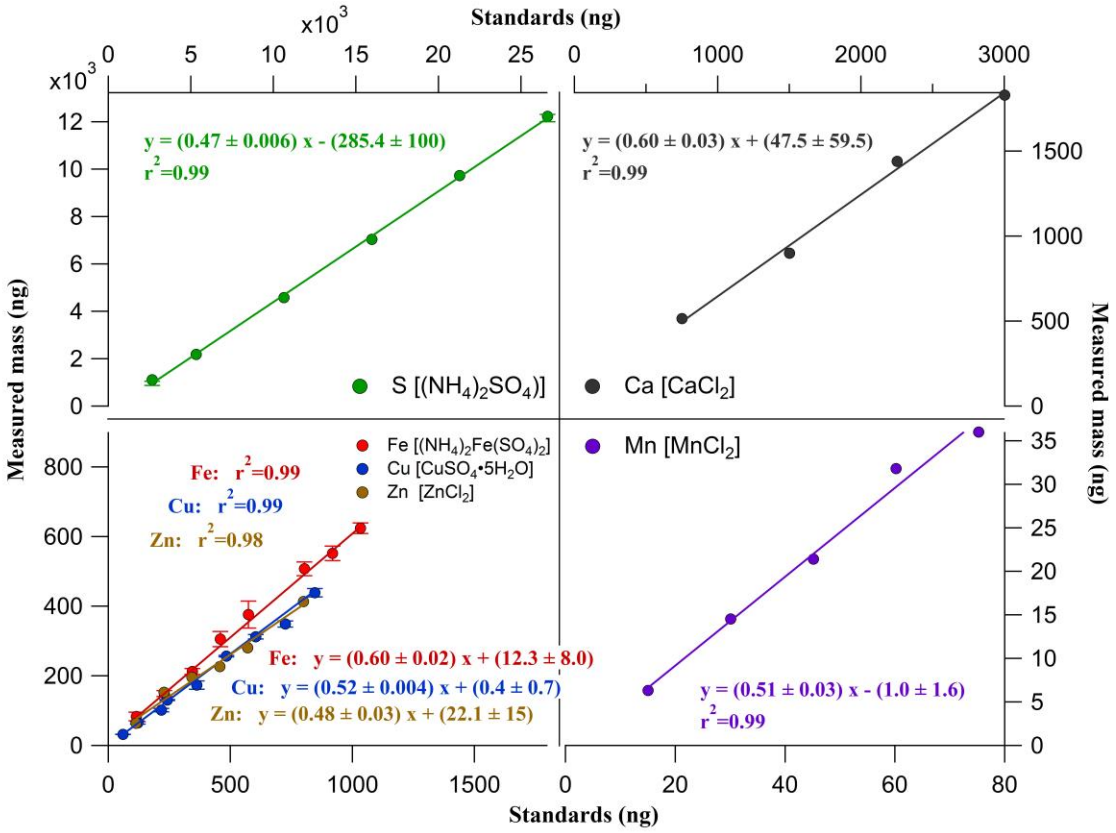

Figure 3-2 System calibration based on multiple element-ion standard solutions. Error bars represent the standard deviation of three replicates. Slopes and intercepts are based on orthogonal regression with errors as one standard deviation.

Figure 3-2 shows the system calibration using serial dilutions of multiple element-ion standards. Linear regression yielded r^2 larger than 0.98 for all cases and similar slopes

(0.47-0.60), indicating that the nebulizer efficiency and other losses in the system were not dependent on the specific element. Slopes from measured mass versus calculated mass of element-ion standard solutions for all standards were averaged and used as the calibration factor (m= 0.53 ± 0.05 in Eq. 4) to interpret all elements in samples. The intercepts were not included in the final ambient concentration calculation (Eq. 4) since the intercept of the sample and blank cancel out after blank subtraction. The standards were made in the range of typical sample concentrations and the intercepts were negligible (<2% of typical ambient levels). One standard ion solution was measured for every five filter samples and the coefficients of variation [CV, calculated as standard deviation (σ) /mean, %] were less than 10% throughout the analyses of all filters, indicating that the system was capable of stable and reproducible operation.

3.3.4 Blanks, LOD, and uncertainties

The limits of detection (LOD) based on blank levels obtained from Hi-Vol filter blanks (N>40), and various uncertainties, as well as overall uncertainties for all elements, are given in Table 3-1. The concentration of blanks was calculated using Eq.4 assuming 23-h sampling at 1.13 m^3 min^{-1} and LOD was determined by three times the standard deviations of blanks. Values below LOD for S, K, Ca, Ti, Mn, Fe, Cu, Zn, As, Se, Br, Sr, Ba, and Pb were assigned as half of LOD values in all the statistical analyses below. Other elements detected by the Xact, such as Sc (Scandium), V (Vanadium), Cr (Chromium), Co (Cobalt), Ni (Nickel), Ge (Germanium), Rb (Rubidium), Ag (Silver), Cd (Cadmium), and Hg (Mercury), for which >50% of aerosol samples were below the detection limits, are not included in the table or subsequent discussion. Calculation of uncertainties is discussed in

section 3.3.5. For most elements, overall uncertainties are less than 20%. Ti, Sr, and Cu have the highest uncertainties of 28%, 25%, and 25%, respectively.

3.3.5 Source apportionment

A source apportionment analysis was performed with Positive Matrix Factorization (PMF) (Paatero and Tapper, 1994) using EPA PMF 5.0 software. PMF analysis was applied on the combined data from JST (summer, fall, winter 2012, and spring 2013), GT (fall, winter 2012, and fall 2013), and RS (winter 2013 and fall 2013) (total N=299). Although the road-side site generally has higher levels of metals than the urban site (JST) and near-road site (GT) (discussed in section 3.4.2.2), merging RS data with JST and GT in the analysis did not alter the PMF solutions substantially (factor profiles and source contributions), but the larger number of input data resulted in a more robust PMF solution. 14 elements (S, K, Ca, Ti, Mn, Fe, Cu, Zn, As, Se, Br, Sr, Ba, and Pb) and WSOC were run in the model with Ti and As categorized as weak species (low S/N signals). The concentrations, together with the uncertainties, were used as the input for PMF runs. Missing data were replaced by species median with 400% uncertainty and values below LOD were assigned as half of LOD values with uncertainties of 5/6 the concentration (Polissar et al., 1998). For other data, uncertainties for each species were determined by multiplying the concentration by overall uncertainties (%). Overall uncertainty was calculated from the sum of the square of various uncertainties including filter sampling (5%), extraction (5%), blanks (1 σ of multiple blanks, 2-15% depending on species), calibration (1 σ of the slope, 10%), and analytical uncertainty. The analytical uncertainty for elements was obtained by analyzing the same sample, a composite of extracts from 11 selected road-side samples 20 times and calculating the coefficient of variation (CV, %). The measured uncertainty for each

element, based on two side-by-side Hi-Vol samplers at JST, was also included in the overall uncertainty. This was done because the calculated uncertainties for some elements (e.g., Cu and Sr) are much smaller than the measured uncertainties from collocated measurements (Table 3-1). By combining two uncertainties, the uncertainties for all elements are slightly overestimating. Uncertainty from collocated measurements was calculated as the relative uncertainty of the slope (1 σ/slope), which was based on an orthogonal regression (discussed below, see Figure 3-4). Both uncertainties and the combined overall uncertainties for each element are given in Table 3-1. The PMF model was executed with 3-8 factors. Based on minimized Q values and physical interpretation of the solutions, a 4-factor solution was found to be optimal. Details on determining the optimal factor and bootstrapping results can be found in the Appendix A.2.

Table 3-1. Limits of detection (LOD), blanks (N>40) and uncertainties for all water-soluble elements

Element	LOD, ng/m^3	Blank, ng/m^3	Analytical uncertainty, %	Sum of square of various uncertainties, %	Uncertainty from collocated measurements, %	Overall uncertainty, %
Sulfur (S)	6.19	6.64	2.19	7.77	2.38	8.13
Potassium (K)	16.45	11.80	2.47	9.89	6.06	11.63
Calcium (Ca)	29.64	32.23	2.38	10.46	11.76	15.87
Titanium (Ti)	0.09	0.06	15.79	21.08	18.68	28.22
Manganese (Mn)	0.11	0.06	3.57	8.54	6.49	10.74
Iron (Fe)	3.11	1.54	12.59	13.94	14.06	19.83
Copper (Cu)	0.91	0.70	2.37	8.57	23.85	25.38
Zinc (Zn)	1.87	1.89	4.56	9.90	8.24	12.90
Selenium (Se)	0.02	0.01	8.94	12.17	7.79	14.46
Bromine (Br)	0.03	0.02	3.93	8.50	4.49	9.62
Strontium (Sr)	0.11	0.08	3.57	9.63	23.53	25.46
Barium (Ba)	1.13	0.37	3.29	10.59	14.08	17.73
Arsenic (As)	-	0	6.97	10.17	3.53	10.77
Lead (Pb)	0.14	0.12	7.45	11.77	1.32	11.85

3.4 Results and Discussions

3.4.1 Comparison with ion chromatography (IC)

As a further test of the system, sulfate concentrations were determined on a subset of the Hi-Vol filter samples by ion chromatography and compared to the elemental analysis of sulfur. 200 filters that included samples from JST and GT were extracted in DI water (same procedure discussed in section Sampling sites and filter preparation, but without adding HNO_3 in the extracts) and inorganic sulfate (IC-sulfate) was measured by an ion chromatography (IC, DX500 with UTAC-ULP1 concentrator column, AG11 guard column, and AS11 anion column, DIONEX, CA). IC-sulfate was then divided by 3 to convert to sulfur mass (molar mass of sulfate and sulfur are 96 and 32 g/mol, respectively) and directly compared to XRF-sulfur. Orthogonal regression shows good quantitative agreement and correlation coefficient (r^2) of 0.96 (Figure 3-3). The discrepancy between sulfur measured by XRF and IC (slope of IC-sulfur vs XRF-sulfur = 0.79 ± 0.01) may be attributed to roughly 20% contributions from additional sulfur species, such as organosulfates that are not detected by the IC. Lower sulfur measured by IC versus XRF has also been observed in other studies (Shakya and Peltier, 2015; Tolocka and Turpin, 2012; He et al., 2001). However, Hidy et al (2014) found no statistical evidence for organosulfates in the Southeast by this difference method.

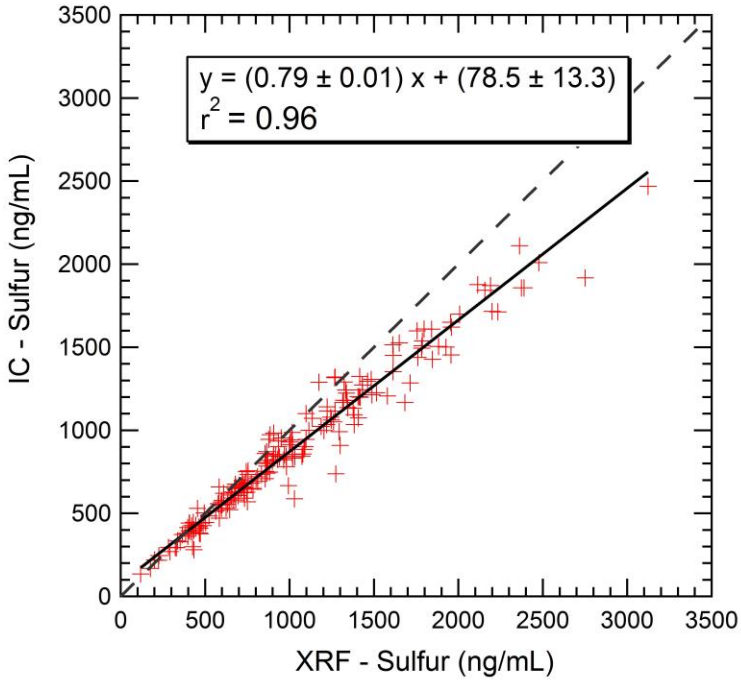

Figure 3-3 Sulfur measured by XRF and 1/3 of sulfate measured by IC (results of orthogonal regression are shown, along with 1:1 ratio by a dotted line).

3.4.2 Water-soluble elements

3.4.2.1 Inter-comparisons of two collocated Hi-Vols

Inter-comparisons of elements from two collocated Hi-Vol samplers (N=11) at JST in November 2012 are shown in Figure 3-4, and results included in Table 3-1. Orthogonal regressions resulted in strong correlations for most elements (r^2 = 0.73-0.99) with moderate correlations for Cu (r^2 = 0.57) and Sr (r^2 = 0.61). The slopes show percentage differences (1-slope) are 1-10% for Cu, K, and Ti, 11-20% for S, Zn, Ca, Br, As, and Sr, and 20-36% for Pb, Mn, Se, Fe, and Ba. Overall, the two Hi-Vols show good agreement for measuring

water-soluble elements, considering the uncertainties from sampling, filter preparations, and extractions. The uncertainties in slope (1 σ) were used in calculating the overall uncertainties (section 3.3.3). The intercepts were relatively small and thus ignored.

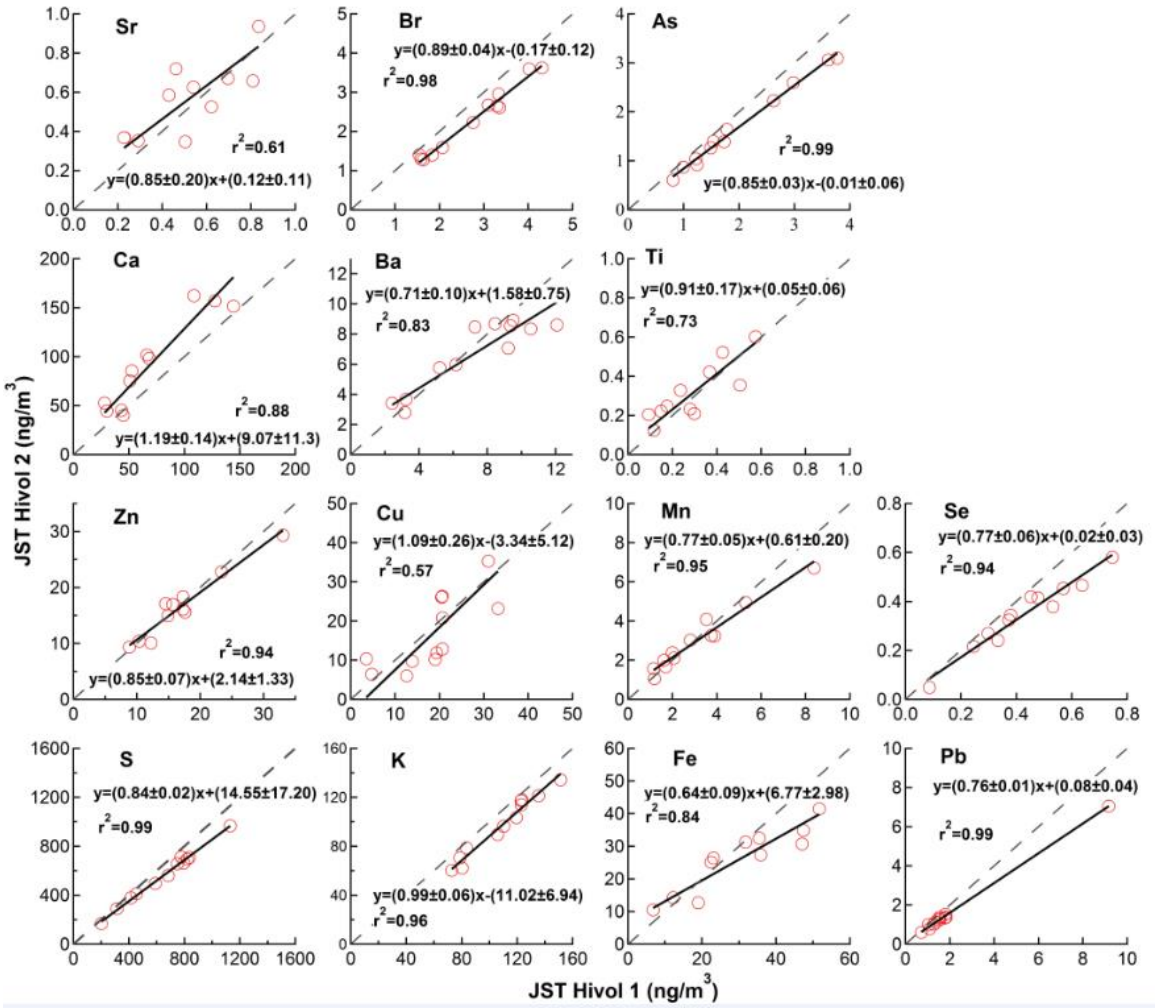

Figure 3-4 Precision from collocated measurements assessed by filter samples (N = 11) collected simultaneously using two Hi-Vol samplers deployed at JST during November 2012 (Analysis was done by orthogonal regression. The dotted line is 1:1).

3.4.2.2 Spatial and temporal trends

Monthly average concentrations of water-soluble elements and WSOC at various sampling sites are given in Figure 3-5 and section 3.6 Figure 3-12, respectively. Three seasons (summer, fall, and winter) were grouped based on the temperature profiles in 2012 and 2013, consistent with our previous work (Fang et al., 2015b; Verma et al., 2014). As seen from Figure 3-5, mass concentrations of water-soluble elements span a wide range, from 0.1 ng/m^3 to 1.2 μg/m^3. S is the most abundant water-soluble element of the group measured, comprising 71 ± 14 % of the total measured element mass. Ca, K, Fe, Cu, Zn, and Ba follow with average (± 1 σ) fractions of 16 (± 12) %, 8 (± 5) %, 1.8 (± 1.3) %, 1.4 (± 2.1) %, 1.4 (± 1.4) %, and 0.5 (± 0.6) %.

Seasonal variability of all elements can be examined from the Atlanta urban sites (JST, GT, and RS). Besides S, commonly found to have a higher concentration in summer due to the higher SO_2 oxidation rates in warm seasons (Hidy et al., 2014), most of the water-soluble elements also had higher concentrations in summer/fall, such as Ca, Fe, Cu, Mn, Sr, and Se. The seasonal variability of these elements may be explained by different causes. Elevated concentration of some elements (Ca, Mn, and Sr) may be attributed to drier conditions in summer favoring the re-suspension of mineral dust; Cu and Fe may be related to secondary formation (discussed in the source apportionment in Sect. 3.4.2.3);and Se is likely due to its coal combustion origins (Bell et al., 2007), thus following a similar trend as S. In contrast, K can be associated with both biomass burning and mineral dust (Zhang et al., 2010; Hueglin et al., 2005) (discussed below &Figure 3-11) and has less seasonal variability, with only slightly higher concentrations in winter due to more biomass burning

during that period. Other metals (Zn, Ba, Br, Pb, Ti, and As) do not exhibit apparent seasonal trends.

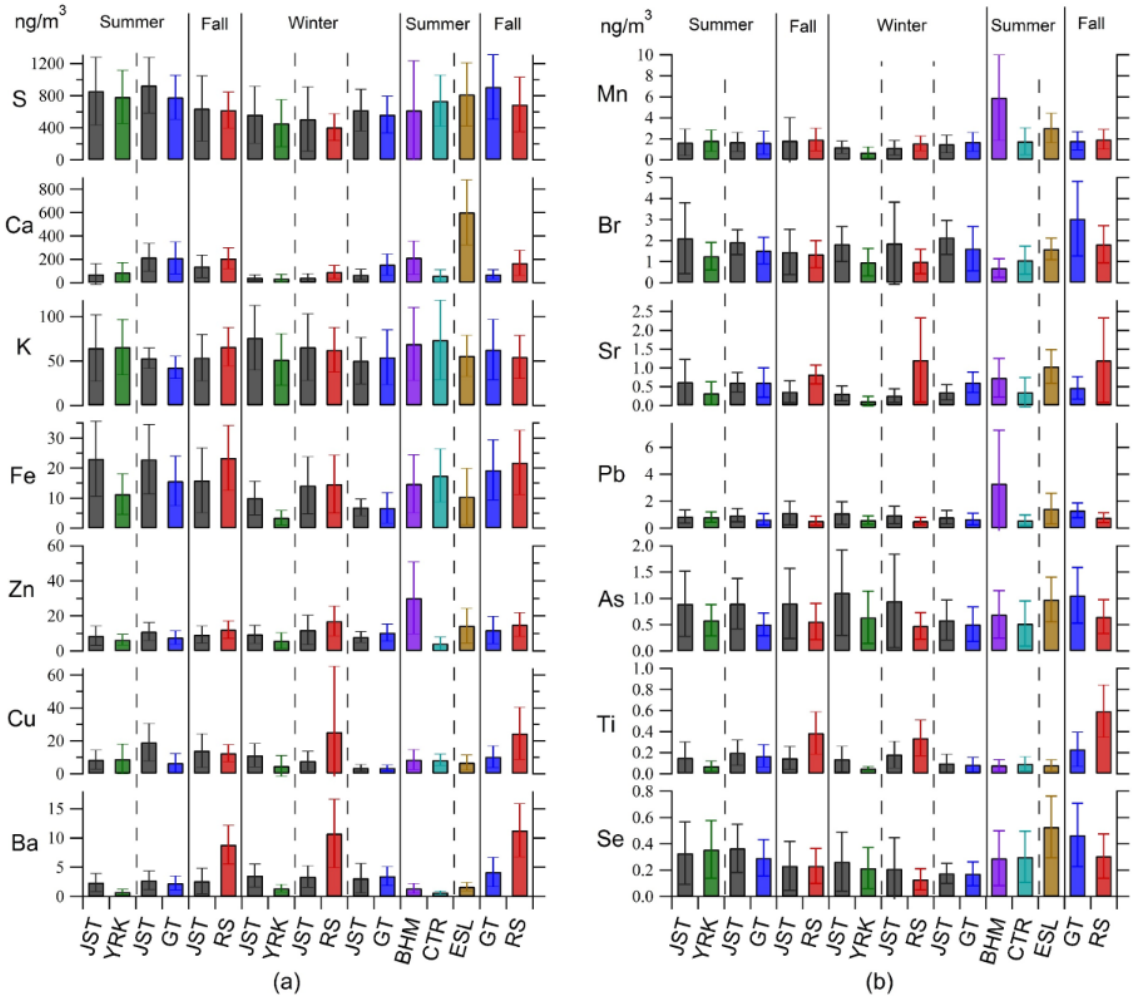

Figure 3-5 Monthly mean (± standard deviation) of water-soluble elements ambient concentration (ng m^{-3}) at various sampling sites. Seasons are separated by solid lines and simultaneous sampling at paired sites are separated by dashed lines (urban – JST, BHM, ESL; rural – YRK, CTR; near-road – GT; road-side – RS).

Spatial variability of water-soluble elements is important in assessing human exposure, within/across cities, for epidemiological studies, and provides insights on sources. The BHM site has a high ambient concentration of most water-soluble metals, such as Mn, Zn, and Pb, with respect to other sites, pointing to industrial sources for these metals in this urban environment. The ratio of averaged Mn, Zn, and Pb at BHM to its paired rural site CTR, is 3.3, 7.0, and 5.7, respectively. ESL, an urban site also strongly impacted by numerous industrial sources (Bae et al., 2006), has the highest Ca and Se concentrations among all sites, and higher Mn and Pb than all Atlanta sites (JST, GT, RS, and YRK). Among the four sites in Atlanta, there was a distinct relationship between the concentration of water-soluble elements and distance to traffic sources. Generally, the road-side (RS) site had much higher element concentrations relative to the rural YRK site, which had notably low concentrations of Cu, Ba, Sr and Ti. For example, the ratio of averaged Cu, Ba, Sr and Ti at RS to its paired Atlanta urban JST site, is 0.9, 3.4, 2.2 and 2.6 in fall and 3.3, 3.1, 4.6 and 1.9 in winter, respectively. Comparing RS to the near-road GT site, ratios are 2.2, 2.7, 2.5 and 2.6 in fall for Cu, Ba, and Ti. Concentrations at YRK were typically much lower than the paired JST urban site, both in summer (ratio of average concentration YRK/JST = 1.1, 0.3, 0.5 and 0.5) and winter (0.4, 0.4, 0.4 and 0.3) for Cu, Ba, Sr, and Ti, respectively.

To further explore the spatial heterogeneity of water-soluble elements in Atlanta and the surrounding region, the coefficient of divergence (COD) (Wilson et al., 2005) and correlation coefficient (Pearson's r) were calculated for each paired site for all elements. A COD close to 0 represents a homogenous distribution, and near 1 indicates heterogeneity. Both are summarized in Table 3-3, and r values are shown in Figure 3-6. The COD and correlation coefficient (r) for WSOC were also included in Table 3-3.

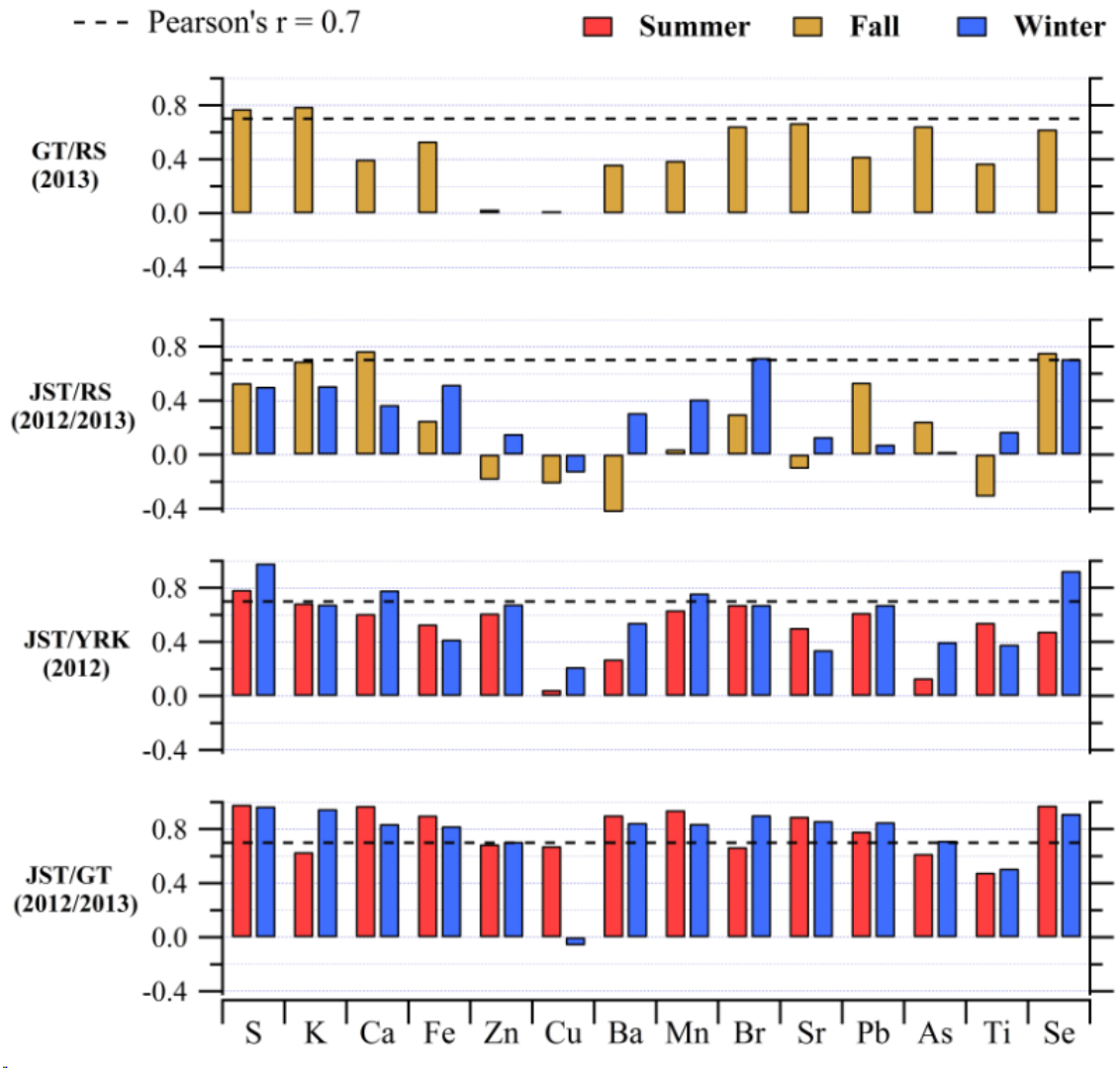

Figure 3-6 Correlations (Pearson's r) between paired sites for various water-soluble elements in Georgia (JST, RS, GT, and YRK).

JST and GT are in close proximity. These two sites had the most similar concentrations for many water-soluble elements, with r ranging from 0.71-0.98 and relatively low CODs (0.06-0.20), except for Cu and Ti. In summer Cu measured at JST and GT have a moderate correlation (r = 0.68) but high COD (0.52), with much higher concentration at JST (mean

= 19.1 ng/m^3, median = 18.5 ng/m^3) than GT (mean = 6.6 ng/m^3, median = 5.1 ng/m^3). In winter, although the average values are similar (3.7 and 3.6 ng/m^3 for JST and GT, respectively), there is no correlation (r = -0.06) and COD is fairly high (0.35). Ti between the two sites has low correlations (r = 0.48 in summer and 0.51 in winter) and high COD (0.38 and 0.36 in summer and winter, respectively).

For the urban/rural (JST/YRK) pair, S, K, Ca, Mn, and Se tended to co-vary and have similar concentrations at the urban and rural sites, pointing to a more regional characteristic (sources) for these elements. The other elements did not co-vary at these two sites and are generally higher at the urban site (JST).

Comparison of the road-side site (RS) to the representative urban site (JST) provides insights into which elements are associated with traffic emissions and how they vary with season. S and K were not correlated well between JST and RS in both fall and winter, suggesting the presence of other local sources for S and K at the RS site, for example, re-suspended dust (Minguillón et al., 2014; Hueglin et al., 2005). For Cu, Ba, Sr, and Ti, the high COD (>0.4), low r values (r < 0.3) between various paired sites, and their concentrations highest at RS, are all indicators of emissions associated with traffic as a dominant source (Figure 3-5).

3.4.2.3 Source apportionment

Positive Matrix Factorization was applied to the combined data from JST, GT, and RS (total N = 299), and four factors were resolved. They are labeled brake/tire wear, biomass burning, secondary formation, and mineral dust, based on the loading of specific elements identified as various source tracers. Note, metals as source tracers are typically based on

total metals, whereas here we are using the measured water-soluble concentrations. Factor profiles and time series plots (from the JST site) are shown in Figure 3-7(a) and (b), respectively. The percentage contribution of the various factors (sources) to the four important health-related metals (Cu, Fe, Zn, and Mn) is shown in Figure 3-8. Breakdown of sources for the other water-soluble elements and WSOC can be found in Figure 3-11.

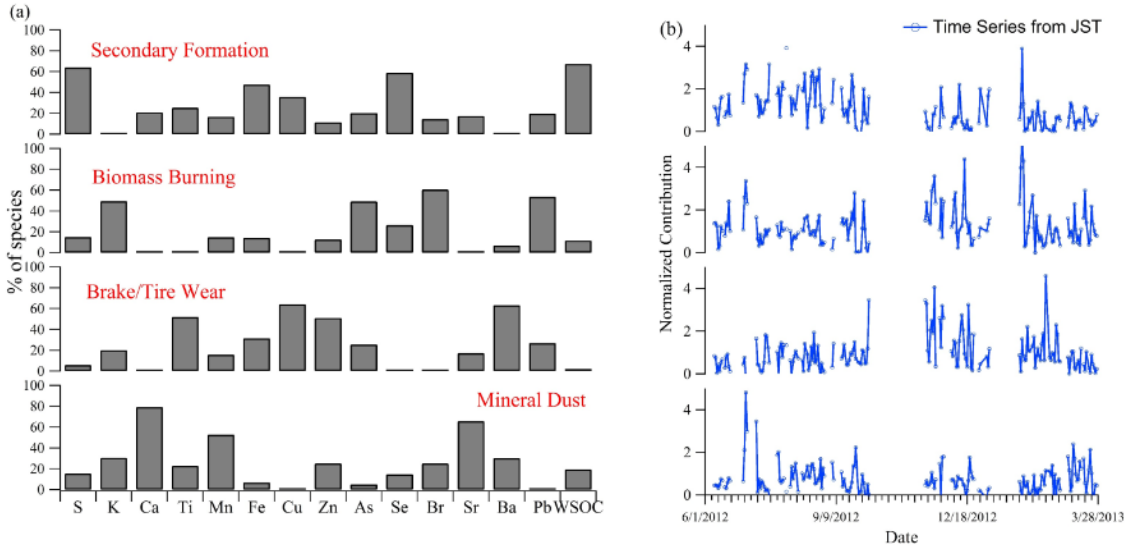

Figure 3-7 Loading of measured water-soluble elements into various PMF resolved factors for all Atlanta sites (a) and factor time series of source contributions resolved from the Jefferson Street Site (JST, urban Atlanta) (b).

The factor with high loadings for Ti, Fe, Cu, Zn, and Ba is identified as a brake/tire wear source as it includes products from brake pads or linings, such as Cu (Adachi and Tainosho, 2004; Sternbeck et al., 2002; Garg et al., 2000), Fe (Adachi and Tainosho, 2004; Garg et al., 2000; Hopke et al., 1980), Ti (Adachi and Tainosho, 2004), and Zn (Adachi and Tainosho, 2004; Sternbeck et al., 2002), and tracers of tire wear, e.g. Zn (Harrison et al.,

2012). A biomass burning factor is identified by high concentrations of K, Br, As, and Pb. While K is a typical component in biomass burning aerosols, Br (Turn et al., 1997) and Pb (Richard et al., 2011) have also been found in wood combustion. The time series plot [Figure 3-7(b)] showed a higher contribution of this factor in winter than in summer ($winter_{avg}/summer_{avg} \approx 1.35$), consistent with the observed winter enhancement of biomass burning emissions in Atlanta (Zhang et al., 2010). Some water-soluble metals (e.g., Se, Fe, Br, Pb, As, Mn, Ba, and Zn) were apportioned to the biomass burning factor (see Figure 3-8& Figure 3-11). The total form of some of these metals (Fe, Mn, Zn, and Cu) (Chang-Graham et al., 2011) and water-soluble Fe have been seen in biomass burning in other studies (Oakes et al., 2012; Chang-Graham et al., 2011). The third factor, referred to as secondary formation, is characterized by high S, WSOC, and Se, and some Fe, with higher contributions in summer than winter ($summer_{avg}/winter_{avg} \approx 2.37$). For the last source, a mineral dust origin is suggested by high loadings of Ca, Mn, and Sr, all indicators of crustal material. The results have implications for health studies.

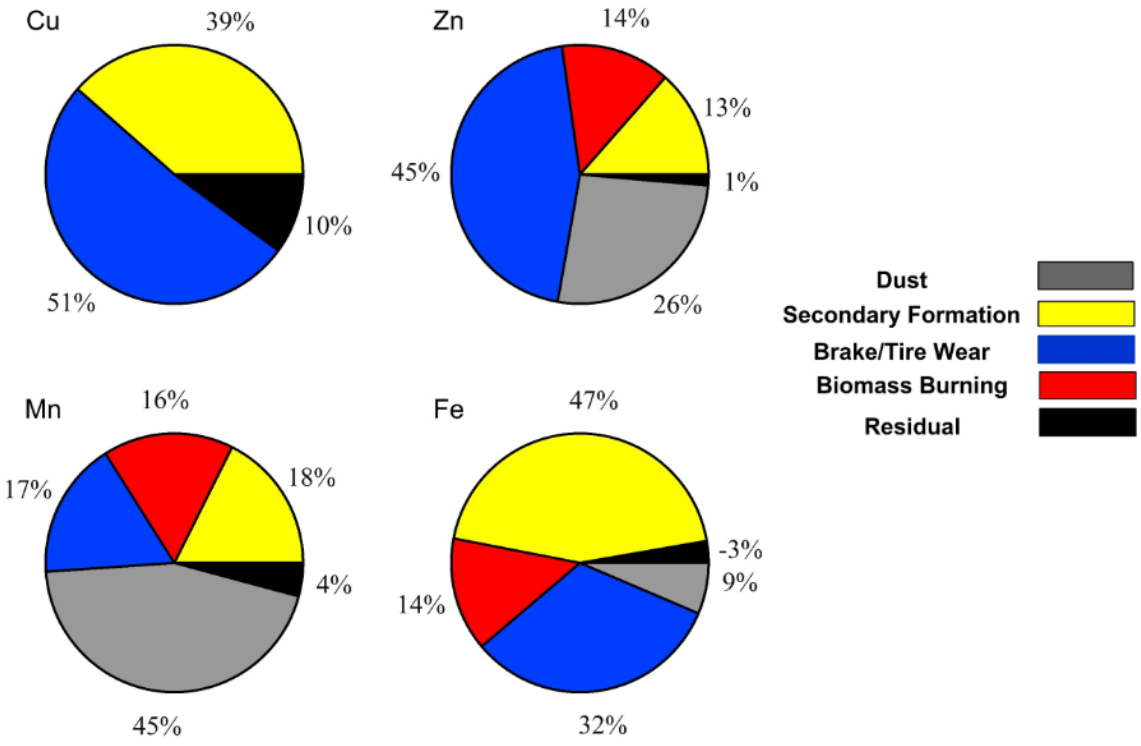

Figure 3-8 Factor contributions for water-soluble Cu, Zn, Mn, and Fe in $PM_{2.5}$ based on the PMF analyses.

3.4.2.4 Redox-active transition metals: Cu, Fe, and Mn

A number of studies have linked water-soluble redox-active Cu, Fe, and Mn to reactive oxygen species (Cheung et al., 2012; Kam et al., 2011; Shen and Anastasio, 2011; Cheung et al., 2010; Akhtar et al., 2010; Landreman et al., 2008; Zhang et al., 2008; Kodavanti et al., 2005). After S, K, and Ca, these metals (i.e., water-soluble Cu, Fe, and Mn) generally have higher ambient concentrations than other measured elements (Figure 3-5). In addition, Cu and Mn are thought to make major contributions to particle-catalyzed ROS generation [e.g., DTT (dithiothreitol) assay (Charrier and Anastasio, 2012)]. Exploring the sources of the water-soluble fractions of these metals is pertinent to our health studies.

As shown in Figure 3-8, tire/brake wear is the dominant source for Cu (51%). It is also strongly correlated with Ba (r = 0.70-0.84, Table 3-4) at the road-side site (RS), and Ba is a good indicator for a brake lining source (Gietl et al., 2010; Torre et al., 2002). The other important contributor to Cu is secondary formation (39%).

Although Zn is not redox-active, we include it here in the discussion since it was also significantly loaded in the tire/brake wear factor (45%) and has been linked to adverse health effects (Akhtar et al., 2010; Kodavanti et al., 2005). PMF analyses suggest that Zn has additional sources, with 26% associated with the mineral dust factor, 14% with the biomass burning, and 13% with secondary formation. Zn is also correlated with other water-soluble metals, to various degrees (Fe, Pb, Mn, Sr, K, Ca, Ti, and Cu with r ranging from 0.70 to 0.89, Table 3-4).

Overall, the results (Figure 3-8) show that brake/tire wear is an important traffic source for Cu (51%), Fe (32%), Mn (17%), and Zn (45%). Studies have specifically linked these metals from brake wear, or traffic sources in general, to pro-inflammatory responses (e.g., (Gasser et al., 2009) and observed adverse health responses (e.g., (Riediker et al., 2004)). Combined with engine combustion emissions, which includes many organic components (e.g., quinones, etc.), the large fraction of water-soluble Cu, along with contributions from Fe and Mn from brake/tire wear, make mobile source emissions important ROS sources (Bates et al., 2015). In contrast, these redox active metals are not found at significant levels in the biomass burning factor (Figure 3-7), which has been found to be a contributor to the $PM_{2.5}$ DTT activity in the SCAPE study (Verma et al., 2014; Verma et al., 2015a), indicating that redox active organic species dominate in that case.

The major identified source for Mn is mineral dust (45%) with other sources making relatively similar contributions: secondary formation (18%), biomass burning (16%), and brake/tire wear (17%). At YRK, the rural site least affected by traffic, Mn correlates best with Ca (r = 0.91) and Sr (r = 0.82, Table 3-4) in summer and K (r = 0.86), Ca (r = 0.86), Zn (r = 0.89), and Sr (r = 0.79) in winter, all indicative of regional mineral dust contributions, consistent with the regional characteristic of Mn discussed in section 3.4.2.2.

For Fe, besides the brake/tire factor, a large fraction (47%) is apportioned to the secondary formation factor, and Fe correlates well with S at JST (r = 0.71), YRK (r = 0.76), and GT (r = 0.73) in summer, and at JST (r = 0.76) in fall 2012 and RS (r = 0.74) in fall 2013. Fe and S are moderately correlated at RS in fall 2012 (r = 0.62), and GT (r = 0.55) in fall 2013. Highest correlations occur when secondary atmospheric processing (oxidation) is strong. These results are consistent with a previous study involving single particle chemical analysis on $PM_{2.5}$ particles in Atlanta, which showed that sulfate is an important proxy for Fe solubility (Oakes et al., 2012) by affecting aerosol pH, or as an indicator of iron sulfates, which are soluble and possibly formed at some point earlier in the particles lifespan under acidic conditions. Metal mobilization by formation of an aqueous particle with secondary acids may also explain the important contribution of secondary formation (39%) to Cu in the Southeastern US, although the correlations between Cu and S were weaker compared to those between Fe and S (Cu - S r=0.51, 0.09, and 0.66 at JST, YRK, and GT in summer, respectively, Table 3-4). The correlation between S and water-soluble Fe and Cu might explain past associations found in other studies between sulfate/sulfur oxide and health endpoints (Atkinson et al., 2010; Sarnat et al., 2008; Pope et al., 2002; Gwynn et al., 2000; Dockery et al., 1996; Raizenne et al., 1996a).

$PM_{2.5}$ mass is regulated and has been associated with adverse health endpoints in many studies (Laden et al., 2000; Pope et al., 2002; Pope et al., 2004; Metzger et al., 2004; Sarnat et al., 2008). Overall, water-soluble iron was highly correlated with $PM_{2.5}$ mass (r = 0.73-0.80, Table 3-5), due to a correlation with sulfate (e.g., the role of sulfate on aerosol pH). Interestingly, Fe was correlated with $PM_{2.5}$ mass even in some cases when S did not co-vary with $PM_{2.5}$ concentration. These cases are all in winter when the r values between $PM_{2.5}$ mass and S were 0.52, 0.35, 0.26, and 0.23, while those with Fe were 0.80, 0.75, 0.76, and 0.74 at JST (Dec), JST (March), GT (March), and RS (Feb), respectively. The exceptions were the two rural sites (YRK and CTR), where water-soluble Fe was moderately or not correlated with $PM_{2.5}$ at all (r = 0.69 at YRK r = 0.3 at CTR) while S and $PM_{2.5}$ still had high correlations (r = 0.78 and 0.75 at YRK and CTR respectively).

Mn and Zn show some correlations with $PM_{2.5}$ mass as well, but only during two periods (for Mn, r = 0.84 at GT and 0.76 at RS, both in winter, for Zn, r = 0.71 and 0.76 at JST in December and March, respectively). No significant correlations were ever found between $PM_{2.5}$ and Cu. It has been demonstrated that water-soluble metals (Zn, Cu, and Fe) can have adverse effects on the respiratory system and our observations suggest that some water-soluble metals, especially Fe, are correlated with $PM_{2.5}$ mass. However, some epidemiological studies point to organic carbon (Peel et al., 2005; Metzger et al., 2004) and $PM_{2.5}$ mass (Sarnat et al., 2008; Pope et al., 2004; Metzger et al., 2004; Pope et al., 2002; Laden et al., 2000) but not metals. Li et al. (2009) suggest that redox-active organic chemicals could play major roles in PM toxicity and metals may synergize with organic PM components to further escalate oxidative stress. Thus, these water-soluble metals could

play both dominant and important secondary roles in driving observed associations between fine particles and adverse health.

3.5 Conclusions

Over 500 $PM_{2.5}$ filter samples (23hr integration time) were collected during 2012-2013 at multiple sites (three urban, two rural, one near-road, and one road-side site) in the Southeastern United States, using paired (simultaneous measurements at two different sites) high-volume samplers, as part of the Southeastern Center for Air Pollution & Epidemiology (SCAPE) project. A focus of SCAPE was assessing the role of $PM_{2.5}$ associated reactive oxygen species (ROS) on health effects. Because water-soluble metals have been linked to ROS, a method was developed to measure the water-soluble elements (S, K, Ca, Ti, Mn, Fe, Cu, Zn, As, Se, Br, Sr, Ba, and Pb) on filters that were also analyzed for aerosol ROS activity by various assays (i.e., DTT and AA assays, discussed in other publications). Water-soluble elements were determined by extracting filters in deionized water, re-aerosolizing the extracts and directing to an instrument designed for online measurements of aerosol elemental composition by non-destructive X-ray fluorescence. The system response was calibrated with standard solutions of multiple elements, which were also used as positive controls when running ambient samples to ensure stability and reproducibility (coefficient of variation < 10%). The method LOD (limit of detection) for each element was reasonably low (< 25% of typical sample levels), and the overall uncertainties were less than 20% for most elements, except for Cu, Sr, and Ti, with overall relative uncertainties of 25%, 25%, and 28%, respectively. The method was further validated by comparing with sulfate measured by ion chromatography on the same ambient filter samples.

Water-soluble elements spanned a wide range of concentrations, from LODs (typically 0.1-30 ng/m^3) to 1.2 µg/m^3, with S as the most abundant element, followed by Ca, K, Fe, Cu, Zn, and Ba. Positive Matrix Factorization (PMF) was used for source apportionment analyses. Four factors were identified; brake/tire wear, characterized by Ba, Zn, Cu, and Ti; biomass burning, characterized by K and Br; secondary formation, characterized by S, Se, Fe, and WSOC; and mineral dust, characterized by Ca, Mn, and Sr. Elements associated with secondary formation and mineral dust were higher during warm/dry seasons when aerosol re-suspension is favored (water-soluble Ca, Mn, and Sr) and secondary formation is high (water-soluble Fe and Cu). S and Se, products from coal combustion, were also at a higher concentration in summer compared to winter. K had only slightly higher concentrations in winter due to contributions from biomass burning (mainly winter) and mineral dust emissions (mainly summer). Other elements (Zn, Ba, Br, Pb, Ti, and As) did not exhibit seasonal trends. Spatially, S, K, Ca, Mn, and Se were generally homogeneously distributed, while Cu, Ba, Sr, and Ti were more heterogeneously distributed, with highest levels near roadways. The other two urban sites outside of Georgia were heavily impacted by industrial sources, contributing to the higher concentration of Zn, Mn, and Pb at Birmingham, AL (BHM), and Ca and Se at the East St. Louis, IL (ESL) site.

The redox-active metals, Cu, Mn, and Fe have been linked to ROS and oxidative stress. Among the four PMF factors, brake/tire wear contributed most to the water-soluble form of these elements in this study, with 51% for Cu, 32% for Fe, and 17% for Mn, pointing to the importance of this source in contributing to fine particle ROS activity. Organic compounds from combustion also contribute to ROS activity, making overall vehicle emissions important sources of $PM_{2.5}$ ROS.

Mn was associated mainly with mineral dust (45%). Water-soluble Zn, a redox-inactive metal, but often identified as toxic in health studies, and among the highest in concentration in this study, was associated with a mixture of factors (45% brake/tire wear, 26% mineral dust, 14% biomass burning, and 13% secondary formation).

Roughly 50% of water-soluble Fe was associated with the secondary formation factor and was highly correlated with S (Pearson's r = 0.71-0.76). There was also substantial loading of Cu (39%) in this factor. Our previous studies in the Southeast have linked water-soluble Fe (measured by a different technique) to sulfate, aerosol pH and soluble iron sulfates (Oakes et al., 2012). The association of Cu with this factor could also be due to increased solubility by sulfur-driven aerosol acidity. Of the four water-soluble metals (Cu, Mn, Fe, and Zn), only Fe was correlated with $PM_{2.5}$ mass (r = 0.73-0.80), due to its association with S. We have previously reported that ROS (DTT assay) measured on these same filters was correlated with $PM_{2.5}$ mass (Fang et al., 2015b). These results indicate that additional aerosol components, such as redox-active organic compounds (Verma et al., 2015a; Verma et al., 2014; Verma et al., 2012) also play a significant role in the ROS activity of aerosols in the Southeastern US, in addition to these water-soluble metals.

3.6 Supporting materials

Table 3-2 Sampling schedule of Hi-Vol filters collected from June 2012 to September 2013.

Month Year	Season	Sampling site	Trailer site
June-July 2012	Summer	JST	YRK
July-August 2012	Summer	JST	GT
September-October 2012	Fall	JST	RS
November 2012	-	JST	JST
December 2012	Winter	JST	YRK
January-February 2013	Winter	JST	RS
March 2013	Winter	JST	GT
June-July 2013	Summer	CTR	BHM
August 2013	Summer	ESL	-
September-October 2013	Fall	GT	RS

JST - Southeastern Aerosol Research and Characterization Study (SEARCH) Jefferson Street, GA; YRK - SEARCH Yorkville, GA; GT - Georgia Tech, GA; RS - Roadside (on Georgia Tech Campus); BHM - SEARCH Birmingham, AL; CTR - SEARCH Centerville, AL; ESL - East St. Louis, IL.

Table 3-3 Coefficient of divergence (COD) and Pearson's r

Paired sites	JST/GT				JST/YRK				JST/RS				GT/RS	
Seasons	Summer		Winter		Summer		Winter		Fall		Winter		Fall	
COD/r	COD	r	COD	r	COD	r	COD	r	COD	r	COD	r	COD	r
S	**0.10**	**0.98**	**0.06**	**0.97**	**0.18**	**0.79**	**0.18**	**0.98**	0.39	0.53	0.26	0.50	0.31	**0.77**
K	**0.15**	0.63	**0.07**	**0.95**	**0.18**	0.69	0.29	**0.68**	**0.18**	0.69	0.28	0.51	**0.16**	**0.79**
Ca	**0.09**	**0.97**	0.36	**0.84**	0.30	0.61	0.28	**0.78**	0.21	**0.77**	0.44	0.37	0.46	0.40
Fe	0.22	**0.90**	0.30	**0.82**	0.46	0.53	0.54	0.42	0.40	0.25	0.29	0.52	0.34	0.53
Zn	0.32	0.69	**0.19**	**0.71**	0.29	0.61	0.38	0.68	0.35	-0.19	0.36	0.15	0.39	0.03
Cu	0.52	0.68	0.35	-0.06	0.41	0.05	0.61	0.21	0.45	-0.21	0.59	-0.13	0.34	0.02
Ba	**0.18**	**0.90**	0.24	**0.85**	0.52	0.27	0.46	0.54	0.61	-0.43	0.53	0.31	0.55	0.36
Mn	**0.14**	**0.94**	**0.13**	**0.84**	0.23	0.64	0.37	**0.76**	0.46	0.04	0.34	0.41	0.33	0.39
Br	**0.18**	0.67	0.26	**0.91**	0.32	0.68	0.43	0.68	0.43	0.30	0.35	**0.72**	0.41	0.65
Sr	**0.13**	**0.89**	0.30	**0.86**	0.46	0.50	0.52	0.34	0.51	-0.11	0.62	0.13	0.51	0.67
Pb	0.28	**0.78**	**0.16**	**0.85**	0.24	0.62	0.34	0.68	0.49	0.53	0.40	0.07	0.40	0.42
As	0.30	0.62	0.21	**0.72**	0.34	0.13	0.42	0.40	0.53	0.25	0.44	0.02	0.41	0.65
Ti	0.38	0.48	0.36	0.51	0.43	0.54	0.46	0.38	0.57	-0.31	0.46	0.17	0.54	0.37
Se	**0.14**	**0.98**	**0.11**	**0.91**	0.28	0.48	0.30	**0.93**	0.28	**0.76**	0.31	**0.71**	0.39	0.62
WSOC	0.30	0.22	0.38	0.49	**0.18**	**0.87**	0.23	**0.79**	**0.19**	0.52	0.48	0.04	0.41	-0.14

Note: COD≤0.2 and r≥0.7 are bolded in blue and red, respectively

The CODs were calculated as follows:

$$COD = \sqrt{\frac{1}{N}\sum_{i=1}^{N}\left[\frac{c_{ij}-c_{ik}}{c_{ij}+c_{ik}}\right]^2} \quad (S1)$$, where c_{ij} and c_{ik} are the water-soluble elements (ng/m^3) measured at paired sites j and k, respectively, and N is the sample size. A COD close to 0 represents a homogenous distribution and near 1 indicates heterogeneity, opposite to correlation coefficients (r). Both are summarized in Table 3-3.

Table 3-4 Correlations (Pearson's r) between water-soluble Cu, Fe, Zn, Mn and other elements

Season. Year	Sites		S	K	Ca	Ti	Mn	Fe	Cu	Zn	As	Se	Br	Sr	Ba	Pb
Summer 2012	JST	Mn	0.61	0.64	0.29	0.62	1	0.66	0.43	0.67	0.03	0.66	**0.80**	**0.80**	0.61	0.52
		Fe	**0.71**	0.48	0.30	**0.81**	0.66	1	0.63	**0.73**	0.41	**0.71**	0.64	0.52	**0.73**	0.67
		Cu	0.51	0.19	0.44	**0.70**	0.43	0.63	1	0.68	0.45	0.59	0.35	0.27	0.68	0.66
		Zn	0.47	0.41	0.32	**0.70**	0.67	**0.73**	0.68	1	0.38	0.59	0.51	0.43	0.64	**0.74**
	YRK	Mn	0.65	0.47	**0.91**	0.21	1	0.44	-0.12	0.53	-0.04	0.53	0.48	**0.82**	0.54	0.37
		Fe	**0.76**	0.60	0.56	0.55	0.44	1	-0.01	0.58	0.02	0.52	**0.73**	0.56	0.33	**0.84**
		Cu	0.09	0.07	-0.05	-0.05	-0.12	-0.01	1	0.20	0.08	0.07	0.13	-0.15	-0.15	0.14
		Zn	0.68	0.54	0.60	0.20	0.53	0.58	0.20	1	-0.02	0.60	0.52	0.51	0.44	0.67
	GT	Mn	0.31	0.61	0.15	0.16	1	0.55	0.17	**0.70**	-0.03	0.27	0.22	**0.79**	0.25	-0.21
		Fe	**0.73**	0.67	0.07	0.52	0.55	1	0.64	0.66	0.51	0.59	0.58	0.35	0.59	0.11
		Cu	0.66	0.25	0.00	0.39	0.17	0.64	1	0.26	0.51	0.54	0.40	0.05	0.44	0.04
		Zn	0.42	0.51	0.22	0.43	**0.70**	0.66	0.26	1	0.35	0.35	0.47	0.57	0.51	0.10
Fall 2012	JST	Mn	0.37	0.30	-0.22	0.30	1	0.61	0.69	0.58	-0.02	0.30	**0.70**	**0.75**	0.36	0.30
		Fe	**0.76**	0.43	0.18	**0.75**	0.61	1	**0.74**	0.65	0.27	0.62	**0.79**	0.56	0.67	0.61
		Cu	0.57	0.55	0.03	**0.73**	0.69	**0.74**	1	0.64	0.59	0.63	0.68	0.24	0.69	**0.75**
		Zn	0.35	0.36	-0.12	0.51	0.58	0.65	0.64	1	0.32	0.38	0.57	0.33	0.47	0.65
	RS	Mn	0.06	**0.76**	0.58	0.30	1	0.18	0.00	0.41	0.09	0.30	0.39	**0.74**	0.46	0.13
		Fe	0.62	0.35	0.38	0.62	0.18	1	0.37	0.60	0.14	0.50	0.62	0.46	0.42	0.34
		Cu	0.27	0.30	0.06	0.39	0.00	0.37	1	0.38	0.00	0.11	0.39	0.43	**0.70**	0.18
		Zn	0.66	0.40	0.42	0.51	0.41	0.60	0.38	1	0.32	0.53	0.63	0.52	0.52	0.28
Winter 2012	JST	Mn	0.24	0.39	0.62	0.35	1	0.38	0.21	0.62	0.30	0.31	0.30	0.68	0.66	0.35
		Fe	0.53	0.56	0.07	0.48	0.38	1	0.63	**0.70**	0.45	0.48	0.51	0.18	0.38	0.62
		Cu	0.25	0.48	-0.11	0.44	0.21	0.63	1	0.51	0.47	0.29	0.19	0.19	0.38	0.52
		Zn	0.29	0.55	0.24	0.48	0.62	**0.70**	0.51	1	0.57	0.46	0.37	0.35	0.50	0.67
	YRK	Mn	0.05	**0.86**	**0.86**	0.19	1	0.53	-0.04	**0.89**	0.18	0.62	0.67	**0.79**	0.63	0.28
		Fe	0.54	0.43	0.23	0.23	0.53	1	0.32	0.50	0.25	**0.83**	0.52	0.11	0.36	**0.76**
		Cu	0.63	0.01	-0.16	0.11	-0.04	0.32	1	0.16	0.08	0.28	-0.04	-0.09	-0.10	0.44
		Zn	0.15	**0.87**	**0.75**	0.38	**0.89**	0.50	0.16	1	0.31	0.62	0.58	**0.73**	0.66	0.42
	GT	Mn	0.15	**0.83**	0.54	0.12	1	0.50	0.63	0.61	0.63	**0.78**	**0.77**	0.52	0.65	0.13
		Fe	0.47	**0.78**	-0.21	0.38	0.50	1	**0.74**	0.59	**0.70**	0.68	**0.72**	0.23	0.52	0.68
		Cu	0.30	0.68	-0.11	0.28	0.63	**0.74**	1	**0.77**	0.44	0.53	0.58	0.06	0.63	0.50
		Zn	0.44	0.46	0.19	0.50	0.61	0.59	**0.77**	1	0.50	0.53	0.39	0.27	**0.81**	0.57
	RS	Mn	0.18	**0.76**	**0.83**	0.55	1	0.56	0.37	0.54	0.49	0.27	0.56	0.35	0.63	0.16
		Fe	0.36	**0.73**	0.16	0.43	0.56	1	0.60	0.48	0.61	0.56	**0.73**	0.34	0.39	0.40
		Cu	0.28	0.59	0.14	**0.73**	0.37	0.60	1	0.42	0.62	0.31	0.46	**0.76**	**0.78**	0.49
		Zn	0.17	0.53	0.20	0.28	0.54	0.48	0.42	1	0.69	0.32	0.44	0.21	0.36	0.49
Fall 2013	GT	Mn	0.57	0.46	0.59	0.47	1	0.57	0.63	0.69	0.35	0.52	0.49	0.36	0.48	0.49
		Fe	0.55	**0.73**	**0.70**	**0.72**	0.57	1	0.63	0.51	0.64	0.46	**0.82**	0.54	0.69	0.62
		Cu	0.35	0.46	0.39	0.54	0.63	0.63	1	0.53	0.58	0.20	0.62	0.35	0.67	0.51
		Zn	0.33	0.28	0.23	0.39	0.69	0.51	0.53	1	0.58	0.31	0.51	0.23	0.62	0.59
	RS	Mn	**0.78**	**0.84**	**0.93**	0.51	1	**0.76**	0.55	**0.85**	0.38	0.64	**0.76**	0.26	0.65	0.31
		Fe	**0.74**	0.67	0.62	**0.71**	**0.76**	1	0.55	0.62	0.62	0.56	**0.82**	0.20	**0.75**	0.47
		Cu	0.30	0.63	0.36	**0.80**	0.55	0.55	1	0.58	0.62	0.21	0.57	0.59	**0.84**	0.37
		Zn	0.64	**0.74**	0.69	0.51	**0.85**	0.62	0.58	1	0.51	0.58	0.62	0.22	0.66	0.57

Note: r≥0.7 are bold and in red.

Table 3-5 Correlations (Pearson's r) between $PM_{2.5}$ and various water-soluble elements

Sites	*Season (Month)*	*S*	*K*	*Ca*	*Ti*	*Mn*	*Fe*	*Cu*	*Zn*	*As*	*Se*	*Br*	*Sr*	*Ba*	*Pb*
JST	Summer (June)	0.66	0.69	0.53	0.67	0.58	0.64	0.54	0.53	0.15	0.65	0.65	0.41	0.48	0.67
	Summer (Aug.)	**0.82**	0.28	0.05	0.45	0.51	**0.80**	0.66	0.58	0.32	0.62	**0.71**	0.39	0.42	0.62
	Fall (Sept.)	**0.83**	**0.80**	0.13	0.69	0.27	**0.80**	0.59	0.69	0.67	**0.78**	0.67	0.52	0.47	**0.77**
	Winter (Dec.)	0.52	0.64	0.23	0.46	0.41	**0.80**	0.54	**0.71**	0.57	**0.73**	0.69	0.17	0.39	0.65
	Winter (Feb.)	**0.78**	0.57	0.06	0.16	0.29	0.68	0.49	0.35	0.24	**0.79**	**0.79**	0.10	0.05	**0.78**
	Winter (March)	0.35	**0.81**	0.27	0.48	0.52	**0.75**	0.30	**0.76**	**0.70**	**0.80**	0.61	0.51	0.41	0.58
YRK	Summer (June)	**0.89**	0.61	0.66	0.57	0.50	**0.73**	0.07	0.53	0.15	**0.70**	**0.83**	0.66	0.41	**0.70**
	Winter (Dec.)	**0.78**	0.48	-0.01	0.07	0.37	0.69	0.56	0.46	0.33	**0.82**	0.57	-0.06	0.21	**0.81**
GT	Summer (Aug.)	**0.86**	0.61	0.33	0.48	0.38	**0.79**	0.60	0.56	0.59	**0.80**	**0.78**	0.38	0.56	0.28
	Winter (March)	0.26	**0.89**	0.11	**0.47**	**0.84**	**0.76**	0.64	0.61	**0.76**	**0.81**	**0.80**	0.31	0.66	0.30
	Fall 2013 (Sept.)	**0.73**	0.24	0.31	0.50	0.33	0.53	0.22	0.08	0.08	0.42	0.58	0.03	0.03	0.08
RS	Fall (Sept.)	0.54	0.65	0.18	0.56	0.45	0.55	0.46	0.57	0.19	0.54	**0.79**	0.50	0.60	0.53
	Winter (Feb.)	0.23	**0.86**	0.53	0.58	**0.76**	**0.74**	0.65	0.51	0.65	0.40	**0.74**	0.40	0.62	0.33
	Fall 2013 (Sept.)	0.65	0.19	0.54	0.18	0.51	0.65	-0.06	0.42	0.32	0.43	0.54	-0.06	0.23	0.11
BHM	Summer 2013 (June)	**0.82**	0.15	0.58	0.41	0.35	**0.77**	0.04	0.20	0.41	0.65	**0.81**	0.17	0.00	0.27
CTR	Summer 2013 (June)	**0.75**	0.57	0.63	0.37	0.55	0.30	-0.18	0.48	0.50	0.64	0.67	0.34	0.39	0.39
ESL	Summer 2013 (Aug.)	0.68	0.67	0.55	0.12	0.04	0.33	0.53	0.11	0.35	0.37	0.34	0.47	0.28	0.49

Note: r≥0.7 are bold and in red.

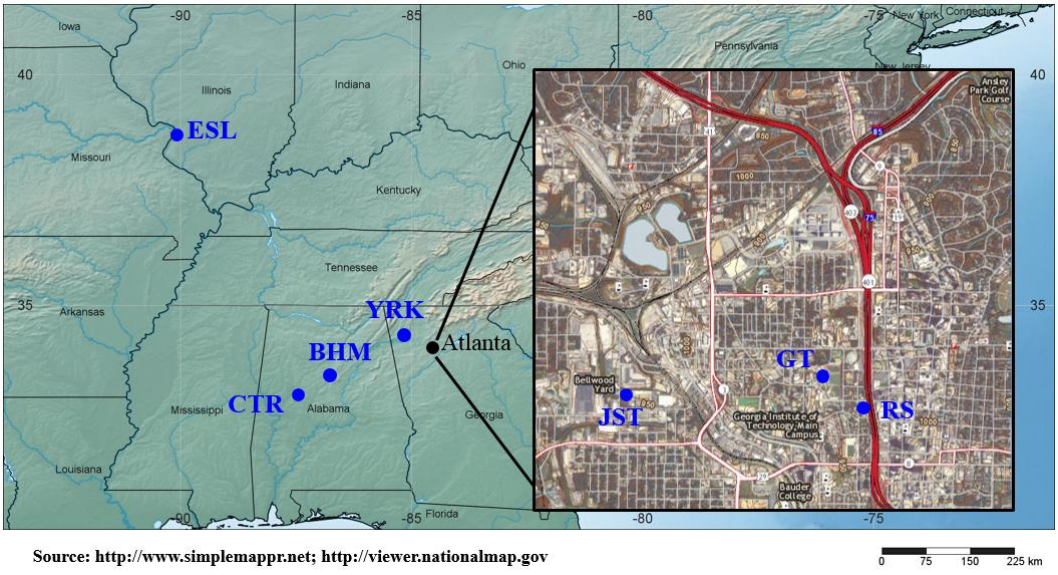

Figure 3-9 Map of sampling sites including three urban site: Jefferson Street, GA (JST); Birmingham, AL (BHM); East St. Louis, IL, two rural sites: Yorkville, GA (YRK); Centerville, AL (CTR), a near-road site - GT, and a road-side site – RS.

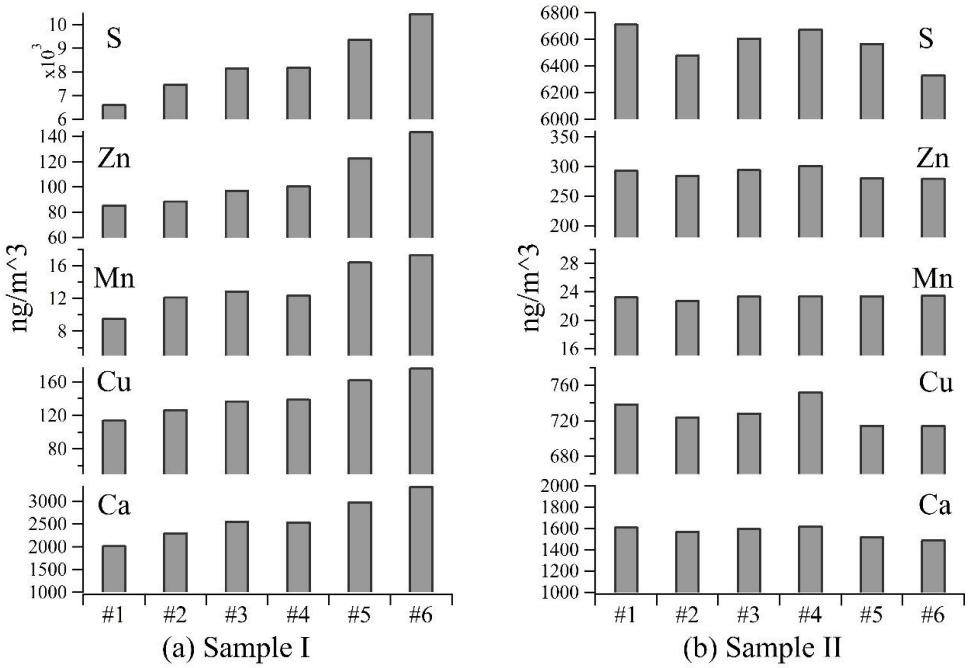

Figure 3-10 Results on selected elements concentration measured by DIONEX-nebulizer-neutralizer-XRF from 6 duplicates from two filter extracts before (a) and after (b) inserting deionized water with 2% HNO3 between samples. It illustrates that inserting DI water with 2% HNO3 is an effect solution to eliminate carry-over issue in the system.

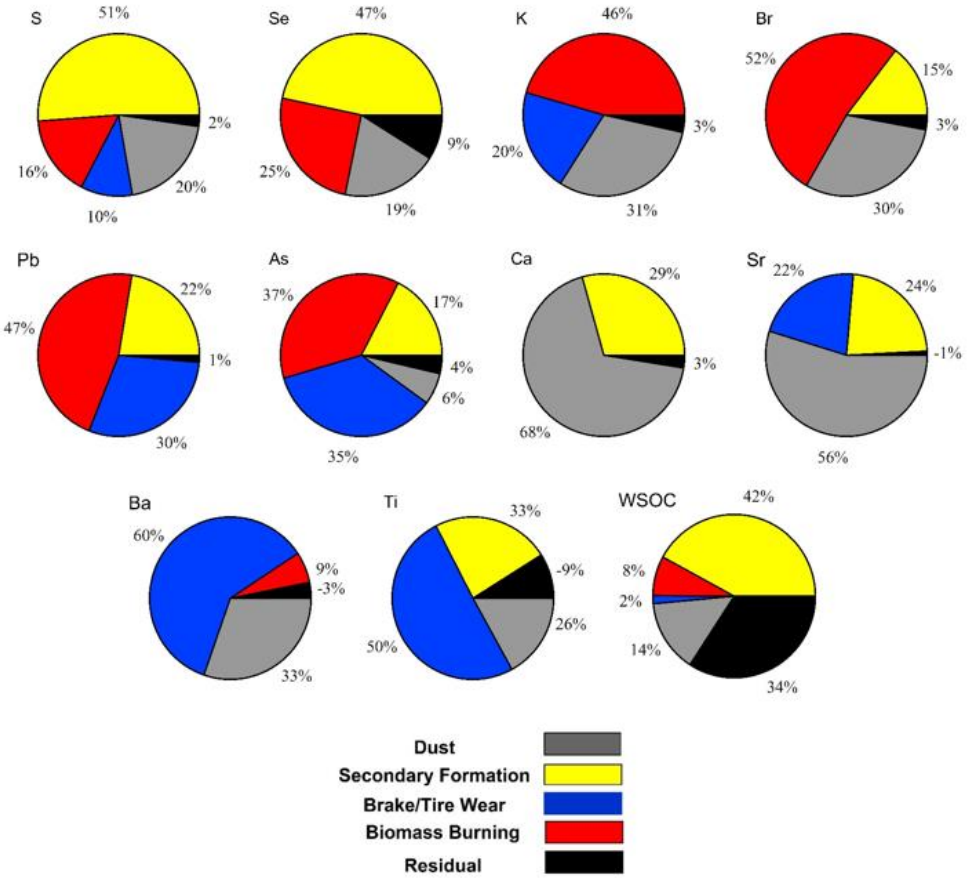

Figure 3-11 Factor contributions for the various water-soluble elements in $PM_{2.5}$ based on the PMF analyses.

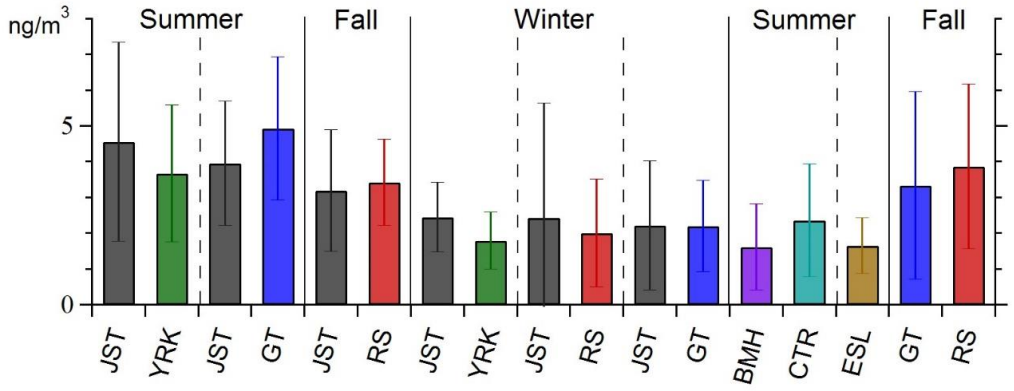

Figure 3-12 Monthly average of ambient concentration of water-soluble organic carbon (WSOC) at the various sites.

CHAPTER 4. OXIDATIVE POTENTIAL OF AMBIENT WATER-SOLUBLE $PM_{2.5}$ IN THE SOUTHEASTERN UNITED STATES: CONTRASTS IN SOURCES AND HEALTH ASSOCIATIONS BETWEEN ASCORBIC ACID (AA) AND DITHIOTHREITOL (DTT) ASSAYS

Ting Fang
Vishal Verma
Josephine T. Bates
Joseph Abrams
Mitchel Klein
Matthew J. Strickland
Stefanie E. Sarnat
Howard H. Chang
James A. Mulholland
Paige E. Tolbert
Armistead G. Russell
Rodney J. Weber

Atmos. Chem. Phys., 16, 3865–3879, 2016
doi:10.5194/acp-16-3865-2016

4.1 Abstract

The ability of certain components of particulate matter to induce oxidative stress through the catalytic generation of reactive oxygen species (ROS) *in vivo* may be one mechanism accounting for observed linkages between ambient aerosols and adverse health outcomes. A variety of assays have been used to measure this so-called aerosol oxidative potential. We developed a semi-automated system to quantify the oxidative potential of filter aqueous extracts utilizing the dithiothreitol (DTT) assay and have recently developed a similar semi-automated system using the ascorbic acid (AA) assay. Approximately 500 $PM_{2.5}$ filter samples collected in contrasting locations in the Southeastern US were analyzed for a host of aerosol species, along with AA and DTT activities. Here we present a detailed contrast in findings from these two assays. Water-soluble AA activity was higher in summer/fall than in winter, with highest levels near highly trafficked highways, whereas DTT activity was higher in winter compared to summer/fall and more spatially homogeneous. AA activity was nearly exclusively correlated with water-soluble Cu (r = 0.70-0.94 at most sites), whereas DTT activity was correlated with organic and metal species. Source apportionment models, Positive Matrix Factorization (PMF) and a Chemical Mass Balance Method with ensemble-averaged source impact profiles (CMB-E), suggest a strong contribution from secondary processes (e.g., organic aerosol oxidation or metal mobilization by formation of an aqueous particle with secondary acids) and traffic emissions to both AA and DTT activities in urban Atlanta. Biomass burning was a large source for DTT activity, but insignificant for AA. AA activity was not correlated with $PM_{2.5}$ mass, while DTT activity covaried strongly with mass (r = 0.49-0.86 across sites/seasons). Various linear models were developed to estimate AA and DTT activities

for the central Atlanta Jefferson Street site, based on the CMB-E sources. The models were then used to estimate daily oxidative potential at this site over the 1998-2009 period. Time-series epidemiological analyses were conducted to assess daily emergency department (ED) visits data for the five-county Atlanta metropolitan area based on the estimated 10-year backcast oxidative potential. Results suggest that estimated AA activity was not statistically associated with any tested health outcomes, while DTT activity was associated with ED visits for both asthma/wheeze and congestive heart failure. The findings point to the importance of both organic components and transition metals from biomass burning and mobile sources to adverse health outcomes in this region.

4.2 Introduction

Studies have linked exposure to fine particulate matter ($PM_{2.5}$) with increased respiratory (Harkema et al., 2004; Aust et al., 2002; Schaumann et al., 2004) and cardiovascular (Pope et al., 2004; Samet et al., 2000) diseases. $PM_{2.5}$ consists of a wide range of chemical components of potentially varying toxicity, implying that $PM_{2.5}$ is not an ideal air quality metric for assessing health impacts. For example, components such as ammonium, sulfate, nitrate, chloride, and some chemical fraction of mineral dust, may be more benign than transition metals (Gasser et al., 2009; Kodavanti et al., 2005; Akhtar et al., 2010), black carbon (or elemental carbon and associated species) (Kleinman et al., 2007; Brunekreef et al., 1997), polycyclic aromatic hydrocarbons (PAHs) (Lundstedt et al., 2007; Burchiel et al., 2005), and other specific organics species (Nel et al., 2001). Although a small mass fraction of $PM_{2.5}$, these components could play a disproportionally large role in the overall adverse health effects of $PM_{2.5}$. A comprehensive set of mechanisms explaining the observed linkage between $PM_{2.5}$ mass and adverse health effects has not been established,

but it has been hypothesized that one possible contributing physiological route is a particle's ability to induce oxidative stress via catalytic generation of reactive oxygen species (ROS) *in vivo*. A number of studies have associated particle oxidative capacity with PM toxicity (Donaldson et al., 2005; Nel, 2005; Shi et al., 2003; Zielinski et al., 1999), but without available large databases of ambient aerosol ROS, large population-based epidemiologic studies of $PM_{2.5}$ oxidative potential have not been possible.

A number of different assays have been developed to quantify the oxidative potential of PM samples (Zomer et al., 2011; Mudway et al., 2011; Ayres et al., 2008; Jung et al., 2006; Cho et al., 2005; Mudway et al., 2005; Venkatachari et al., 2005). Two commonly used approaches are the dithiothreitol (DTT) assay (Cho et al., 2005) and the ascorbic acid (AA) assay (Ayres et al., 2008; Mudway et al., 2005). It may be expected that these two different assays respond to different aerosol components and are linked to different health endpoints. The AA assay has been shown to be most sensitive to transition metals (Janssen et al., 2014; Strak et al., 2012; DiStefano et al., 2009; Künzli et al., 2006) but quinone compounds may react with AA as well (Roginsky et al., 1999). For the DTT assay, identified DTT-active PM components are organic species, including water-soluble organic carbon (WSOC) (Verma et al., 2009a; Cho et al., 2005), or of increasing specificity, HUmic-LIke Substances (HULIS) (Verma et al., 2012; Lin and Yu, 2011), and quinones (Chung et al., 2006; Kumagai et al., 2002) (a component of HULIS). Other studies, however, have emphasized the role of transition metals, such as Cu and Mn (Vejerano et al., 2015; Charrier and Anastasio, 2012). Some differences between studies may arise due to differing source characteristics of the specific regions studied.

Both assays involve incubating the anti-oxidant (DTT or AA) with filter aqueous extracts of $PM_{2.5}$ at a controlled temperature (37 °C) and pH (7.4), and measuring the depletion of the antioxidant over time, typically detected as a decrease in light absorption at a certain wavelength (412 and 265 nm for DTT and AA, respectively). The antioxidant loss rate is interpreted as a measure of the ability of aerosol redox-active species to catalytically transfer electrons from DTT or AA to oxygen (O_2). DTT can be considered a chemical surrogate to cellular reductants, such as NADH or NADPH, which reduces O_2 to superoxide anion ($O_2^{\cdot}$) and induces oxidative stress (Kumagai et al., 2002). Unlike DTT, AA is a physiological antioxidant in lung lining fluid, which prevents the oxidation of lipids and proteins (Valko et al., 2005). Asthmatic patients have markedly decreased the concentration of AA in lung lining fluid compared to healthy control subjects (Kelly et al., 1999). Therefore, the *in vitro* oxidation of these two antioxidants by PM might represent the interaction of PM with biological antioxidants *in vivo* leading to the induction of oxidative stress and ultimately adverse health effects.

Among the various available methods for measuring oxidative potential, these two assays are relatively straightforward and reproducible, allowing high-throughput routine measurements and the generation of large data sets for exploring links between aerosol components and health through epidemiology, or also as an initial screening step for identifying different redox components for more detailed cell or animal studies (Ayres et al., 2008).

We recently developed a semi-automated system (Fang et al., 2015b) to measure DTT activity and here describe its adaption to the AA assay. Utilizing our automated analytical system, we measured the water-soluble oxidative potential of over 500 filter samples

collected as part of the Southeastern Center for Air Pollution & Epidemiology (SCAPE) study. Although insoluble components are important, since there is no current standard protocol for measuring the water-insoluble oxidative potential, we focus solely on the water-soluble AA and DTT activities. We evaluate and compare these two assays in order to identify specific aerosol components the AA assay is responsive to. We perform a source apportionment analysis and assess these results through observed AA activity seasonal and spatial variability. AA source profiles are used to generate a model that estimates AA activities, which is then used to backcast AA levels over the past 10 years for use in a time-series epidemiological analysis in the Atlanta metropolitan area. Throughout, we compare the AA results to our previously published DTT findings (Bates et al., 2015, Fang et al., 2015b, Verma et al., 2014) to provide a contrast between these two commonly utilized assays to assess aerosol water-soluble oxidative potential and possible associations with health endpoints.

4.3 Methods

4.3.1 Sampling

Sampling methods have been described in detail elsewhere (Fang et al., 2015b; Verma et al., 2014). In brief, $PM_{2.5}$ (quartz filters, Pallflex® Tissuquartz™, 8 × 10 inches) was sampled at seven locations in the Southeastern US, with different source characteristics, using two sets of high-volume samplers (Hi-Vol) (Thermo Anderson, flow rate normally 1.13 m^3 min^{-1}). Sampling in the metropolitan Atlanta area was carried out from June 2012 through March 2013 (noon - 11 a.m., 23 hours) and involved paired-sites with one Hi-Vol sampler fixed at an urban background site (Jefferson Street, referred as JST) whilst the other sampler was deployed at three other sites on a monthly basis, and at least twice during different seasons. These three sites were: a rural site (Yorkville, YRK), a road-side site (RS, adjacent to the interstate highway I75/85), and a near-road site (GT, 840 m from the RS site). Following sampling in Atlanta, the two samplers were moved to Birmingham, AL (BHM, within a few kilometers of significant transportation and industrial sources) and Centerville, AL (CTR, surrounded by forests and a lightly traveled county road) for a month of sampling in June-July 2013, followed by one-month August sampling at East St. Louis, IL, an urban residential/light commercial area about 3 km east of the central business district of St. Louis, MO (Sauvain et al.). Finally, a GT-RS pair was conducted in September 2013. A table providing the sampling schedule and a map can be found in the supporting material (Table 4-1 & Figure 3-9). JST, YRK, BHM, and CTR are all part of the Southeastern Aerosol Research and Characterization Study (SEARCH) network sites (Hansen et al., 2003). Collected samples were immediately wrapped in prebaked aluminum foil and stored at −18°C until analyzed. DTT, water-soluble organic carbon, and brown

carbon analyses on the filters were conducted within a year of sample collection, water-soluble elements were within a year and a half, and AA measurements were conducted within two years of sample collection.

4.3.2 Oxidative potential measurement

Filter extraction: One punch of the collected Hi-Vol filter (5.07 cm^2) was extracted in 30 mL of deionized (DI) water (> 18 MΩ cm^{-1}) in a sterile polypropylene centrifuge tube (VWR International LLC, Suwanee, GA, USA) by sonication using an Ultrasonic Cleanser (VWR International LLC, West Chester, PA, USA) for half an hour. For those having activities close to blanks, 15 mL was used instead. Extracts were then filtered using PTFE 0.45 µm syringe filters (Fisherbrand™) to remove insoluble material larger than 0.45 µm. Although OH may form during sonication (Miljevic et al., 2014), it appears to have little effect on our ROS measurement since we compared the water-soluble ROS activities from the same sample that had been extracted by shaking for 3 hours vs sonication and found no significant differences (average ratio and standard deviation is 1.08 ± 0.20, n = 7).

AA determination: The method in this study was based on an ascorbate-only model (Mudway et al., 2005; Ayres et al., 2008) that is a simplified and alternative high throughput approach to a synthetic respiratory tract lining fluid model (RTLF) containing ascorbate, urate, and reduced glutathione (GSH) (Zielinski et al., 1999; Mudway et al., 2004). The method protocol is shown in Figure 4-1 and system setup can be found in Figure 4-6 in the supporting materials. The method involves two steps.

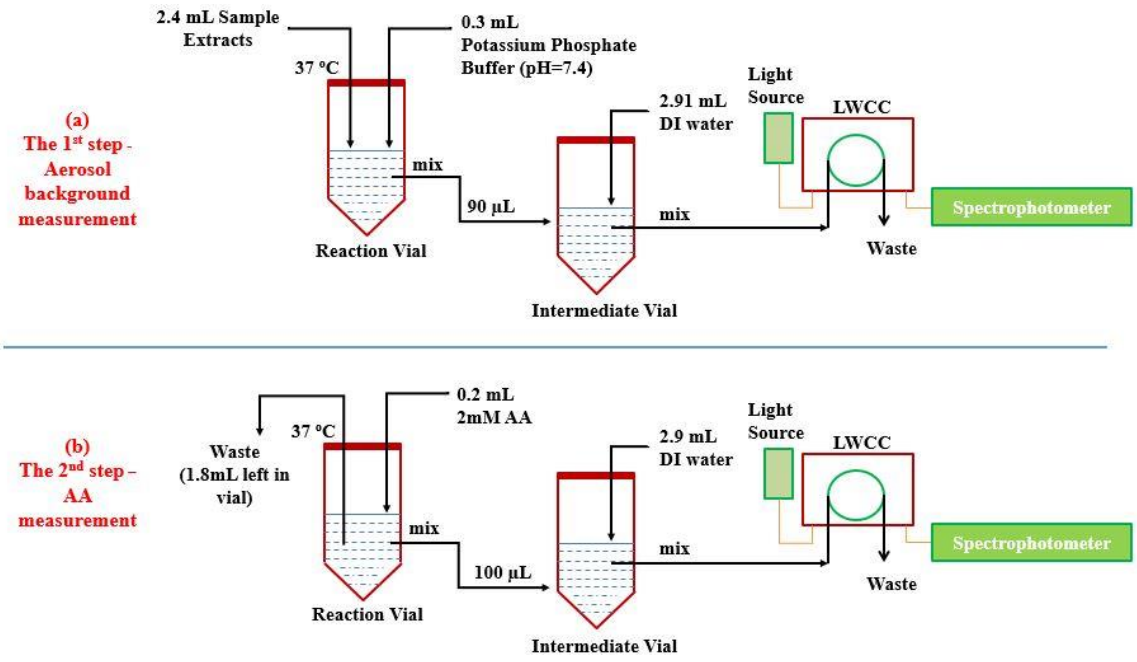

Figure 4-1 Protocol schematics for conducting Ascorbic Acid assay

The first step is an aerosol background measurement (Figure 4-1). In order to control for the contribution of absorbance of particles themselves at 265 nm wavelength, an AA-free control was measured and subtracted from the sample absorbance readings. 2.4 mL aerosol extracts and 0.3 mL 0.5 mM Kbuffer were loaded into a reaction vial (sterile polypropylene centrifuge tube, VWR International LLC, Suwanee, GA, USA) using a programmable syringe pump (A) with a 5 mL syringe (Kloehn, Inc., Las Vegas, NV, USA). Following mixing, 90 µL of the mixture was transferred to an intermediate vial using Pump B with a 250 µL syringe and diluted to 3 mL. Pump A then withdrew the diluted mixture from the intermediate vial and pushed it through a Liquid Wave-guide Capillary Cell (LWCC-M-100; World Precision Instruments, Inc., FL, USA) with an optical path length of 100 mm. The waveguide was coupled to an online spectrophotometer, which included a UV-VIS

light source (Ocean Optics DT-Mini-2, Ocean Optics, Inc., Dunedin, FL, USA), and a multi-wavelength light detector (USB4000 Miniature Fiber Optic Spectrometer, Ocean Optics, Inc., Dunedin, FL, USA). Aerosol background absorbance at 265 and 700 nm (baseline) were recorded at two-second intervals using data acquisition software (SpectraSuite). For the samples collected in this study, backgrounds due to the aerosol absorption at 265 nm were <10% of the sample absorbance readings. Prior to the second step, the system performed a self-cleaning by flushing the intermediate vial and the two syringes with DI water three times.

The second step is the AA measurement (Figure 4-1). Following the aerosol background measurement, Pump A discarded a fraction of the sample-Kbuffer mixture and left only 1.8 mL in the reaction vial. 0.2 mL 2 mM AA solution was then loaded to the reaction vial using Pump B. Both the reaction and intermediate vial were continuously shaken at 400 rpm in a ThermoMixer (Eppendorf North America, Inc., Hauppauge, NY, USA), which also maintained the incubation temperature at 37 °C. At five different specified times (7, 15, 24, 32, 40 minutes), a small aliquot (100 µL) was transferred to the intermediate vial, diluted to 3 mL, and pushed through the LWCC, generating a total of five data points quantifying the remaining AA concentration. The system then again performed a self-cleaning before analyzing the next sample. A multi-position valve (14-port, VICI® Valco Instrument Co. Inc., USA) was used to select samples for analysis. To ensure the suspension of PM in the extract, each sample was mixed by pushing 5mL of air through the extract before loading to the reaction vial.

Final AA activity is calculated as follows:

$$\boldsymbol{\sigma AA = -\sigma Abs \times \frac{N_0}{Abs_0}} \quad \textbf{(Equation 5),}$$

$$\boldsymbol{AAv = \frac{\sigma AA_s - \sigma AA_b}{\frac{V_a}{V_e} \times V_p}} \quad \textbf{(Equation 6).}$$

Following the notation above, σAbs is the slope of absorbance versus time, where the absorbance is the absorbance of each time interval subtracting the corresponding aerosol background absorbance; Abs_0 is the initial absorbance calculated from the intercept of linear regression of absorbance versus time; N_0 is the initial moles of AA added in the reaction vial (400 nmol); σAA_s (σAA_b) is the rate of AA consumption for a sample (blank); V_e and V_a are the extraction volume (30 or 15 mL) and sample volume added to the reaction (1.6 mL), respectively. V_p is the ambient air volume (m^3) represented by the sample in the extraction volume. AAv represents volume normalized AA activity, in units of nmol min^{-1} m^{-3}. Similarly, here DTTv represents the volume normalized DTT activity. Note that AAv and DTTv, although with the same unit, cannot be compared in magnitude as their responses are different.

4.3.3 Chemical analysis on PM filters

4.3.3.1 Water-soluble organic carbon and brown carbon

An automated system (details in Figure 4-7) was used to measure water-soluble organic carbon (WSOC) and brown carbon (BrC) on the water-soluble extracts from the same Hi-Vol filters. Filter extracts (~6mL, same extraction protocol outlined above), after loading onto a 5 mL sample loop (Upchurch Scientific, Inc., Oak Harbor, WA), were first passed through a 1 m LWCC (LWCC-2100; World Precision Instruments, Inc., FL, USA), where absorbance at 365 nm wavelength (BrC) was measured using an online spectrophotometer (Ocean Optics, Inc., Dunedin, FL, USA). The extracts then entered a TOC analyzer

(Sievers Model 900, GE Analytical Instruments, Boulder, CO, USA) for determining WSOC concentration.

4.3.3.2 Water-soluble elements

A similar automated system was developed to determine the water-soluble elements, including S (Sulfur), Ca (Calcium), K (Potassium), Fe (Iron), Cu (Copper), Zn (Zinc), Ba (Barium), Pb (Lead), As (Arsenic), Sr (Strontium), Se (Selenium), Br (Bromine), Mn (Manganese), and Ti (Titanium). Details of the method are described in Fang et al. (2015a) and section 3.3.2.

4.3.3.3 $PM_{2.5}$ mass

$PM_{2.5}$ mass concentration was measured by a Tapered Element Oscillating Microbalance (TEOM) by Atmospheric Research Analysis (ARA, Inc.) at SEARCH sites (JST, YRK, BHM, and CTR) and ESL. For the RS and GT sites, since $PM_{2.5}$ mass were not available, the PM mass concentrations were estimated from the sum of chemical components analyzed on the same Hi-Vol filters (Verma et al., 2014; Fang et al., 2015b) (Details in the section 2.3.4).

4.3.4 Source apportionment

Source apportionment of AAv was performed using a Positive Matrix Factorization (PMF) model (EPA PMF 5.0 software) (Paatero and Tapper, 1994) and a Chemical Mass Balance model (version 8.2) with ensemble-averaged source impact profiles (CMB-E)(Balachandran et al., 2012). PMF is a commonly used source apportionment approach that does not require source profiles as CMB-E, whereas CMB-E has better performance

and lower relative uncertainties as compared to the PMF method (Balachandran et al., 2012). Source contributions to DTTv using PMF and CMB-E are discussed in our other publications (Verma et al., 2014). A PMF analysis on the water-soluble elements (S, K, Ca, Ti, Mn, Fe, Cu, Zn, As, Se, Br, Sr, Ba, and Pb) and WSOC from JST, GT, and RS sites has been reported in Fang et al.(Fang et al., 2015a). AAv was simply added to the data sets to generate the AAv results shown here. The PMF results on DTTv in our prior analyses were based on JST and GT sites.

In PMF, the uncertainties for each species were determined by multiplying the concentration by overall uncertainties (%), which were obtained by propagating the uncertainties from filter sampling (assumed to be 5%), extraction (assumed to be 5%), blanks (1 σ of multiple blanks), calibration (1 σ of slope, for water-soluble elements), collocated measurements (for water-soluble elements and AA, Figure 4-8), and analytical uncertainties. The analytical uncertainties were obtained by analyzing the same sample/standards multiple times; for example, a composite of extracts from 11 samples for water-soluble elements (coefficient of variation, CV = 2-16 %); 9,10-phenanthrenequinone for AA (CV = 13%), and sucrose standard solutions for WSOC (CV = 10%). Missing data were replaced by species medians with 400% uncertainty, and values below LOD were assigned as half of LOD values with uncertainties of 5/6 the concentration(Polissar et al., 1998). Uncertainty from collocated measurements was calculated as the relative uncertainty of the slope (1 σ/slope), which was based on an orthogonal regression.

An ensemble-trained source apportionment approach (Balachandran et al., 2012) (CMB-E) was also used to construct the source impacts on AAv based on $PM_{2.5}$ species (sulfate, nitrate, ammonium, OC, EC, and total metals) and AAv measured during SCAPE sampling

periods (2012-2013). The source profiles cover a range of sources, including light-duty gasoline vehicles (LDGV), heavy-duty diesel vehicles (HDDV), ambient sulfate (AMSULF), ambient nitrate (AMNITR), ammonium bisulfate (AMBSLF), not otherwise apportioned organic carbon (OTHER_OC), dust, biomass burning (BURN), coal-fired power plants, cement, and cooking. An ensemble average was calculated for each source category using ten different runs developed from four individual source apportionment methods. Since the filters for the source impact profiles were collected from midnight to midnight, while the filters collected for AAv measurement were collected from noon to 11 a.m. next day, the sources identified were linearly interpolated using a fixed ratio. For example, two consecutive filters (filter 1 and 2) collected from midnight to midnight, 12/24*filter1 + 11/24*filter2 would be used to produce the estimated AAv to compared with actual measured data.

4.3.5 Epidemiological assessment

4.3.5.1 Backcast-estimates of AA activities

To undertake a time-series epidemiological analysis with sufficient power, retrospective data sets of daily AAv levels from 1 August 1998 to 31 December 2009 at an Atlanta site representative of the urban airshed air quality are needed. Previous epidemiological studies by the study team, assessing Atlanta air quality and emergency department (ED) visits, have used data from the SEARCH JST site, the anchor site for our AAv measurements. To generate daily estimates of retrospective AAv at JST, first, a linear model was used to estimate the contribution of various sources to our observed AAv measured at JST. This was done through separate linear regressions for AAv with the ensemble-predicted sources

as independent variables. In previous work (Balachandran et al., 2012), a source times-series from August 1998 to December 2009 was generated for JST using the same CMB-E model with the same independent variables measured at JST. The AAv regression was then applied to this time series to construct a time series of estimated AAv for the epidemiology study time period, during which direct measurements of AAv were not available. In order to test the sensitivity of epidemiologic results to different backcast models, two other models are generated for AAv (discussed in section 3.2.1). Identical methods were applied to DTTv to obtain three different models for comparisons with those from AAv.

4.3.5.2 Epidemiological analyses

Epidemiological time-series analysis (Strickland et al., 2010; Winquist et al., 2015) was employed to assess associations of retrospective DTTv and AAv with health effects as reflected in ED visits. Relationships between ED visits data from Atlanta area hospitals and typical ambient air quality characteristics, as well as the impact of exposure misclassification and other factors, have been extensively studies (Strickland et al., 2010; Winquist et al., 2015; Metzger et al., 2004; Peel et al., 2005). For the present analysis, we apply these previously reported epidemiologic modeling approach to the backcast-estimates of AAv and DTTv, in order to assess associations of these oxidative potential air quality descriptors with selected outcomes in the ED visits data collected from hospitals serving the five-county metropolitan Atlanta area during 1998-2009. The health outcomes investigated in the current analysis are daily visits for respiratory diseases, including pneumonia (n=145,610 total visits for study period), chronic obstructive pulmonary disease (n=49,251), and asthma/wheeze (n=263,665), and cardiovascular diseases, including

ischemic heart disease (n=73,477) and congestive heart failure (CHF) (n=70,587). The air quality was modeled as a three-day moving average ("lag 0-2", the moving average of estimated pollutant level for that day, the previous day, and the day before). Poisson generalized linear regression was performed; to control for temporal trends and meteorological variables, models included cubic splines with monthly knots for time, linear, quadratic and cubic terms for mean daily dew point (lag 0-2), maximum daily temperature (lag 0), and minimum daily temperature (lag 1-2), indicators of hospital contribution time periods, season of year, day of week and holiday, and interaction terms between season and maximum temperature, and between season and day of week. These covariates were chosen based on prior studies (Strickland et al., 2010; Winquist et al., 2015) which identified important confounders to the relationship between daily ambient pollution levels and ED visits. Risk ratios (the relative risks of ED visit associated with an increase of one interquartile range of the exposure metric) and 95% confidence intervals (CI) were used to describe the observed health associations. Risk ratios with confidence intervals above 1 are indicative of statistically significant positive associations. International classification of disease codes used to define the health outcomes can be found in the Appendix A.3.

4.4 Results and Discussion

4.4.1 AAv for measurements during 2012-2013 and comparisons to DTTv

4.4.1.1 Spatio-temporal distribution

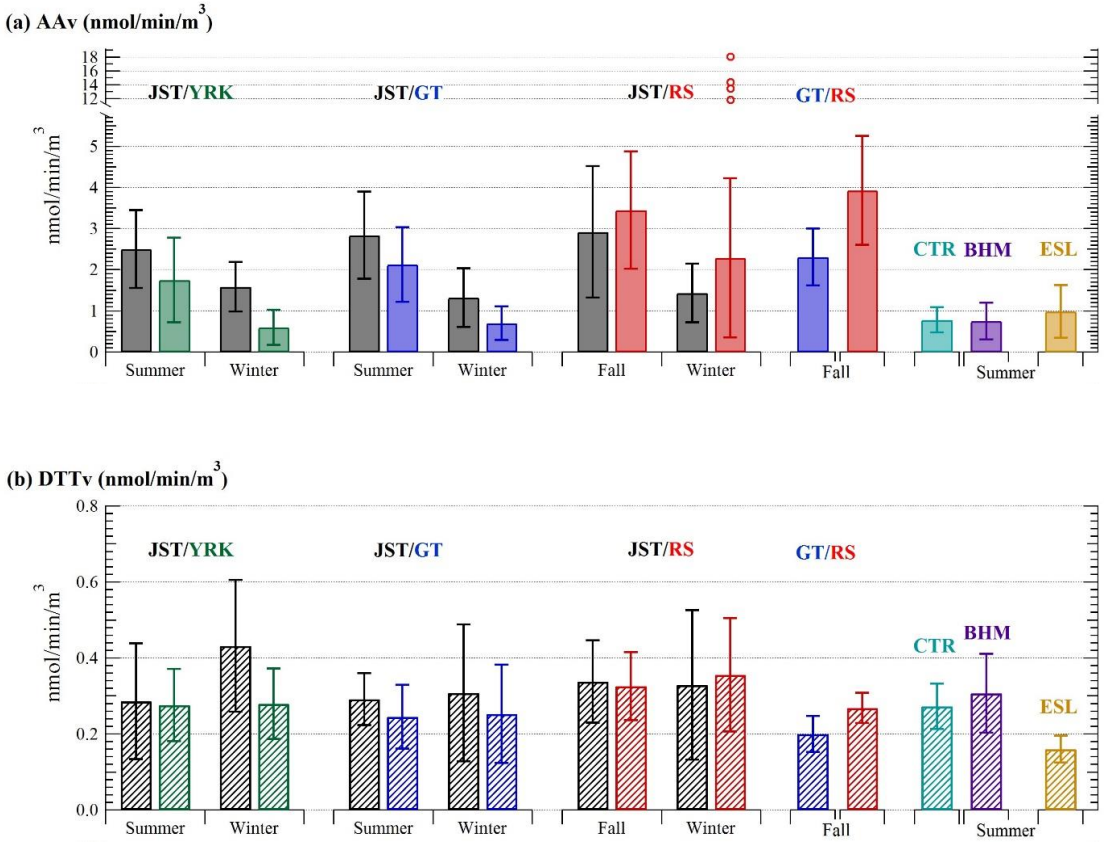

Figure 4-2 Monthly average (±SD) of $PM_{2.5}$ oxidative potential based on the (a) AA and (b) DTT assays from the water-soluble extracts from filters collected at three urban (JST, BHM, and ESL), two rural (YRK and CTR), a near-road (GT), and a road-side (RS) site in the Southeastern United States.

Monthly average water-soluble AAv at various sampling sites are given in Figure 4-2(a). AAv was heterogeneously distributed, indicated by the significant variability between

sites. Highest AAv was found at the roadside site (RS) and lowest at rural sites. For example, the ratio of average AAv at RS to its paired Atlanta urban JST site was 1.2 in fall and 1.6 in winter [(2.7 when including the four high data points in Figure 4-2(a)] and RS to near-road GT was 1.7 in fall 2013. AAv at the rural site was generally lower compared to the urban environments, the average YRK/JST ratio was 0.7 in summer and 0.4 in winter, respectively. An exception is that BHM (urban) and CTR (rural) had similar AAv (BHM_{avg} = 0.75 ± 0.45 nmol min^{-1} m^{-3} and CTR_{avg} = 0.78 ± 0.31 nmol min^{-1} m^{-3}). Comparing AAv in different cities, BHM and the other urban site, ESL (average AAv= 0.98 ± 0.63 nmol min^{-1} m^{-3}), had lower AAv relative to the Atlanta urban sites (average of JST and GT in summer = 2.5 ± 1.0 nmol min^{-1} m^{-3}). The higher AAv near traffic sources has also been found in other studies (Janssen et al., 2014; Strak et al., 2012; Janssen et al., 2015). In contrast, Figure 4-2(b) shows that DTTv was largely spatially uniform, differences between paired sites is much less than those for AAv.

The seasonal distribution can be examined from the Atlanta sites, JST, GT, RS, and YRK. The AA activity was higher in summer/fall compared to winter; the ratio of summer or fall to winter was 1.8, 2.9, 1.0, and 3.1 (average ratio is 2.2 ± 0.9) for JST, YRK, RS, and GT, respectively. In contrast, JST DTTv had an opposite seasonal trend, with the highest level in December (winter), while there was no significant seasonal variation observed at YRK, GT and the RS site. These results indicate that there are differences in the sources for water-soluble AAv and DTTv, with traffic emissions a more significant source for AAv. Correlation analysis with specific aerosol components provides further insights.

4.4.1.2 Correlations with chemical components

To further identify the major sources for AAv and compare to DTTv , a correlation analysis was performed between the assays and the following selected chemical components; BrC (an indicator of incomplete combustion, i.e., biomass burning), WSOC and S (secondary processes), Ca (mineral dust), and selected transition metals (Cu, Fe, Mn, and Zn) that have been related to adverse health outcomes (Cheung et al., 2012; Kam et al., 2011; Shen and Anastasio, 2011; Cheung et al., 2010; Akhtar et al., 2010; Landreman et al., 2008; Zhang et al., 2008; Kodavanti et al., 2005). Correlation coefficients based on linear regressions between AAv or DTTv and chemical species (Pearson's r) are shown graphically in Figure 4-3. A detailed matrix showing the correlations at individual sites is given in Table 4-1. To simplify Figure 4-3, JST and GT were combined into one metric given their close proximity and high correlation ($r>0.7$) for many PM species, such as EC, WSOC, and water-soluble elements (Fang et al., 2015a). As shown in Figure 4-3, AAv was almost exclusively correlated with water-soluble Cu. The r value ranged from 0.70-0.94 for most sites/seasons except RS in fall 2012, JST/GT in winter, ESL in summer, and GT in fall 2013. High correlations between AAv and Cu are consistent with other studies (Janssen et al., 2014; Künzli et al., 2006), although the correlation coefficients (r) in our work (0.70-0.94) were higher (0.60-0.74 in other studies), possibly because we used water-soluble Cu and the other studies used elemental (total) concentrations. Strak et al (Strak et al., 2012) also report a higher r value between AAv and water-soluble Cu ($r = 0.82$) than that between AAv and total Cu ($r = 0.76$) from the same sample set.

Compared to AAv, DTTv is more broadly correlated with aerosol species: high correlations were observed with S ($r = 0.66$-0.74) and WSOC ($r = 0.71$- 0.77) in summer, which

diminished in fall (r = 0.14-0.66 for S and r = 0.20-0.65 for WSOC) and was weaker in winter (r<0.4) for S. Instead, higher correlations were found with BrC (r = 0.78-0.88) and WSOC (r = 0.60-0.84) in winter. The decreasing correlation between DTTv and S going from summer to winter suggests the important role of secondary processing in summer (Verma et al., 2009a; McWhinney et al., 2013b) and the increasing contribution of biomass burning to winter DTTv; AAv did not show similar trends, i.e., AAv did not correlate with S (r = -0.12-0.60) and low r values were observed with K in winter (r = 0.07-0.19, one exception was JST in December r = 0.7), suggesting incomplete combustion (e.g., biomass burning) was not a significant source for AAv. Whereas AAv was nearly exclusively correlated with Cu, DTTv was correlated with various metals, including Ca, Mn, Fe, Cu, and Zn. In Figure 4-2, counting the number of sampling sites at which r values between AAv and various metals were larger than 0.65 (i.e. black solid bars), we observed eight times for Cu and once for Mn (r = 0.82). Whereas for DTTv (see the striped bars in Figure 4-3), we found twice (r= 0.67 and 0.77) for Ca, 3 times for Mn (r = 0.65-0.75), 6 times for Fe (r = 0.68-0.90), once for Cu (r = 0.68), and 3 times for Zn (r = 0.70-0.82). There were, however, no apparent seasonal patterns for the correlations between these water-soluble metals and DTTv since they were related to mineral dust (68% of Ca, 45% of Mn, and 26% of Fe) and vehicle brake/tire wear emissions (51% of Cu, 45% of Zn, 32% of Fe, and 17% of Mn).

The comparison of AAv and DTTv's correlation with $PM_{2.5}$ mass is noteworthy. DTTv was fairly well correlated with $PM_{2.5}$ mass (r = 0.49-0.86, Figure 4-3), whereas AAv did not correlate as well (r = -0.17 to 0.59), as also found by Künzli et al. (Künzli et al., 2006) (r = 0.34). $PM_{2.5}$ mass has been linked with adverse health endpoints in many epidemiological

studies (Laden et al., 2000; Pope et al., 2002; Pope et al., 2004; Metzger et al., 2004; Sarnat et al., 2008), thus the lack of correlation of AAv with $PM_{2.5}$ mass may be suggestive of an expected lack of linkage between AA-measured oxidative potential and health endpoints (tested in section 4.4.2). In summary, AA and DTT assays have differing associations with PM chemical species, further suggested by a lack of strong correlation between the two assays at all sites ($r<0.55$), similar to findings from other studies ($r<0.65$) (Janssen et al., 2014; Yang et al., 2014; Janssen et al., 2015). A source apportionment analysis is performed to attempt to quantify contributions of various sources to $PM_{2.5}$ AAv.

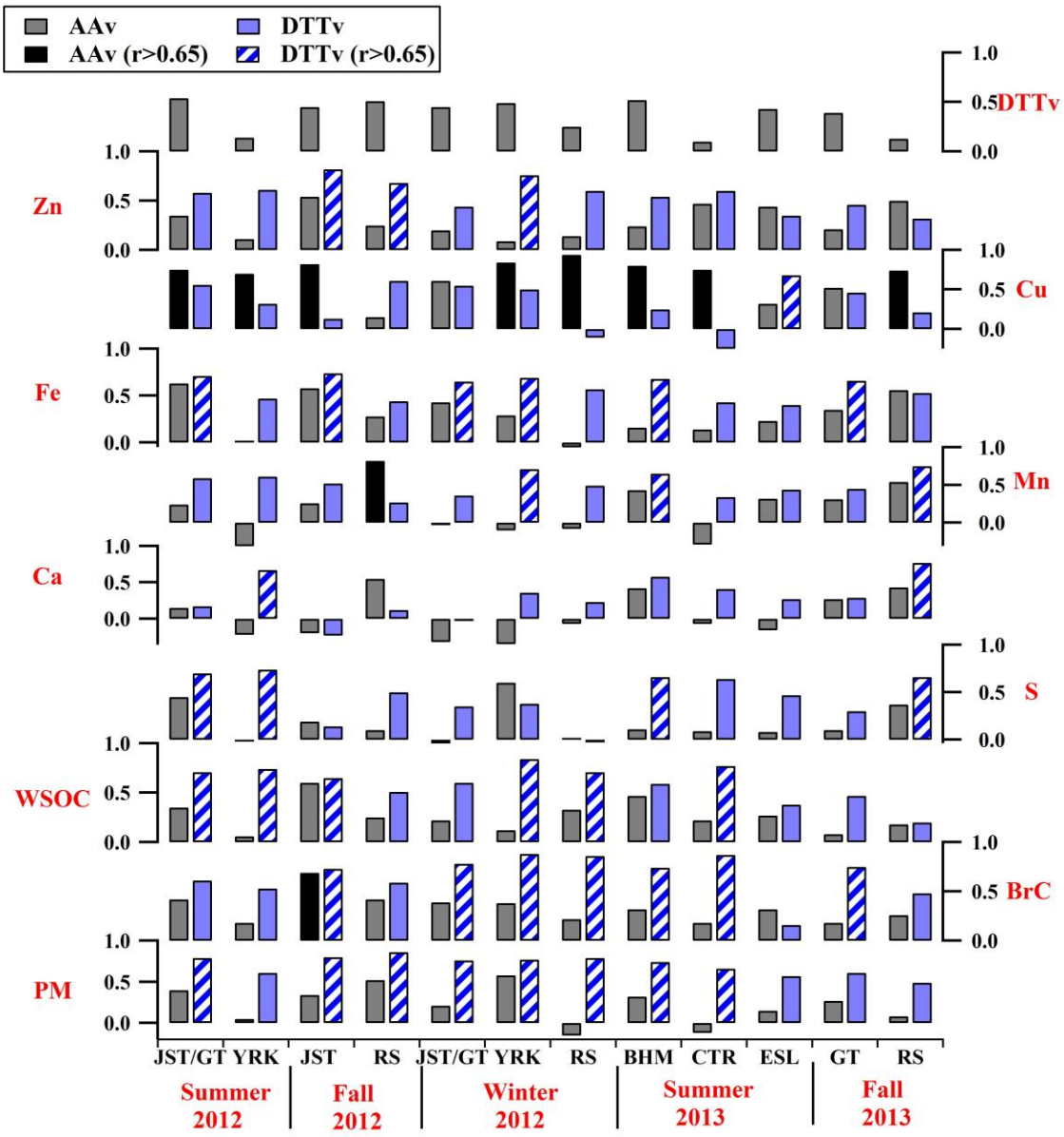

Figure 4-3 Correlation coefficient (Pearson's r) of fine particle water-soluble AA or DTT activities with $PM_{2.5}$ mass and selected chemical species at various sites in the Southeastern US. A more detailed correlation table is provided in Table 4-2.

4.4.1.3 Source apportionment

Various source contributions to water-soluble AAv and DTTv resolved from PMF and CMB-E based on measured data during 2012-2013 are shown in Figure 4-4(a, b) and (c, d), respectively. For AAv, the detailed loadings of various species and time series of each PMF factor can be found in Figure 4-9.

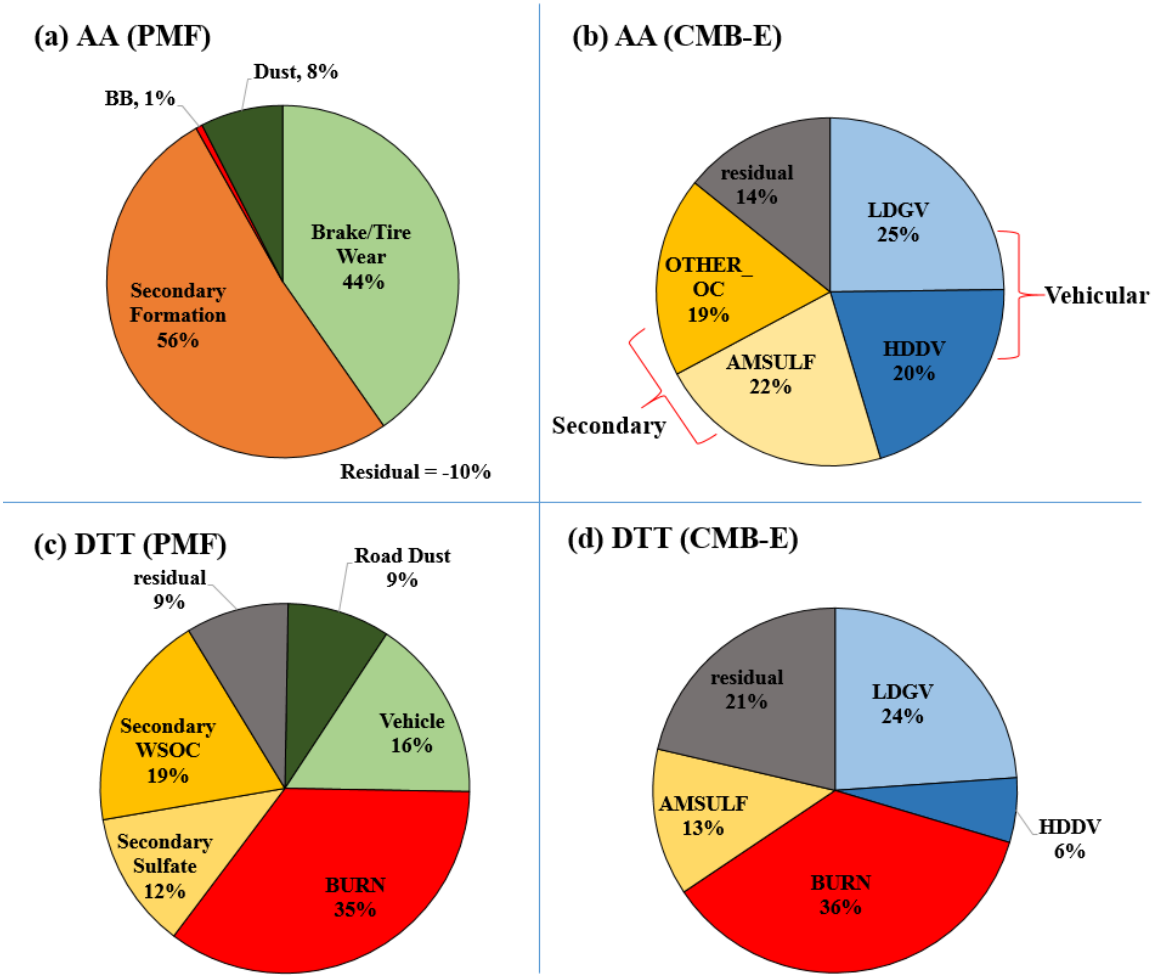

Figure 4-4 Contribution of various factors resolved by PMF (a, c), and ensemble (b, d), to the water-soluble AA (a, b) and DTT (c, d) activities measured during 2012-2013. BURN – biomass burning; AMSULF – ammonium sulfate; HDDV – heavy-duty diesel vehicles; LDGV – light-duty gasoline vehicles; OTHER_OC – other organic

carbon which secondary organic aerosols from biogenic emissions, and possible additional contributions from other VOC sources.

AA Sources: Comparing Figure 4-4 (a) and (b) shows that CMB-E and PMF gave consistent and complementary results for AAv sources. Consistent with the spatial distributions, CMB-E indicated that vehicles comprise almost half of the total source contributions to $PM_{2.5}$ AAv with roughly equal contributions from light and heavy duty vehicles. PMF also found vehicle emissions as a major source, but, based on loadings of source tracers in the various factors, resolved the source as mechanical generation processes (44% from brake/tire wear). Both methods also found sources of AAv associated with secondary processes. CMB-E provides more details on this factor in that it separated out secondary organic and ambient sulfate sources. This is consistent with our source apportionment analyses on water-soluble metals (Fang et al., 2015a), which showed that Cu was mainly associated with secondary formation and brake/tire wear, consistent with AAv being highly correlated with Cu. The 19% other OC source in Figure 4-3(b) is related to un-apportioned OC, which includes secondary organic aerosols from biogenic emissions, and possible additional contributions from other VOC sources. At this point, the role it plays as a source of AAv is not clear. It should be noted that the residual for PMF was -10% and 14% for CMB-E, which means the PMF model over-predicted and CMB-E under-estimated AAv. The source apportionment analysis is consistent with the spatial distribution, which indicated vehicle emissions as a main source for AAv activity.

AAv compared to DTTv Sources: Comparisons of the source apportionment results for water-soluble AAv using PMF and CMB-E to a similar analysis for DTTv is insightful.

PMF source apportionment analyses [Figure 4-4(a) and (c)] suggest a common contribution from traffic emissions and secondary processes to both water-soluble AAv and DTTv, but the contributions were stronger for AAv than DTTv. For example, 44% AAv was attributed to vehicles and 56% to secondary processes, compared to 16% and 31% for DTTv, respectively. Higher fractional contributions of these two sources for AAv is because unlike DTTv, biomass burning does not contribute to AAv (1%), whereas it makes a large contribution to the overall study DTTv (35%). CMB-E also found no contribution of biomass burning to AAv, but identified a fractional contribution from biomass burning [36% BURN in Figure 4-4(d)] to DTTv similar to PMF. CMB-E points to ammonium sulfate (AMSULF) as a source for both AAv and DTTv. Neither AA nor DTT assay responds to pure ammonium sulfate, meaning that ammonium sulfate is an indicator of some source or process. It may be a marker for atmospheric processed or aged aerosols. For example, both assays respond to water-soluble transition metals, and a significant fraction of these metals, when emitted, are not water-soluble [solubilities of Zn is ~50%, Cu and Mn 10-40%, Fe < 10% (Birmili et al., 2006; Espinosa et al., 2002)]. Mobilization by acidic aerosols can increase the soluble fraction, which requires a low aerosol pH and time, both can be linked to sulfate aerosol. For example, at pH < 2, 1-2% of mineral dust Fe is mobilized within 3-5 days (Meskhidze et al., 2003). Previous measurements in this study region have also shown water-soluble Fe associated with sulfate in individual particles (Oakes et al., 2012).

It is worth noting that both assays appear to be linked to emissions from traffic, but the actual sources from traffic differ. AAv was almost exclusively associated with mechanically generated aerosols (i.e. brake/tire wear), whereas for water-soluble DTTv,

traffic emissions included both metals and organic aerosol species, i.e., from mechanically generated (brake/tire wear) and combustion (tailpipe emissions). Finally, correlations to specific aerosol species and source apportionment analysis can be confounded by co-variability with other unmeasured components or processes, as demonstrated by the associations with ammonium sulfate, or nonlinear responses of these assays to specific components (Charrier et al., 2015). However, the major sources identified for both AAv and DTTv, and the contrasts between their sources, is consistent with the season trends and spatial distributions observed and discussed above for each assay, indicating that the source apportionment analysis is robust.

4.4.2 AAv association with health endpoints and contrasts to DTTv

4.4.2.1 Backcast-estimates of AAv using Source Impacts

Although over roughly 1 year of AAv data were generated for the central JST site in Atlanta, longer data sets are generally needed for a time series epidemiological study. To generate these data, multiple linear regression was used to estimate AAv from the CMB-E identified sources (denoted here as AA_v^e). We follow the same approach as that used for DTTv (Bates et al., 2015). Water-soluble AAv (nmol min^{-1} m^{-3}) measured between 2012 and 2013 at JST were regressed against all CMB-E sources. Insignificant sources (p of F-statistic of coefficient>0.05, Table 4-3) and the significant sources with negative coefficients were removed. The latter occurred for BURN (biomass burning) and AMNITR (ammonium nitrate), likely due to their opposite seasonal trends to the measured AAv. These two sources also did not contribute to AAv [see Figure 4-4(a)]. The final regression for AAv is:

AA_v^e=0.079+0.19 LDGV+0.23 HDDV+0.063 AMSULF+0.075 OTHER_OC (Equation 7)

For direct comparison with DTTv, we used the same criteria for including various sources in the DTTv regression model, with the result:

DTT_v^e=0.067+0.11 LDGV+0.045 HDDV+0.02 AMSULF+0.069 BURN (Equation 8)

(Note, the DTT_v^e regression is different from that in Bates et al., (2015) in that AMSULF (ammonium sulfate) was included in this model).

AA_v^e and DTT_v^e are the estimated ROS activities of $PM_{2.5}$ (nmol min^{-1} m^{-3}), which are related to the following sources (μg m^{-3}): light-duty gasoline vehicles (LDGV), heavy-duty diesel vehicles (HDDV), ammonium sulfate (AMSULF), biomass burning (BURN), and other organic carbon (OTHER_OC). The coefficients in the equations represent the intrinsic activities (nmol min^{-1} μg^{-1}) of the sources, a measure of the strength of the source on a per $PM_{2.5}$ mass basis for water-soluble AAv or DTTv. Interestingly, for both assays, the traffic sources (LDGV+HDDV) has the highest ROS intrinsic activity, while secondary sources or biomass burning have relatively lower ROS intrinsic activities. The high intrinsic activity in the traffic sources might be attributed to metals that have much higher intrinsic ROS activities (Charrier and Anastasio, 2012; Verma et al., 2015a). The much higher coefficients of LDGV and HDDV in the AA_v^e regression than those in DTT_v^e highlight the larger role of metals from these sources contributing to the overall AA_v^e. Although biomass burning has a lower DTT intrinsic activity compared to the other sources in the DTT_v^e model, it was the largest contributor to DTT_v^e due to the strength of this source over the measurement period (e.g., large magnitude of BURN). The regression positive intercepts indicate some unidentified source for AAv and DTTv. Insight on the ability of the models

to predict AA_v^e and DTT_v^e is given by the correlation between the model and measurements (AA_v^e vs AAv and DTT_v^e vs DTTv). The r values are 0.60 and 0.68 for AA_v^e and DTT_v^e, respectively, indicating the models can only account for about 40% (r^2 or 36 to 46%) of the observed variability. Regression coefficients, p-values, and r values are summarized in section 4.6 Table 4-3.

To test the sensitivity of the epidemiological results to other predictive models, two other regressions were used to predict AAv and DTTv: 1) all sources included, 2) only significant sources with positive coefficients (above), but with AMSULF removed. The latter was done because sulfate has substantially decreased over the last decade due to emission reductions in the southeastern US (Hidy et al., 2014; Hand et al., 2012), which may have unknown effects on AA_v^e and DTT_v^e. These models and various statistics are also summarized in Table S3. For both assays, the models with all sources included had highest correlations coefficients between model and observed activities (r ~ 0.7, or model explains ~50% of the variability).

4.4.2.2 Health associations from time-series epidemiological models

Backcast AA_v^e and DTT_v^e were next generated for the study period corresponding to the health (ED) data. The various regression models (including Equation.7 and 8) were used to generate daily retrospective estimates of AAv and DTTv at the JST site for the period of 1998-2009, based on existing source impacts generated in a previous study for the same site. AA_v^e and DTT_v^e were run separately in epidemiological models of ED visits for selected outcomes (section 4.3.5.2). The risk ratios for AA_v^e and DTT_v^e for asthma/wheeze and congestive heart failure are presented in Figure 4-5 (data given in Table 4-4). The other

health outcomes (chronic obstructive pulmonary disease, pneumonia, and ischemic heart disease) did not show significant associations with AA_v^e or DTT_v^e (results given in Table 4-4).

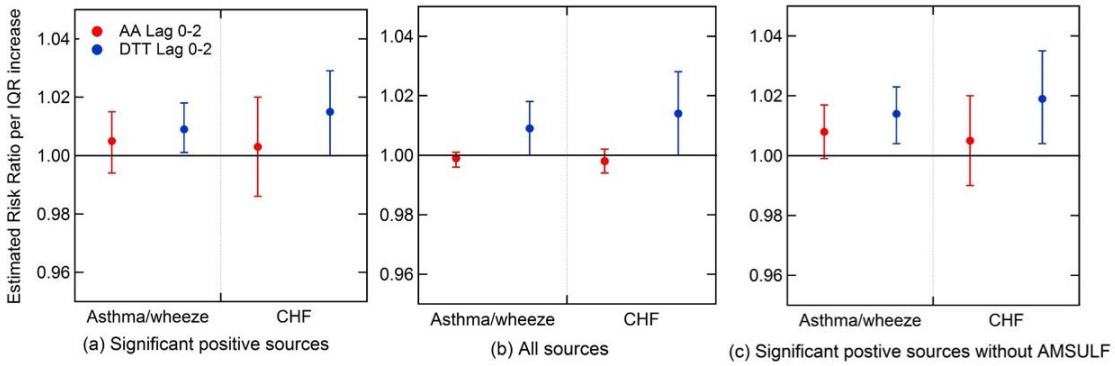

Figure 4-5 Associations between backcast-estimated AA and DTT activities based on estimated sources for the previous 10 years (1998-2009) and emergency department (ED) visits for asthma/wheeze and congestive heart failure (CHF) in the greater metropolitan Atlanta, GA, region. The estimated AA and DTT were based on linear regression models that include (a) only statistically significant (p of F-statistic of coefficient<0.05) sources with positive coefficients; (b) all sources; and (c) significant positive sources without AMSULF (ammonium sulfate). The models were generated from a multiple regression of the measured AA activities or DTT, on a per volume air bases, with all sources from CMB-E as independent variables. Risk ratios and associated 95% confidence intervals are presented for an increase of one interquartile range (IQR) increment of the exposure metric. A risk ratio with 95% confidence intervals (CI) for interquartile range above 1 indicates a statistically significant positive association. Risk ratio data and related statistics can be found in Table 4-4**.**

For asthma/wheeze and congestive heart failure, although the risk ratios for an increase of an interquartile range for AA_v^e were above 1 [1.005 and 1.003 for Asthma/wheeze and CHF, respectively, Figure 4-5(a)], the 95 % confidence intervals crossed 1 (0.994-1.015 and 0.986-1.020 for Asthma/wheeze and congestive heart failure, respectively), indicating a

non-statistically significant association between AA_v^e and the ED visits for these health outcomes. In contrast, both of the health outcomes showed statistically significant associations with the DTT_v^e. The same results were found for estimates based on the two other regressions [Figure 4-5(b) and (c)], suggesting that the null relationship of AA_v^e and positive association of DTT_v^e with these health outcomes are to some extent robust, despite the high uncertainties in oxidative potential from the back-cast models. A possible cause for the differences in AA_v^e and DTT_v^e health associations, at least for this study region, is the more narrow selectivity of the AA assay to specific aerosol components (i.e., mostly sensitive to Cu). Thus, the AA assay may not capture the overall oxidative potential of all the various PM components as well as the DTT assay.

PM-induced oxidative stress has been proposed to exacerbate asthma (Li et al., 2003a) and adverse cardiovascular responses (Donaldson et al., 2001). Linkages seen here between $PM_{2.5}$ oxidative potential measured with the DTT assay and morbidity due to asthma/wheeze and congestive heart failure are consistent with these studies. Our results are also consistent with a recent study which found children's respiratory health was more strongly associated with oxidative potential measured with the DTT assay than by electron spin resonance (ESR) (Yang et al., 2016); the ESR assay has been shown to be highly correlated with AA-measured oxidative potential (Janssen et al., 2014). However, their sample preparation method before oxidative potential measurements involves extracting the particles in pure methanol, evaporating the methanol, and reconstituting in DI water, whereas our work focuses only on the water-soluble fraction. The contrast between the DTT with the AA results suggest the importance of organic components and transition metals from biomass burning and vehicular emissions in the Southeastern US, and support

aerosol particle oxidative potential as a mechanism contributing to these PM-induced adverse health effects. Although this work shows a contrast between these two assays and association with health endpoints, Janssen et al. (2015) found significant associations between both assays and nasal and airway inflammation based on a small panel study (n=31). Finally, some studies have shown that ROS plays a key role in COPD (O'Donnell et al., 2006), IHF (Lakshmi et al., 2009; Giordano, 2005), and Pneumonia (Kuwano et al., 2003), however, we did not observe a significantly positive association between our tested oxidative potential assays with these health outcomes.

4.5 Conclusions

Approximately 500 $PM_{2.5}$ high-volume filter samples collected in the Southeastern US were analyzed for aerosol oxidative potential using the ascorbic acid (AA) assay. The AA activities reported are from the same filters for which water-soluble dithiothreitol (DTT) activities had already been determined. We found that water-soluble AA activity on a per air volume basis (AAv) was highest near roadways and lowest at rural sites. AAv was higher in summer/fall than winter. These results are in contrast to DTTv, which was more spatially uniform and had an opposite seasonal trend at the urban Atlanta site (higher in winter than summer/fall). AAv was most consistently correlated with water-soluble metals (especially water-soluble Cu), whereas DTTv was correlated with organic species and water-soluble metals (Fe, Cu, Zn, Mn, and Ca), and also $PM_{2.5}$ mass. A source apportionment analysis indicated that traffic emissions and secondary processes were strong contributors to both AAv and DTTv in urban Atlanta. For AAv only road dust was responsible, in contrast to both combustion emissions and road dust contributing to the DTTv from this source. Biomass burning did not contribute to AAv, but was a substantial

source for DTTv, consistent with AAv being mainly associated with transition metals. These source apportionment results are also consistent with observed seasonal trends and spatial distributions for both assays. Time-series large population epidemiological analyses using backcast-estimates of AAv and DTTv from a number of linear models based on 10-year historical source impacts suggest that AAv was not linked with any emergency department (ED) visits for all tested health outcomes at 95% confidence levels. DTTv was associated with ED visits for both asthma/wheeze and congestive heart failure, for all the linear models tested. Neither AAv nor DTTv was associated with chronic obstructive pulmonary disease (COPD), Ischemic heart failure (IHD) or pneumonia at a statistically significant level. Based on the wide-ranging comparisons between these assays, we conclude that, for the region investigated here, the DTT assay was a more comprehensive multi-pollutant indicator of $PM_{2.5}$ oxidative potential than the AA assay. Finally, the ability to readily measure both $PM_{2.5}$ AA and DTT activities with the automated systems outlined here enables large-scale studies involving direct measurements of PM oxidative potential. These types of future studies are needed to test if our health findings based on backcast-estimated AA and DTT levels are robust and applicable to other regions.

4.6 Supporting materials

Table 4-1 Sampling schedule of Hi-Vol filters collected from June 2012 to September 2013.

Month Year	Season	Anchor site	Trailer site
June-July 2012	Summer	JST	YRK
July-August 2012	Summer	JST	GT
September-October 2012	Fall	JST	RS
November 2012	-	JST	JST
December 2012	Winter	JST	YRK
January-February 2013	Winter	JST	RS
March 2013	Winter	JST	GT
June-July 2013	Summer	CTR	BHM
August 2013	Summer	ESL	-
September-October 2013	Fall	GT	RS

JST - Southeastern Aerosol Research and Characterization Study (SEARCH) Jefferson Street, GA; YRK - SEARCH Yorkville, GA; GT - Georgia Tech, GA; RS - Roadside (on Georgia Tech Campus); BHM - SEARCH Birmingham, AL; CTR - SEARCH Centerville, AL; ESL - East St. Louis, IL.

Table 4-2 Water-soluble AA and DTT activity correlations (Pearson's r) with water-soluble species in $PM_{2.5}$

	Site-Month. Year	BrC	WSOC	PM	S	K	Ca	Ti	Mn	Fe	Cu	Zn	As	Se	Br	Sr	Ba	Pb	DTT
	JST-June 2012	0.58	0.59	0.59	0.47	0.23	0.35	0.58	0.41	0.64	**0.91**	0.52	**0.74**	0.49	0.36	0.37	0.52	0.42	0.57
	JST-Aug. 2012	0.43	0.36	0.08	0.32	0.32	0.04	0.59	**0.65**	0.60	**0.74**	0.23	0.37	0.30	0.56	0.30	0.61	0.43	0.52
	JST-Sept. 2012	**0.69**	0.60	0.34	0.19	0.26	-0.20	0.48	0.26	0.58	**0.82**	0.54	**0.71**	0.23	0.21	0.16	0.34	0.47	0.45
	JST- Dec. 2012	0.42	**0.65**	0.56	-0.12	**0.70**	0.24	0.36	0.28	**0.66**	**0.81**	0.66	0.64	0.27	0.28	0.35	0.60	0.49	**0.70**
	JST-Feb. 2013	0.38	0.30	0.36	0.16	0.18	-0.21	-0.15	-0.06	0.14	0.29	-0.09	0.02	0.25	0.34	-0.15	-0.18	0.32	0.49
	JST-March 2013	-0.03	-0.03	-0.17	0.01	0.19	-0.08	-0.15	0.02	0.30	**0.78**	0.23	0.24	0.14	-0.30	-0.13	0.08	0.26	0.10
	GT-Aug. 2012	0.57	0.10	0.58	0.55	0.41	0.12	0.44	0.10	**0.77**	**0.75**	0.13	0.61	0.51	0.49	0.03	0.38	0.16	0.62
	GT-March 2013	0.43	0.47	0.40	0.05	0.37	0.06	0.05	0.37	0.36	0.63	0.36	0.03	0.40	0.31	-0.01	0.38	0.16	0.54
AA	GT-Sept 2013	0.18	0.08	0.27	0.10	0.32	0.27	0.38	0.37	0.35	0.52	0.18	0.17	0.07	0.33	0.10	0.45	0.07	0.39
	RS-Sept.2012	0.42	0.25	0.52	0.10	**0.72**	0.55	0.27	**0.82**	0.28	0.15	0.25	-0.29	0.17	0.28	**0.71**	0.49	-0.16	0.51
	RS-Feb.2013	0.22	0.13	-0.15	0.01	0.15	-0.07	0.17	-0.08	-0.05	**0.94**	0.14	-0.03	0.01	-0.04	0.12	0.14	-0.14	0.25
	RS-Sept 2013	0.26	0.18	0.08	0.37	0.58	0.43	0.52	0.54	0.56	**0.74**	0.50	0.33	0.21	0.67	0.06	0.62	0.40	0.13
	YRK-June.2012	0.18	0.06	0.05	-0.02	0.24	-0.22	-0.23	-0.31	0.00	**0.70**	0.11	0.02	0.06	0.27	-0.25	-0.24	0.17	0.14
	YRK-Dec.2012	0.38	0.12	0.58	0.60	0.07	-0.35	0.04	-0.10	0.29	**0.84**	0.09	0.27	0.39	0.10	-0.28	-0.04	0.54	0.49
	BHM-June 2013	0.32	0.47	0.32	0.11	0.46	0.42	0.15	0.43	0.16	**0.80**	0.24	-0.01	-0.04	0.09	0.19	0.08	-0.04	0.52
	CTR-June 2013	0.18	0.22	-0.12	0.09	0.12	-0.07	0.03	-0.29	0.14	**0.75**	0.47	0.27	0.15	0.19	-0.41	-0.24	0.38	0.10
	ESL-Aug 2013	0.32	0.27	0.15	0.08	0.17	-0.16	0.09	0.32	0.23	0.32	0.44	0.18	0.31	0.17	-0.14	0.00	0.20	0.43
	JST-June 2012	**0.77**	**0.91**	**0.85**	**0.74**	**0.71**	0.59	**0.66**	0.63	0.62	0.53	0.58	0.36	**0.69**	**0.72**	0.50	0.49	0.61	1
	JST-Aug. 2012	**0.66**	0.62	**0.80**	**0.77**	0.48	0.06	**0.68**	**0.77**	**0.90**	**0.79**	0.59	0.42	**0.74**	**0.79**	0.36	**0.65**	**0.71**	1
	JST-Sept. 2012	**0.73**	**0.65**	**0.80**	0.14	0.30	-0.23	0.53	0.52	**0.74**	0.13	**0.82**	0.13	0.20	0.28	0.10	0.55	0.27	1
	JST- Dec. 2012	**0.81**	**0.78**	**0.75**	0.07	**0.73**	0.51	0.55	0.54	**0.79**	0.63	**0.82**	**0.67**	0.43	0.38	0.39	**0.73**	0.59	1
	JST-Feb. 2013	**0.70**	**0.65**	**0.84**	**0.70**	**0.71**	0.25	-0.02	0.33	**0.70**	0.37	0.30	0.19	**0.66**	**0.77**	0.16	0.13	**0.75**	1
	JST-March 2013	**0.88**	0.63	**0.77**	0.05	**0.67**	0.26	0.63	0.51	0.57	0.36	0.58	**0.78**	**0.69**	0.44	0.44	0.58	0.52	1
	GT-Aug. 2012	0.37	0.38	0.63	0.59	0.53	0.00	0.26	0.60	**0.77**	**0.67**	0.62	0.54	0.52	0.45	0.35	0.53	0.09	1
	GT-March 2013	**0.83**	0.49	**0.88**	0.34	**0.78**	0.11	0.23	**0.71**	**0.84**	**0.83**	**0.70**	0.61	**0.74**	0.61	0.33	0.63	0.36	1
DTT	GT-Sept 2013	**0.75**	0.47	0.61	0.30	**0.65**	0.29	0.34	0.58	**0.66**	0.46	0.36	0.22	0.20	0.50	0.15	0.38	0.23	1
	RS-Sept.2012	0.59	0.51	**0.86**	0.50	0.52	0.12	0.51	0.27	0.44	0.61	0.55	-0.06	0.39	0.61	0.36	0.56	0.35	1
	RS-Feb.2013	**0.86**	0.71	**0.79**	-0.03	**0.69**	0.23	0.32	0.49	0.57	-0.11	0.60	0.63	0.33	0.57	0.20	0.34	0.34	1
	RS-Sept 2013	0.48	0.20	0.49	**0.66**	0.53	**0.77**	0.09	**0.75**	0.53	0.21	0.32	-0.13	0.41	0.64	0.16	0.29	-0.51	1
	YRK-June.2012	0.53	**0.74**	0.59	**0.74**	0.60	**0.67**	0.23	0.61	0.47	0.32	0.61	0.36	**0.67**	0.59	**0.73**	0.19	0.56	1
	YRK-Dec.2012	**0.88**	**0.84**	**0.77**	0.38	**0.74**	0.36	0.31	**0.71**	**0.69**	0.50	**0.76**	0.39	**0.83**	**0.73**	0.32	0.49	**0.74**	1
	BHM-June 2013	**0.74**	0.59	**0.74**	**0.66**	0.42	0.58	0.29	**0.65**	**0.68**	0.25	0.54	0.45	0.60	**0.69**	0.27	0.21	0.49	1
	CTR-June 2013	**0.87**	**0.77**	**0.66**	0.64	**0.66**	0.41	0.36	0.34	0.43	-0.25	0.60	0.47	0.62	0.62	0.03	0.12	0.61	1
	ESL-Aug 2013	0.16	0.38	0.57	0.47	0.48	0.27	0.17	0.44	0.40	**0.68**	0.35	0.52	0.41	0.51	0.25	0.44	0.36	1

r>0.65 in red and bold; Data below LOD was replaced by half of LOD values.

Table 4-3 Water-soluble AA and DTT regressions with all CMB-E sources, with only significant (positive) sources, and with only significant (positive) sources without AMSULF

	Regressions		Intercept	LDGV	HDDV	SDUST	BURN	AMSULF	AMBSLF	AMNITR	OTHER_OC	*r
AA	All sources	Coefficient	0.19 ± 0.059	0.31 ± 0.046	0.28 ± 0.062	-0.020 ± 0.029	-0.098 ± 0.029	0.078 ± 0.020	0.018 ± 0.032	-0.088 ± 0.039	0.060 ± 0.020	0.71
		p-value	<0.01	<0.01	<0.01	0.50	<0.01	<0.01	0.59	0.03	<0.01	
	Significant sources	Coefficient	0.17 ± 0.055	0.32 ± 0.044	0.32 ± 0.060		-0.14 ± 0.023	0.076 ± 0.019		-0.077 ± 0.035	0.072 ± 0.019	0.69
		p-value	<0.01	<0.01	<0.01		<0.01	<0.01		0.03	<0.01	
	Significant positive sources	Coefficient	0.079 ± 0.058	0.19 ± 0.043	0.23 ± 0.064			0.063 ± 0.021			0.075 ± 0.075	0.60
		p-value	0.18	<0.01	<0.01			<0.01			<0.01	
	Significant positive sources without AMSULF	Coefficient	0.18 ± 0.047	0.19 ± 0.044	0.24 ± 0.066						0.083 ± 0.022	0.57
		p-value	<0.01	<0.01	<0.01						<0.01	
DTT	All sources	Coefficient	0.050 ± 0.025	0.11 ± 0.021	0.038 ± 0.028	0.012 ± 0.012	0.065 ± 0.012	0.023 ± 0.009	0.015 ± 0.016	-0.001 ± 0.017	0.004 ± 0.010	0.69
		p-value	0.048	<0.01	0.17	0.32	<0.01	0.011	0.35	0.94	0.68	
	Significant sources	Coefficient	0.067 ± 0.02	0.11 ± 0.02	0.045 ± 0.024		0.063 ± 0.01	0.022 ± 0.01				0.68
		p-value	<0.01	<0.01	0.07		<0.01	0.01				
	Significant sources without AMSULF	Coefficient	0.095 ± 0.018	0.11 ± 0.020	0.052 ± 0.024		0.069 ± 0.010					0.67
		p-value	<0.01	<0.01	0.04		<0.01					

*- r value represents the correlations between measured and predicted data.

The sources are light-duty gasoline vehicles (LDGV), heavy-duty diesel vehicles (HDDV), soil dust (SDUST), biomass burning (BURN), ammonium sulfate (AMSULF), ammonium bisulfate (AMBSLF), ammonium nitrate (AMNITR), and other organic carbon (OTHER_OC) which mostly contains biogenic carbon.

Table 4-4 Risk ratios (95% confidence interval for interquartile range) and p-values for backcast-estimated AA and DTT activities (1998-2009) from the epidemiological analyses on asthma/wheeze, congestive heart failure (CHF), Chronic obstructive pulmonary disease (COPD), Ischemic heart disease (IHD), and Pneumonia

	Regressions	Asthma/wheeze (AS_WHZ)		Congestive heart failure (CHF)	
		Lag 0-2		Lag 0-2	
AA	**All sources**	0.999 (0.997-1.002)	p=0.64	0.998 (0.994-1.002)	p=0.29
	Significant positive sources	1.005 (0.994-1.015)	p=0.38	1.003 (0.986-1.020)	p=0.74
	Significant positive sources without AMSULF	1.008 (0.999-1.017)	p=0.07	1.005 (0.990-1.020)	p=0.50
DTT	**All sources**	1.009 (1.000-1.018)	p=0.04	1.014 (1.000-1.028)	p=0.05
	Significant positive sources	1.009 (1.001-1.018)	p=0.04	1.015 (1.000-1.029)	p=0.04
	Significant positive sources without AMSULF	1.014 (1.004-1.023)	p=0.01	1.019 (1.004-1.035)	p=0.01

	Regressions	Chronic obstructive pulmonary disease (COPD)		Ischemic heart disease (IHD)		Pneumonia	
		Lag 0-2		Lag 0-2		Lag 0-2	
AA	**All sources**	0.997 (0.992-1.002)	p=0.25	0.996 (0.993-1.000)	p=0.05	0.998 (0.995-1.001)	p=0.18
	Significant positive sources	1.010 (0.992-1.028)	p=0.29	0.991 (0.976-1.006)	p=0.25	0.996 (0.985-1.006)	p=0.38
	Significant positive sources without AMSULF	0.996 (0.979-1.013)	p=0.63	0.989 (0.975-1.003)	p=0.11	0.992 (0.982-1.002)	p=0.13
DTT	**All sources**	1.008 (0.991-1.025)	p=0.35	0.989 (0.975-1.002)	p=0.10	0.997 (0.987-1.006)	p=0.50
	Significant positive sources	0.996 (0.976-1.016)	p=0.67	0.983 (0.967-0.998)	p=0.03	0.994 (0.982-1.006)	p=0.29
	Significant positive sources without AMSULF	1.007 (0.990-1.024)	p=0.40	0.989 (0.976-1.002)	p=0.11	0.997 (0.988-1.007)	p=0.57

The AA and DTT activities were estimated from three different linear regressions including all sources from CMB-E, statistically significant (p of F-statistic of coefficient<0.05) sources with positive coefficients, and significant positive sources without AMSULF (ammonium sulfate).

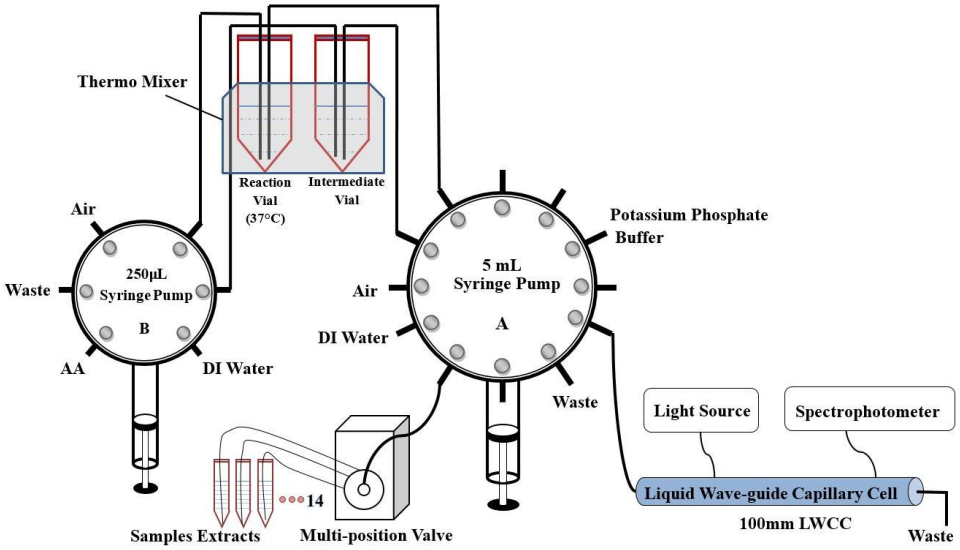

Figure 4-6 Semi-automated system setup for Ascorbic Acid activities determination

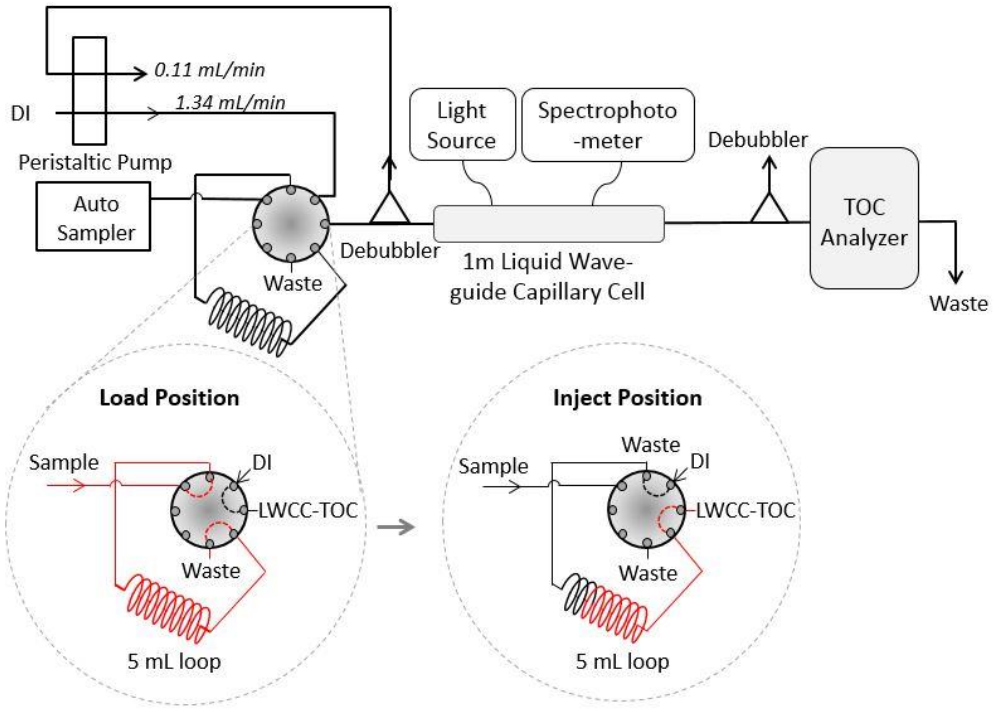

Figure 4-7 Automated system that utilized an auto-sampler (AS40, DIONEX Corporation, Sunnyvale, CA, USA), a SelectPro two-position fluid processor valve (Alltech, Deerfield, IL, USA), and a peristaltic pump (Ismatec, Cole-Parmer Instrument Company, Vernon Hills, IL, USA) for measuring water-soluble organic carbon (WSOC) and brown carbon (BrC) from aqueous extracts.

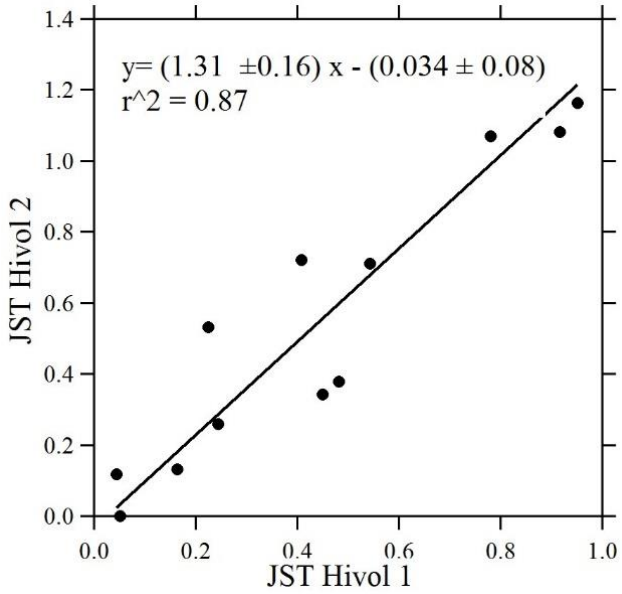

Figure 4-8 Collocated measurements using two Hi-Vol samplers deployed at JST during November 2012 (Analysis was done by orthogonal regression.)

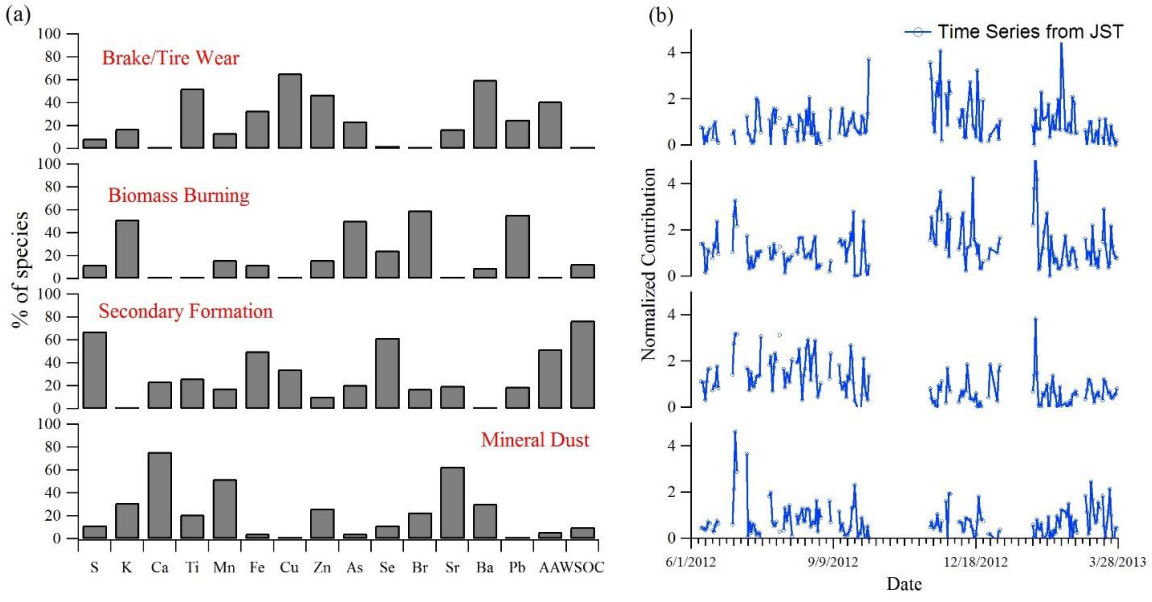

Figure 4-9 Loading of various water-soluble species and AA activity into various factors resolved by PMF analyses for all Atlanta urban sites (JST, GT, and RS) (a) and factors' time series (b) from the JST site.

CHAPTER 5. HIGHLY ACIDIC AMBIENT PARTICLES, SOLUBLE METALS AND OXIDATIVE POTENTIAL: A LINK BETWEEN SULFATE AND AEROSOL TOXICITY

Ting Fang
Hongyu Guo
Linghan Zeng
Vishal Verma
Athanasios Nenes
Rodney J. Weber

Environ. Sci. Technol., 51, 2611–2620, 2017
doi: 10.1021/acs.est.6b06151

5.1 Abstract

Soluble transition metals in particulate matter (PM) can generate reactive oxygen species *in vivo* by redox cycling, leading to oxidative stress and adverse health effects. Most metals, such as those from roadway traffic, are emitted in an insoluble form but must be soluble for redox cycling. Here we present the mechanism of metals dissolution by highly acidic sulfate aerosol and the effect on particle oxidative potential (OP) through analysis of size distributions. Size-segregated ambient PM was collected from a road-side and representative urban site in Atlanta, GA. Elemental and organic carbon, ions, total and water-soluble metals, and water-soluble OP were measured. Particle pH was determined with a thermodynamic model using measured ionic species. Sulfate was spatially uniform and found mainly in the fine mode, whereas total metals and mineral dust cations were highest at the road-side site and in the coarse mode, resulting in a fine mode pH<2 and near neutral coarse mode. Soluble metals and OP peaked at the intersection of these modes demonstrating that sulfate plays a key role in producing highly acidic fine aerosols capable of dissolving primary transition metal ions that contribute to aerosol OP. Sulfate-driven metals dissolution may account for sulfate-health associations reported in past studies.

5.2 Introduction

Although a substantial number of studies have supported the association between particulate matter (PM) and adverse health outcomes (Metzger et al., 2004; Pope et al., 2004; Samet et al., 2000), many questions remain on the underlying drivers of PM toxicity. Oxidative stress, an *in vivo* state of disequilibrium due to an imbalance between antioxidant defense capacity and reactive oxygen species (ROS), has been suggested as a mechanistic

explanation for PM toxicity (Nel, 2005; Xia et al., 2006; Valavanidis et al., 2008). Oxidative potential (OP), referred to as the ability of particles to generate ROS by consumption of antioxidants and/or generation of oxidants, has been used as a health-based exposure measure of PM in several recent studies (Bates et al., 2015; Yang et al., 2016; Akhtar et al., 2010; Ayres et al., 2008; Weichenthal et al., 2016b). Methods to measure OP include cellular (Xia et al., 2006; Kubátová et al., 2006) and acellular assays (Mudway et al., 2011; Jung et al., 2006; Cho et al., 2005; Venkatachari et al., 2005; Frampton et al., 1999). Cellular assays involve culturing and exposing cells, whereas acellular assays generally involve more straightforward chemical analysis making them easier to perform and automate. The ascorbic acid (AA) (OP^{AA}) and dithiothreitol (DTT) (OP^{DTT}) assays are two commonly used acellular measures of aerosol OP. AA is a physiological antioxidant present in the lung and DTT is used as a chemical surrogate of antioxidants, such as glutathione and NADPH. Both assays measure the depletion of AA or DTT through oxidation under biological relevant temperature of 37 °C and pH of 7.4, mimicking the interaction between PM and cellular antioxidants *in vivo*, providing an index of PM's ability to generate ROS. OP^{DTT} has been widely used. It has been linked to airway inflammation markers (Delfino et al., 2013), cellular oxidative stress markers (Li et al., 2003b), cellular cytotoxicity (Steenhof et al., 2011; Velali et al., 2016), and more recently, cardiorespiratory health endpoints in epidemiological studies (Bates et al., 2015; Yang et al., 2016). These results support the use of OP as a highly health relevant air quality parameter.

To mitigate adverse health effects, ambient particle OP sources, and atmospheric transformations that alter OP, need to be known. A number of aerosol components have

been found to correlate with aerosol OP^{DTT}. These include bulk water-soluble organic carbon (WSOC) (Saffari et al., 2014a; Verma et al., 2014; Fang et al., 2016), humic-like substances (HULIS) (Dou et al., 2015; Lin and Yu, 2011) and highly oxygenated organic aerosols (Verma et al., 2015a), and more specific aerosol components, such as polycyclic aromatic hydrocarbons (PAHs) (Cheung et al., 2010; Ntziachristos et al., 2007; Saffari et al., 2014a), quinones (Sauvain et al., 2015; Kumagai et al., 2002), and water-soluble transition metals (e.g., manganese (Mn) and copper (Cu) (Charrier and Anastasio, 2012; Verma et al., 2014; Sauvain et al., 2015; Saffari et al., 2014a; Fang et al., 2016)). Source apportionment points to incomplete combustion from biomass and fossil fuels (gas and diesel engines), and sources associated with transition metals, such as mineral dust and resuspended road dust from tire or brake wear (Fang et al., 2016; Verma et al., 2014). In contrast to OP^{DTT}, correlations suggest that transition metals (i.e., Cu) are the main aerosol component contributing to OP^{AA}, with road-traffic a major source (Mudway et al., 2004; Fang et al., 2016). In past studies, both $OP^{DTT}$and OP^{AA} source apportionment found a significant contribution from sources associated with sulfate. Since the AA and DTT assays do not respond to pure sulfate, these associations suggest that secondary processing related to sulfate sources is driving the correlations.

Mechanistic studies have linked increased OP to secondary atmospheric reactions. For example, although correlated with OP^{DTT}, PAHs are not DTT active, but PAHs can be oxidized to redox-active quinones or nitro-PAHs (Cho et al., 2005). Highly oxygenated aromatic compounds, such as hydroxyquinones, make significant contributions to OP^{DTT} (Verma et al., 2015b), consistent with OP^{DTT} correlations to WSOC and highly oxygenated OA. Aged diesel exhaust PM showed higher OP^{DTT} than fresh diesel exhaust emissions

and the OP^{DTT}increased with time (Li et al., 2009). Secondary processing also applies to transition metals, which as noted are common drivers of both OP^{DTT} and OP^{AA}. Metals sources include industry (Quiterio et al., 2004), vehicles (Lough et al., 2005; Manoli et al., 2002), mineral dust (Manoli et al., 2002), and ship engine emissions(Moldanová et al., 2009; Oeder et al., 2015) which are emitted mainly in an insoluble form. Ambient aerosol water-soluble fractions of Cu and Mn range between 10 to 40 %, and less than 10 % for iron (Fe), even after atmospheric processing (Birmili et al., 2006; Espinosa et al., 2002), suggesting that concentrations of water-soluble forms are limited by the atmospheric conversion process. Thus, to contribute to OP, primary insoluble metals must undergo some form of atmospheric processing to become soluble, a state that could be arrived at by acidification (Nenes et al., 2011; Shi et al., 2011; Meskhidze et al., 2003) or complexation with an organic ligand (Paris and Desboeufs, 2013; Xu and Gao, 2008). Soluble metals, such as Fe and Cu participate in redox cycling reactions, which may lead to enhanced lipid peroxidation, DNA damage, and altered calcium and sulfhydryl homeostasis (Valko et al., 2005; Stohs and Bagchi, 1995; Valavanidis et al., 2005). Common mechanisms involve the Fenton reaction that catalytically converts hydrogen peroxide to the more toxic hydroxyl radicals (Liochev and Fridovich, 2002; Valavanidis et al., 2000). Epidemiological studies have found associations of water-soluble transition metals with health endpoints, such as reductions in birth weight (Darrow et al., 2011) and preterm birth (Darrow et al., 2009).

Sulfate, as a main component of $PM_{2.5}$, has shown a strong association with mortality in many studies (Dockery et al., 1993; Pope et al., 1995; Sarnat et al., 2008; Feng et al., 2000; Maynard et al., 2007). Sulfate contributes to aerosol acidity (Waldman et al., 1990) and there is a historical record of associations between so-called particle “strong acidity”

(Spengler et al., 1989; Koutrakis et al., 1992; Koutrakis et al., 1988; Appel et al., 1980) and adverse health effects (Dockery et al., 1996; Thurston et al., 1994; Gwynn et al., 2000; Raizenne et al., 1996b; Spengler et al., 1996; Thurston et al., 1991). Since fine particle OP has been linked to aerosol toxicity, and water-soluble transition metals and sulfate sources correlated with OP, it may be that sulfate linkages to health are largely through its role in acid dissolution of primary metals commonly found in ambient particles. Here we investigate metals dissolution and its effect on OP by measuring the size distributions of aerosol chemical species to predict particle pH and compare to water-soluble and total metals, and measures of OP.

5.3 Methods

5.3.1 Sample collection

Size-fractionated aerosol samples were collected at a road-side and urban site in Atlanta, GA using two Micro-Orifice Uniform Deposit Impactors (MOUDI, MSP Corp., Shoreview, MN, USA). The road-side site (RS) was adjacent (within 5 meters) to the interstate I75/85 highway that passes through downtown Atlanta and is highly utilized by light duty vehicles due to heavy duty vehicle (trucks with six wheels or more) restrictions. The 75/85 interstate-connector in Atlanta had an annual average daily traffic of 301,000 vehicles in 2015, making it one of the busiest corridors in the US (http://geocounts.com/gdot/). For contrast, the urban site (GT) was located on the rooftop of the Environmental Science and Technology building on the Georgia Tech campus roughly 420 meters from the RS site. The MOUDIs collected samples in a non-rotating mode without a back-up filter and divided particles into ten different size bins under

ambient conditions (e.g., RH and T). Aerodynamic particle diameters at 50% collection efficiency for the stages (so-called cut-off sizes) were 18, 10, 5.6, 3.2, 1.8, 1.0, 0.56, 0.32, 0.18, 0.1, and 0.056 μm. Particles with sizes between these cutoffs are collected on separate stages. Two sets of samples were collected at each site, with one set using particle collection impaction substrates of pre-baked quartz filters (47 mm Tissuquartz™ Filters, Pall Corp., Ann Arbor, MI, USA) and the other Zefluor filters (47 mm, PTFE Membrane, 2 μm pore size, Pall Corp., Ann Arbor, MI, USA). For each MOUDI, sampling was conducted for approximately 7 days continuously. The GT set was collected on 3/16-3/23/2016 and RS set 3/28-4/4/2016. These samples were analyzed for various PM chemical components, including organic carbon (OC), elemental carbon (EC), anions, cations, and total and water-soluble Fe, Cu, and Mn, as well as OP. Four other sets of MOUDI samples were collected at each site for OP analysis only, and two out of these four sets were sampled at both sites simultaneously. Collected filter samples were immediately sealed in Petri dishes and stored at −18 °C until analyzed, which typically occurred within 3 days following collection, except for metals analysis, which was done after a 2-month storage period.

5.3.2 PM chemical components

Each quartz filter from the MOUDI samples was cut into portions for determining various chemical components. A 1.5 cm^2 portion was used for OC and EC thermal optical determination using a Sunset OCEC Analyzer (Sunset Laboratory Inc., Tigard, OR, IMPROVE method). Another same size portion was extracted with DI water and filtered (0.45 μm syringe filter) for ion measurement via ion chromatography with conductivity detection (Metrohm 761 Compact ICs, Riverside, FL, USA). The remaining fraction of the

filter was cut in half and analyzed for total and water-soluble metals using an Inductively Coupled Plasma Mass Spectrometry (ICP-MS) (Agilent 7500a series, Agilent Technologies, Inc., CA, USA). Details on how the mass was determined on divided filters and how the OCEC analysis was done on MOUDI samples is provided in the Appendix A.5.

For determining total metals, samples were digested in 1:3 HNO_3:HCl solution, diluted with DI water, then filtered with 0.45 µm syringe filters. For measuring water-soluble metals, filters were sonicated in DI water for 0.5 hr with an Ultrasonic Cleanser (VWR International LLC, West Chester, PA, USA). After sonication, the extracts were filtered using 0.45 µm syringe filters, then HNO_3 was added to produce a final concentration of 2%. Here we focus on Fe, Cu, and Mn as they are common transition metals linked to aerosol toxicity (Pardo et al., 2015; Shuster-Meiseles et al., 2016; Costa and Dreher, 1997; Ghio et al., 1999b; Kadiiska et al., 1997). A set of standards of these metals were treated following the same procedures as samples to establish filter mass concentrations from the ICP-MS responses. R^2 of the standard calibration curves ranged from 0.9918 to 0.9995 (N=8) for various metals. A 25 ppb internal standard of scandium (Sc) was added to all samples and standards to monitor analytical drift. The overall uncertainty that included the precision of standards, variability in sample airflow rate, extraction procedure (assuming 5%), and blanks, (all one standard deviation), was estimated to be 8% for Cu, 8% for Fe, and 6% for Mn. Limits of detection for the water-soluble metals method were 0.0003 ng m^{-3} for Cu, 0.26 ng m^{-3} for Fe, and 0.003 ng m^{-3} for Mn, and those for total metals method were 0.098 ng m^{-3} for Cu, 0.95 ng m^{-3} for Fe, and 0.004 ng m^{-3} for Mn.

5.3.3 Oxidative potential

Oxidative potential (OP) was measured on a half portion of the MOUDI Zefluor filters. Sample preparation and the OP methods are described in detail in other publications (Fang et al., 2016; Fang et al., 2015b). Filters were extracted in DI water, filtered with 0.45 μm syringe filters, then separated into two fractions. One was analyzed with the Ascorbic Acid (AA) method via a simplified approach to the AA analysis method that uses a synthetic respiratory tract lining fluid model (Mudway et al., 2005; Zielinski et al., 1999) to determine water-soluble AA activity (OP_{ws}^{AA}). The other filter fraction was measured for water-soluble DTT activity (OP_{ws}^{DTT}) with the dithiothreitol (DTT) assay. These two assays measure the oxidative capacity of particles by monitoring the consumption rate of AA and DTT at pH = 7.4 and T = 37 °C. Final OP data are reported as DTT consumption per volume of sample air (units of nmol min^{-1} m^{-3}).

5.3.4 Aerosol pH

pH is defined as the logarithmic scale of the hydronium ion activity in an aqueous solution.

$$\boldsymbol{pH = -\log_{10} \gamma_{H^+} H_{aq}^{+} \cong -\log_{10} \frac{1000 \gamma_{H^+} H_{air}^{+}}{W_i}} \qquad \textbf{(Equation 9)}$$

Where γ_{H^+} is the hydronium ion activity coefficient (assumed = 1) and H_{aq}^{+} (mole L^{-1}) is the hydronium ion concentration within the ambient particle liquid water. H_{aq}^{+} can be also be viewed as the hydronium ion concentration per volume of air H_{air}^{+} (μg m^{-3}) divided by the concentration of particle liquid water, W_i (μg m^{-3}). Since most particle water is associated with the highly hygroscopic inorganic species, such as sulfate, liquid water is often estimated from only the inorganic species concentrations, ignoring smaller

contributions by organic aerosol components (Guo et al., 2015). We follow that approach here.

There is no accurate way to directly measure the pH of ambient $PM_{2.5}$. Methods to infer pH based on ion balances or ratios of measured anion and cations (which does not include OH^- or H^+) are not good surrogates for pH (Guo et al., 2015; Hennigan et al., 2015; Guo et al., 2016; Bougiatioti et al., 2016). Measurements of "strong acidity" (Koutrakis et al., 1988) often used in previous health studies, are also not an accurate measure of actual particle pH since in that approach H_{aq}^+ is determined in a vastly more dilute solution than what exits in the ambient aerosol and so is essentially an ion balance approach. Currently, the most accurate way to determine particle pH is to run a thermodynamic model to predict pH based on measured gas and particle species that contribute to pH, assuming the thermodynamic system is in equilibrium. Here we use the model ISORROPIA-II (Nenes et al., 1999; Fountoukis and Nenes, 2007), which predicts both H_{air}^+ and W_i to determine pH. Ideally, inputs to the model include total (gas plus particle) concentrations of all species that affect pH. The model then predicts equilibrium partitioning of species between the gas and particle phases. A number of studies show the equilibrium condition is met for fine particles (Weber et al., 2016; Guo et al., 2016; Guo et al., 2015), which can occur fairly rapidly (15 to 30 minutes) (Fountoukis et al., 2009). This is not true for the coarse mode due to kinetic limitations (Cruz et al., 2000; Dassios and Pandis, 1999; Fountoukis et al., 2009). Thus pH was calculated using different methods for fine and coarse modes. First, since no gas phase species were available, we determined pH in the fine mode through an iteration procedure that used the measured particulate species (SO_4^{2-}, NO_3^-, Cl^-, NH_4^+, Na^+, K^+, Ca^{2+}, and Mg^{2+}) and ISORROPIA-II to predict gas species. Total fine mode aerosol

concentrations for each ion were determined by summing measured concentrations for MOUDI stages below and including 3.2 µm cut size. Then, under the assumption that the fine mode ions were in equilibrium with the gas phase, ISORROPIA-II was run in forward mode and gas phase concentrations of NH_3, HNO_3, HCl were determined; predicted gas phase concentrations from the *i-1* run were applied to the i^{th} iteration, until the gas concentrations converged. The converged gas concentrations were similar to what has been observed in this region [e.g., ammonia, being the most important was predicted to be between 0.6 and 0.7 µg m^{-3}, similar to that recorded in the southeastern US (0.1-0.8 µg m^{-3}) (Weber et al., 2016)]. We have used this iterative method in a previous study (Guo et al., 2016). With these gas phase concentrations, ISORROPIA-II was run for each MOUDI stage using that stage's measured aerosol ion concentrations and estimated gas concentrations to determine pH for each stage. Since equilibrium is not expected between the gas and particles of the coarse mode due to kinetic limitations, and because these measurements were made fairly close to the source of the coarse mode particles, pH was determined by ignoring interaction with the gas phase. ISORROPIA-II was run in forward mode with zero gas concentrations. A similar result was found for ISORROPIA-II run in reverse mode for the coarse particles, although the numerical solution can be more unstable. The fine mode pH predicted here (pH of 1 to 2) is similar to levels found in other studies in this region where more complete data sets (i.e., gases measured) were available. We assumed particles to be internally mixed (i.e., homogeneous pH within each size bin) when calculating pH for each size bin. Freshly emitted particles and coarse mode particles may be largely external mixtures. A similar assumption has been made when calculating bulk pH of PM_1 and $PM_{2.5}$ in our past studies and good agreement was still found between

observed and predicted partitioning of semivolatile species (Guo et al., 2016; Guo et al., 2015; Weber et al., 2016). Insoluble ions are not an issue as their concentration is too low that they don't affect the equilibrium of H^+ in the aqueous solution unless they impede dissolution or mass transport within the particle or between the particle and the gas phase (Meskhidze et al., 2005). The uncertainty of pH prediction based on known sources was estimated to be 13% in a previous study (Guo et al., 2015) and expected to be higher in this study considering the estimated gaseous concentrations and the lower inorganic mass loadings distributed in MOUDI stages. The accuracy of the pH prediction is predominantly judged by the reproduction of semi-volatile components partitioning between gas and particle phases (i.e., how do predicted gas NH_3 or HNO_3 and particle NH_4^+ or NO_3^- compare to the measurements of these species, as these predictions depend on other ions and RH, T. Details on ISORROPIA-II and verification of predicted pH for $PM_{2.5}$ in both the southeastern and northeastern US has been reported (Weber et al., 2016; Guo et al., 2016; Guo et al., 2015).

5.4 Results

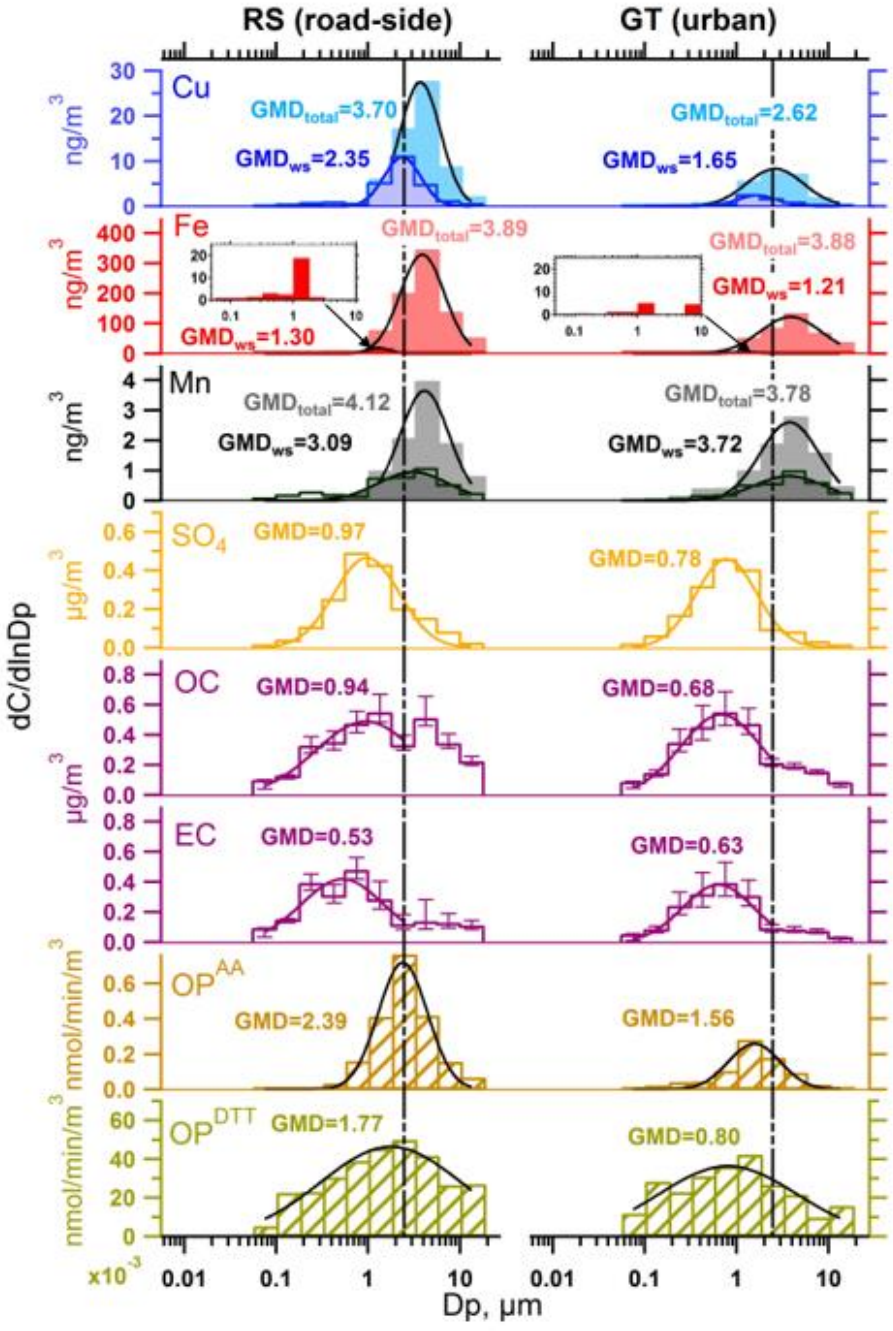

Figure 5-1 Ambient size distributions of PM chemical components and water-soluble oxidative potential at a road-side site (left panel, RS, measurements 3/28-4/4/2016) and an urban background site (right panel, GT, measurements 3/16-3/23/2016) in Atlanta, GA, USA. OC and EC were fitted with a lognormal curve (intercept forced to zero) for size ranges < 2.5 μm while others were fitted for the whole size range.

GMD is the geometric mean diameter (μm). The vertical dotted line is aerodynamic diameter at 2.5 μm, the so-called upper limit of $PM_{2.5}$. Water-soluble (denoted as ws) Fe had low concentrations relative to total. Water-soluble Fe with enlarged scale can be found in Figure 5-8 in section 5.7.

Figure 5-1 shows the measured size distributions of various PM components and oxidative potential at a road-side (RS) and urban (GT) site in Atlanta, GA. Measurements of OP from other sampling times show similar distributions (Figure 5-4 to Figure 5-8). The fitted distribution equation and parameters, (geometric mean diameters (GMD) and geometric standard deviation (σ_g)), and the associated uncertainties can be found in Table 5-1. Although the MOUDI samples at the two sites in Figure 5-1 were collected at different times, given the samples were averaged over 7 days, and that both were collected close in time, the size distributions are taken to represent the general characteristics of the two sites. (Note that the comparisons of OP in Figure 5-1 lead to similar observations to those from OP measured simultaneously at the two sites, see Figure 5-5 and Figure 5-7).

5.4.1 Size distributions of metals

Cu, Fe, and Mn exhibited a single mode for both total (elemental) and water-soluble components. As expected for mechanically generated aerosols (Willeke and Whitby, 1975), total metals were predominantly found in the coarse mode. Water-soluble metals, however, peaked at smaller sizes. Differences in particle GMD between total and water-soluble metals were more obvious for Cu and Fe than for Mn. At the two sites, the GMD for water-soluble Cu and Fe ranged from 1.24 to 2.35 μm, whereas for total Cu and Fe, GMDs were between 2.63 and 3.90 μm. Mn had more similar GMDs for water-soluble (3.17 and 3.78 μm) fractions versus total (3.83 and 4.13 μm).

Concentrations also differed between sites. The RS site had much higher levels of total Cu and Fe compared to the GT site, indicating a primary traffic emission source. Total Mn was more uniform between the two sites. This is consistent with known sources. Past studies have attributed Cu to brake/tire wear (Adachi and Tainosho, 2004; Sternbeck et al., 2002; Garg et al., 2000), Fe to brake/tire wear (Adachi and Tainosho, 2004; Hopke et al., 1980) and mineral dust (Rodríguez et al., 2004; Choi et al., 2001), and some Mn to brake/tire wear (Birmili et al., 2006) and a significant source from mineral dust (Rodríguez et al., 2004; Choi et al., 2001). For water-soluble comparisons between the two sites, Cu and Fe concentrations were also higher by the RS site, whereas Mn levels were similar. This is consistent with our previous findings for the Atlanta region where water-soluble Mn had a more regional characteristic, consistent with a mineral dust source, while water-soluble Cu and Fe had a stronger traffic-related source (Fang et al., 2015a). Thus, comparisons between the two sites show that the RS metals were associated with generally larger particles, consistent with expectations that sedimentation would deplete larger particles as transported further from the source (i.e., metals in smaller particle sizes are enhanced relative to larger particles at the GT site).

Comparisons of the water-soluble to total fractions indicate the extent of their solubility. The average (± SD) water-soluble fraction for all size ranges from all data were 13 ± 14%, 44 ± 36%, and 50 ± 30% for Fe, Cu, and Mn, respectively. In general, Fe was the least soluble among the three metals, consistent with other studies (Birmili et al., 2006; Espinosa et al., 2002). A box plot showing the span of metal solubility over the whole size range is shown in Figure 5-2. For all three metals, $PM_{2.5}$ had substantially higher soluble fractions than the coarse mode (see Figure 5-9).

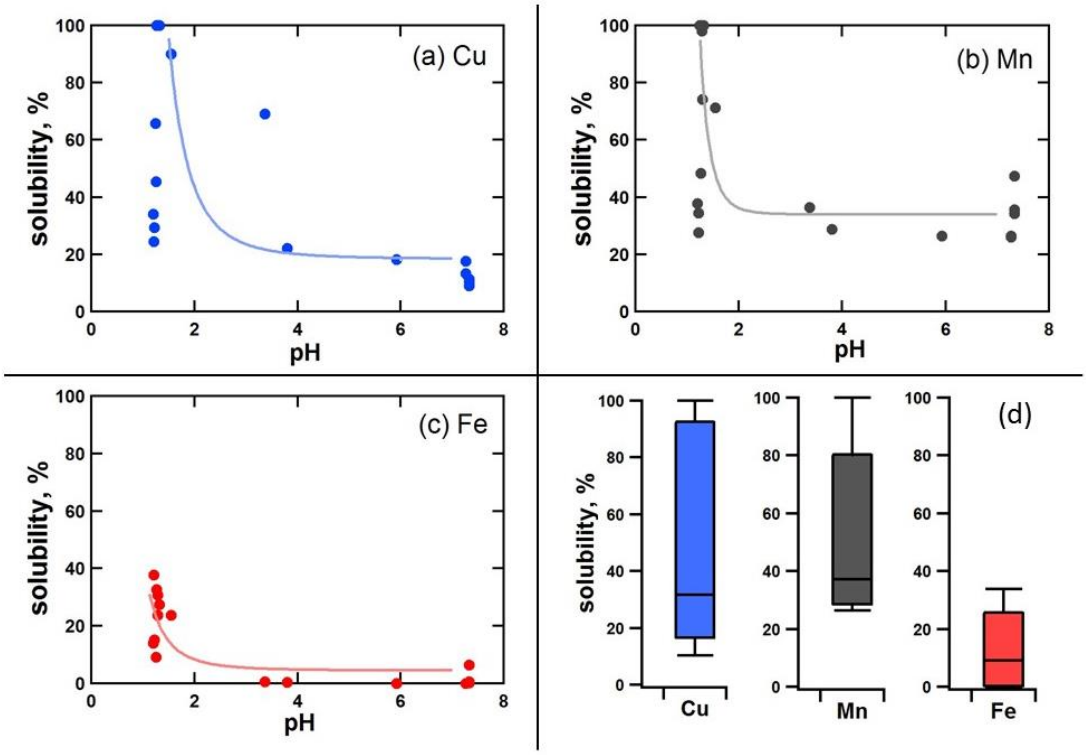

Figure 5-2 Metal solubility in relation to pH for (a) Cu, (b) Mn and (c) Fe. (d) shows box plots of metals solubility across all size ranges. Top whisker – 90%, bottom whisker – 10%, line in the box – median, box top – third quartile, box bottom – first quartile. The finest stage (Dp = 0.056-0.1 µm) and the stage with Dp = 0.1-0.18 µm (only for Fe) had metal concentrations below the detection limit and not included in solubility calculations.

5.4.2 Size distributions of carbonaceous particles and sulfate

Organic and elemental carbon (OC and EC) in ambient particles showed a typical aerosol bi-modal distribution with a clear fine-mode ($\leq PM_{2.5}$) and coarse-mode ($PM_{2.5-10}$), with a minimum between modes at about 2.5 µm. At the RS site, OC had a more prominent coarse mode and EC was generally associated with smaller particles. In contrast, sulfate was most abundant in the fine mode. Although SO_2 is mainly from point sources, such as coal-fired electric generating units, the conversion of SO_2 to form secondary sulfate results in a

regional characteristic for sulfate (Hidy et al., 2014), accounting for similar concentrations between the two sites (Figure 5-1).

5.4.3 Size distributions of water-soluble particulate oxidative potential

Both OP_{ws}^{AA} and OP_{ws}^{DTT} had a mono-modal distribution, which peaked near the separation between fine and coarse modes (i.e., 2.5 μm). However, the peaks in the modes were at slightly higher sizes at the RS site, similar to what was observed for water-soluble Cu and Fe. In terms of OP magnitude, OP_{ws}^{AA} levels were substantially higher at the RS than the GT site, whereas OP_{ws}^{DTT} were similar at both sites, indicating, like sulfate, a more regional characteristic for OP_{ws}^{DTT}. OP_{ws}^{AA} appear mainly associated with roadway emissions. In comparing the two measures of OP, OP_{ws}^{DTT} peaked at a smaller size than OP_{ws}^{AA} at both sites and had a much broader distribution. Other studies have also reported OP size distributions, but only focused on differences between broad aerosol modes; e.g., ultrafine, fine, and coarse. The more highly size-resolved data reported here are generally consistent with other studies (see Figure 5-10), but provide substantially more insight on the sources and processes leading to aerosol OP.

5.5 Discussion

The OP size distributions are unique in that they peak near 2.5 μm, which is the minimum separating the mass-based coarse and fine modes (see sulfate and OCEC distributions, for example). This affects where particles are deposited in the respiratory tract (Peters et al., 1997; Lippmann, 2010). The cause for the OP distributions being largely centered near 2.5

μm can be explained by how the fine and coarse mode interaction contributes to water-soluble metals.

5.5.1 Metals dissolution by acid processing

There are two ways that a metal can become soluble, acid dissociation under low pH conditions (Nenes et al., 2011; Shi et al., 2011; Meskhidze et al., 2003), or by forming a ligand with an organic species, such as oxalate, at higher pH (Schwertmann, 1991; Ali and Dzombak, 1996). A concentration of water-soluble metals peaking at the overlap between sulfate and the total metals suggests an acidity-driven metals dissolution process. Taking Cu as an example, size distributions of sulfate, water-soluble and total Cu are plotted together in Figure 5-3 for the RS and GT site. The water-soluble Cu peak was within the overlap of the lower tail of the primary total Cu distribution in the coarse mode and upper tail of the secondary sulfate distribution in the fine mode. If in this overlap area, sulfate and total Cu were internally mixed (within a single particle), insoluble Cu may be mobilized over time by sulfuric acid, creating a soluble form of Cu.

Calculated particle pH for each MOUDI stage is also shown in Figure 5-3 and supports this hypothesis. Concentrations of the various ions measured on the MOUDI stages that went into the pH calculation are shown in section 5.7 Figure 5-11. Predominance of sulfate and lack of mineral cations in the fine mode (Dp less than approximately 1.8 μm) results in a very low pH, ranging between 1 and 2, whereas low levels of sulfate and high levels of cations, such as Ca^{2+} and Mg^{2+} (see Figure 5-11), likely in the form of carbonates ($CaCO_3$ and $MgCO_3$) (Ito and Feng, 2010) in the coarse mode leads to a more neutral coarse mode, with pH approximately near 7. The transition between these two modes is where the soluble

metals are found. Metals solubility in relation to pH at each MOUDI stage from both sites are shown in Figure 5-2 (a-c). When pH is near neutral, metals solubility was low; as pH decreased, solubility substantially increased, further supporting the association of pH with metals solubility and the mechanism of acid processing. Longo et al. (Longo et al., 2016a) also found increasing mineral dust Fe solubility with particle acidity in Saharan dust. The very low pH levels for the fine mode reported here are also consistent with more detailed calculations of pH we have reported for the same region (Guo et al., 2015; Weber et al., 2016) and in other locations (Bougiatioti et al., 2016; Guo et al., 2016), indicating that this mechanism of metals solubility may apply to many regions.

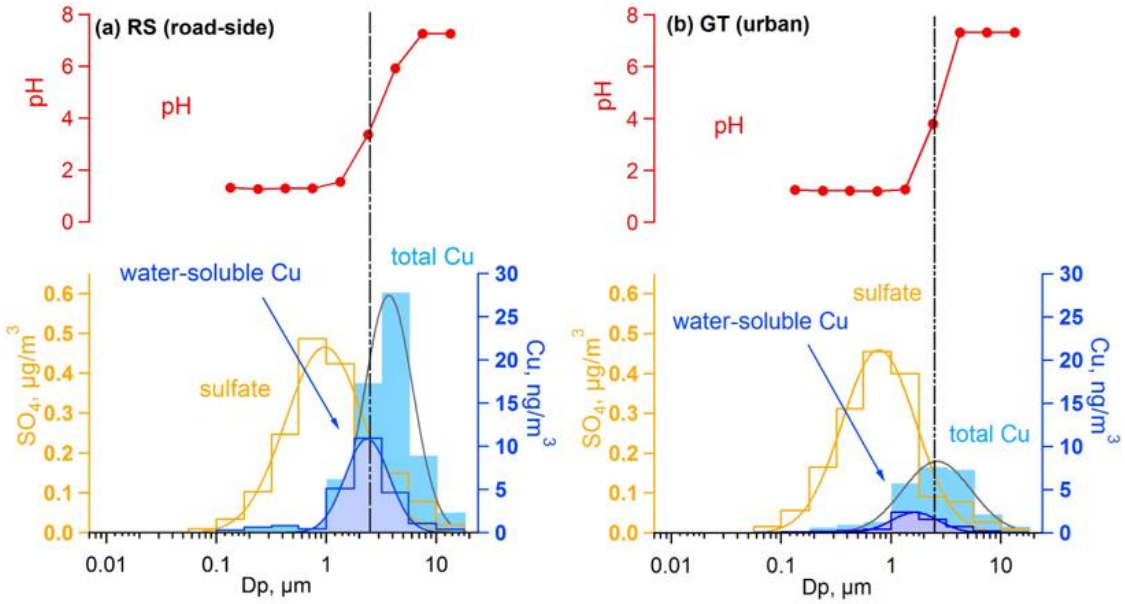

Figure 5-3 Metals (e.g. Cu) dissolution by sulfate under acidic conditions. The vertical dotted line is aerodynamic diameter (Dp) at 2.5 μm, the upper limit of so-called $PM_{2.5}$. pH was estimated from ISORROPIA-II based on ionic species from MOUDI samples collected on 3/28-4/4/2016 and 3/16-3/23/2016 at road-side and urban site, respectively.

The dissolution of metal oxides at low pH takes time, from hours up to weeks (Shi et al., 2011). Meskhidze et al. (Meskhidze et al., 2003) found that 2-5% Fe was mobilized after 4 days at pH = 1 and that at low pH, the dissolution is much faster since the dissolution rate depends exponentially on pH. Given that the sampling was done continuously for 7 days, particles collected on the filters were subject to possible post-collection dissolution for an average of 3.5 days. As shown in Figure 5-2 and Figure 5-3, for fine particles, pH values were in the range of 1 to 2, therefore, the solubility of fine-mode Fe could be over-estimated by up to roughly 5% compared to ambient aerosols, since the collected particles remained at ambient conditions for an extended period of time during the sampling period. As for coarse particles, the predicted pH was larger than 4 and so this effect will be negligible. In our study, the metal analysis was done after a 2-month storage period in a freezer. Majestic et al. (Majestic et al., 2006) showed that Fe particles collected on a filter and stored frozen didn't change significantly over 3 months. Therefore, continuous dissolution during storage did not likely happen. The toxicity of aerosols is highly sensitive to pH since over their lifespan only a fraction of the total elemental metal is solubilized. Sulfate plays a key role; its high hygroscopicity leads to the formation of the aqueous drops and provides H^+ that dissolves the metals, forming soluble forms of metal sulfates.

Our other studies in Atlanta support these findings. Correlations have been observed between water-soluble Fe and sulfate (r^2 = 0.62 - 0.76, N=181) in summer and fall (Fang et al., 2015a). Single particle X-ray fluorescence (XRF) measurements has shown that Fe solubility was associated with particle sulfur content (Oakes et al., 2012) and that approximately 50% of the sulfate within individual particles between 1 and 2.5 μm was associated with a metal cation, likely in the form of iron or copper sulfates (Longo et al.,

2016b). These results are also consistent with our source apportionment analysis for aerosols in metropolitan Atlanta, where we found that in $PM_{2.5}$, roughly 50% of the water-soluble Fe and 40% of the water-soluble Cu were associated with secondary processing (Fang et al., 2015a). The remaining fraction of these metals was largely associated with a primary brake/tire wear source (32% of Fe and 51% of Cu) consistent with high levels at the RS site.

Because of water-soluble transition metals contribution to OP, these processes play an important role in shaping the size distributions of OP_{ws}^{AA} and OP_{ws}^{DTT}. Our previous study showed that Cu is a common contributor to OP_{ws}^{AA} and OP_{ws}^{DTT} in PM2.5 ambient samples (Fang et al., 2016). In fact, water-soluble Cu was nearly exclusively correlated with OP_{ws}^{AA} ($r = 0.70$-0.94), consistent with identical size distributions for water-soluble Cu and OP_{ws}^{AA}, and OP_{ws}^{AA} higher at the RS than the GT site (Figure 5-1). In contrast, we have reported that OP_{ws}^{DTT} was sensitive to water-soluble Cu as well as certain organic species from combustion sources (Verma et al., 2014). The combined contribution from these two different aerosol components to OP_{ws}^{DTT} can explain the differences between OP_{ws}^{AA} and OP_{ws}^{DTT} distributions; that is the OP_{ws}^{DTT} distribution peaking between the fine-mode OC peak and water-soluble Cu peak, resulting in a broader distribution than OP_{ws}^{AA}.

5.5.2 Role of metals in OP and health

The size distribution results presented here, along with our previous single particle analysis, demonstrate that acid processing of metals by sulfate increased the metals solubility and particle OP, providing a linkage between sulfate and adverse health effects that may explain some of the past associations often found between sulfate or "strong

acidity" and various health endpoints (Dockery et al., 1993; Pope et al., 1995; Sarnat et al., 2008; Gwynn et al., 2000; Thurston et al., 1994; Thurston et al., 1991; Burnett et al., 1997; Fairley, 1999; Schwartz et al., 1996). Our results are consistent with the earlier findings of Ghio et al.(Ghio et al., 1999a), who pointed out a linkage between ambient aerosol sulfate content, soluble metals, and oxidant generation. However, they hypothesized Fe solubility was driven by ligand formation, and not acid-driven dissolution. Other processes involving sulfate may also adversely affect health, such as catalyzing the formation of secondary hazardous organic aerosols (Jang et al., 2002) and chemical reactions involving hydrogen peroxide (Friedlander and Yeh, 1998). In addition, other particle pH effects are possible, for example, pH below 5 can enhance the formation of ozonide at the air-lung surface, leading to ROS generation *in vivo*, inducing oxidative stress due to ozone (Enami et al., 2008).

Changing emissions may increase the importance of aerosol pH health effects in the future. Although particulate sulfate has substantially decreased in the southeast US over the past 15 years due to the reduction of sulfur dioxide emissions from electrical generating units (Hand et al., 2012), we have shown that fine particle pH has not significantly changed, remaining highly acidic with pH between -1 and 2 (Weber et al., 2016). pH below nominally 3 is likely required to solubilize iron in ambient particles within a reasonable time (Meskhidze et al., 2003), (other transition metals, such as Cu, will solubilize at a higher pH), making it possible for this effect to be widespread given our observations of a ubiquitous low fine particle pH (Guo et al., 2016; Guo et al., 2015). Traffic-related metals emissions are not expected to decrease substantially in the near future; traffic counts have increased over the past ten years (http://geocounts.com/gdot/). Adaptation to electric

powered vehicles will end tail-pipe emissions, but mechanically generated tire/brake wear emissions will continue. Metals mobilization by acidification is therefore likely to remain an important factor in future aerosol OP and the health effects of PM.

5.6 Conclusions

Size distributions of various PM components were used to investigate how sulfate, through particle pH, affects the mobilization of metals, and its effect on aerosol oxidative potential (OP) measured by the AA and DTT assays. Comparisons were made between a road-side and an urban site in Atlanta, GA. Our results suggest that the very low pH (< 2) of fine particles results in an increase in highly toxic water-soluble particulate matter transition metal ions. This happens by the interaction between acidic fine mode particles and primary insoluble metal particles in the coarse mode. The intersecting tails of these two distributions result in a soluble metal size distribution that peaks near particles with aerodynamic diameter of 2.5 μm, the minimum between the fine and coarse mass modes and the upper limit of $PM_{2.5}$. Size-resolved OP showed similar atypical ambient aerosol distributions, which will impact deposition patterns in the respiratory system. These findings highlight how atmospheric processing of aerosol emissions can substantially increase their toxicity, and the role of sulfate in this process may help to explain reported linkages between sulfate, or "strong acidity", and adverse health outcomes in many past studies.

5.7 Supporting materials

Table 5-1 Summary of size distribution geometric mean diameters (GMD) and geometric standard deviation (σ_g) for lognormal fits (intercept forced to zero) of various PM components and water-soluble ascorbic acid (OP_{ws}^{AA}) and dithiothreitol (OP_{ws}^{DTT}) activities from MOUDI samples collected in Atlanta, GA.

	Road-side (RS)				Urban (GT)			
Species	**GMD**	**GMD_SD**	**σ_g**	**σ_g _SD**	**GMD**	**GMD_SD**	**σ_g**	**σ_g _SD**
water-soluble Cu	2.35	0.06	1.58	1.02	1.65	0.10	1.65	1.06
total Cu	3.70	0.12	1.65	1.03	2.62	0.13	2.04	1.05
water-soluble Fe	1.30	0.08	1.31	1.03	1.21	0.39	1.33	1.25
total Fe	3.89	0.15	1.74	1.04	3.88	0.23	2.14	1.06
water-soluble Mn	3.09	0.41	2.42	1.15	3.72	0.38	2.44	1.11
total Mn	4.12	0.21	1.84	1.05	3.78	0.23	2.09	1.06
SO_4	0.97	0.06	2.27	1.07	0.78	0.04	2.16	1.06
OC	0.94	0.15	3.47	1.20	0.68	0.04	2.74	1.07
EC	0.53	0.08	2.79	1.19	0.63	0.05	2.42	1.08
OP_{ws}^{AA}	2.39	0.09	1.85	1.04	1.56	0.11	1.92	1.07
OP_{ws}^{DTT}	1.77	0.21	5.79	1.16	0.80	0.15	5.59	1.25

SD – standard deviation from log normal fit using IGOR software.

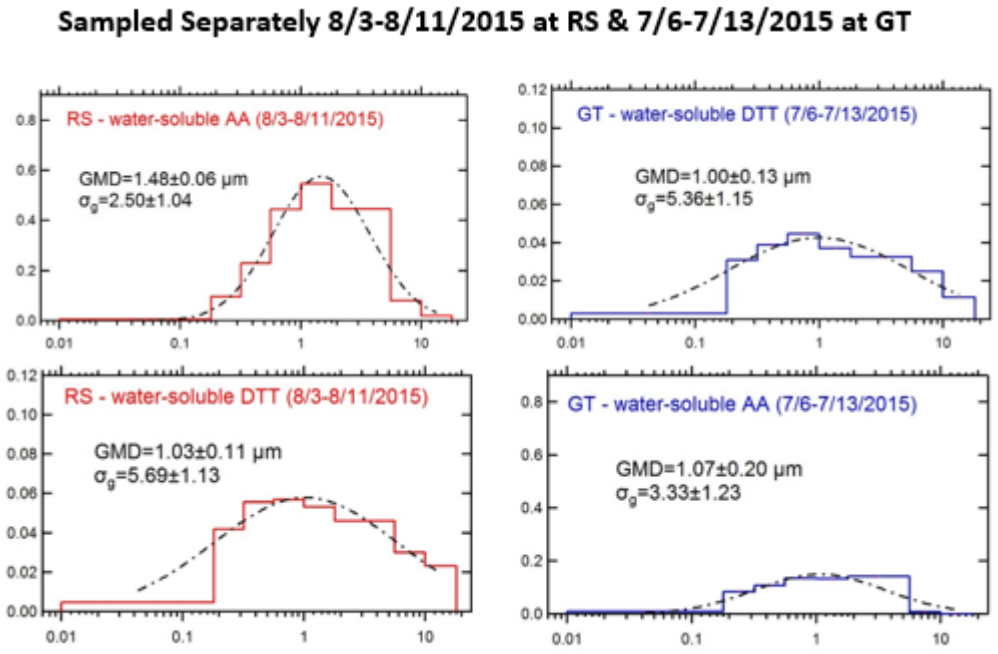

Figure 5-4 Ambient size distribution of OP from MOUDIs collected in summer 2015.

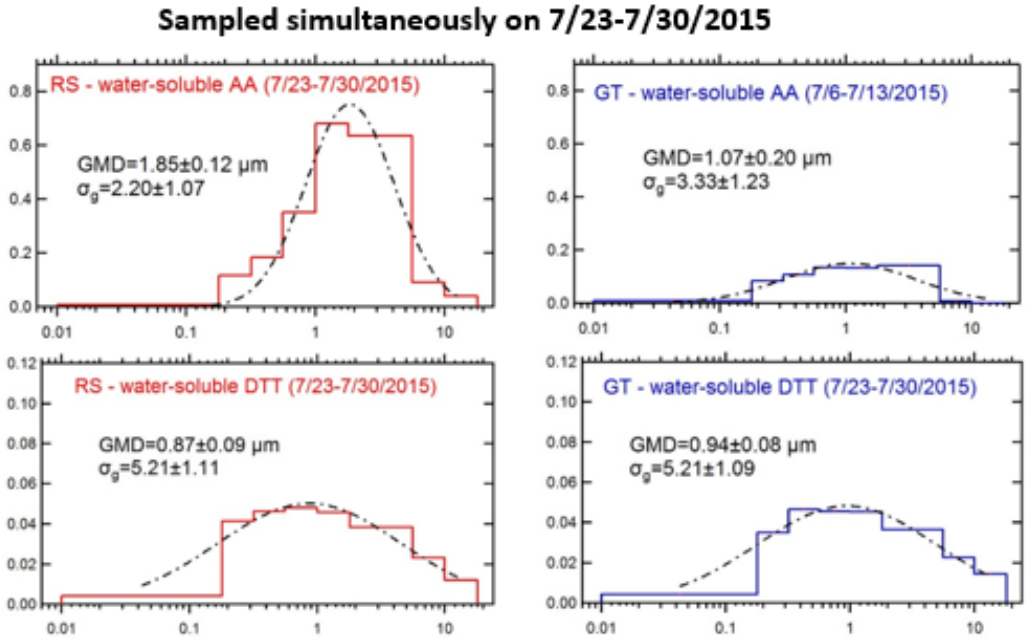

Figure 5-5 Ambient size distribution of OP from MOUDIs collected in summer 2015.

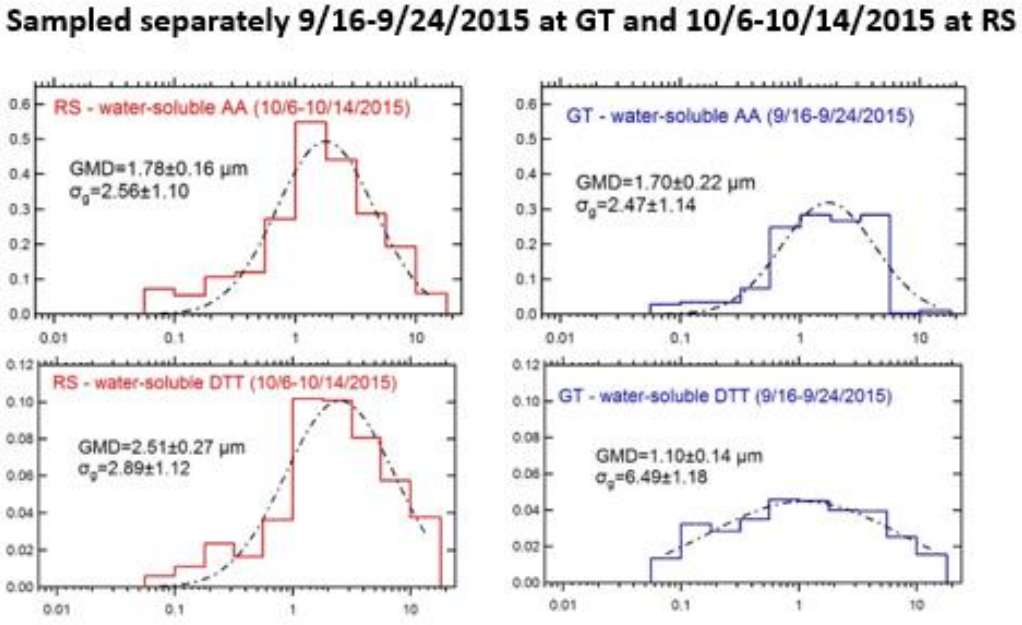

Figure 5-6 Ambient size distribution of OP from MOUDIs collected in fall 2015.

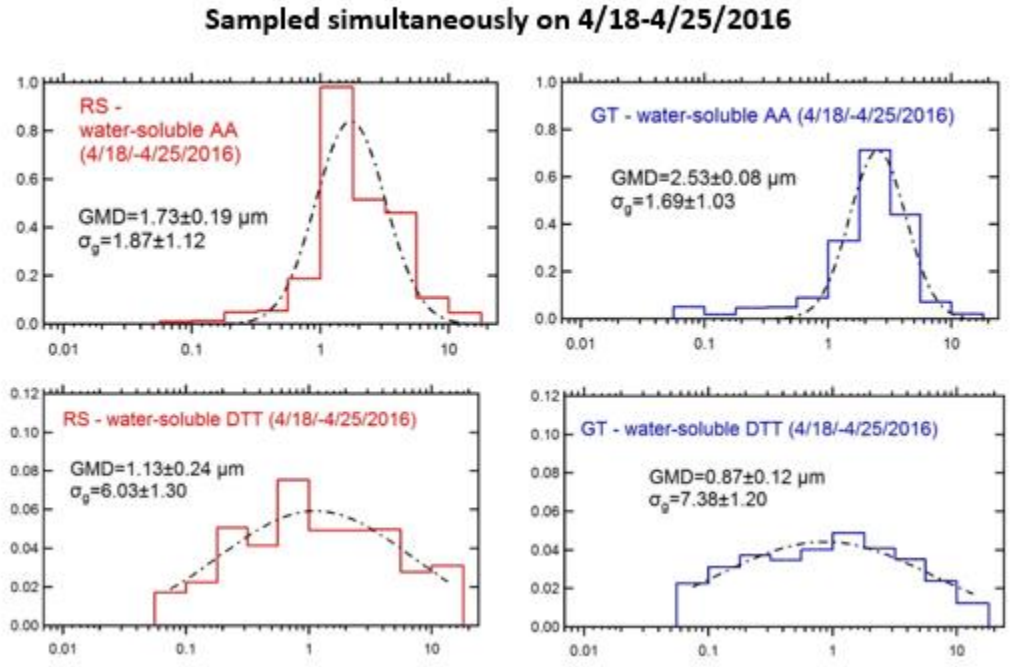

Figure 5-7 Ambient size distribution of OP from MOUDIs collected in spring 2016.

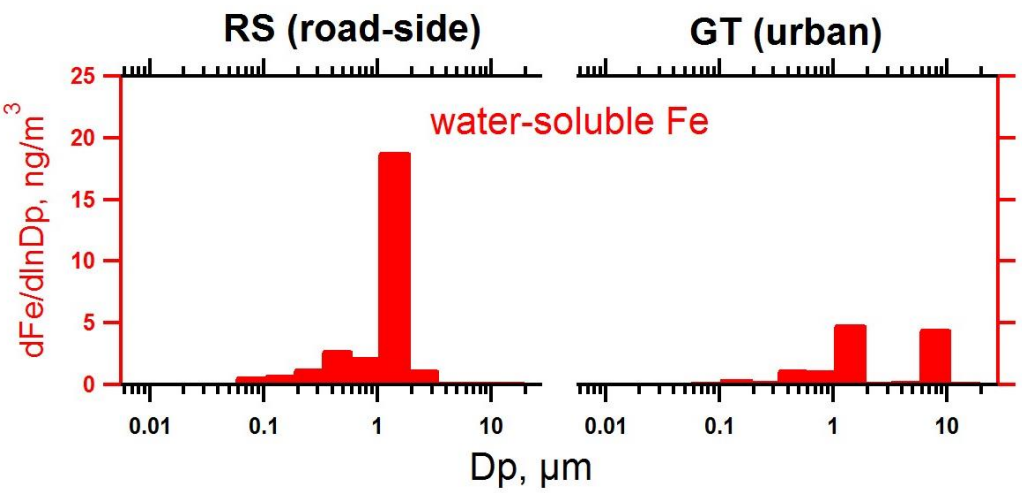

Figure 5-8 Ambient size distribution of water-soluble Fe from MOUDIs collected on 3/28-4/4/2016 and 3/16-3/23/2016 at a road-side and urban site, respectively.

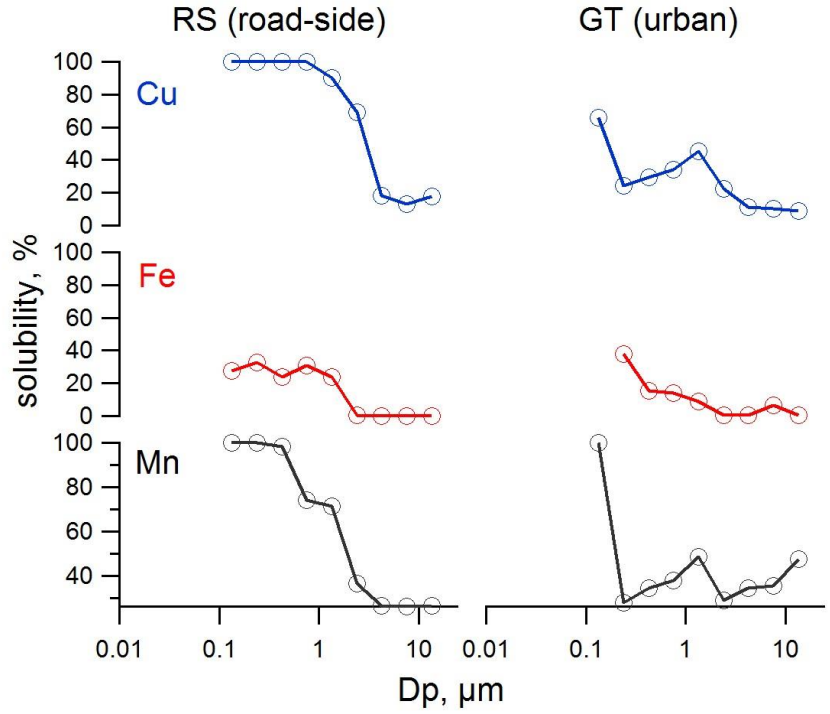

Figure 5-9 Water-soluble fraction (solubility) of Cu, Fe, and Mn from MOUDIs collected on 3/28-4/4/2016 and 3/16-3/23/2016 at road-side and urban site, respectively. The finest stage (0.056-0.1 µm) and the stage with Dp = 0.1-0.18 µm (only for Fe) had metal concentrations below detection limit and not included in solubility calculations.

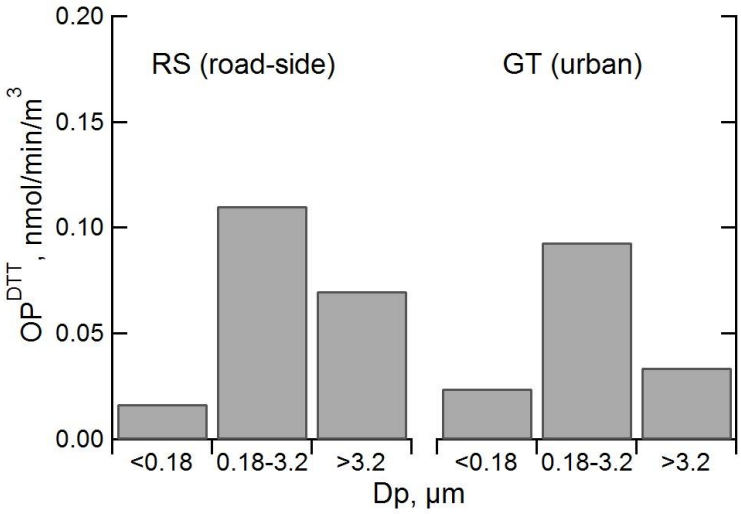

Figure 5-10 Water-soluble DTT activity of particle size fractions over broad ranges for comparisons with OP distributions reported in the literature.

Comparison of highly size-resolved MOUDI OP^{DTT} to that of other studies.

Other studies have compared OP_{ws}^{DTT} of different size modes, including ultrafine (Dp < 0.18 µm), fine (0.18 ≤ Dp ≤ 2.5 µm), and coarse (Dp > 2.5 µm), and found that fine particles had the highest OP_{ws}^{DTT} in both traffic and urban environments (Li et al., 2003b; Steenhof et al., 2011; Cho et al., 2005; Ntziachristos et al., 2007). Another study found particles with Dp within 0.49-3 µm range had the highest OP_{ws}^{DTT} (Velali et al., 2016). Integrating our OP_{ws}^{DTT} size distributions to match the less size-resolved data of these other studies (Dp < 0.18, 0.18-3.2, and >3.2 µm) shows general consistency with the previous studies (see Figure 5-10). In contrast, Steenhof et al. (Steenhof et al., 2011) found that fine mode had the lowest OP_{ws}^{DTT} in stop-and-go traffic and at an underground site.

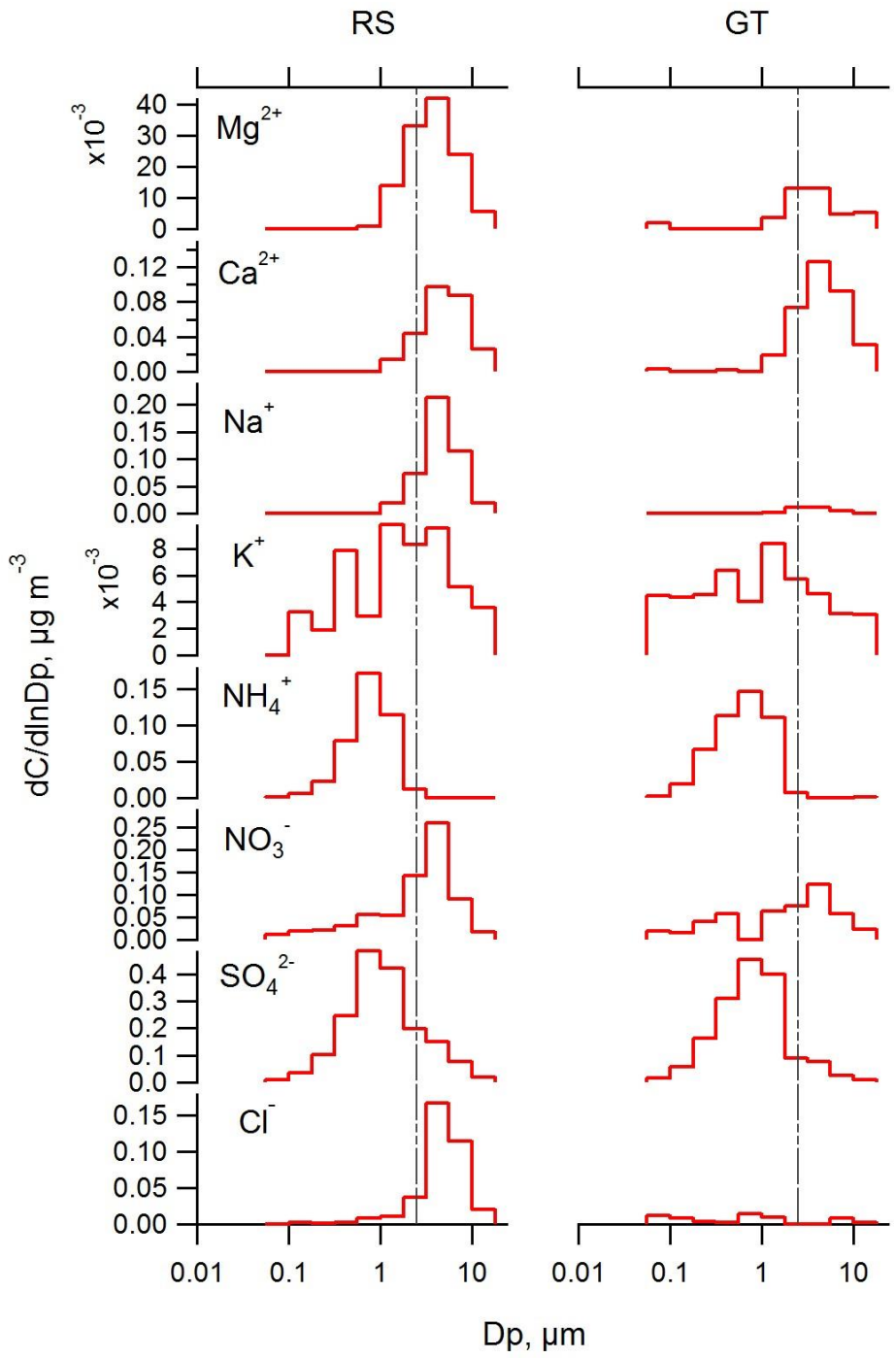

Figure 5-11 Ambient size distribution of cations and anions from MOUDIs collected on 3/28-4/4/2016 and 3/16-3/23/2016 at road-side and urban site, respectively. The vertical dotted line is aerodynamic diameter at 2.5 µm.

CHAPTER 6. AMBIENT SIZE DISTRIBUTIONS AND LUNG DEPOSITION OF AEROSOL DITHIOTHREITOL-MEASURED OXIDATIVE POTENTIAL: CONTRAST BETWEEN SOLUBLE AND INSOLUBLE PARTICLES

Ting Fang
Linghan Zeng
Dong Gao
Vishal Verma
Aleksandr B. Stefaniak
Rodney J. Weber

Environ. Sci. Technol., 51, 6802–6811, 2017
doi: 10.1021/acs.est.7b01536

6.1 Abstract

Ambient particulate matter may upset redox homeostasis leading to oxidative stress and adverse health effects. Size distributions of water-insoluble and water-soluble OP^{DTT} (dithiothreitol assay, a measure of oxidative potential per air volume) are reported for a roadside site and an urban site. The average water-insoluble fractions were 23% and 51%, and 37% and 39%, for fine and coarse modes at the road-side and urban site, respectively, measured during different periods. Water-soluble OP^{DTT} was unimodal, peaked near 1-2.5 μm due to contributions from fine-mode organic components plus coarse-mode transition metal ions. In contrast, water-insoluble OP^{DTT} was bimodal, with both fine and coarse modes. The main chemical components that drive both fractions appear to be the same, except that for water-insoluble OP^{DTT} the compounds were absorbed on surfaces of soot and non-tailpipe traffic dust. They were largely externally mixed and deposited in different regions in the respiratory system, transition metal ions predominately in the upper regions and organic species, such as quinones, deeper in the lung. Although OP^{DTT} per mass (toxicity) was highest for ultrafine particles, estimated lung deposition was mainly from accumulation and coarse particles. Contrasts in the phases of these forms of OP^{DTT} deposited in the respiratory system may have differing health impacts.

6.2 Introduction

Studies have associated exposure to particulate matter (PM) with adverse health effects (Hoek et al., 2013; Brook et al., 2010; Pope et al., 2004). Oxidative stress, an imbalance toward an excess of reactive oxygen species (ROS), is considered to induce inflammation, a possible mechanism leading to adverse health effects (Xia et al., 2006). In an effort to

find a more biologically relevant metric than bulk PM mass concentration to represent the integrated effects from multiple toxic components in PM, oxidative potential (OP), defined as the capability of particles to deplete physiological antioxidants (reductants) and generate ROS, has been proposed. Positive associations between cardiorespiratory health endpoints and OP measured with the dithiothreitol (DTT) assay (OP^{DTT}) have been reported (units for OP^{DTT} are loss of DTT per time per volume of air sampled) (Yang et al., 2016; Bates et al., 2015; Delfino et al., 2013). Physiologically relevant assays, glutathione (OP^{GSH}) and ascorbic acid (OP^{AA}) (both antioxidants found in lung fluid), tested in a synthetic respiratory tract lining fluid model show mixed results; OP^{GSH} has been associated with lung cancer mortality (Weichenthal et al., 2016a) and myocardial infarction (Weichenthal et al., 2016b) while OP^{AA} was not. In other studies, neither OP^{GSH} nor OP^{AA} was associated with respiratory function (Strak et al., 2012; Steenhof et al., 2013) or cardiorespiratory mortality (Atkinson et al., 2016). Comparing OP^{DTT} and OP^{AA}, we found positive associations between asthma/wheeze and congestive heart failure with OP^{DTT}, but not with OP^{AA} (Fang et al., 2016). Here, we focus on OP^{DTT}, but the analysis could be repeated for other OP assays.

In many cases, when implementing the DTT assay, particles are extracted in water followed by liquid filtration to remove solid or insoluble fractions. But studies show that OP^{DTT} can also be associated with insoluble aerosol components. Daher et al. (Daher et al., 2011) found that the OP^{DTT} values of particles collected using a Biosampler without filtration, thought to collect both water-soluble and insoluble fractions, were substantially higher than those of the aqueous extracts of the particles collected with a filter. McWhinney et al. (McWhinney et al., 2013a) found that approximately 25% and 90% of the OP^{DTT} was in

the water-insoluble fraction for urban PM and diesel exhaust particles, respectively. These studies and others (Li et al., 2013; Yang et al., 2014; Verma et al., 2012) provide evidence that insoluble aerosol species contribute to OP and should be considered when assessing health effects.

Elemental carbon (EC, black carbon or soot) is one of the insoluble species in PM identified as a serious health hazard. Research has shown that exposure to soot exacerbates cardiovascular and respiratory symptoms (McCreanor et al., 2007; Grahame and Schlesinger, 2010; Janssen et al., 2012). Soot is usually found mainly in the fine mode ($PM_{2.5}$, meaning all particles with aerodynamic diameter less than 2.5 μm) and is a product of incomplete combustion (Homann, 1998). In terms of OP, studies have linked reactive oxygen intermediates formed on the surface of soot, such as quinones from the oxidation of polycyclic aromatic hydrocarbons (PAHs) by ozone, to increased OP^{DTT} (Shiraiwa et al., 2011; Antinolo et al., 2015). Both representative (Li et al., 2013) and real (McWhinney et al., 2013a; McWhinney et al., 2011) diesel exhaust soot, when oxidized by ozone, exhibited much higher OP^{DTT}. The OP^{DTT} associated with diesel exhaust soot was not extractable by acid (Pan et al., 2004) or organics solvents, including methanol (McWhinney et al., 2013a) and dichloromethane (DCM) (McWhinney et al., 2013a; Pan et al., 2004), indicating that the DTT-active species were strongly adsorbed to the soot surface. Association between OP^{DTT} and the number of surface sites on nanoparticles (Sauvain et al., 2012) has been reported. These laboratory findings indicate that OP^{DTT} is contiguous with the surface of soot and that OP^{DTT} may play a key role in the adverse health effects of soot. Soot also provides a surface for the formation and stabilization of some ROS, e.g.

"environmentally persistent free radicals" (EPFRs) (Dellinger et al., 2007; Arangio et al., 2016), which may also be related to soot toxicity.

Coarse-mode aerosol ($PM_{2.5-10}$, meaning particles with a size between 2.5 and 10 μm) also has been linked to adverse health effects (Ostro et al., 1999; Osornio-Vargas et al., 2011; Hetland et al., 2004) and a significant fraction of the coarse-mode particle species are insoluble, remaining solid when deposited in liquid environments. Although variable levels of soot can be found in particles larger than $PM_{2.5}$, most insoluble species are associated with mechanically generated aerosols, such as mineral and fugitive dust. In urban environments, this has been linked to tire/brake wear components from traffic and construction activities in non-arid regions (Shirmohammadi et al., 2015; Furusjö et al., 2007; Weinbruch et al., 2014). Minerals (e.g. silicates, calcium carbonates, metal oxides, or clay minerals (Klein et al., 2008)) can induce ROS formation as a solid particle binding to a cell surface or entering the cell by engulfment and lead to ROS production, or as a "carrier" of more toxic species such as metals and surface-sorbed PAHs (Schoonen et al., 2006).

Aerodynamic size, in part, affects the location of deposition in the respiratory system (Peters et al., 1997; Lippmann, 2010). Particles deposited deep within the lung are most damaging due to difficulty in clearance and more readily enter the bloodstream when deposed in the alveoli (Nemmar et al., 2002; Furuyama et al., 2009). The circulatory system translocates soluble species and insoluble particles and the associated OP from the lung to other critical organs such as kidneys (De Jong et al., 2008; Li et al., 2017), heart (De Jong et al., 2008) and liver (De Jong et al., 2008; Oberdorster et al., 2002; Li et al., 2017), among others (Li et al., 2017), causing localized effects. In addition, recent studies show that

particles deposited in the nasal region translocate into the central nervous system via the olfactory bulb and cause brain lesions, dementia (Oberdorster et al., 2004; Maher et al., 2016; Chen et al., 2017) and impaired cognitive development (Sunyer et al., 2015). Particle size is also related to different toxic effects. Various studies have attempted to link PM size to adverse health effects. Some studies indicate that coarse particles are more potent at inducing hemolysis and DNA degradation (Osornio-Vargas et al., 2011), and pro-inflammatory cytokines in vitro (Hetland et al., 2004) than fine particles ($PM_{2.5}$), whereas some show that inhibition of cell proliferation is significantly stronger by $PM_{2.5}$ (Osornio-Vargas et al., 2011). The ultrafine fraction ($PM_{0.1}$) is often viewed as highly toxic. $PM_{0.1}$ is observed to cause airway inflammation in vivo (De Haar et al., 2006), more strongly associated with biomarkers of systemic inflammation than larger-size fractions (Delfino et al., 2009), and the small size enables penetration of pulmonary barriers and travel to other organs or cell membranes leading to damage of cell organelles, such as mitochondria (Li et al., 2003b), whereas accumulation ($PM_{0.1\text{-}2.5}$) and coarse fractions do not show similar behaviors, however more recent studies show that solid particles up to 1.75 μm in diameter also translocate to various organs from the lung (Li et al., 2017).

Although there has been substantial research on the toxicity of ambient PM in relation to particle size, there are limited studies on the ambient size distribution of OP. Several studies (Steenhof et al., 2011; Cho et al., 2005; Li et al., 2003b; Ntziachristos et al., 2007) have examined the OP^{DTT} of different size fractions of PM collected by the Versatile Aerosol Concentration Enrichment System (VACES), contrasting OP between broad aerosol modes, e.g. quasi-ultrafine (aerodynamic diameter, $D_p < 0.18$ μm), accumulation ($0.18 \leq D_p \leq 2.5$ μm), and coarse fractions ($D_p > 2.5$ μm). It is generally found that on a

per unit air volume basis, accumulation-mode particles have the highest OP^{DTT} per volume air, whereas ultrafine particles show much higher OP^{DTT} per unit mass than accumulation and coarse particles.

Here, we investigate the ambient size distribution and the major chemical players of both water-soluble and -insoluble OP^{DTT} for particles collected from two contrasting sites. Specifically, we study the relationship between fine-mode soot and coarse-mode dust and water-insoluble OP^{DTT}. The size distributions of OP were also used to assess the deposition of both forms of OP^{DTT} in the human respiratory system.

6.3 Methods

6.3.1 Size-Segregated Sampling of PM

Details on the sampling and chemical analysis can be found in section 5.3.1 and Fang et al. (Fang et al., 2017a). Two 10-stage Micro-Orifice Uniform Deposit Impactors (MOUDI, MSP Corp., Shoreview, MN, USA) were used to collect size-segregated ambient particles at a roadside (RS) site and an urban representative (GT) site in Atlanta, GA, from summer 2015 to spring 2016. The RS site was adjacent to highly congested interstate highway (I75/85), and the GT site was located on the rooftop of a building on the Georgia Tech campus, roughly 420 m from the RS site. The 50% cutoff aerodynamic diameters of the MOUDI are 18, 10, 5.6, 3.2, 1.8, 1.0, 0.56, 0.32, 0.18, 0.1, and 0.056 μm. The MOUDIs were operated in a non-rotating mode without a backup filter at a flow rate of 30 L min^{-1}. Methods to account for non-uniform deposits of particles due to non-rotating mode on chemical analysis are described in the Appendix A.5. Fourteen MOUDI samples were collected (seven at each site), while four from these samples (i.e., two pairs) were collected

simultaneously at both sites. For each MOUDI run, sampling was conducted under ambient RH and temperature (MOUDIs located outdoors) for approximately 7 days to provide sufficient mass loadings for various analyses. Studies on the stability of OP at ambient temperature are currently lacking, but Sauvain et al. (Sauvain et al., 2015) found that OP^{DTT} of particles collected on Teflon™ filters were stable after about 170 h (~7 days), indicating a 7-day sampling period will not significantly affect OP^{DTT}. All OP analyses in this work were done after a maximum of 3-day sample storage in sealed Petri dishes at -18 °C. Sampling periods, filter types used, and species quantified are summarized in section 6.6 Table 6-1. For every MOUDI sample, one field blank was included. All data were blank corrected with the averages from all blanks combined. Consistency between the two MOUDIs was first assessed by comparing water-soluble OP^{DTT} (OP_{ws}^{DTT}) when operated simultaneously at the GT site. Orthogonal regression yielded a slope of 1.0 ± 0.1 (value ± one standard deviation), low intercept ($-6.0 \times 10^{-5} \pm 0.002$ nmol min^{-1} m^{-3}), and high r^2 (0.92) (Figure 6-7).

6.3.2 Chemical Components Analysis

Teflon (47 mm PTFE Membrane Filters, 2 μm pore size, Pall Corp., Ann Arbor, MI, USA) and quartz filters (47 mm, Tissuquartz™ Filters, Pall Corp., Ann Arbor, MI, USA) were used as impaction surfaces, depending on the chemical analyses. For simultaneous sets, Teflon filters were used for one MOUDI at each site; for different-day collection, both quartz and Teflon filters were used for two MOUDIs at one site. Along with OP^{DTT}, particle chemical components measured included organic carbon (OC), elemental carbon (EC), ions, water-soluble, and total metals. OC, EC, ions, and metals were measured on quartz filters, and OP^{DTT} was measured on Teflon filters. OC and EC were measured using a

Sunset OCEC Analyzer (Sunset Laboratory Inc., Tigard, OR) following the IMPROVE protocol (Chow et al., 2007). Water-soluble and total metals including copper, manganese, and iron were measured using inductively coupled plasma mass spectrometry (ICP-MS) (Agilent 7500a series, Agilent Technologies, Inc., CA, USA). For water extracts, filters were sonicated in deionized (DI) water (> 18 MΩ cm^{-1}) with an Ultrasonic Cleanser (VWR International LLC, West Chester, PA, USA) for half an hour, and filtered with PTFE 0.45 μm syringe filters (Fisherbrand™). For determining total metals (elemental), filters were first digested in 2 mL of 1:3 HNO_3:HCl solution, diluted in DI water to a final volume of 10 mL, and then filtered with 0.45 μm syringe filters. Both water-soluble and total samples were then acidified by adding HNO_3 to achieve a final concentration of 2% HNO_3. A 25 ppb internal standard of scandium was added to every sample to monitor analytical drift. Only Cu data are discussed since our previous studies (Fang et al., 2016; Verma et al., 2014) show Cu is the main transition metal contributing to the OP^{DTT}. Ions were determined on the water-extracted samples (filtered with 0.45 μm filters) using ion chromatography (Metrohm 761 Compact ICs, Riverside, FL, USA). Surface area size distributions of OC, EC and $CaCO_3$ were calculated assuming spherical particles and the same density across all size ranges using the following equation:

$$\frac{dn_s}{d\ln D_p} = \frac{6}{\rho\, D_{pg}\, 10^6} \times \frac{dn_m}{d\ln D_p} \qquad \textbf{(Equation 10)}$$

where $\frac{dn_s}{d\ln D_p}$ and $\frac{dn_m}{d\ln D_p}$ are the surface area and mass distribution functions, respectively; D_p is aerodynamic diameter (μm); D_{pg} is the geometric mean diameter of each MOUDI stage (the square root of the product of upper and lower D_p of each MOUDI stage, μm); 10^6 is the unit conversion factor, and ρ is the particle density; 1.27 g cm^{-3} for OC (Turpin

and Lim, 2001), 1.77 g cm^{-3} for EC (Turpin and Lim, 2001), and 2.71 g cm^{-3} for $CaCO_3$. ($CaCO_3$ was calculated from Ca^{2+}; although the $CaCO_3$ concentration is likely underestimated since only water-soluble Ca^{2+} was measured and $CaCO_3$ is not highly soluble. $CaCO_3$ is taken as a surrogate of mineral dust (Tang et al., 2015; Zhao et al., 2013) and the shape of the $CaCO_3$ surface area distribution is taken to be identical as ambient mineral dust distribution). The surface area size distribution of OC, EC, and $CaCO_3$ can be found in section 6.6 Figure 6-8.

6.3.3 Oxidative Potential (OP)

OP measurement on Teflon MOUDI filters include OP_{ws}^{DTT} and total DTT (OP_{total}^{DTT}) activities. Water-insoluble OP^{DTT} was determined by difference ($OP_{wi}^{DTT} = OP_{total}^{DTT} - OP_{ws}^{DTT}$). The DTT assay was conducted manually or by a semi-automated instrument (Fang et al., 2015b; Fang et al., 2016) on the filtered DI water extracts to determine OP_{ws}^{DTT}. A 1 mM DTT solution was added to the sample extract with potassium phosphate buffer (Kbuffer, pH = 7.4) at 37 °C. At five different specific time intervals, a small aliquot from the mixture was withdrawn to determine remaining DTT concentration with a light absorption method. DTT consumption rate was used to calculate final OP. The DTT analysis explicitly followed the method described by Cho et al. (Cho et al., 2005).

OP_{total}^{DTT} was determined manually with the same method as that for OP_{ws}^{DTT}, except that the extract was not filtered. The sample filter was also left in the sample-Kbuffer-DTT mixture such that the DTT-active species from insoluble particles suspended in the extracts, and those still on the filter surface, could be in contact with added DTT and consume DTT over time. That is, after 0.5-h sonication, Kbuffer and DTT (1 mM) were added to the extract

with the sample filter included. At five time intervals, a small aliquot was withdrawn to determine remaining DTT concentration using the same light absorption method as stated above. A detailed method for measuring OP_{total}^{DTT} can be found in the Appendix A.6. The consistency of the manual DTT method was monitored with 9,10-phenanthraquinone as a positive control run on different days with the samples (N = 10, the coefficient of variation < 10%). Lognormal distributions were fit to all data. Fit equations are summarized in the Appendix A.4. For OP, geometric mean diameters (GMD) and geometric standard deviation (σ_g), total OP, and the associated uncertainties for each MOUDI set can be found in Table 6-2, Table 6-3. These tables also give the overall combined mean GMD and σ_g for both measures of OP at the RS and GT site. This mean GMD and σ_g were used to calculate the averaged frequency distribution ($df/dlnD_p$) of OP at each site. Average distribution ($dOP/dlnD_p$) was calculated differently. Each stage of the average distribution was the mean of corresponding stages from all MOUDI samples. The MOUDI sets collected in summer 2015 had a different cutoff diameter of 2.5 μm instead of a standard cutoff diameter of 1.8 μm; for these MOUDI sets, only stages with the same cut-off diameters as other MOUDI samples were included in calculating the average distribution. All OP^{DTT} reported is in unit of DTT loss rate per volume of air.

Intrinsic OP was calculated by dividing measured OP with PM mass concentration. Given that direct mass measurement was not done, PM mass concentration for each MOUDI stage was estimated from the sum of measured chemical components, including elemental carbon (EC), organic mass (OC*1.6 (Turpin and Lim, 2001)), total metals, and ions (SO_4^{2-}, NO_3^-, Cl^-, and NH_4^+). Total metals were represented by their oxide forms (K_2O, $CaCO_3$, MgO, CuO, MnO_2, and Fe_2O_3), except elemental mass was used for Cu and Mn for stages

below 1.8 μm, given that Cu and Mn particles smaller than 1.8 μm are mostly water-soluble (Fang et al., 2017a) and studies show likely in the form of metal sulfates (and sulfate was measured) (Oakes et al., 2012; Longo et al., 2016b). The PM mass distributions for both sites can be found in Figure 6-9.

6.3.4 Modeling Deposition in the Human Respiratory System

Deposition efficiency in the human respiratory tract represents the mean probability of an inhaled particle being deposited in a given compartment. Particle deposition efficiency estimates are based on empirical expressions derived from human inhalation data (ICRP, 1994) (ICRP., 1994). Deposition was modeled for an adult male at light work (breathing rate = 1.5 m^3 h^{-1}, respiration frequency = 20 min^{-1}, and tidal volume = 1250 cm^3) assuming unit density spherical particles (i.e., 1 g cm^{-3}). Regional deposition in different compartments of the respiratory tract (extrathoracic, bronchial, and alveolar regions) was calculated for nose-only breathing and are summarized in Figure 6-10. Deposition of OP in the respiratory system was obtained by multiplying the averaged frequency distributions of OP with the deposition efficiency. OP deposition was integrated over three particle size modes (ranges): quasi-ultrafine (<0.18 μm), accumulation (0.18-3.2 μm), and coarse (3.2-18 μm). Only total, alveolar, and extrathoracic deposition are discussed.

6.4 Results and discussion

6.4.1 Soluble fraction and size distribution of particulate oxidative potential

Figure 6-1 shows the size distribution of OP_{ws}^{DTT} and OP_{total}^{DTT}; the difference is OP_{wi}^{DTT}. The OP_{wi}^{DTT} to OP_{total}^{DTT} fraction depended on particle size. Average OP_{wi}^{DTT} to OP_{total}^{DTT} ratios at the

roadside (RS) were 23% and 51% in the fine and coarse mode, respectively. The average insoluble fraction at the urban (GT) site was similar in the fine (37%) and coarse (39%) mode. Note that these ratios were averaged from all MOUDI data.

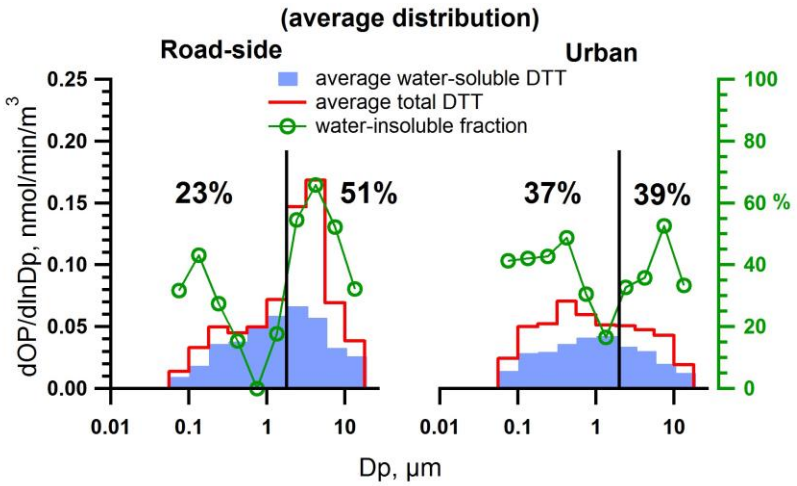

Figure 6-1 Average distribution of total and water-soluble DTT activities from all MOUDI samples. The mean water-insoluble fractions were calculated from the average distribution for fine and coarse modes separated by the vertical line at aerodynamic diameter D_p = 1.8 µm.

Frequency distributions are plotted to compare shapes of OP distributions for all MOUDI data since they are independent of the ambient OP levels, which can vary substantially between sites and measurement periods. Lognormal fitted frequency distribution for individual MOUDI measurement (N = 5 for OP_{ws}^{DTT}, and N = 2 for OP_{wi}^{DTT}) at RS and GT sites and the average frequency distribution of OP are shown in Figure 6-2 for OP_{ws}^{DTT} and OP_{wi}^{DTT}.

OP_{wi}^{DTT} had a bimodal distribution with a peak in the accumulation and coarse modes, in stark contrast to OP_{ws}^{DTT}, which was unimodal with peak near the minimum between the

two OP_{wi}^{DTT} modes (geometric mean diameter, GMD, ranged from 0.80 to 2.51 μm at both sites, Table 6-2). The sources and/or atmospheric processes producing OP_{ws}^{DTT} and OP_{wi}^{DTT} clearly differ.

Contrasting the OP frequency distributions at the two sites provides insights on the contributions of highway emissions to OP_{ws}^{DTT} and OP_{wi}^{DTT}. Small variations were observed in OP_{ws}^{DTT} frequency size distributions (Figure 6-2), especially at the GT site. OP_{ws}^{DTT} from one MOUDI sample collected in fall at the RS site, however, showed a peak at a much larger size (GMD = 2.51 μm) than the average frequency distribution (GMD_{mean} = 1.46 μm), suggesting that roadside OP_{ws}^{DTT} was occasionally affected largely by non-tailpipe traffic sources, which pushed the GMD to a larger size range. When removing this measurement, the GMD_{mean} for OP_{ws}^{DTT} at the RS site was 1.20 μm, much closer to that at the GT site, showing that OP_{ws}^{DTT} had a more regional character, consistent with earlier findings in the same region (Fang et al., 2015b; Verma et al., 2014). For OP_{wi}^{DTT}, the coarse-mode peak was larger than the accumulation mode at the RS site, while the opposite was observed at the GT site, indicating coarse-mode OP_{wi}^{DTT} was more affected by non-tailpipe traffic emissions. More limited transport of large size particles due to sedimentation, resulting in lower OP_{wi}^{DTT} at the GT site also would play a role.

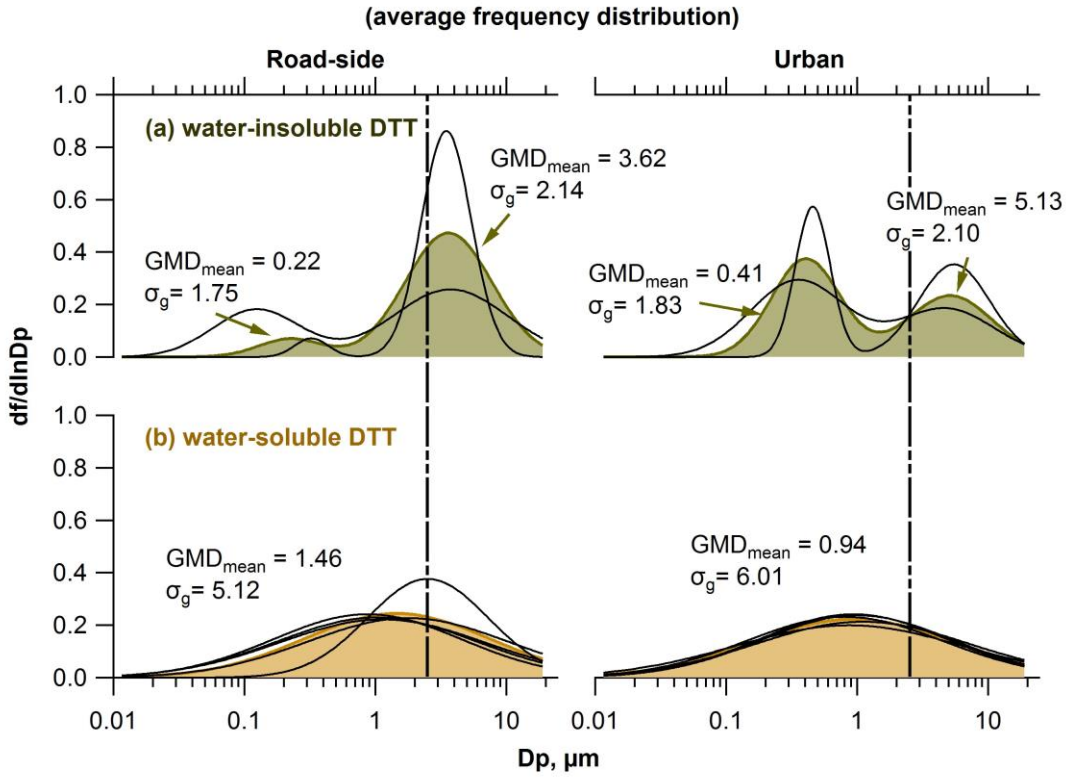

Figure 6-2 Averaged frequency distributions of (a) water-insoluble DTT and (b) water-soluble DTT activities at a road-side site (RS, left panels) and an urban background (GT, right panels) in Atlanta, GA, USA. The vertical dotted line is aerodynamic diameter D_p = 2.5 µm. GMD_{mean} and σ_g are the mean of the fit geometric mean diameter (µm) and geometric standard deviation, respectively, of multiple MOUDI samples (two sets for water-insoluble DTT, five sets for water-soluble DTT, per volume of air). Shaded color represents the mean frequency distribution. Each black curve represents the frequency distribution from each MOUDI measurement. The equation for the frequency distribution can be found in the Appendix A.4.

Comparing simultaneous measurements at the two sites (Figure 6-3) supports the above inferences. For example, OP_{wi}^{DTT} collected simultaneously at both sites exhibited much higher coarse mode levels at the RS site than at the GT site, suggestive of a major contribution from non-tailpipe traffic emissions to coarse-mode OP_{wi}^{DTT}. Accumulation-mode OP_{wi}^{DTT} and OP_{ws}^{DTT} levels were similar at both sites, indicating mainly a regional influence on accumulation-mode OP_{wi}^{DTT} and OP_{ws}^{DTT} for these MOUDI data sets.

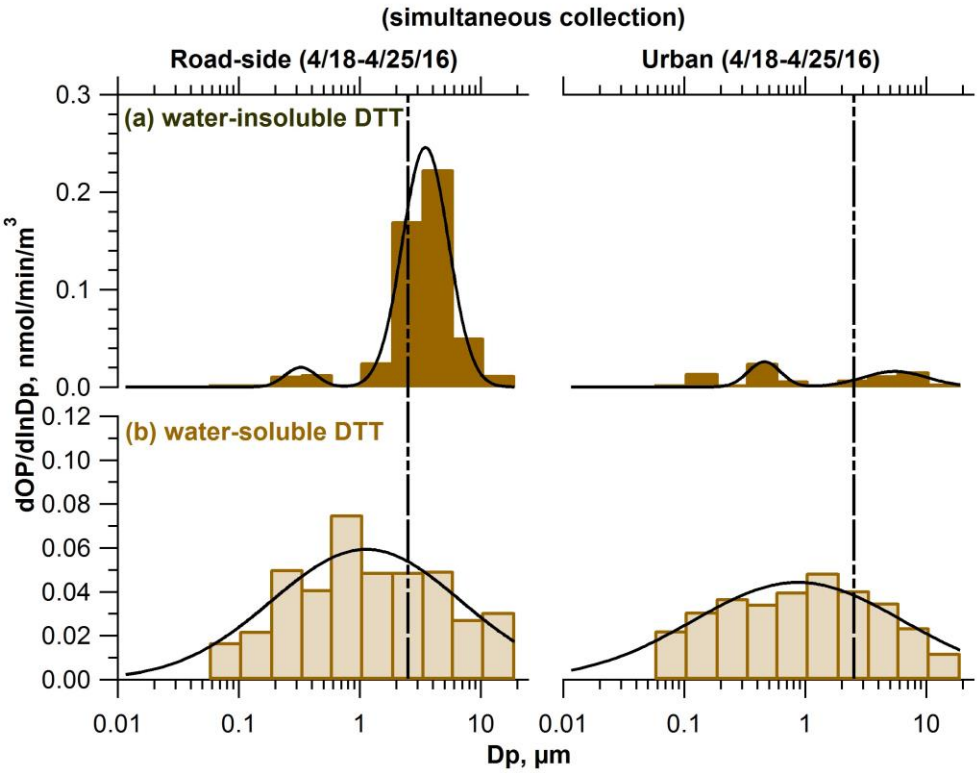

Figure 6-3 Ambient size distribution of oxidative potential from MOUDI samples collected simultaneously at a roadside site (RS, left panels) and a representative urban site (GT, right panels) in Atlanta, GA, USA. The vertical dotted line is aerodynamic diameter D_p = 2.5 µm.

6.4.2 Sources and processes based on other measured species

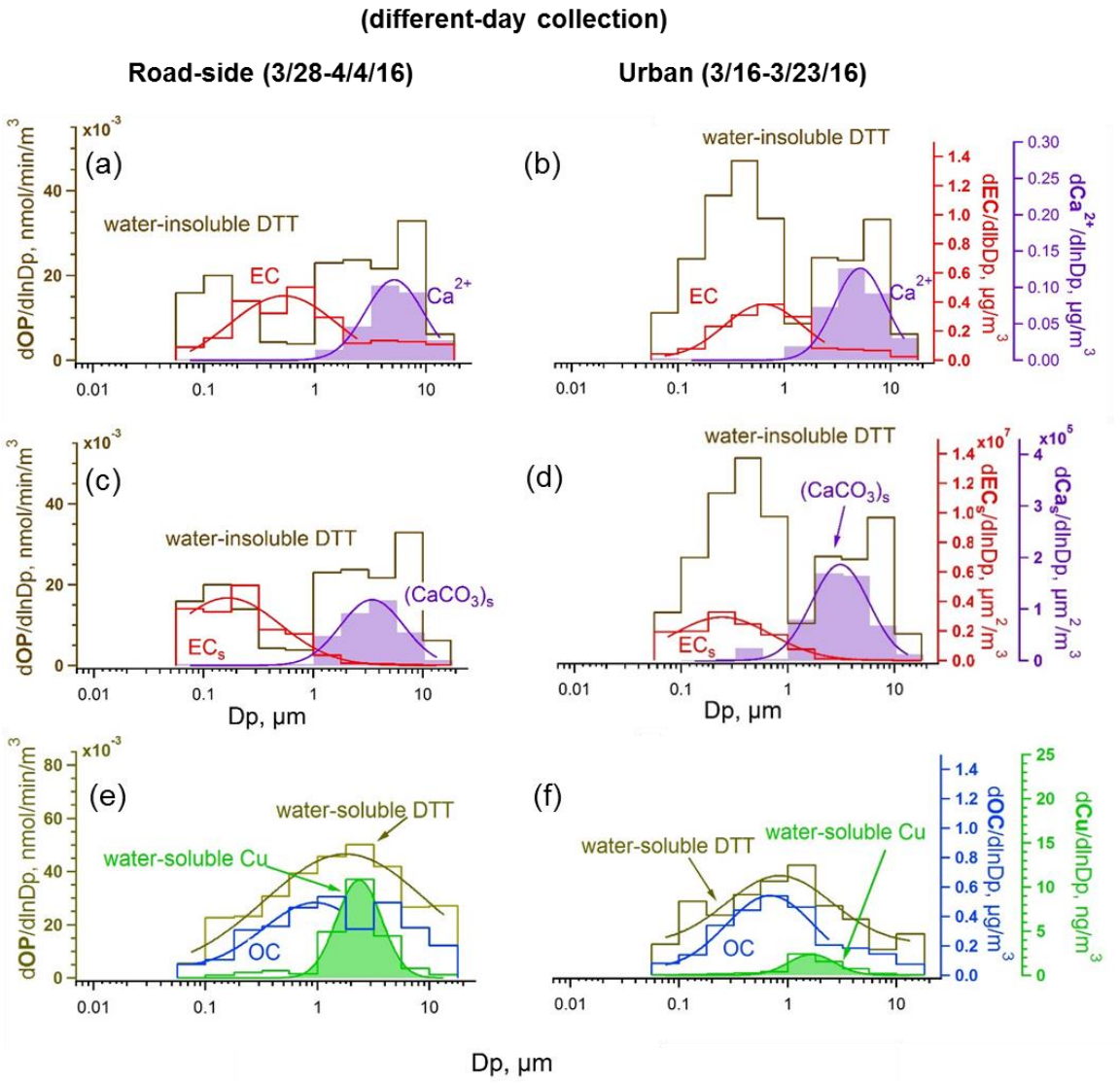

Figure 6-4 Size distributions of chemical species and oxidative potential at a road-side site (RS, left panels, 3/28-4/4/2016) and a representative urban site (GT, right panels, 3/16-3/23/2016) in Atlanta, GA. EC_s and $(CaCO_3)_s$ in (c) and (d) represent surface area distributions of EC and estimated $CaCO_3$; others are mass distributions.

Figure 6-4 shows the ambient size distributions of OP_{wi}^{DTT} and OP_{ws}^{DTT}, OC, EC, Ca^{2+} and water-soluble Cu, and the estimated surface area distribution of EC and $CaCO_3$ at both

sites. Ambient size distributions of chemical species provide clues to the sources and processes that led to the observed OP distributions. Fang et al. (Fang et al., 2017a) has reported on particle size-dependent processes relating to metals dissolution that affect OP_{ws}^{DTT}, here we focus mainly on OP_{wi}^{DTT}. Note that the MOUDI samples shown in Figure 6-4 at GT and RS sites were collected in different time periods. As is common, OC and EC had bimodal distributions with a larger accumulation-mode peak and a smaller peak in the coarse mode. Total Cu was most abundant in the coarse mode (data not shown, see Fang et al. (Fang et al., 2017a)), consistent with insoluble Cu particles mainly emitted from mechanical generation, such as braking components and resuspended dust (Adachi and Tainosho, 2004; Garg et al., 2000). Compared to total Cu, water-soluble Cu peaked at a smaller size, which can be explained by a combination of primary emissions (i.e., brake wear) and secondary processing by sulfate particles forming acidic conditions (Fang et al., 2015a; Fang et al., 2017a). Our previous paper (Fang et al., 2017a) showed that sulfate can produce highly acidic fine aerosols capable of dissolving Cu emitted in an insoluble form, and this acid-dissolved Cu played an important role in shaping the distribution of OP_{ws}^{DTT}. It is noted that Mn is also an important transition metal ion contributing to OP_{ws}^{DTT} (Verma et al., 2015a; Verma et al., 2014). Since Mn had a size distribution similar to that of Cu (Fang et al., 2017a), Mn may be involved the same processes in shaping the distribution of OP_{ws}^{DTT}. In addition to water-soluble metals, other evidence points to organic species from combustion playing an important role in fine-mode OP_{ws}^{DTT} (~ 60% from organics and 40% from metals) (Verma et al., 2015a). Thus, contributions from both water-soluble metals and organic species can explain why OP_{ws}^{DTT} had a broad distribution that peaked between fine-mode OC and water-soluble Cu [Figure 6-4 (e) and (f)]. The variation in GMD at the

roadside OP_{ws}^{DTT} can also be attributed to the varying relative contribution from water-soluble Cu and organic species; for example, a higher concentration of Cu may shift the distribution toward the coarse mode.

Bimodal OP_{wi}^{DTT} follow distributions of insoluble species in the accumulation and coarse modes. A main insoluble fine-mode aerosol is soot (or EC). Figure 6-4 (c) and (d) show that measured EC mass size distributions converted to EC surface area distributions match well with OP_{wi}^{DTT}, consistent with OP_{wi}^{DTT} being associated with the EC surface. Note that OC and EC have similar surface area distributions, Figure 6-8, but much of OC is soluble so it is difficult to infer insoluble OC size distributions from this data. We will show below that some of this insoluble OC, e.g., quinones or similar compounds, appear to coat soot. Studies reporting oxidation of PAHs (Antinolo et al., 2015) and diesel exhaust soot or black carbon (McWhinney et al., 2011; McWhinney et al., 2013a; Li et al., 2013) by ozone, forming surface-bound quinones and increasing OP^{DTT}, are consistent with our fine-mode OP_{wi}^{DTT} being associated with surfaces of EC. Measurements of fine-mode particle-bound PAHs in Atlanta traffic were highly correlated with black carbon ($r = 0.86$) (Greenwald et al., 2014). Furthermore, fine-mode number distributions of solid particles that remain insoluble when ambient aerosol was collected in water were highly correlated with EC mass concentrations (Greenwald et al., 2007) and had size distributions similar to that of EC (Figure 6-11), consistent with EC being the main insoluble fine-mode species.

The data also show the importance of time for atmospheric aging on fine-mode OP_{wi}^{DTT}. This can be seen by comparing the OP_{wi}^{DTT}/EC surface area ratio at the RS site, which is heavily influenced by primary emissions, to the GT site of more atmospheric processed

aerosols. Fine-mode (Dp < 1 μm) OP_{wi}^{DTT} per EC surface area concentration values were 4 to 5 times higher at the GT site (mean of OP_{wi}^{DTT} per EC surface area (mean ± standard deviation) was $(1.5 \pm 0.6) \times 10^{-8}$ and $(3.2 \pm 1.6) \times 10^{-9}$ nmol min^{-1} μm^{-2} for GT and RS site, respectively, see Figure 6-12 and Figure 6-13). A longer study also shows higher OP_{wi}^{DTT} per EC concentrations at the GT site based on bulk $PM_{2.5}$ samples collected simultaneously at both sites (Figure 6-14). This is consistent with PAH-coated EC being emitted by the road, but requiring oxidation to convert EC-surface PAHs to quinones. Higher O_3 levels away from the road due to less NOx titration may also play a role. These processes explain the observed similar fine-mode OP_{wi}^{DTT} levels when measured simultaneously at the RS and GT sites. Because fresh soot per mass (or surface area) does not have as high OP^{DTT} as aged aerosol, OP^{DTT} is clearly not related solely to a soot surface property formed during emission.

Soluble transition metals also contribute to OP^{DTT} but are typically not found in particles smaller than 1 μm. However, they may account for much of the coarse-mode OP_{wi}^{DTT}. Primary coarse-mode particles are generated by mechanical processes. There is limited information on which chemical species may contribute to coarse-mode OP_{wi}^{DTT}, but the $CaCO_3$ surface area distribution is seen to be similar to that of OP_{wi}^{DTT} in coarse mode at both sites, suggesting that it is also related to a surface property. Soluble metals (and possibly some contribution from adsorbed EC and quinones, see Figure 6-15 and Figure 6-16 for EC and OC in the coarse mode) may remain bound to these large mineral dust particles during the water extraction process and account for at least some of the coarse-mode OP_{wi}^{DTT}.

6.4.3 Intrinsic OP distributions

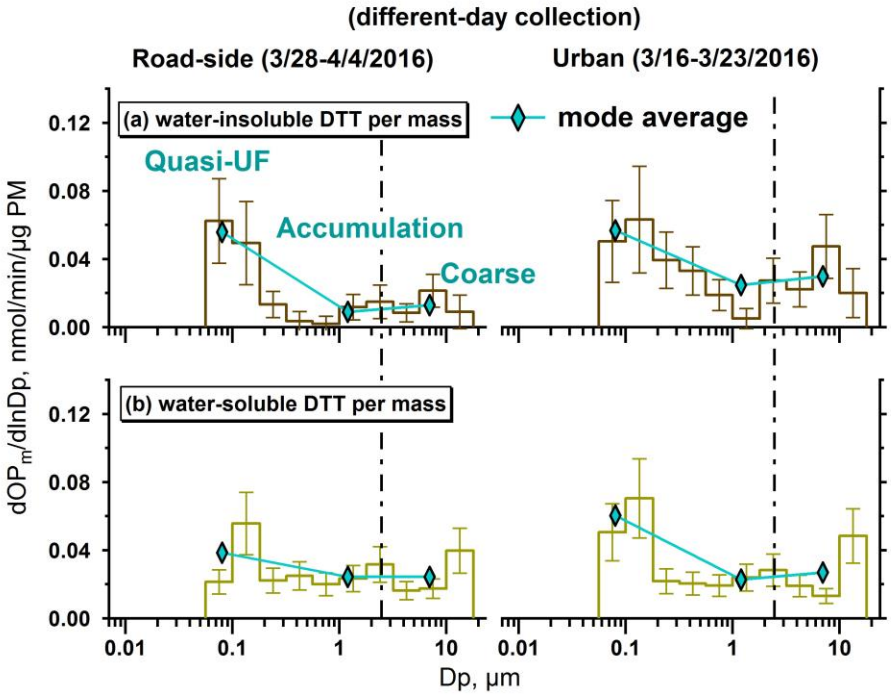

Figure 6-5 Oxidative potential distributions on a per PM mass basis at a road-side site (RS, left panels, 3/28-4/4/2016) and a representative urban site (GT, right panels, 3/16-3/23/2016) in Atlanta, GA, USA. Average OP per mass for three modes, quasi-ultrafine (< 0.18 µm), accumulation (0.18 ≤ D_p ≤ 3.2 µm), and coarse (3.2 < D_p <10 µm) is also shown (diamonds with line). PM mass on each MOUDI stage was estimated from the sum of measured chemical components. The dotted line is aerodynamic diameter D_p = 2.5 µm. Error bars were based on uncertainties associated with OP per mass calculated by propagation of uncertainties from OP per air volume and PM mass estimates.

Comparing the oxidative activity of different size particles on a per PM mass basis (intrinsic activity) can provide a measure of aerosol toxicity. Figure 6-5 shows that both OP_{ws}^{DTT} and OP_{wi}^{DTT} per mass are highest for quasi-ultrafine particles where the mass is low. (Note that OP^{DTT} per mass is also high for the large particles, but in this case, masses may be underestimated due to inferring total $CaCO_3$ from soluble measured Ca^{2+}). In terms of

modes, OP_{ws}^{DTT} per mass was the highest for quasi-ultrafine, in agreement with some other studies (Cho et al., 2005; Ntziachristos et al., 2007). OP_{wi}^{DTT} also had the highest per mass activity for the quasi-ultrafine mode, consistent with high soot (EC) toxicity. Although the intrinsic activities provide contrast in the OP potency of particles of differing sizes, overall potential for adverse health effects depends on exposure; the OP activity per volume of air, which has a very different distribution than that of OP^{DTT} per PM mass, and the efficiency of particle deposition as a function of size in the respiratory system.

6.4.4 Respiratory OP deposition

Particle deposition patterns in the respiratory tract, in part, depend on particle size. Since chemical components driving OP_{wi}^{DTT} and OP_{ws}^{DTT} vary with particle size, different components of OP^{DTT} will be deposited in different regions. OP^{DTT} deposition was calculated for the whole respiratory tract (extrathoracic and all lung compartments) and two sub-regions, the extrathoracic compartment and the alveolar. In each region we compare the relative importance of OP^{DTT} associated with quasi-ultrafine, accumulation, and coarse modes. The results are shown in Figure 6-6. For the whole respiratory tract, coarse-mode OP_{wi}^{DTT} (DTT loss rate per volume of air) deposition dominated at both the urban and road-side sites, accumulation-mode OP_{wi}^{DTT} deposition was also high and quasi-ultrafine OP^{DTT} was minimal. For OP_{ws}^{DTT} a similar pattern was found, except accumulation-mode particles made greater contributions or were on par with coarse-mode particle contributions to whole respiratory tract deposition. Extrathoracic deposition patterns for both forms of OP^{DTT} were similar to those of the whole respiratory tract, accumulation and coarse particles made the most contributions; coarse mode was larger for OP_{wi}^{DTT} and coarse

and accumulation were similar for OP_{ws}^{DTT}. For alveolar deposition, there was much less contribution from coarse-mode particles (coarse particle alveolar deposition was < 4% of the whole respiratory tract deposition), because the majority was deposited in the upper respiratory tract. Alveolar deposition was dominated by accumulation-mode particles for both OP_{wi}^{DTT} andOP_{ws}^{DTT}.

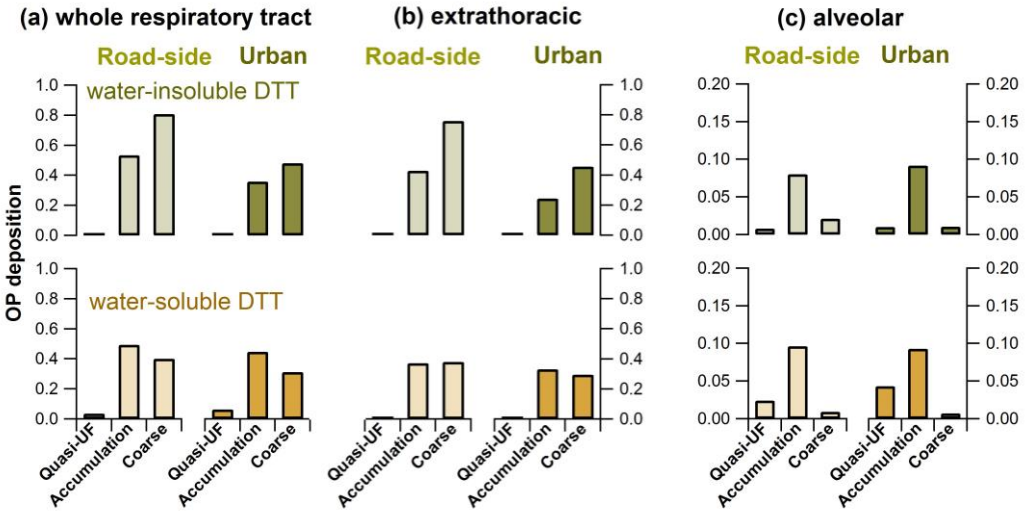

Figure 6-6 Estimated whole respiratory tract, extrathoracic, and alveolar deposition of PM oxidative potential in the human respiratory system for three aerosol size modes: quasi-ultrafine (D_p < 0.18 µm), accumulation (0.18 ≤ D_p ≤ 3.2 µm), and coarse (3.2 < D_p <10 µm). Whole-lung deposition refers to the total OP deposited in the whole respiratory tract. Deposition of OP equals the deposition efficiency times the average OP frequency distribution (vertical axis is unitless), both a function of particle size. Deposition efficiencies were based on an empirical expression assuming unit density spheres for steady breathing with a flow rate of 1.5 cm^3 h^{-1}, breathing frequency of 20 min^{-1}, and tidal volume of 1500 cm^3. OP deposition on the vertical axis was calculated by integrating the deposition of OP over the three particle size modes.

These comparisons show that although quasi-ultrafine particles are more DTT-active per mass and are deposited in the alveoli with higher efficiencies than accumulation and coarse particles (close to 100%), the deposition levels of quasi-ultrafine OP-containing particles were small in this study, and so less important. These results are as expected; coarse-mode particles are deposited in the upper respiratory tract (extrathoracic and tracheobronchial regions) and accumulation-mode particles predominantly in the alveoli. Consequently, upper respiratory deposition of OP_{wi}^{DTT} would be related to soluble metals, with minor contributions from quinones adsorbed to dust (or quinones adsorbed to soot adsorbed to dust). Similarly, for upper airway deposition of OP_{ws}^{DTT}, soluble transition metals would dominate (Fang et al., 2017a). For alveolar deposition of OP_{wi}^{DTT}, the main aerosol components would be those associated with or adsorbed to, soot surfaces, the latter mostly quinones (or similar compounds). Alveolar deposition of OP_{ws}^{DTT} is also mainly associated with quinones, soluble transition metal ions would play a minor role (Fang et al., 2017a). Limited mixing between the organic aerosol (e.g., quinones) and transition metal ions in single particles due to association with different sizes (e.g., for $PM_{2.5}$, mixing is only likely in the 1 to 2.5 μm size range) raises the question if these main components of OP^{DTT} will extensively interact when deposited in the lung. Bulk measurements of OP^{DTT} that mix components of all sizes for $PM_{2.5}$ samples may produce interactions between DTT-active organic species and transition metal ions that would not occur to the same extent in lung lining fluid, leading to artifacts. Finally, it remains to be determined if water-soluble and water-insoluble OP^{DTT} are linked to differing health end points, despite both forms of OP^{DTT} being driven by similar size-dependent aerosol chemical components.

6.5 Summary

Ambient size distributions of water-soluble and water-insoluble OP^{DTT}, and various chemical components at a road-side and urban site were used to study the sources and atmospheric processes that contribute to both fractions of OP^{DTT}. The results show that the two main chemical components that drive water-soluble and water-insoluble OP^{DTT} are the same, transition metal ions and organic species, such as quinones. The difference is that for water-insoluble OP^{DTT}, these two major players were absorbed on solid surfaces; transition metal ions on coarse-mode mineral-tire-brake dust or soot surfaces, while quinones on fine-mode soot surface, resulting in a bimodal distribution with a fine and coarse mode for water-insoluble OP^{DTT}. In contrast, water-soluble OP^{DTT} was unimodal with a peak near 1-2.5 μm due to contributions from fine-mode organic components plus acid-processed coarse-mode transition metal ions. The data show the importance of secondary processing for both fractions of OP^{DTT}. Lung deposition analyses suggest that although ultrafine particles had the highest OP^{DTT} per mass (toxicity), lung deposition was mainly contributed by fine and coarse modes. Upper respiratory deposition of OP^{DTT} was mainly associated with transition metal ions while alveolar deposition was mainly with organic species. Contrasts in the phases of these forms of OP^{DTT} deposited in the respiratory system may have differing health impacts.

6.6 Supporting materials

Table 6-1 Summary of MOUDIs filter collection and analysis

Season Year	Sampling Period	RS (road-side)		GT (urban)	
		MOUDI #1	**MOUDI #2**	**MOUDI #1**	**MOUDI #2**
Summer 2015	7/6-7/13/2015			*Teflon (OP_{ws}^{DTT})	
	7/23-7/30/2015		Teflon (OP_{ws}^{DTT})	Teflon (OP_{ws}^{DTT})	
	8/3-8/11/2015	Teflon (OP_{ws}^{DTT})			
Fall 2015	9/16-9/24/2015			Teflon (OP_{ws}^{DTT})	Quartz (OC, EC, ions)
	10/6-10/14/2015	Teflon (OP_{ws}^{DTT})	Quartz (OC, EC, ions)		
Spring 2016	3/16-3/23/2016			Teflon (OP_{ws}^{DTT}, OP_{total}^{DTT})	Quartz (OC, EC, ions, metals)
	3/28-4/4/2016	Teflon (OP_{ws}^{DTT}, OP_{total}^{DTT})	Quartz (OC, EC, ions, metals)		
	4/18-4/25/2016		Teflon (OP_{ws}^{DTT}, OP_{total}^{DTT})	Teflon (OP_{ws}^{DTT}, OP_{total}^{DTT})	

* filter type (species measured), Organic carbon (OC), elemental carbon (EC), ions, and metals were determined from the pre-baked quartz filters (47 mm, Tissuquartz™ Filters, Pall Corp., Ann Arbor, MI, USA), and the Zefluor filters (47 mm PTFE Membrane Filters, 2 μm pore size, Pall Corp., Ann Arbor, MI, USA) were used for determining the OP of particles.; OP_{ws}^{DTT} – water-soluble DTT activity; OP_{total}^{DTT} – total DTT activity.

Table 6-2 Summary of size distribution geometric mean diameters (GMD) in μm for lognormal fits of OP from all MOUDIs sets collected in Atlanta, GA (Parameters for OP_{wi}^{DTT} are shown for fine and coarse mode due to bimodal distribution)

Season Year	Sampling Period	RS (road-side)			GT (urban)		
		OP_{ws}^{DTT}	OP_{wi}^{DTT}		OP_{ws}^{DTT}	OP_{wi}^{DTT}	
			Fine	coarse		Fine	coarse
Summer 2015	7/6-7/13/2015	-	-	-	1.00	-	-
	7/23-7/30/2015	0.87	-	-	0.94	-	-
	8/3-8/11/2015	1.03	-	-	-	-	-
Fall 2015	9/16-9/24/2015	-	-	-	1.10	-	-
	10/6-10/14/2015	2.51	-	-	-	-	-
Spring 2016	3/16-3/23/2016	-	-	-	0.80	0.35	4.76
	3/28-4/4/2016	1.77	0.12	3.76	-	-	-
	4/18-4/25/2016	1.13	0.32	3.48	0.87	0.46	5.50
* GMD, **Mean ± SD**		**1.46 ± 0.68**	**0.22 ± 0.14**	**3.62 ± 0.20**	**0.94 ± 0.12**	**0.41 ± 0.07**	**5.13 ± 0.52**

Table 6-3 Summary of size distribution geometric standard deviation (σ_g) [unitless] for lognormal fits of OP from all MOUDIs sets collected in Atlanta, GA (Parameters for OP_{wi}^{DTT} are shown for fine and coarse mode due to bimodal distribution)

Season Year	Sampling Period	RS (road-side)			GT (urban)		
		OP_{ws}^{DTT}	OP_{wi}^{DTT}		OP_{ws}^{DTT}	OP_{wi}^{DTT}	
			Fine	coarse		Fine	coarse
Summer 2015	7/6-7/13/2015	-	-	-	5.36	-	-
	7/23-7/30/2015	5.21	-	-	5.21	-	-
	8/3-8/11/2015	5.69	-	-	-	-	-
Fall 2015	9/16-9/24/2015	-	-	-	6.49	-	-
	10/6-10/14/2015	2.89	-	-	-	-	-
Spring 2016	3/16-3/23/2016	-	-	-	5.59	2.29	2.33
	3/28-4/4/2016	5.79	2.16	2.74	-	-	-
	4/18-4/25/2016	6.03	1.35	1.55	7.38	1.36	1.87
* σ_g, **Mean ± SD**		**5.12 ± 1.28**	**1.75 ± 0.57**	**2.14 ± 0.84**	**6.01 ± 0.92**	**1.83 ± 0.66**	**2.10 ± 0.32**

Table 6-4 Summary of total OP (OPt) for each lognormal fit of OP [nmol min^{-1} m^{-3}] from all MOUDIs sets collected in Atlanta, GA (Parameters for OP_{wi}^{DTT} are shown for fine and coarse mode due to bimodal distribution)

Season Year	Sampling Period	RS (road-side)			GT (urban)		
		OP_{ws}^{DTT}	OP_{wi}^{DTT}		OP_{ws}^{DTT}	OP_{wi}^{DTT}	
			Fine	coarse		Fine	coarse
Summer 2015	7/6-7/13/2015	-	-	-	0.18	-	-
	7/23-7/30/2015	0.21	-	-	0.20	-	-
	8/3-8/11/2015	0.25	-	-	-	-	-
Fall 2015	9/16-9/24/2015	-	-	-	0.21	-	-
	10/6-10/14/2015	0.27	-	-	-	-	-
Spring 2016	3/16-3/23/2016	-	-	-	0.16	0.10	0.07
	3/28-4/4/2016	0.20	0.04	0.07	-	-	-
	4/18-4/25/2016	0.27	0.02	0.27	0.22	0.02	0.03
* OPt, **Mean ± SD**		**0.24 ± 0.03**	**0.03 ± 0.01**	**0.17 ± 0.14**	**0.20 ± 0.02**	**0.06 ± 0.06**	**0.05 ± 0.03**

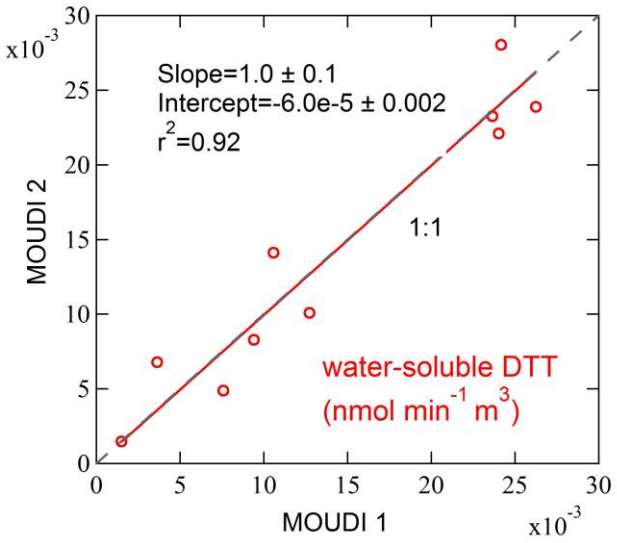

Figure 6-7 Comparison between two MOUDIs deployed side-by-side at the GT site where OP_{ws}^{DTT} were measured at each stage. Each data point is for the same impactor stage on the two MOUDIs. Linear fits were done by orthogonal regression. The dotted line is 1:1.

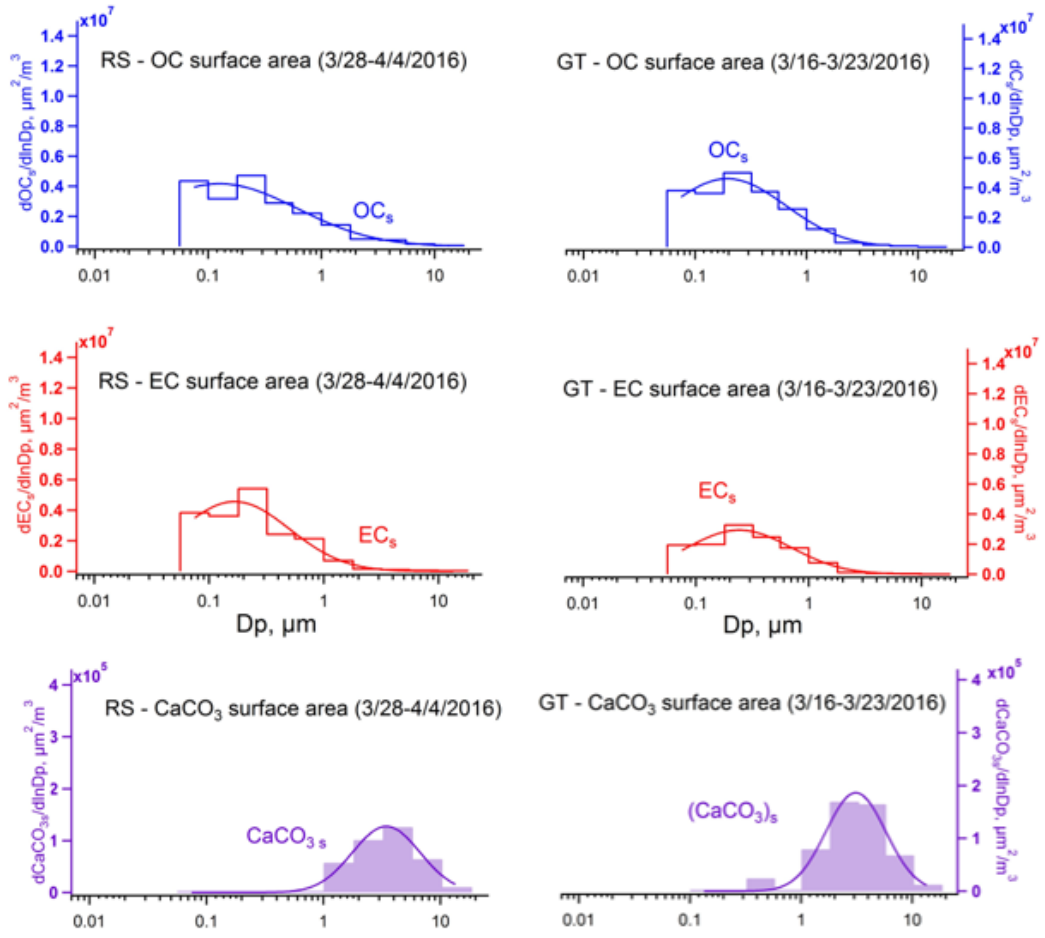

Figure 6-8 Surface area distribution of OC, EC, and $CaCO_3$ from MOUDI set collected in spring 2016.

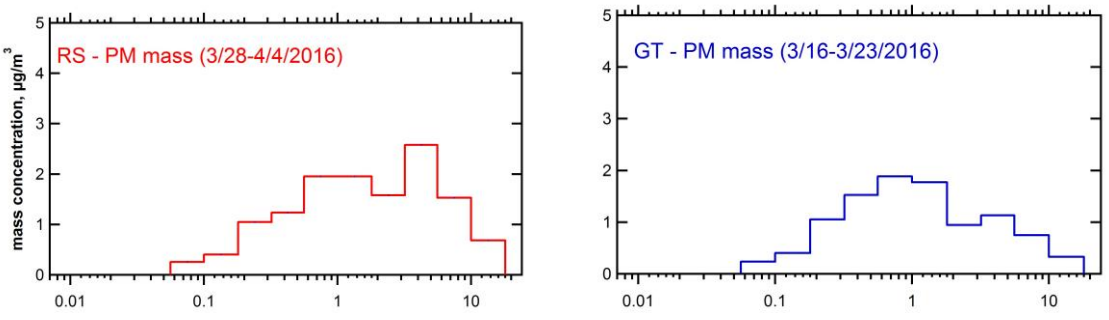

Figure 6-9 Estimated PM mass size distribution from the sum of elemental carbon (EC), organic mass (OC*1.6), total metals, and ions (SO_4^{2-}, NO_3^-, Cl^-, and NH_4^+) from MOUDI samples collected in Spring 2016. Total metals were represented by their

oxides forms (K_2O, $CaCO_3$, MgO, CuO, MnO_2, and Fe_2O_3), except for Cu and Mn that their total metals (elemental) were used for stages below 1.8 µm, given that Cu and Mn particles smaller than 1.8 µm are mostly water-soluble (Fang et al., 2017a) and metal sulfates (Oakes et al., 2012; Longo et al., 2016b).

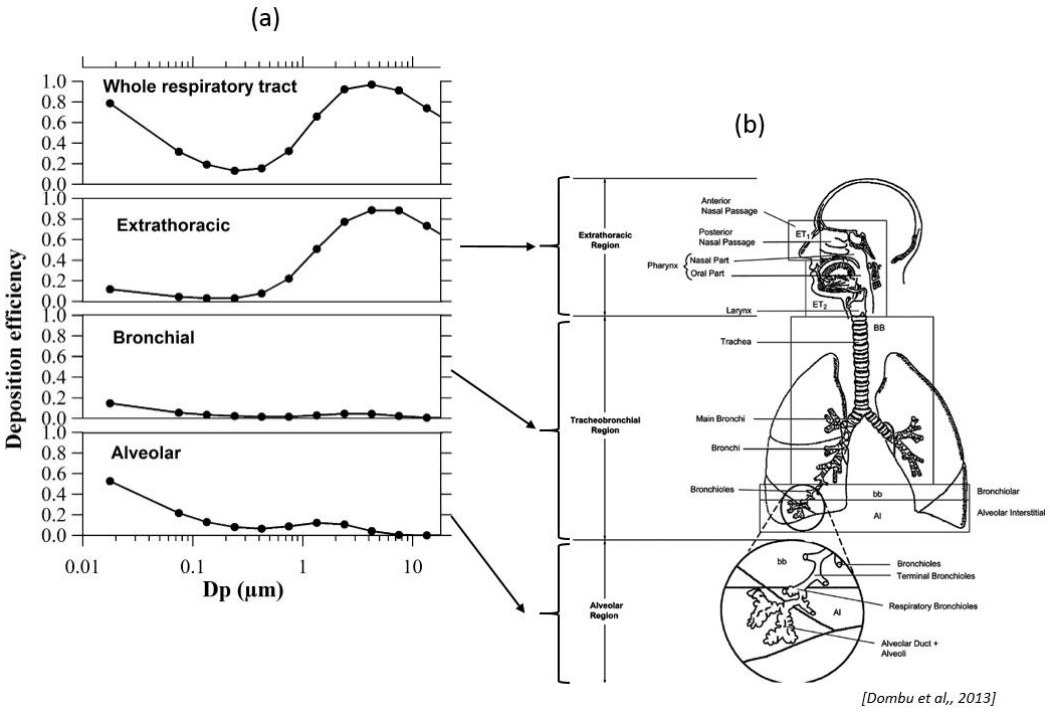

Figure 6-10 Whole respiratory tract and regional deposition efficiency of aerosols assuming unit density spherical particle and nose-only breathing at a steady breathing with a flow rate of 1.5 m^3 h^{-1}, respiration frequency of 20 min^{-1}, and tidal volume of 1250 cm^3. Regional deposition refers to the collection of particles in extrathoracic, bronchial, and alveolar regions. (b) was adapted from Dombu et al., 2013 (Dombu and Betbeder, 2013).

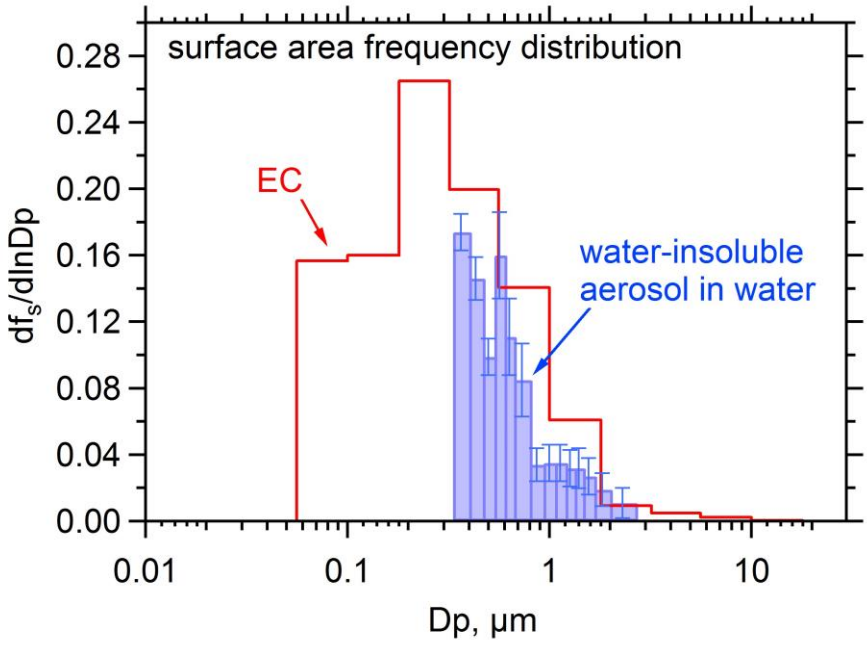

Figure 6-11 Water-insoluble aerosol (WIA) surface area frequency distribution adapted from the number concentration distribution from Greenwald et al. (Greenwald et al., 2007) in comparison with EC surface area frequency distribution at the urban site from this work. The WIA instrument collects ambient aerosols into water with a high flow rate liquid impinger and measures the solid particles in the liquid with optical diameters from 0.25 to 2.0 μm with an optical particle counter to determine the number concentration distribution of ambient insoluble particles in water. This WIA instrument provides evidence of the size distribution of insoluble particles when deposited in the lung, in contrast to the distribution in the ambient atmosphere that may be internally mixed with soluble species, assuming the water-soluble components have similar solubilities in water as lung lining fluid. The surface area function was calculated from the measured number concentration using the equation $\frac{dS}{d\ln D_p} = \frac{dN}{d\ln D_p} \pi D_{pg}^2$, where D_p and D_{pg} is the aerodynamic and geometric mean aerodynamic diameter in each MOUDI stage (μm). The optical diameter from Greenwald et al. (Greenwald et al., 2007) was converted to aerodynamic D_p using the equation $D_p = D_{optical}\ \rho^{0.5}$ (referred to Murphy et al. (Murphy et al., 2004)), where $D_{optical}$ is the optical diameter (μm) and ρ is the density, 1.77 g cm^{-3}. Error bars on the WIA surface distribution represent the standard deviations from four sets of data collected from May to June in 2004.

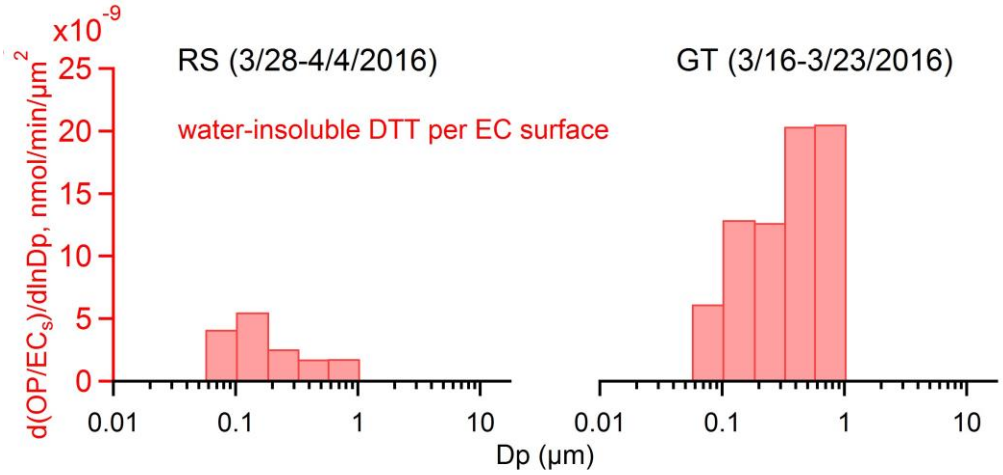

Figure 6-12 Water-insoluble DTT per EC surface area for Dp smaller than 1 µm. MOUDI samples were collected during different time periods at a road-side (RS) and urban (GT) site in Atlanta. OP_{wi}^{DTT} per EC surface area (mean ± standard deviation) was (1.5 ± 0.6) × 10^{-8} and (3.2 ± 1.6) × 10^{-9} nmol min^{-1} $µm^{-2}$ for GT and RS, respectively.

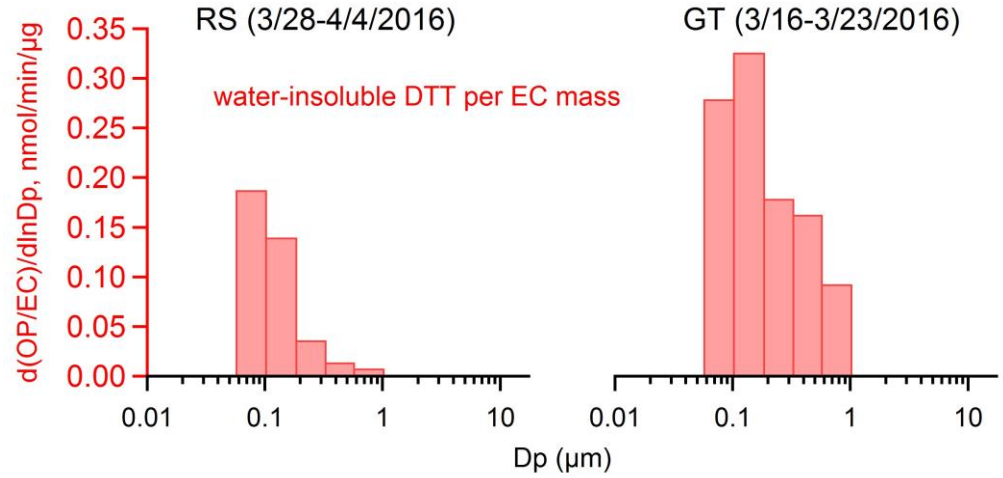

Figure 6-13 Water-insoluble DTT per EC mass for Dp smaller than 1 µm. MOUDI samples were collected during different time periods at a road-side (RS) and urban (GT) site in Atlanta. OP_{wi}^{DTT} per EC mass (mean ± standard deviation) was 0.21 ± 0.09 and 0.08 ± 0.08 nmol min^{-1} $µg^{-1}$ for GT and RS, respectively.

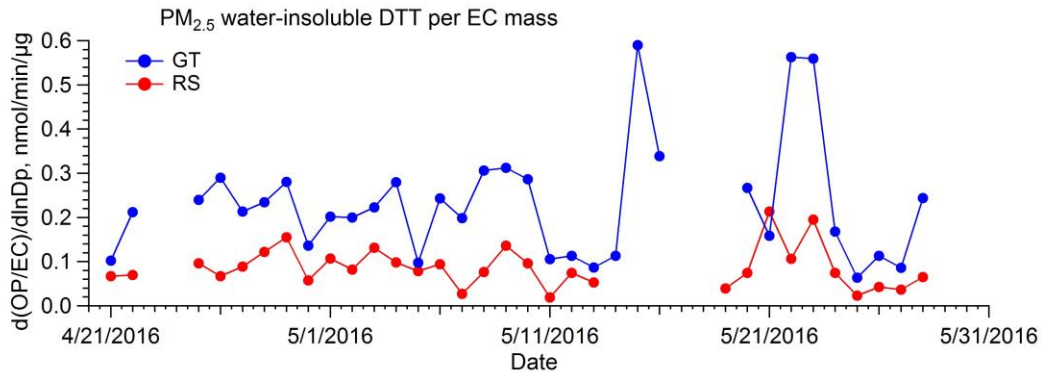

Figure 6-14 Water-insoluble DTT per EC mass from $PM_{2.5}$ samples collected on filters at road-side (RS) and urban site (GT). OP_{wi}^{DTT} per EC mass was 0.23 ± 0.13 and 0.09 ± 0.05 nmol min^{-1} μg^{-1} for GT and RS, respectively.

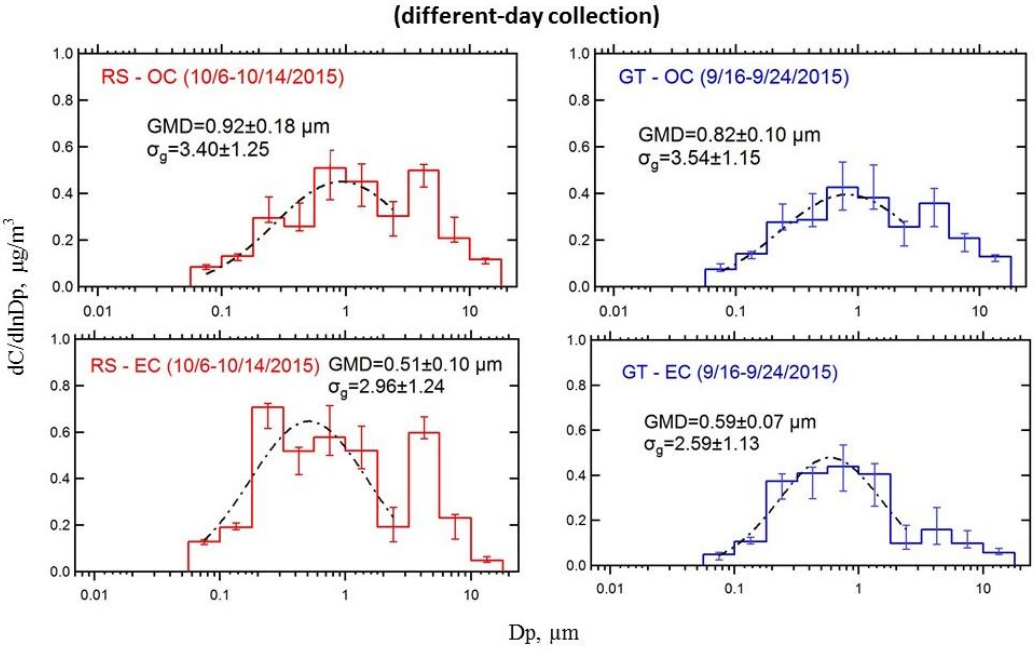

Figure 6-15 Ambient size distribution of OC and EC from MOUDI sets collected in fall 2015.

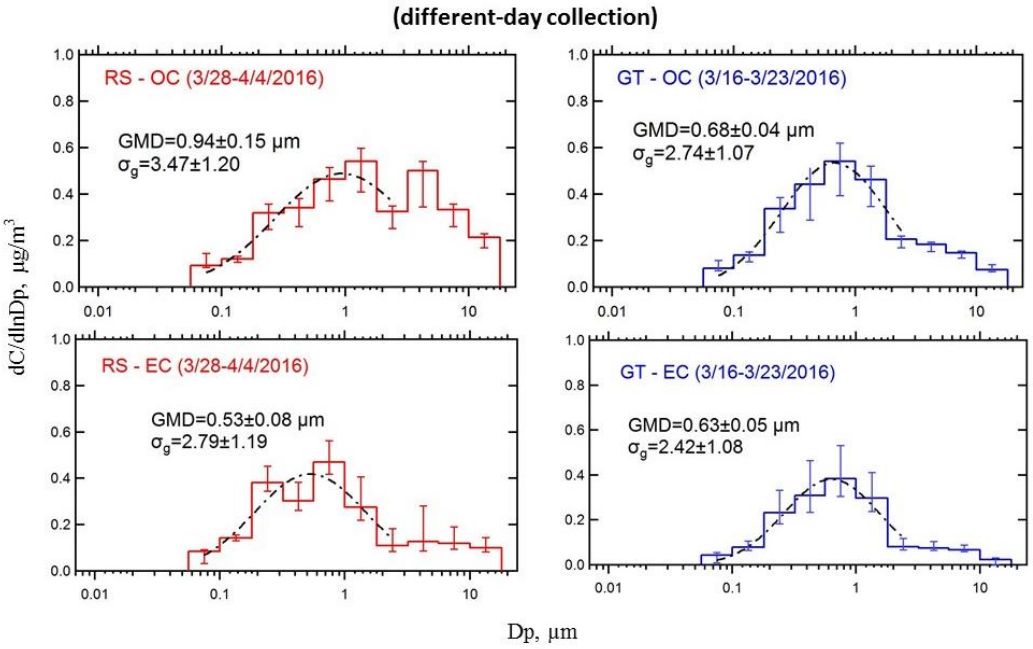

Figure 6-16 Ambient size distribution of OC and EC from MOUDI sets collected in spring 2016.

CHAPTER 7. FUTURE WORK

In this thesis, we have assessed aerosol oxidative potential (OP) as a health indicator from epidemiological models and extensively studied the sources and processes leading to OP. OP measured by the dithiothreitol (DTT) method represent the capability of multiple toxic components in the PM mixture (organic species and transition metal ions, comprising only a minor proportion of the total mass) to generate reactive oxygen species (ROS) that lead to oxidative stress, making OP a better health indicator than PM mass concentration and OP measured by the Ascorbic Acid (AA) assay with a narrower chemical sensitivity. Policies that focus on reducing the total mass concentration of PM should be set in terms of OP, focusing more heavily upon sources and processes emitting toxic transition metal ions and organic species. Overall, the results of this thesis have improved our understanding of oxidative potential in aerosol health studies and offered a promising way forward; however, there are a few critical issues needing further attention or research.

Measurement of OP

This thesis used two common measures of OP, the dithiothreitol DTT and AA assays. The DTT assay is based on the same protocol from Cho et al. (Cho et al., 2005), and the AA assay is a simplified approach to a more complex synthetic respiratory tract lining fluid (RTLF) model (Mudway et al., 2004; Zielinski et al., 1999). A major challenge associated with the DTT assay is that there is substantial variation in the DTT method used in different studies, making inter-comparisons between studies difficult. One important cause of the difficulty is the different initial DTT concentration used in different studies, i.e., the

concentration of DTT solution at the beginning of DTT consumption process (at time 0). Standardization of the DTT measurement method is needed.

Most part of this thesis is based on the OP measured from water extracts of particles collected onto a filter subtract. While filter-based collection approaches with long sampling duration are commonly needed for high mass loadings for OP analysis, they entail artifacts due to losses of semi-volatile species during sampling and handling procedures. Studies have shown that semi-volatile components of particles contribute to OP^{DTT} (Verma et al., 2011). Besides, composite samples collected over a long period of time do not capture the diurnal variations in the aerosol OP. Developing online and high time-resolved OP measurement systems could avoid these artifacts and provide diurnal profiles of OP for further understand the sources and processes contributing to OP. Sameenoi et al. have developed a microfluidic electrochemical sensor for online monitoring of OP^{DTT} (Sameenoi et al., 2012a) and a microfluidic paper-based analytical device using the DTT assay which skips the extraction procedure (Sameenoi et al., 2012b). However, these systems have not been further tested in field studies. Eiguren-Fernandez et al. (Eiguren-Fernandez et al., 2017) developed an online DTT system (o-MOCA) collecting particles directly into small volume of liquid using a Liquid Spot Sampler (LSS). This system was tested in the ambient only for 3 days. Further studies on the online system development for OP measures are needed.

The DTT and AA assays only represent two of the many OP measures that are available. Other commonly used a-cellular OP assays include $OH\cdot$ production in a surrogate lung fluid (Jung et al., 2006), electron spin resonance (ESR) (Shi et al., 2003), chemiluminescent reductive acridinium triggering (CRAT) (Zomer et al., 2011), and glutathione reductase

recycling (GSH) (Li et al., 2003) methods. Although studies have compared some of these methods together (Yang et al., 2014; Ayres et al., 2008; Fang et al., 2016), so far there has been a lack of systematic comparisons of all OP methods. Associations between different OP measures and health were only limited to two OP comparison, e.g. OP^{ESR} vs OP^{DTT} (Yang et al., 2016), OP^{GSH} vs OP^{AA} (Weichenthal et al., 2016a; Weichenthal et al., 2016b; Strak et al., 2012), and OP^{DTT} vs OP^{AA} from this thesis (Fang et al., 2016). Attempts to synthesize different studies to achieve comprehensive comparisons between OP measures are impossible due to the differences in ambient environments, extraction medium, measured chemical species, and selected health outcomes. There remains a need to compare all different OP measures to find out the relative merits of different OP assays and construct an invaluable standard protocol (one assay or several complementary assays) for initial screening of particle toxicity.

Metals and organics

Acid processing has been identified as an important mechanism driving metal solubility. While this thesis provides some evidence of acidity driven mechanism from the ambient size distributions of metals, sulfate, and particle pH, our data do not provide information related to other factors that could potentially affect the acid dissolution of metals, for example, time for dissolution, temperature, phase state of the aerosol, mixing state, and complexation between metals and organic species. There is clearly a need for more studies examining the acidity-driven dissolution process and the role of these factors in aerosol OP.

One important finding of this thesis is that both transition metal ions and organic species are important to health since water-soluble OP^{DTT}, attributed to both organics and metals, not water-soluble OP^{AA}, driven mainly by metals, are found statistically significant associated with health outcomes. Preliminary laboratory studies in our lab suggest a synergistic effect between metals and quinones in ambient samples. In addition, we tested the behaviors of pure metal solutions and ambient aerosol water extracts on a C-18 column designed to separate the hydrophilic (those pass through the column) and hydrophobic (those retained on the column) fractions (data not presented in the thesis). The results showed that pure metals were all retained by the C18 columns, while fractions of metals in ambient samples passed through, suggesting a complexation of metals with organics. The complexation of metals with organics might possibly limit their participation in the electron transfer reactions that produce ROS. This suggests that although metals and organic species are the main drivers to OP^{DTT}, since there is synergistic effect between them affecting their OP, there is advantage of using OP^{DTT} over species when studying the health effects of aerosol. Future studies should focus on the synergistic effects between organic species and metals and the effects on their toxicity.

The same idea can be applied to OP vs sources. Our results showed that secondary processing was the main contributor to OP^{DTT} in summer and biomass burning played a more important role in winter. It is interesting to compare the health associations between sources and OP^{DTT} in different seasons.

Cellular work

This thesis linked ambient OP measurement with hospital data from epidemiology, there is a big gap from a cellular level. One important issue with chemical assays is that they don't simulate the real interaction between PM and cells. Although the DTT assay mimics the electron-transfer mechanism based on the catalytic ability of redox-active species to transfer elections from DTT to oxygen, whether OP^{DTT} is associated with the cellular oxidative stress responses is still an open question. Some evidence has shown that OP^{DTT} is associated with hemeoxygenase (HO-1), an enzyme responsive to oxidative stress and mitochondrial damage (Li et al., 2003). However, more studies on cellular oxidation by PM are needed.

APPENDIX A. SUPPLEMENT

A.1 Chemical preparation and storage information

PQN standard: 5 mM 9,10-phenanthraquinone (PQN) standard stock was made by dissolving 10.4 mg of 9,10-phenanthraquinone in 10 mL DMSO. The stock was kept in the freezer when not in use. For routine analysis, final PQN standard was prepared from stock in deionized water (DI water, Nanopure Infinity^{TM} ultrapure water system; >18 MΩ cm^{-1}) before feeding to the system.

1 mM DTT: 10 mM stock DTT solution was made by dissolving 154.24 mg DTT in 100 mL DI water and stored in the fridge no longer than one month. 1 mM DTT was made fresh from 10mM stock solution every time for immediate use.

0.2 mM DTNB: 0.2 mM DTNB was prepared in Methanol (MeOH), stored in the fridge for no longer than 6 months.

0.08 M Tris buffer with 4 mM EDTA: Tris buffer was first prepared by dissolving 96.92 g of Tris Base and 11.69 g of EDTA in DI water. This will bring the pH to ~10. Then adjust the pH to 8.9 by adding a small amount of HCl. Add DI water to make a final volume of 10 L as the stock and store in room temperature.

0.5 M Potassium Phosphate Buffer (KBuffer): 0.5 M Kbuffer was made by mixing 13.47 g of KH_2PO_4 (Monopotassium Phosphate) and 69.85 g of K_2HPO_4 (Dipotassium Phosphate) in 1 L DI water. The mixture was then chelexed using Chelex® 100 resin (BIO-

RAD Laboratories, Inc., USA) to remove binding polyvalent metal ions (especially Cu and Fe).

1% w/v TCA was prepared in DI water and stored in room temperature.

A.2 Water-soluble metals PMF results

Input

Positive Matrix Factorization (PMF) analysis was applied to the data from JST (summer, fall, winter 2012, spring 2013), GT (fall, winter 2012, fall 2013), and RS (fall 2012, winter 2013) (total N=299). Missing data were replaced by species median. 15 species including S, K, Ca, Ti, Mn, Fe, Cu, Zn, As, Se, Br, Sr, Ba, Pb, and WSOC were run in the model.

PMF solutions

1) **Q/Qexp criterion**

Q/Qexp as a function of P (numbers of factors) was used to narrow down the range of factors to 3, 4 and 5 (see Figure A - 1).

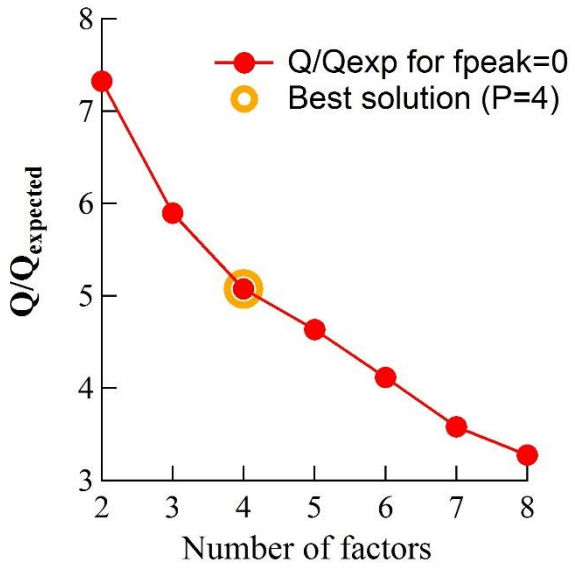

Figure A - 1 Q/Qexp as a function of the numbers of factors used in the PMF solution.

2) Determining # of factors

Best solution P=4 was determined by closer examination of factor spectra, time series and results from bootstrapping for P= 3, 4, and 5.

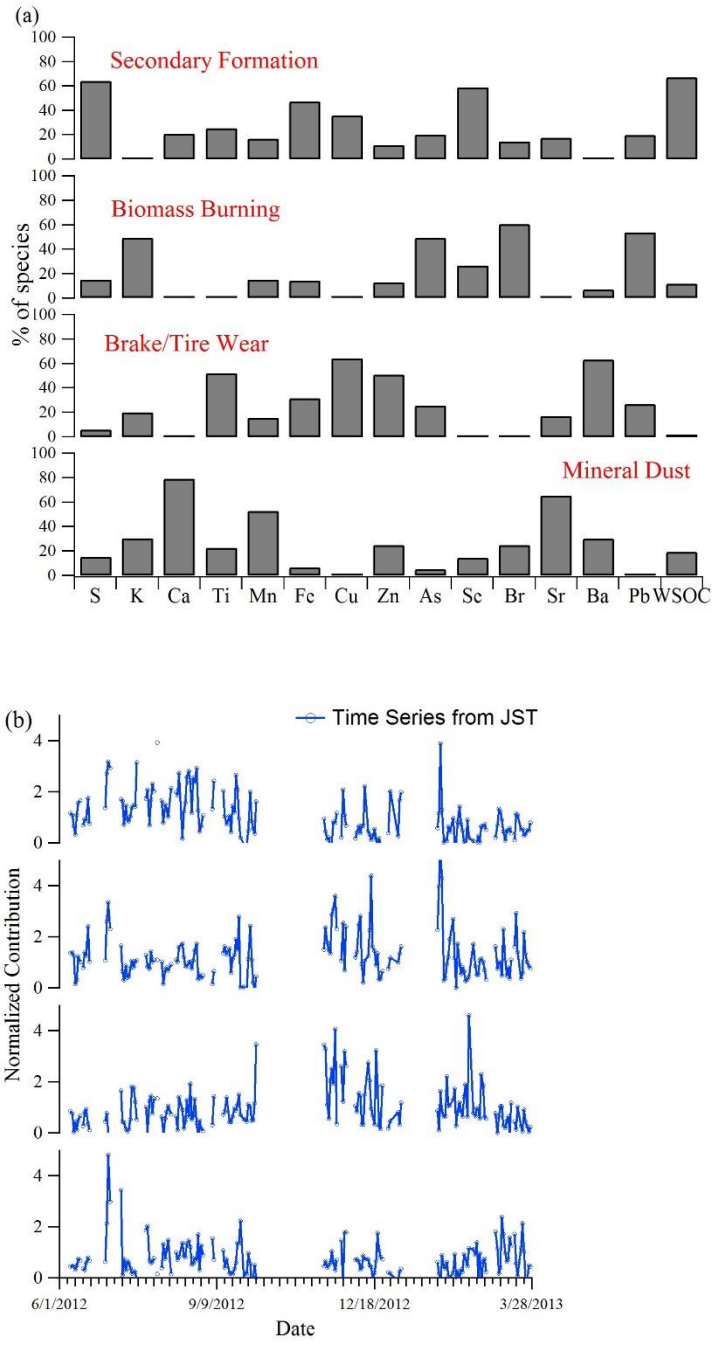

Figure A - 2 Factor profiles (a) and time series (b) for 4-factor solution

Table A - 1 Bootstrapping results on 4-factor solution

	Factor 1	Factor 2	Factor 3	Factor 4	Unmapped
Boot Factor 1	100	0	0	0	0
Boot Factor 2	0	100	0	0	0
Boot Factor 3	1	0	99	0	0
Boot Factor 4	0	0	0	100	0

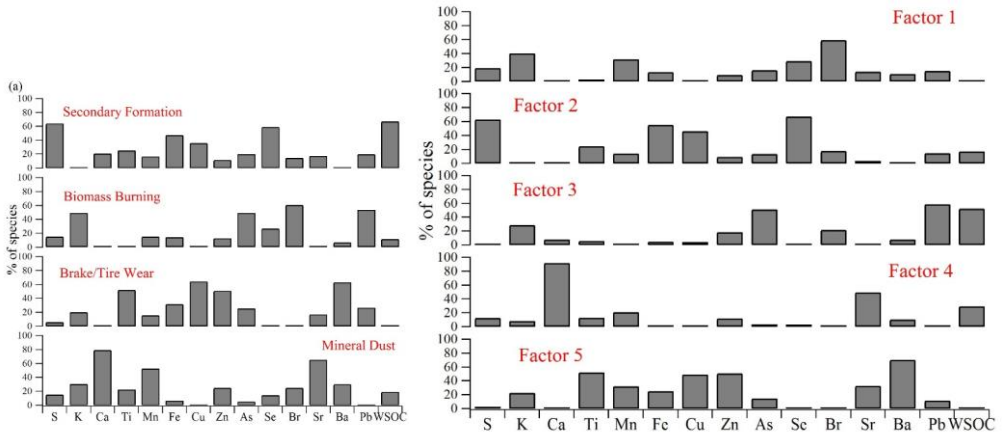

(a) (b)

Figure A - 3 Factor profiles for 4-factor solution (a) and 5-factor solution (b).

The 5-factor solution resulted in splitting of the "biomass burning" source (Factor 2 in panel a, Fig. A - 3) into two factors (Factor 1 and 3 in panel b, Fig A - 3) with no clear identification. Moreover, the bootstrap calculations (Table A - 1) highlight the bootstrapping factor 5 in 5-facor solution were matched to other factors, indicating less stability of the 5-factor solution.

Table A - 2 Bootstrapping results on 5-factor solution

	Factor 1	Factor 2	Factor 3	Factor 4	Factor 5	Unmapped
Boot Factor 1	83	4	12	0	1	0
Boot Factor 2	0	98	2	0	0	0
Boot Factor 3	0	0	100	0	0	0
Boot Factor 4	0	0	0	99	1	0
Boot Factor 5	0	0	0	0	100	0

In the case of 3 factors, source apportionment leads to factors with no clear physical interpretations (Fig. A - 4 & Table A - 3).

Table A - 3 Bootstrapping results on 3-factor solution

	Factor 1	Factor 2	Factor 3	Unmapped
Boot Factor 1	97	3	0	0
Boot Factor 2	0	99	1	0
Boot Factor 3	3	3	94	0

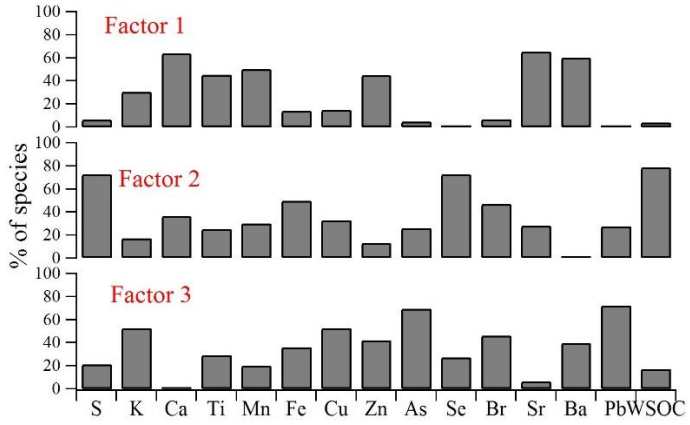

Figure A - 4 Factor profiles for 3-factor solution

3) Rotational ambiguity: fpeak variation

The rotational ambiguity of the 4-factor PMF solution was explored via the Fpeak parameter in the range ±2 (Fig. A - 5). The results indicate that Q/Qexp is at a minimum for Fpeak=0, justifying the decision to use Fpeak=0 in the case of the optimal 4-factor solution.

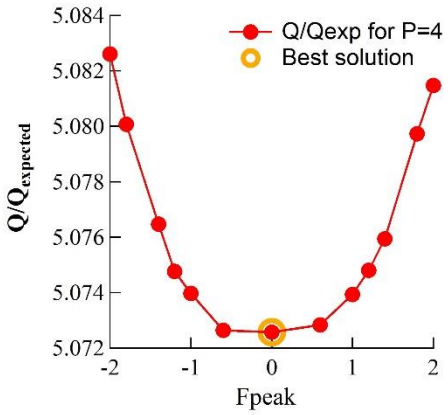

Figure A - 5 Q/Qexp as function of Fpeak parameter

A.3 Codes for health outcomes used in the epidemiological models

The health outcomes in the epidemiological models are asthma or wheeze with a primary International Classification of Disease, 9th Revision, (ICD-9) code of 493 and 786.07, congestive heart failure (428), chronic obstructive pulmonary disease (491, 492, 496), cardiovascular disease (410-414, 427, 428, 433-437, 440, 443-445, 451-453), ischemic heart disease (410-414), and pneumonia (480-486) for a patient with a home ZIP code within the Atlanta 5-county metro area (Fulton, DeKalb, Gwinnett, Cobb, Clayton) recorded in an Atlanta hospital from 8/1/1998 through 12/31/2009.

A.4 Equations to fit the distributions and averaged frequency OP distribution

Equations to fit the distributions

$$\frac{dC}{dlnD_p} = \frac{C_t}{(2\pi)^{1/2} ln\sigma_g} \exp\left(-\frac{(lnD_p - lnGMD)^2}{2ln^2\sigma_g}\right),$$

where C is the concentration of PM species (μg m^{-3} or ng m^{-3}) or oxidative potential (OP, nmol min^{-1} m^{-3}), D_p is the aerodynamic diameter (μm), and GMD and σ_g are geometric mean diameter (μm) and geometric standard deviation for the lognormal fits. C_t is the total level of PM species or OP; it's the area under the curve, same unit as C.

Averaged frequency OP distribution:

$$\frac{df}{dlnD_p} = \frac{1}{(2\pi)^{1/2} ln\sigma_{g_{mean}}} \exp\left(-\frac{(lnD_p - lnGMD_{mean})^2}{2ln^2\sigma_{g_{mean}}}\right),$$

where GMD_{mean} and $\sigma_{g_{mean}}$ are the mean of the GMD and σ_g obtained from a lognormal fit of each MOUDI sets, respectively.

A.5 Method for dividing deposits between cut filter portions and OCEC analysis on MOUDI samples

The MOUDI sampler collects particles as discrete points on the substrate filter, each point being associated with an impact jet. For the upper size stages where the number of impactor jets are few, this leads to highly non-uniform deposits. This raises issues when cutting the filter and for the OCEC analysis which depends on a laser transmission through the filter to assess the spit in OC and EC. At smaller size stages the number of jets is so large the deposit can be assumed to be uniform. In order to calculate the total deposits of different chemical components on the filters, the chemical mass on the corresponding filter portion was multiplied by the ratio of the number of dots on the whole filter versus those on the analyzed filter portion. This was done for stages with a cut size larger than 0.56 μm; for smaller stages filter surface areas were used. Since the laser beam in the OCEC analyzer may pass through blank filter space due to the non-uniform deposition in MOUDI samples, OC/EC separation was done by manual split at 800 seconds. This specific split time was based on the split time (800 ± 100 seconds) obtained from a set of uniform deposited filter samples collected at another urban site in Atlanta, GA. Split times of 700 and 900 seconds were applied to the data and shown as error bars on OC and EC distributions.

.

A.6 Coarse mode particle pH

As notes in the main text, gas-phase data (i.e., NH_3, HNO_3, and HCl) were estimated by iterating ISORROPIA-II with fine mode particle-phase data assuming the gas was only in equilibrium with the fine mode aerosol. At the RS site, NH_3, HNO_3, HCl were predicted to 0.6, 0.6, 2.5 μg m^{-3}, respectively, whereas at the GT site, these gases were 0.7, 0.5, 2.2 μg m^{-3}. With these estimated gases, the model fairly accurately predicted fine mode NH_4^+ and NO_4^- concentrations, Figure A -1.

Unlike the fine mode, coarse mode particles are unlikely to reach equilibrium with the gas phase due to kinetic limitations (Fountoukis et al., 2009; Cruz et al., 2000; Dassios and Pandis, 1999). Assuming coarse mode particles in equilibrium with the gas phase generally leads to a large positive bias between predicted coarse particle NO3- and NH4+, as seen in Figure A - 1. The pH associated with this calculation, compared to that predicted assuming the lack of equilibrium in the coarse mode, is shown in Figure A -2.

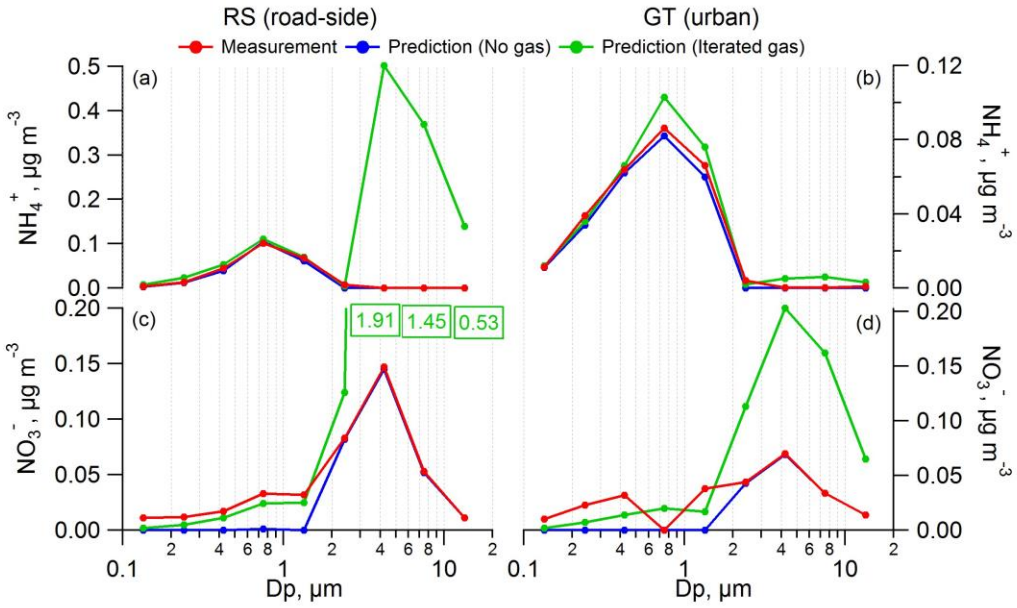

Figure A - 1 Comparison of ISORROPIA-II predicted NH_4^+ and NO_3^- with measurements for each MOUDI stage. Two versions of forward mode predictions are shown above: input without gas phase data (blue) and with gases assuming

equilibrium (green). Three points are beyond y-axis range in graph (c); their y-values are listed.

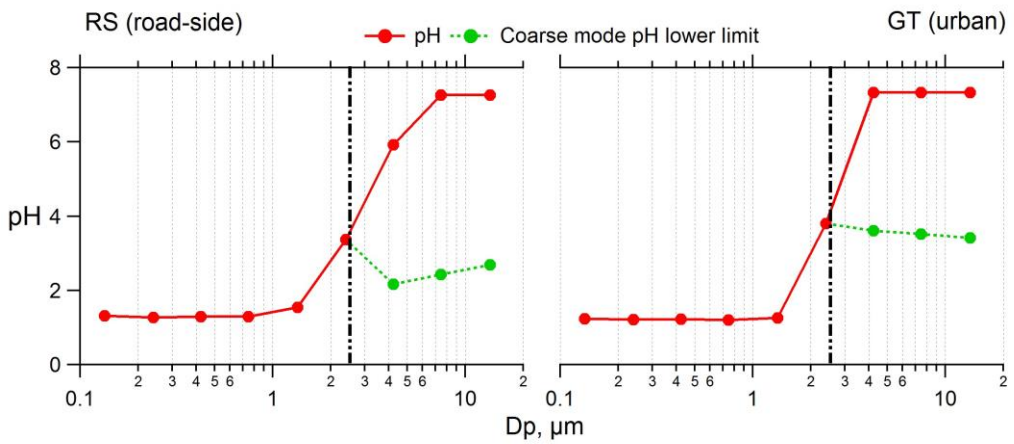

Figure A - 2 Predicted particle pH size distribution, as Figure 5-3, with added coarse mode pH lower limit. Note that, the lower limit is not realistic due to kinetic limitations and large over-predictions of NO_3^- (hence overestimated acidity), but shows possible pH range the coarse mode could reach given sufficient time.

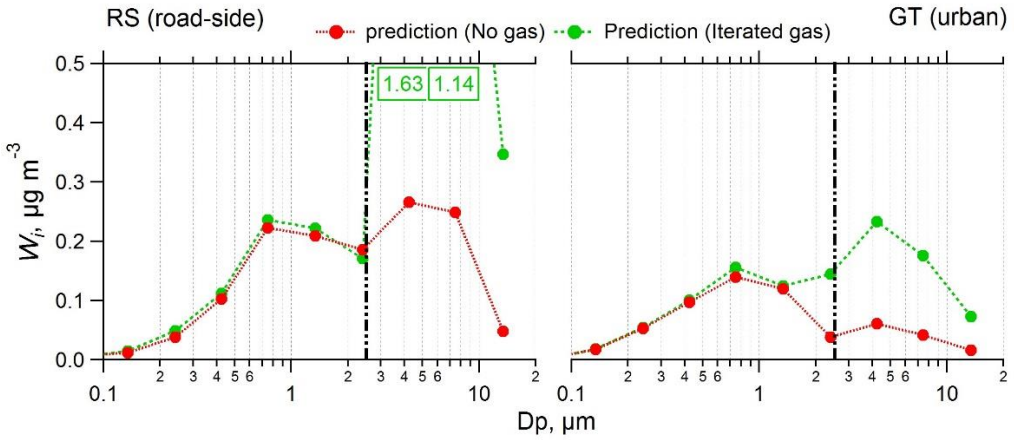

Figure A - 3 Predicted particle water size distribution, Liquid water predicted by assuming gas equilibrium is much higher than that assuming no interaction between the gas and coarse mode particles due to the long equilibration timescale. The largest deviation between the green and red lines was at Dp = 3.2-5.6 µm range, which only leads to pH within a factor of $\log_{10}(5)$ uncertainty. The lower coarse mode liquid water levels (red line) realistically reproduce aerosol composition data, however, liquid water was not measured so no comparison with measurements is possible.

A.7 Detailed method for measuring total DTT activity on MOUDIs filters

a) **Filter extraction**: filter sample (half of a 47 mm MOUDI Teflon filter) was sonicated in 4.9 mL DI water in a 15 mL centrifuge tube for 30 min with an Ultrasonic Cleanser (VWR International LLC, West Chester, PA, USA);
b) **Total DTT activity (OP_{total}^{DTT}) measurement**:

After sonication, 1.4 mL potassium phosphate buffer (pH = 7.4) was added to the centrifuge tube containing the sample filter and extract, after that the tube was placed in a ThermoMixer (Eppendorf North America, Inc., Hauppauge, NY, USA) for approximately 5 min to ensure the temperature of the tube reached 37 °C. At time zero, 0.7 mL 1mM DTT solution was added to the Kbuffer-sample mixture. DTT was consumed over time. At five different time intervals (7, 15, 25, 32, 40 min), 100 µL of the mixture was transferred to another centrifuge tube preloaded with 1 mL 1% v/v Trichloroacetic acid (TCA) to quench the DTT consumption. To determine the concentration of DTT remaining in the tube, 2 mL Tris buffer (0.08 M with 4 mM EDTA) and 0.2 mL DTNB (0.5 mM) were added to the quenched mixture with residual DTT. The reaction between the residual DTT and DTNB forms a light absorbing compound, 2-nitro-5-thiobenzoic acid (TNB), which has a high extinction coefficient at 412 nm wavelength. The final mixture with TNB was then passed through a Liquid Waveguide Capillary Cell (LWCC-M-100; World Precision Instruments, Inc., FL, USA) coupled to a UV-VIS light source (Ocean Optics DT-Mini-2B, Ocean Optics, Inc., Dunedin, FL, USA), and a multi-wavelength light detector (USB4000 Miniature Fiber Optic Spectrometer, Ocean Optics, Inc., Dunedin, FL, USA) to determine the absorbance at 412 nm wavelength, respectively. The absorbance measured via this method was calibrated with a known concentration of DTT, and the calibration curve was used to calculate the remaining amount of DTT in the sample-Kbuffer-DTT mixture.

c) **Final OP calculations**:

The final OP can be calculated as follows:

$$OP\ (nmol\ min^{-1}\ m^{-3}) = \frac{\sigma_{sample}(nmol\ min^{-1}) - \sigma_{blank}(nmol\ min^{-1})}{\frac{V_a\ (mL)}{V_e\ (mL)} \times V_p(m^3) \times \frac{A_p}{A_{total}}} \qquad \text{Eq. (1)}$$

σ_{sample} and σ_{blank} are the consumption rates of sample and blank, i.e. the slopes by taking a linear fit to the remaining amount of DTT in the sample-Kbuffer-DTT mixture over time (nmol min^{-1}); V_e and V_a are the extraction volume and sample volume added to the sample-Kbuffer-DTT mixture, respectively; V_p is the total air volume sampled through the whole filter; A_{total} and A_p are total area and the area taken for OP analysis, respectively. For stages with a cut-off size of 0.56 μm and up, A_{total} and A_p represent the number of dots on the whole Teflon filter and that taken for OP analysis.

REFERENCES

REFERENCES

Adachi, K., and Tainosho, Y.: Characterization of heavy metal particles embedded in tire dust, Environ. Int., 30, 1009-1017, 10.1016/j.envint.2004.04.004, 2004.

Akhtar, U. S., McWhinney, R. D., Rastogi, N., Abbatt, J. P. D., Evans, G. J., and Scott, J. A.: Cytotoxic and proinflammatory effects of ambient and source-related particulate matter (PM) in relation to the production of reactive oxygen species (ROS) and cytokine adsorption by particles, Inhalation Toxicol., 22, 37-47, 10.3109/08958378.2010.518377, 2010.

Alfadda, A. A., and Sallam, R. M.: Reactive oxygen species in health and disease, Journal of Biomedicine and Biotechnology, 2012, 10.1155/2012/936486, 2012.

Ali, M. A., and Dzombak, D. A.: Effects of simple organic acids on sorption of Cu2+ and Ca2+ on goethite, Geochim. Cosmochim. Acta, 60, 291-304, http://dx.doi.org/10.1016/0016-7037(95)00385-1, 1996.

Allen, C. L., and Bayraktutan, U.: Oxidative Stress and Its Role in the Pathogenesis of Ischaemic Stroke, International Journal of Stroke, 4, 461-470, 10.1111/j.1747-4949.2009.00387.x, 2009.

Antinolo, M., Willis, M. D., Zhou, S., and Abbatt, J. P. D.: Connecting the oxidation of soot to its redox cycling abilities, Nat. Commun., 6, 6812, 10.1038/ncomms7812, 2015.

Antonini, J. M., Clarke, R. W., Krishna Murthy, G. G., Sreekanthan, P., Jenkins, N., Eagar, T. W., and Brain, J. D.: Freshly generated stainless steel welding fume induces greater lung inflammation in rats as compared to aged fume, Toxicology Letters, 98, 77-86, http://dx.doi.org/10.1016/S0378-4274(98)00103-9, 1998.

Appel, B. R., Wall, S. M., Haik, M., Kothny, E. L., and Tokiwa, Y.: Evaluation of techniques for sulfuric acid and particulate strong acidity measurements in ambient air, Atmos. Environ. (1967-1989), 14, 559-563, http://dx.doi.org/10.1016/0004-6981(80)90086-4, 1980.

Arangio, A. M., Tong, H., Socorro, J., Pöschl, U., and Shiraiwa, M.: Quantification of environmentally persistent free radicals and reactive oxygen species in atmospheric aerosol particles, Atmos. Chem. Phys., 16, 13105-13119, 10.5194/acp-16-13105-2016, 2016.

Atkinson, R. W., Fuller, G. W., Anderson, H. R., Harrison, R. M., and Armstrong, B.: Urban ambient particle metrics and health: a time-series analysis, Epidemiology, 21, 501-511, 10.1097/EDE.0b013e3181debc88, 2010.

Atkinson, R. W., Samoli, E., Analitis, A., Fuller, G. W., Green, D. C., Anderson, H. R., Purdie, E., Dunster, C., Aitlhadj, L., Kelly, F. J., and Mudway, I. S.: Short-term associations between particle oxidative potential and daily mortality and hospital admissions in London, Int. J. Hyg. Environ. Health, 219, 566-572, http://dx.doi.org/10.1016/j.ijheh.2016.06.004, 2016.

Aust, A. E., Ball, J. C., Hu, A. A., Lighty, J. S., Smith, K. R., Straccia, A. M., Veranth, J. M., and Young, W. C.: Particle characteristics responsible for effects on human lung epithelial cells, Health Effects Institute, 2002.

Ayres, J. G., Borm, P., Cassee, F. R., Castranova, V., Donaldson, K., Ghio, A., Harrison, R. M., Hider, R., Kelly, F., and Kooter, I. M.: Evaluating the toxicity of airborne particulate matter and nanoparticles by measuring oxidative stress potential-a workshop report and consensus statement, Inhalation Toxicol., 20, 75-99, 2008.

Bae, M.-S., Schauer, J. J., and Turner, J. R.: Estimation of the monthly average ratios of organic mass to organic carbon for fine particulate matter at an urban site, Aerosol Science and Technology, 40, 1123-1139, 10.1080/02786820601004085, 2006.

Balachandran, S., Pachon, J. E., Hu, Y., Lee, D., Mulholland, J. A., and Russell, A. G.: Ensemble-trained source apportionment of fine particulate matter and method uncertainty analysis, Atmospheric Environment, 61, 387-394, http://dx.doi.org/10.1016/j.atmosenv.2012.07.031, 2012.

Bates, J. T., Weber, R. J., Abrams, J., Verma, V., Fang, T., Klein, M., Strickland, M. J., Sarnat, S. E., Chang, H. H., Mulholland, J. A., Tolbert, P. E., and Russell, A. G.: Reactive Oxygen Species Generation Linked to Sources of Atmospheric Particulate Matter and Cardiorespiratory Effects, Environ. Sci. Technol., 49, 13605-13612, 10.1021/acs.est.5b02967, 2015.

Bell, M. L., Dominici, F., Ebisu, K., Zeger, S. L., and Samet, J. M.: Spatial and temporal variation in PM(2.5) chemical composition in the United States for health effects studies, Environmental Health Perspectives, 115, 989-995, 10.1289/ehp.9621, 2007.

Birmili, W., Allen, A. G., Bary, F., and Harrison, R. M.: Trace Metal Concentrations and Water Solubility in Size-Fractionated Atmospheric Particles and Influence of Road Traffic, Environ. Sci. Technol., 40, 1144-1153, 10.1021/es0486925, 2006.

Bonvallot, V., Baeza-Squiban, A., Baulig, A., Brulant, S., Boland, S., Muzeau, F., Barouki, R., and Marano, F.: Organic compounds from diesel exhaust particles elicit a proinflammatory response in human airway epithelial cells and induce cytochrome p450 1A1 expression, American Journal of Respiratory Cell and Molecular Biology, 25, 515-521, 10.1165/ajrcmb.25.4.4515, 2001.

Borrowman, C. K., Zhou, S., Burrow, T. E., and Abbatt, J. P. D.: Formation of environmentally persistent free radicals from the heterogeneous reaction of ozone and polycyclic aromatic compounds, Physical Chemistry Chemical Physics, 18, 205-212, 10.1039/C5CP05606C, 2016.

Bougiatioti, A., Nikolaou, P., Stavroulas, I., Kouvarakis, G., Weber, R., Nenes, A., Kanakidou, M., and Mihalopoulos, N.: Particle water and pH in the eastern Mediterranean: source variability and implications for nutrient availability, Atmos. Chem. Phys., 16, 4579-4591, 10.5194/acp-16-4579-2016, 2016.

Brook, R. D., Rajagopalan, S., Pope, C. A., Brook, J. R., Bhatnagar, A., Diez-Roux, A. V., Holguin, F., Hong, Y., Luepker, R. V., Mittleman, M. A., Peters, A., Siscovick, D., Smith, S. C., Whitsel, L., Kaufman, J. D., on behalf of the American Heart Association Council on, E., Prevention, C. o. t. K. i. C. D., Council on Nutrition, P. A., and Metabolism: Particulate matter air pollution and cardiovascular disease: an update to the scientific statement from the american heart association, Circulation, 121, 2331-2378, 2010.

Brunekreef, B., Janssen, N. A., de Hartog, J., Harssema, H., Knape, M., and van Vliet, P.: Air pollution from truck traffic and lung function in children living near motorways, Epidemiology, 8, 298-303, 10.1097/00001648-199705000-00012, 1997.

Burchiel, S. W., Lauer, F. T., Dunaway, S. L., Zawadzki, J., McDonald, J. D., and Reed, M. D.: Hardwood smoke alters murine splenic T cell responses to mitogens following a 6-month whole body inhalation exposure, Toxicology and Applied Pharmacology, 202, 229-236, http://dx.doi.org/10.1016/j.taap.2004.06.024, 2005.

Burnett, R. T., Cakmak, S., Brook, J. R., and Krewski, D.: The role of particulate size and chemistry in the association between summertime ambient air pollution and hospitalization for cardiorespiratory diseases, Environ. Health Perspect., 105, 614-620, 1997.

Burnett, R. T., Brook, J., Dann, T., Delocla, C., Philips, O., Cakmak, S., Vincent, R., Goldberg, M. S., and Krewski, D.: Association between particulate- and gas-phase components of urban air pollution and daily mortality in eight Canadian cities, Inhal Toxicol, 12 Suppl 4, 15-39, 10.1080/08958370050164851, 2000.

Bylund, J., Brown, K. L., Movitz, C., Dahlgren, C., and Karlsson, A.: Intracellular generation of superoxide by the phagocyte NADPH oxidase: How, where, and what for?, Free Radical Biology and Medicine, 49, 1834-1845, https://doi.org/10.1016/j.freeradbiomed.2010.09.016, 2010.

Chang-Graham, A. L., Profeta, L. T. M., Johnson, T. J., Yokelson, R. J., Laskin, A., and Laskin, J.: Case study of water-soluble metal containing organic constituents of biomass burning aerosol, Environmental Science & Technology, 45, 1257-1263, 10.1021/es103010j, 2011.

Charrier, J. G., and Anastasio, C.: On dithiothreitol (DTT) as a measure of oxidative potential for ambient particles: evidence for the importance of soluble transition metals, Atmos. Chem. Phys., 12, 9321-9333, 10.5194/acp-12-9321-2012, 2012.

Chen, H., Kwong, J. C., Copes, R., Tu, K., Villeneuve, P. J., van Donkelaar, A., Hystad, P., Martin, R. V., Murray, B. J., Jessiman, B., Wilton, A. S., Kopp, A., and Burnett, R. T.: Living near major roads and the incidence of dementia, Parkinson's disease, and multiple sclerosis: a population-based cohort study, The Lancet, 389, 718-726, 10.1016/s0140-6736(16)32399-6, 2017.

Cheung, K., Shafer, M. M., Schauer, J. J., and Sioutas, C.: Diurnal trends in oxidative potential of coarse particulate matter in the Los Angeles basin and their relation to sources and chemical composition, Environmental Science & Technology, 46, 3779-3787, 10.1021/es204211v, 2012.

Cheung, K. L., Ntziachristos, L., Tzamkiozis, T., Schauer, J. J., Samaras, Z., Moore, K. F., and Sioutas, C.: Emissions of particulate trace elements, metals and organic species from gasoline, diesel, and biodiesel passenger vehicles and their relation to oxidative potential, Aerosol Sci. Technol., 44, 500-513, 10.1080/02786821003758294, 2010.

Chevion, M.: A site-specific mechanism for free radical induced biological damage: The essential role of redox-active transition metals, Free Radical Biology and Medicine, 5, 27-37, http://dx.doi.org/10.1016/0891-5849(88)90059-7, 1988.

Cho, A. K., Sioutas, C., Miguel, A. H., Kumagai, Y., Schmitz, D. A., Singh, M., Eiguren-Fernandez, A., and Froines, J. R.: Redox activity of airborne particulate matter at different sites in the Los Angeles Basin, Environ. Res., 99, 40-47, 10.1016/j.envres.2005.01.003, 2005.

Cho, W.-S., Duffin, R., Poland, C. A., Duschl, A., Oostingh, G. J., MacNee, W., Bradley, M., Megson, I. L., and Donaldson, K.: Differential pro-inflammatory effects of metal oxide nanoparticles and their soluble ions in vitro and in vivo; zinc and copper nanoparticles, but not their ions, recruit eosinophils to the lungs, Nanotoxicology, 6, 22-35, 10.3109/17435390.2011.552810, 2011.

Choi, J. C., Lee, M., Chun, Y., Kim, J., and Oh, S.: Chemical composition and source signature of spring aerosol in Seoul, Korea, J. Geophys. Res.: Atmos., 106, 18067-18074, 10.1029/2001JD900090, 2001.

Chow, J. C., Watson, J. G., Chen, L. W. A., Chang, M. C. O., Robinson, N. F., Trimble, D., and Kohl, S.: The IMPROVE_A Temperature Protocol for Thermal/Optical Carbon Analysis: Maintaining Consistency with a Long-Term Database, J. Air Waste Manage. Assoc., 57, 1014-1023, 10.3155/1047-3289.57.9.1014, 2007.

Chung, M. Y., Lazaro, R. A., Lim, D., Jackson, J., Lyon, J., Rendulic, D., and Hasson, A. S.: Aerosol-borne quinones and reactive oxygen species generation by particulate matter extracts, Environmental Science & Technology, 40, 4880-4886, 10.1021/es0515957, 2006.

Cohen, A. J., Brauer, M., Burnett, R., Anderson, H. R., Frostad, J., Estep, K., Balakrishnan, K., Brunekreef, B., Dandona, L., Dandona, R., Feigin, V., Freedman, G., Hubbell, B., Jobling, A., Kan, H., Knibbs, L., Liu, Y., Martin, R., Morawska, L., Pope, C. A., III, Shin, H., Straif, K., Shaddick, G., Thomas, M., van Dingenen, R., van Donkelaar, A., Vos, T.,

Murray, C. J. L., and Forouzanfar, M. H.: Estimates and 25-year trends of the global burden of disease attributable to ambient air pollution: an analysis of data from the Global Burden of Diseases Study 2015, The Lancet, 389, 1907-1918, 10.1016/S0140-6736(17)30505-6, 2017.

Costa, D. L., and Dreher, K. L.: Bioavailable transition metals in particulate matter mediate cardiopulmonary injury in healthy and compromised animal models, Environ. Health Perspect., 105, 1053-1060, 1997.

Cruz, C. N., Dassios, K. G., and Pandis, S. N.: The effect of dioctyl phthalate films on the ammonium nitrate aerosol evaporation rate, Atmos. Environ., 34, 3897-3905, http://dx.doi.org/10.1016/S1352-2310(00)00173-4, 2000.

Daher, N., Ning, Z., Cho, A. K., Shafer, M., Schauer, J. J., and Sioutas, C.: Comparison of the chemical and oxidative characteristics of particulate matter (PM) collected by different methods: filters, impactors, and biosamplers, Aerosol Sci. Technol., 45, 1294-1304, 10.1080/02786826.2011.590554, 2011.

Darrow, L. A., Klein, M., Flanders, W. D., Waller, L. A., Correa, A., Marcus, M., Mulholland, J. A., Russell, A. G., and Tolbert, P. E.: Ambient air pollution and preterm birth: a time-series analysis, Epidemiology, 20, 689-698, 10.1097/EDE.0b013e3181a7128f, 2009.

Darrow, L. A., Klein, M., Strickland, M. J., Mulholland, J. A., and Tolbert, P. E.: Ambient air pollution and birth weight in full-term infants in Atlanta, 1994-2004, Environ. Health Perspect., 119, 731-737, 10.1289/ehp.1002785, 2011.

Dassios, K. G., and Pandis, S. N.: The mass accommodation coefficient of ammonium nitrate aerosol, Atmos. Environ., 33, 2993-3003, http://dx.doi.org/10.1016/S1352-2310(99)00079-5, 1999.

Davies, K. J. A.: Oxidative stress: the paradox of aerobic life, Biochemical Society Symposium, 61, 1, 1995.

De Haar, C., Hassing, I., Bol, M., Bleumink, R., and Pieters, R.: Ultrafine but not fine particulate matter causes airway inflammation and allergic airway sensitization to co-administered antigen in mice, Clin. Exp. Allergy, 36, 1469-1479, 10.1111/j.1365-2222.2006.02586.x, 2006.

De Jong, W. H., Hagens, W. I., Krystek, P., Burger, M. C., Sips, A. J., and Geertsma, R. E.: Particle size-dependent organ distribution of gold nanoparticles after intravenous administration, Biomaterials, 29, 1912-1919, 10.1016/j.biomaterials.2007.12.037, 2008.

Delfino, R. J., Staimer, N., Tjoa, T., Gillen, D. L., Polidori, A., Arhami, M., Kleinman, M. T., Vaziri, N. D., Longhurst, J., and Sioutas, C.: Air pollution exposures and circulating biomarkers of effect in a susceptible population: clues to potential causal component mixtures and mechanisms, Environ. Health Perspect., 117, 1232-1238, 10.1289/ehp.0800194, 2009.

Delfino, R. J., Staimer, N., Tjoa, T., Gillen, D. L., Schauer, J. J., and Shafer, M. M.: Airway inflammation and oxidative potential of air pollutant particles in a pediatric asthma panel, J. Exposure Sci. Environ. Epidemiol., 23, 466-473, 10.1038/jes.2013.25, 2013.

Dellinger, B., Pryor, W. A., Cueto, R., Squadrito, G. L., Hegde, V., and Deutsch, W. A.: Role of Free Radicals in the Toxicity of Airborne Fine Particulate Matter, Chemical Research in Toxicology, 14, 1371-1377, 10.1021/tx010050x, 2001.

Dellinger, B., Lomnicki, S., Khachatryan, L., Maskos, Z., Hall, R. W., Adounkpe, J., McFerrin, C., and Truong, H.: Formation and stabilization of persistent free radicals, Proc. Combust. Inst., 31, 521-528, http://dx.doi.org/10.1016/j.proci.2006.07.172, 2007.

Dias, V., Junn, E., and Mouradian, M. M.: The Role of Oxidative Stress in Parkinson's Disease, Journal of Parkinson's disease, 3, 461-491, 10.3233/JPD-130230, 2013.

DiStefano, E., Eiguren-Fernandez, A., Delfino, R. J., Sioutas, C., Froines, J. R., and Cho, A. K.: Determination of metal-based hydroxyl radical generating capacity of ambient and diesel exhaust particles, Inhal Toxicol, 21, 731-738, 10.1080/08958370802491433, 2009.

Dockery, D. W., Pope, C. A., Xu, X., Spengler, J. D., Ware, J. H., Fay, M. E., Ferris, B. G., and Speizer, F. E.: An Association between Air Pollution and Mortality in Six U.S. Cities, N. Engl. J. Med., 329, 1753-1759, 10.1056/NEJM199312093292401, 1993.

Dockery, D. W., Cunningham, J., Damokosh, A. I., Neas, L. M., Spengler, J. D., Koutrakis, P., Ware, J. H., Raizenne, M., and Speizer, F. E.: Health effects of acid aerosols on North American children: respiratory symptoms, Environ. Health Perspect., 104, 500-505, 1996.

Dombu, C. Y., and Betbeder, D.: Airway delivery of peptides and proteins using nanoparticles, Biomaterials, 34, 516-525, 10.1016/j.biomaterials.2012.08.070, 2013.

Donaldson, K., Stone, V., Seaton, A., and MacNee, W.: Ambient particle inhalation and the cardiovascular system: potential mechanisms, Environmental Health Perspectives, 109, 523-527, 2001.

Donaldson, K., Tran, L., Jimenez, L., Duffin, R., Newby, D., Mills, N., MacNee, W., and Stone, V.: Combustion-derived nanoparticles: a review of their toxicology following inhalation exposure, Part Fibre Toxicol, 2, 10, 10.1186/1743-8977-2-10, 2005.

Dou, J., Lin, P., Kuang, B.-Y., and Yu, J. Z.: Reactive Oxygen Species Production Mediated by Humic-like Substances in Atmospheric Aerosols: Enhancement Effects by Pyridine, Imidazole, and Their Derivatives, Environ. Sci. Technol., 49, 6457-6465, 10.1021/es5059378, 2015.

Eiguren-Fernandez, A., Kreisberg, N., and Hering, S.: An online monitor of the oxidative capacity of aerosols (o-MOCA), Atmos. Meas. Tech., 10, 633-644, 10.5194/amt-10-633-2017, 2017.

Enami, S., Hoffmann, M. R., and Colussi, A. J.: Acidity enhances the formation of a persistent ozonide at aqueous ascorbate/ozone gas interfaces, Proc. Natl. Acad. Sci. U. S. A., 105, 7365-7369, 2008.

Espinosa, A. J. F., Rodríguez, M. T., de la Rosa, F. J. B., and Sánchez, J. C. J.: A chemical speciation of trace metals for fine urban particles, Atmos. Environ., 36, 773-780, 10.1016/S1352-2310(01)00534-9, 2002.

Fairley, D.: Daily mortality and air pollution in Santa Clara County, California: 1989-1996, Environ. Health Perspect., 107, 637-641, 1999.

Fang, T., Guo, H., Verma, V., Peltier, R. E., and Weber, R. J.: PM2.5 water-soluble elements in the southeastern United States: automated analytical method development, spatiotemporal distributions, source apportionment, and implications for heath studies, Atmos. Chem. Phys. , 15, 11667-11682, 10.5194/acpd-15-17189-2015, 2015a.

Fang, T., Verma, V., Guo, H., King, L. E., Edgerton, E. S., and Weber, R. J.: A semi-automated system for quantifying the oxidative potential of ambient particles in aqueous extracts using the dithiothreitol (DTT) assay: results from the Southeastern Center for Air Pollution and Epidemiology (SCAPE), Atmos. Meas. Tech., 8, 471-482, 10.5194/amt-8-471-2015, 2015b.

Fang, T., Verma, V., Bates, J. T., Abrams, J., Klein, M., Strickland, M. J., Sarnat, S. E., Chang, H. H., Mulholland, J. A., Tolbert, P. E., Russell, A. G., and Weber, R. J.: Oxidative potential of ambient water-soluble PM2.5 in the southeastern United States: contrasts in sources and health associations between ascorbic acid (AA) and dithiothreitol (DTT) assays, Atmos. Chem. Phys., 16, 3865-3879, 10.5194/acp-16-3865-2016, 2016.

Fang, T., Guo, H., Zeng, L., Verma, V., Nenes, A., and Weber, R. J.: Highly acidic ambient particles, soluble metals, and oxidative potential: a link between sulfate and aerosol toxicity, Environ. Sci. Technol., 51, 2611-2620, 10.1021/acs.est.6b06151, 2017a.

Fang, T., Zeng, L., Gao, D., Verma, V., Stefaniak, A. B., and Weber, R. J.: Ambient Size Distributions and Lung Deposition of Aerosol Dithiothreitol-Measured Oxidative Potential: Contrast between Soluble and Insoluble Particles, Environmental Science & Technology, 51, 6802-6811, 10.1021/acs.est.7b01536, 2017b.

Feng, C. T., Michael, G. A., and Joan, M. D.: An Exploratory Analysis of the Relationship between Mortality and the Chemical Composition of Airborne Particulate Matter, Inhalation Toxicol., 12, 121-135, 10.1080/08958378.2000.11463204, 2000.

Fountoukis, C., and Nenes, A.: ISORROPIA II: a computationally efficient thermodynamic equilibrium model for K^+–Ca^{2+}–Mg^{2+}–$NH4^+$–Na^+–SO_4^{2-}–NO^{3-}–Cl^-–H_2O aerosols, Atmos. Chem. Phys., 7, 4639-4659, 10.5194/acp-7-4639-2007, 2007.

Fountoukis, C., Nenes, A., Sullivan, A., Weber, R., Van Reken, T., Fischer, M., Matías, E., Moya, M., Farmer, D., and Cohen, R. C.: Thermodynamic characterization of Mexico

City aerosol during MILAGRO 2006, Atmos. Chem. Phys., 9, 2141-2156, 10.5194/acp-9-2141-2009, 2009.

Frampton, M. W., Ghio, A. J., Samet, J. M., Carson, J. L., Carter, J. D., and Devlin, R. B.: Effects of aqueous extracts of PM10 filters from the Utah Valley on human airway epithelial cells, Am. J. Physiol.: Lung Cell. Mol. Physiol, 277, L960-L967, 1999.

Friedlander, S. K., and Yeh, E. K.: The Submicron Atmospheric Aerosol as a Carrier of Reactive Chemical Species: Case of Peroxides, Appl. Occup. Environ. Hyg., 13, 416-420, 10.1080/1047322X.1998.10389566, 1998.

Furusjö, E., Sternbeck, J., and Cousins, A. P.: PM10 source characterization at urban and highway roadside locations, Sci. Total Environ., 387, 206-219, https://doi.org/10.1016/j.scitotenv.2007.07.021, 2007.

Furuyama, A., Kanno, S., Kobayashi, T., and Hirano, S.: Extrapulmonary translocation of intratracheally instilled fine and ultrafine particles via direct and alveolar macrophage-associated routes, Arch. Toxicol., 83, 429-437, 10.1007/s00204-008-0371-1, 2009.

Garg, B. D., Cadle, S. H., Mulawa, P. A., Groblicki, P. J., Laroo, C., and Parr, G. A.: Brake wear particulate matter emissions, Environ. Sci. Technol., 34, 4463-4469, 10.1021/es001108h, 2000.

Gasser, M., Riediker, M., Mueller, L., Perrenoud, A., Blank, F., Gehr, P., and Rothen-Rutishauser, B.: Toxic effects of brake wear particles on epithelial lung cells in vitro, Particle and Fibre Toxicology, 6, 30, 10.1186/1743-8977-6-30, 2009.

Ghio, A. J., Stoneheurner, J., McGee, J. K., and Kinsey, J. S.: Sulfate content correlates with iron concentrations in ambient air pollution particles, Inhalation Toxicol., 11, 293-307, 10.1080/089583799197104, 1999a.

Ghio, A. J., Stonehuerner, J., Dailey, L. A., and Carter, J. D.: Metals associated with both the water-soluble and insoluble fractions of an ambient air pollution particle catalyze an oxidative stress, Inhalation Toxicol., 11, 37-49, 10.1080/089583799197258, 1999b.

Gholampour, A., Nabizadeh, R., Naseri, S., Yunesian, M., Taghipour, H., Rastkari, N., Nazmara, S., Faridi, S., and Mahvi, A. H.: Exposure and health impacts of outdoor particulate matter in two urban and industrialized area of Tabriz, Iran, Journal of Environmental Health Science and Engineering, 12, 27, 2014.

Gietl, J. K., Lawrence, R., Thorpe, A. J., and Harrison, R. M.: Identification of brake wear particles and derivation of a quantitative tracer for brake dust at a major road, Atmospheric Environment, 44, 141-146, http://dx.doi.org/10.1016/j.atmosenv.2009.10.016, 2010.

Grahame, T. J., and Schlesinger, R. B.: Cardiovascular health and particulate vehicular emissions: a critical evaluation of the evidence, Air Qual., Atmos. Health, 3, 3-27, 10.1007/s11869-009-0047-x, 2010.

Greenwald, R., Bergin, M. H., Weber, R., and Sullivan, A.: Size-resolved, real-time measurement of water-insoluble aerosols in metropolitan Atlanta during the summer of 2004, Atmos. Environ., 41, 519-531, http://dx.doi.org/10.1016/j.atmosenv.2006.08.035, 2007.

Greenwald, R., Bergin, M. H., Yip, F., Boehmer, T., Kewada, P., Shafer, M. M., Schauer, J. J., and Sarnat, J. A.: On-roadway in-cabin exposure to particulate matter: measurement results using both continuous and time-integrated sampling approaches, Aerosol Sci. Technol., 48, 664-675, 10.1080/02786826.2014.912745, 2014.

Guo, H., Xu, L., Bougiatioti, A., Cerully, K. M., Capps, S. L., Hite, J. R., Carlton, A. G., Lee, S. H., Bergin, M. H., Ng, N. L., Nenes, A., and Weber, R. J.: Fine-particle water and pH in the southeastern United States, Atmos. Chem. Phys., 15, 5211-5228, 10.5194/acp-15-5211-2015, 2015.

Guo, H., Sullivan, A. P., Campuzano-Jost, P., Schroder, J. C., Lopez-Hilfiker, F. D., Dibb, J. E., Jimenez, J. L., Thornton, J. A., Brown, S. S., Nenes, A., and Weber, R. J.: Fine particle pH and the partitioning of nitric acid during winter in the northeastern United States, J. Geophys. Res.: Atmos., 121, 10355-10376, 10.1002/2016JD025311, 2016.

Gurgueira, S. A., Lawrence, J., Coull, B., Murthy, G. G., and Gonzalez-Flecha, B.: Rapid increases in the steady-state concentration of reactive oxygen species in the lungs and heart after particulate air pollution inhalation, Environ Health Perspect, 110, 749-755, 2002.

Gwynn, R. C., Burnett, R. T., and Thurston, G. D.: A time-series analysis of acidic particulate matter and daily mortality and morbidity in the Buffalo, New York, region, Environ. Health Perspect., 108, 125-133, 2000.

Halliwell, B.: Antioxidants and human disease: a general introduction, Nutrition reviews, 55, S44-49; discussion S49-52, 1997.

Hand, J. L., Schichtel, B. A., Malm, W. C., and Pitchford, M. L.: Particulate sulfate ion concentration and SO2 emission trends in the United States from the early 1990s through 2010, Atmos. Chem. Phys., 12, 10353-10365, 10.5194/acp-12-10353-2012, 2012.

Hansen, D. A., Edgerton, E. S., Hartsell, B. E., Jansen, J. J., Kandasamy, N., Hidy, G. M., and Blanchard, C. L.: The Southeastern aerosol research and characterization study: Part 1—Overview, Journal of the Air & Waste Management Association, 53, 1460-1471, 10.1080/10473289.2003.10466318, 2003.

Harkema, J. R., Keeler, G., Wagner, J., Morishita, M., Timm, E., Hotchkiss, J., Marsik, F., Dvonch, T., Kaminski, N., and Barr, E.: Effects of concentrated ambient particles on normal and hypersecretory airways in rats, Res Rep Health Eff Inst, 120, 1-68, 2004.

Harrison, R. M., Jones, A. M., Gietl, J., Yin, J., and Green, D. C.: Estimation of the contributions of brake dust, tire wear, and resuspension to nonexhaust traffic particles derived from atmospheric measurements, Environmental Science & Technology, 46, 6523-6529, 10.1021/es300894r, 2012.

Hayyan, M., Hashim, M. A., and AlNashef, I. M.: Superoxide Ion: Generation and Chemical Implications, Chemical Reviews, 116, 3029-3085, 10.1021/acs.chemrev.5b00407, 2016.

He, K., Yang, F., Ma, Y., Zhang, Q., Yao, X., Chan, C. K., Cadle, S., Chan, T., and Mulawa, P.: The characteristics of PM2.5 in Beijing, China, Atmospheric Environment, 35, 4959-4970, http://dx.doi.org/10.1016/S1352-2310(01)00301-6, 2001.

Heal, M. R., Hibbs, L. R., Agius, R. M., and Beverland, I. J.: Total and water-soluble trace metal content of urban background PM10, PM2.5 and black smoke in Edinburgh, UK, Atmospheric Environment, 39, 1417-1430, 10.1016/j.atmosenv.2004.11.026, 2005.

Hennigan, C. J., Izumi, J., Sullivan, A. P., Weber, R. J., and Nenes, A.: A critical evaluation of proxy methods used to estimate the acidity of atmospheric particles, Atmos. Chem. Phys., 15, 2775-2790, 10.5194/acp-15-2775-2015, 2015.

Hetland, R. B., Cassee, F. R., Refsnes, M., Schwarze, P. E., Låg, M., Boere, A. J. F., and Dybing, E.: Release of inflammatory cytokines, cell toxicity and apoptosis in epithelial lung cells after exposure to ambient air particles of different size fractions, Toxicol. In Vitro, 18, 203-212, 10.1016/s0887-2333(03)00142-5, 2004.

Hidy, G. M., Blanchard, C. L., Baumann, K., Edgerton, E., Tanenbaum, S., Shaw, S., Knipping, E., Tombach, I., Jansen, J., and Walters, J.: Chemical climatology of the southeastern United States, 1999-2013, Atmos. Chem. Phys., 14, 11893-11914, 10.5194/acp-14-11893-2014, 2014.

Hiura, T. S., Kaszubowski, M. P., Li, N., and Nel, A. E.: Chemicals in diesel exhaust particles generate reactive oxygen radicals and induce apoptosis in macrophages, the Journal of Immunology, 163, 5582-5591, 1999.

Hoek, G., Krishnan, R. M., Beelen, R., Peters, A., Ostro, B., Brunekreef, B., and Kaufman, J. D.: Long-term air pollution exposure and cardio- respiratory mortality: a review, Environ. Health, 12, 1-16, 10.1186/1476-069X-12-43, 2013.

Homann, K.-H.: Fullerenes and soot formation— new pathways to large particles in flames, Angew. Chem., Int. Ed., 37, 2434-2451, 10.1002/(SICI)1521-3773(19981002)37:18<2434::AID-ANIE2434>3.0.CO;2-L, 1998.

Hopke, P. K., Lamb, R. E., and Natusch, D. F. S.: Multielemental characterization of urban roadway dust, Environ. Sci. Technol., 14, 164-172, 10.1021/es60162a006, 1980.

Hu, S., Polidori, A., Arhami, M., Shafer, M. M., Schauer, J. J., Cho, A., and Sioutas, C.: Redox activity and chemical speciation of size fractioned PM in the communities of the Los Angeles-Long Beach harbor, Atmos. Chem. Phys., 8, 6439-6451, 10.5194/acp-8-6439-2008, 2008.

Huang, Y. C., Ghio, A. J., Stonehuerner, J., McGee, J., Carter, J. D., Grambow, S. C., and Devlin, R. B.: The role of soluble components in ambient fine particles-induced changes in human lungs and blood, Inhal Toxicol, 15, 327-342, 10.1080/08958370304460, 2003.

Hueglin, C., Gehrig, R., Baltensperger, U., Gysel, M., Monn, C., and Vonmont, H.: Chemical characterisation of PM2.5, PM10 and coarse particles at urban, near-city and rural sites in Switzerland, Atmospheric Environment, 39, 637-651, http://dx.doi.org/10.1016/j.atmosenv.2004.10.027, 2005.

Hung, H.-F., and Wang, C.-S.: Experimental determination of reactive oxygen species in Taipei aerosols, Journal of Aerosol Science, 32, 1201-1211, https://doi.org/10.1016/S0021-8502(01)00051-9, 2001.

ICRP.: Publication 66: Human Respiratory Tract Model for Radiological Protection, Oxford, UK: Pergamon, 36-52, 1994.

Ito, A., and Feng, Y.: Role of dust alkalinity in acid mobilization of iron, Atmos. Chem. Phys., 10, 9237-9250, 10.5194/acp-10-9237-2010, 2010.

Jang, M., Czoschke, N. M., Lee, S., and Kamens, R. M.: Heterogeneous Atmospheric Aerosol Production by Acid-Catalyzed Particle-Phase Reactions, Science, 298, 814-817, 10.1126/science.1075798, 2002.

Janssen, N. A., Gerlofs-Nijland, M. E., Lanki, T., Salonen, R. O., Cassee, F., Hoek, G., Fischer, P., Brunekreef, B., and Krzyzanowski, M.: Health effects of black carbon, World Health Organization, Denmark, 2012.

Janssen, N. A. H., Yang, A., Strak, M., Steenhof, M., Hellack, B., Gerlofs-Nijland, M. E., Kuhlbusch, T., Kelly, F., Harrison, R., Brunekreef, B., Hoek, G., and Cassee, F.: Oxidative potential of particulate matter collected at sites with different source characteristics, Science of The Total Environment, 472, 572-581, 10.1016/j.scitotenv.2013.11.099, 2014.

Janssen, N. A. H., Strak, M., Yang, A., Hellack, B., Kelly, F. J., Kuhlbusch, T. A. J., Harrison, R. M., Brunekreef, B., Cassee, F. R., Steenhof, M., and Hoek, G.: Associations between three specific a-cellular measures of the oxidative potential of particulate matter and markers of acute airway and nasal inflammation in healthy volunteers, Occupational and environmental medicine, 72, 49-56, 2015.

Jung, H., Guo, B., Anastasio, C., and Kennedy, I. M.: Quantitative measurements of the generation of hydroxyl radicals by soot particles in a surrogate lung fluid, Atmos. Environ., 40, 1043-1052, http://dx.doi.org/10.1016/j.atmosenv.2005.11.015, 2006.

Kadiiska, M. B., Mason, R. P., Dreher, K. L., Costa, D. L., and Ghio, A. J.: In Vivo Evidence of Free Radical Formation in the Rat Lung after Exposure to an Emission Source Air Pollution Particle, Chem. Res. Toxicol., 10, 1104-1108, 10.1021/tx970049r, 1997.

Kam, W., Ning, Z., Shafer, M. M., Schauer, J. J., and Sioutas, C.: Chemical characterization and redox potential of coarse and fine particulate matter (PM) in

underground and ground-level rail systems of the Los Angeles metro, Environmental Science & Technology, 45, 6769-6776, 10.1021/es201195e, 2011.

Kanti Das, T., Wati, M. R., and Fatima-Shad, K.: Oxidative Stress Gated by Fenton and Haber Weiss Reactions and Its Association With Alzheimer's Disease, Arch Neurosci, 2, e20078, 10.5812/archneurosci.20078, 2015.

Kehrer, J. P.: The Haber–Weiss reaction and mechanisms of toxicity, Toxicology, 149, 43-50, https://doi.org/10.1016/S0300-483X(00)00231-6, 2000.

Kelly, F. J., Mudway, I., Blomberg, A., Frew, A., and Sandström, T.: Altered lung antioxidant status in patients with mild asthma, The Lancet, 354, 482-483, http://dx.doi.org/10.1016/S0140-6736(99)01812-7, 1999.

Kelly, F. J., and Fussell, J. C.: Size, source and chemical composition as determinants of toxicity attributable to ambient particulate matter, Atmospheric Environment, 60, 504-526, http://dx.doi.org/10.1016/j.atmosenv.2012.06.039, 2012.

Klein, C., Dutrow, B., and Dana, J. D.: The 23rd edition of the manual of mineral science: (after James D. Dana), 23rd ed., J. Wiley, Hoboken, N.J., 2008.

Kleinman, M. T., Sioutas, C., Froines, J. R., Fanning, E., Hamade, A., Mendez, L., Meacher, D., and Oldham, M.: Inhalation of concentrated ambient particulate matter near a heavily trafficked road stimulates antigen-induced airway responses in mice, Inhalation toxicology, 19, 117-126, 10.1080/08958370701495345, 2007.

Kodavanti, U. P., Schladweiler, M. C., Ledbetter, A. D., McGee, J. K., Walsh, L., Gilmour, P. S., Highfill, J. W., Davies, D., Pinkerton, K. E., Richards, J. H., Crissman, K., Andrews, D., and Costa, D. L.: Consistent pulmonary and systemic responses from inhalation of fine concentrated ambient particles: roles of rat strains used and physicochemical properties, Environmental Health Perspectives, 113, 1561-1568, 10.1289/ehp.7868, 2005.

Koutrakis, P., Wolfson, J. M., and Spengler, J. D.: An improved method for measuring aerosol strong acidity: Results from a nine-month study in St Louis, Missouri and Kingston, Tennessee, Atmos. Environ. (1967-1989), 22, 157-162, http://dx.doi.org/10.1016/0004-6981(88)90308-3, 1988.

Koutrakis, P., Thompson, K. M., Wolfson, J. M., Spengler, J. D., Keeler, G. J., and Slater, J. L.: Determination of aerosol strong acidity losses due to interactions of collected particles: Results from laboratory and field studies, Atmos. Environ., Part A, 26, 987-995, http://dx.doi.org/10.1016/0960-1686(92)90030-O, 1992.

Kubátová, A., Dronen, L. C., Picklo, M. J., and Hawthorne, S. B.: Midpolarity and nonpolar wood smoke particulate matter fractions deplete glutathione in RAW 264.7 macrophages, Chem. Res. Toxicol., 19, 255-261, 10.1021/tx050172f, 2006.

Kumagai, Y., Koide, S., Taguchi, K., Endo, A., Nakai, Y., Yoshikawa, T., and Shimojo, N.: Oxidation of proximal protein sulfhydryls by phenanthraquinone, a component of diesel exhaust particles, Chem. Res. Toxicol., 15, 483-489, 10.1021/tx0100993, 2002.

Künzli, N., Mudway, I. S., Götschi, T., Shi, T., Kelly, F. J., Cook, S., Burney, P., Forsberg, B., Gauderman, J. W., Hazenkamp, M. E., Heinrich, J., Jarvis, D., Norbäck, D., Payo-Losa, F., Poli, A., Sunyer, J., and Borm, P. J. A.: Comparison of Oxidative Properties, Light Absorbance, and Total and Elemental Mass Concentration of Ambient PM(2.5) Collected at 20 European Sites, Environmental Health Perspectives, 114, 684-690, 10.1289/ehp.8584, 2006.

Laden, F., Neas, L. M., Dockery, D. W., and Schwartz, J.: Association of fine particulate matter from different sources with daily mortality in six U.S. cities, Environmental Health Perspectives, 108, 941-947, 10.2307/3435052, 2000.

Landreman, A. P., Shafer, M. M., Hemming, J. C., Hannigan, M. P., and Schauer, J. J.: A macrophage-based method for the assessment of the Reactive Oxygen Species (ROS) activity of atmospheric particulate matter (PM) and application to routine (daily-24 h) aerosol monitoring studies, Aerosol Science and Technology, 42, 946-957, 10.1080/02786820802363819, 2008.

Li, N., Hao, M., Phalen, R. F., Hinds, W. C., and Nel, A. E.: Particulate air pollutants and asthma: A paradigm for the role of oxidative stress in PM-induced adverse health effects, Clinical Immunology, 109, 250-265, http://dx.doi.org/10.1016/j.clim.2003.08.006, 2003a.

Li, N., Sioutas, C., Cho, A. K., Schmitz, D., Misra, C., Sempf, J., Wang, M., Oberley, T., Froines, J., and Nel, A.: Ultrafine particulate pollutants induce oxidative stress and mitochondrial damage, Environ. Health Perspect., 111, 455-460, 10.1289/ehp.6000, 2003b.

Li, Q., Shang, J., and Zhu, T.: Physicochemical characteristics and toxic effects of ozone-oxidized black carbon particles, Atmos. Environ., 81, 68-75, http://dx.doi.org/10.1016/j.atmosenv.2013.08.043, 2013.

Li, Q. F., Wyatt, A., and Kamens, R. M.: Oxidant generation and toxicity enhancement of aged-diesel exhaust, Atmos. Environ., 43, 1037-1042, http://dx.doi.org/10.1016/j.atmosenv.2008.11.018, 2009.

Li, R., Ning, Z., Majumdar, R., Cui, J., Takabe, W., Jen, N., Sioutas, C., and Hsiai, T.: Ultrafine particles from diesel vehicle emissions at different driving cycles induce differential vascular pro-inflammatory responses: Implication of chemical components and NF-kappaB signaling, Particle and Fibre Toxicology, 7, 6, 10.1186/1743-8977-7-6, 2010.

Li, X.-Y., Hao, L., Liu, Y.-H., Chen, C.-Y., Pai, V. J., and Kang, J. X.: Protection against fine particle-induced pulmonary and systemic inflammation by omega-3 polyunsaturated fatty acids, Biochim. Biophys. Acta, Gen. Subj., 1861, 577-584, http://dx.doi.org/10.1016/j.bbagen.2016.12.018, 2017.

Lin, P., and Yu, J. Z.: Generation of reactive oxygen species mediated by Humic-like Substances in atmospheric aerosols, Environ. Sci. Technol., 45, 10362-10368, 10.1021/es2028229, 2011.

Liochev, S. I., and Fridovich, I.: The Haber-Weiss cycle - 70 years later: an alternative view, Redox Rep., 7, 55-57, 10.1179/135100002125000190, 2002.

Lippmann, M.: Regional deposition of particles in the human respiratory tract, in: Comprehensive Physiology, John Wiley & Sons, Inc., 2010.

Lomnicki, S., Truong, H., Vejerano, E., and Dellinger, B.: Copper Oxide-Based Model of Persistent Free Radical Formation on Combustion-Derived Particulate Matter, Environmental Science & Technology, 42, 4982-4988, 10.1021/es071708h, 2008.

Longo, A. F., Feng, Y., Lai, B., Landing, W. M., Shelley, R. U., Nenes, A., Mihalopoulos, N., Violaki, K., and Ingall, E. D.: Influence of Atmospheric Processes on the Solubility and Composition of Iron in Saharan Dust, Environ. Sci. Technol., 50, 6912-6920, 10.1021/acs.est.6b02605, 2016a.

Longo, A. F., Vine, D. J., King, L. E., Oakes, M., Weber, R. J., Huey, L. G., Russell, A. G., and Ingall, E. D.: Composition and oxidation state of sulfur in atmospheric particulate matter, Atmos. Chem. Phys., 16, 13389-13398, 10.5194/acp-16-13389-2016, 2016b.

Lough, G. C., Schauer, J. J., Park, J.-S., Shafer, M. M., DeMinter, J. T., and Weinstein, J. P.: Emissions of Metals Associated with Motor Vehicle Roadways, Environ. Sci. Technol., 39, 826-836, 10.1021/es048715f, 2005.

Lundstedt, S., White, P. A., Lemieux, C. L., Lynes, K. D., Lambert, I. B., Öberg, L., Haglund, P., and Tysklind, M.: Sources, fate, and toxic hazards of oxygenated polycyclic aromatic hydrocarbons (PAHs) at PAH- contaminated sites, AMBIO: A Journal of the Human Environment, 36, 475-485, 10.1579/0044-7447(2007)36[475:sfatho]2.0.co;2, 2007.

Maher, B. A., Ahmed, I. A. M., Karloukovski, V., MacLaren, D. A., Foulds, P. G., Allsop, D., Mann, D. M. A., Torres-Jardón, R., and Calderon-Garciduenas, L.: Magnetite pollution nanoparticles in the human brain, Proc. Natl. Acad. Sci. U. S. A., 201605941, 10.1073/pnas.1605941113, 2016.

Majestic, B. J., Schauer, J. J., Shafer, M. M., Turner, J. R., Fine, P. M., Singh, M., and Sioutas, C.: Development of a Wet-Chemical Method for the Speciation of Iron in Atmospheric Aerosols, Environ. Sci. Technol., 40, 2346-2351, 10.1021/es052023p, 2006.

Manoli, E., Voutsa, D., and Samara, C.: Chemical characterization and source identification/apportionment of fine and coarse air particles in Thessaloniki, Greece, Atmos. Environ., 36, 949-961, http://dx.doi.org/10.1016/S1352-2310(01)00486-1, 2002.

Maynard, D., Coull, B. A., Gryparis, A., and Schwartz, J.: Mortality risk associated with short-term exposure to traffic particles and sulfates, Environ. Health Perspect., 115, 751-755, 10.1289/ehp.9537, 2007.

McCreanor, J., Cullinan, P., Nieuwenhuijsen, M. J., Stewart-Evans, J., Malliarou, E., Jarup, L., Harrington, R., Svartengren, M., Han, I.-K., Ohman-Strickland, P., Chung, K. F., and Zhang, J.: Respiratory effects of exposure to diesel traffic in persons with asthma, N. Engl. J. Med., 357, 2348-2358, 10.1056/NEJMoa071535, 2007.

McWhinney, R. D., Gao, S. S., Zhou, S., and Abbatt, J. P. D.: Evaluation of the effects of ozone oxidation on redox-cycling activity of two-stroke engine exhaust particles, Environ. Sci. Technol., 45, 2131-2136, 10.1021/es102874d, 2011.

McWhinney, R. D., Badali, K., Liggio, J., Li, S.-M., and Abbatt, J. P. D.: Filterable redox cycling activity: a comparison between diesel exhaust particles and secondary organic aerosol constituents, Environ. Sci. Technol., 47, 3362-3369, 10.1021/es304676x, 2013a.

McWhinney, R. D., Zhou, S., and Abbatt, J. P. D.: Naphthalene SOA: redox activity and naphthoquinone gas–particle partitioning, Atmos. Chem. Phys., 13, 9731-9744, 10.5194/acp-13-9731-2013, 2013b.

Meskhidze, N., Chameides, W. L., Nenes, A., and Chen, G.: Iron mobilization in mineral dust: Can anthropogenic SO2 emissions affect ocean productivity?, Geophys. Res. Lett., 30, 2085, 10.1029/2003GL018035, 2003.

Meskhidze, N., Chameides, W. L., and Nenes, A.: Dust and pollution: A recipe for enhanced ocean fertilization?, J. Geophys. Res., 110, 2156-2202, 10.1029/2004JD005082, 2005.

Metzger, K. B., Tolbert, P. E., Klein, M., Peel, J. L., Flanders, W. D., Todd, K., Mulholland, J. A., Ryan, P. B., and Frumkin, H.: Ambient air pollution and cardiovascular emergency department visits, Epidemiology, 15, 46-56, 10.1097/01.EDE.0000101748.28283.97, 2004.

Minguillón, M. C., Cirach, M., Hoek, G., Brunekreef, B., Tsai, M., de Hoogh, K., Jedynska, A., Kooter, I. M., Nieuwenhuijsen, M., and Querol, X.: Spatial variability of trace elements and sources for improved exposure assessment in Barcelona, Atmospheric Environment, 89, 268-281, http://dx.doi.org/10.1016/j.atmosenv.2014.02.047, 2014.

Moldanová, J., Fridell, E., Popovicheva, O., Demirdjian, B., Tishkova, V., Faccinetto, A., and Focsa, C.: Characterisation of particulate matter and gaseous emissions from a large ship diesel engine, Atmos. Environ., 43, 2632-2641, 10.1016/j.atmosenv.2009.02.008, 2009.

Mudway, I. S., Stenfors, N., Duggan, S. T., Roxborough, H., Zielinski, H., Marklund, S. L., Blomberg, A., Frew, A. J., Sandström, T., and Kelly, F. J.: An in vitro and in vivo investigation of the effects of diesel exhaust on human airway lining fluid antioxidants,

Arch. Biochem. Biophys., 423, 200-212, http://dx.doi.org/10.1016/j.abb.2003.12.018, 2004.

Mudway, I. S., Duggan, S. T., Venkataraman, C., Habib, G., Kelly, F. J., and Grigg, J.: Combustion of dried animal dung as biofuel results in the generation of highly redox active fine particulates, Part. Fibre Toxicol., 2, 6, 10.1186/1743-8977-2-6, 2005.

Mudway, I. S., Fuller, G., Green, D., Dunster, C., and Kelly, F. J.: Report: Quantifying the London specific component of PM10 oxidative activity, University of London, Defra, UK, 2011.

Murphy, D. M., Cziczo, D. J., Hudson, P. K., Schein, M. E., and Thomson, D. S.: Particle density inferred from simultaneous optical and aerodynamic diameters sorted by composition, J. Aerosol Sci., 35, 135-139, http://dx.doi.org/10.1016/S0021-8502(03)00386-0, 2004.

Nel, A. E., Diaz-Sanchez, D., and Li, N.: The role of particulate pollutants in pulmonary inflammation and asthma: evidence for the involvement of organic chemicals and oxidative stress, Current opinion in pulmonary medicine, 7, 20-26, 10.1097/00063198-200101000-00004, 2001.

Nel, A. E.: Air pollution-related illness: effects of particles, Science, 308, 804-806, 10.1126/science.1108752, 2005.

Nemat, K., Yadollah, S., and Mahdi, M.: Chronic Inflammation and Oxidative Stress as a Major Cause of Age- Related Diseases and Cancer, Recent Patents on Inflammation & Allergy Drug Discovery, 3, 73-80, http://dx.doi.org/10.2174/187221309787158371, 2009.

Nemmar, A., Hoet, P. H. M., Vanquickenborne, B., Dinsdale, D., Thomeer, M., Hoylaerts, M. F., Vanbilloen, H., Mortelmans, L., and Nemery, B.: Passage of inhaled particles into the blood circulation in humans, Circulation, 105, 411, 2002.

Nenes, A., Pandis, S. N., and Pilinis, C.: Continued development and testing of a new thermodynamic aerosol module for urban and regional air quality models, Atmos. Environ., 33, 1553-1560, http://dx.doi.org/10.1016/S1352-2310(98)00352-5, 1999.

Nenes, A., Krom, M. D., Mihalopoulos, N., Van Cappellen, P., Shi, Z., Bougiatioti, A., Zarmpas, P., and Herut, B.: Atmospheric acidification of mineral aerosols: a source of bioavailable phosphorus for the oceans, Atmos. Chem. Phys., 11, 6265-6272, 10.5194/acp-11-6265-2011, 2011.

Norris, G., YoungPong, S. N., Koenig, J. Q., Larson, T. V., Sheppard, L., and Stout, J. W.: An association between fine particles and asthma emergency department visits for children in Seattle, Environmental Health Perspectives, 107, 489-493, 1999.

Ntziachristos, L., Froines, J. R., Cho, A. K., and Sioutas, C.: Relationship between redox activity and chemical speciation of size-fractionated particulate matter, Part. Fibre Toxicol., 4, 5, 10.1186/1743-8977-4-5, 2007.

Oakes, M., Ingall, E. D., Lai, B., Shafer, M. M., Hays, M. D., Liu, Z. G., Russell, A. G., and Weber, R. J.: Iron solubility related to particle sulfur content in source emission and ambient fine particles, Environ. Sci. Technol., 46, 6637-6644, 10.1021/es300701c, 2012.

Oberdorster, G., Sharp, Z., Atudorei, V., Elder, A., Gelein, R., Lunts, A., Kreyling, W., and Cox, C.: Extrapulmonary translocation of ultrafine carbon particles following whole-body inhalation exposure of rats, J. Toxicol. Environ. Health, Part A, 65, 1531-1543, 10.1080/00984100290071658, 2002.

Oberdorster, G., Sharp, Z., Atudorei, V., Elder, A., Gelein, R., Kreyling, W., and Cox, C.: Translocation of inhaled ultrafine particles to the brain, Inhalation Toxicol., 16, 437-445, 10.1080/08958370490439597, 2004.

Oeder, S., Kanashova, T., Sippula, O., Sapcariu, S. C., Streibel, T., Arteaga-Salas, J. M., Passig, J., Dilger, M., Paur, H. R., Schlager, C., Mulhopt, S., Diabate, S., Weiss, C., Stengel, B., Rabe, R., Harndorf, H., Torvela, T., Jokiniemi, J. K., Hirvonen, M. R., Schmidt-Weber, C., Traidl-Hoffmann, C., BeruBe, K. A., Wlodarczyk, A. J., Prytherch, Z., Michalke, B., Krebs, T., Prevot, A. S., Kelbg, M., Tiggesbaumker, J., Karg, E., Jakobi, G., Scholtes, S., Schnelle-Kreis, J., Lintelmann, J., Matuschek, G., Sklorz, M., Klingbeil, S., Orasche, J., Richthammer, P., Muller, L., Elsasser, M., Reda, A., Groger, T., Weggler, B., Schwemer, T., Czech, H., Ruger, C. P., Abbaszade, G., Radischat, C., Hiller, K., Buters, J. T., Dittmar, G., and Zimmermann, R.: Particulate matter from both heavy fuel oil and diesel fuel shipping emissions show strong biological effects on human lung cells at realistic and comparable in vitro exposure conditions, PLoS One, 10, e0126536, 10.1371/journal.pone.0126536, 2015.

Ore, S.: Oxidative Stress Relaxation of Natural Rubber Vulcanized with Di-Tertiary-Butyl Peroxide, Rubber Chemistry and Technology, 29, 1043-1046, 10.5254/1.3542575, 1956.

Osornio-Vargas, A. R., Serrano, J., Rojas-Bracho, L., Miranda, J., Garcia-Cuellar, C., Reyna, M. A., Flores, G., Zuk, M., Quintero, M., Vazquez, I., Sanchez-Perez, Y., Lopez, T., and Rosas, I.: In vitro biological effects of airborne PM(2.5) and PM(10) from a semi-desert city on the Mexico-US border, Chemosphere, 83, 618-626, 10.1016/j.chemosphere.2010.11.073, 2011.

Ostro, B. D., Hurley, S., and Lipsett, M. J.: Air pollution and daily mortality in the coachella valley, california: a study of PM10 dominated by coarse particles, Environ. Res., 81, 231-238, http://dx.doi.org/10.1006/enrs.1999.3978, 1999.

Øvrevik, J., Refsnes, M., Låg, M., Holme, A. J., and Schwarze, E. P.: Activation of Proinflammatory Responses in Cells of the Airway Mucosa by Particulate Matter: Oxidant- and Non-Oxidant-Mediated Triggering Mechanisms, Biomolecules, 5, 10.3390/biom5031399, 2015.

Paatero, P., and Tapper, U.: Positive matrix factorization: A non-negative factor model with optimal utilization of error estimates of data values, Environmetrics, 5, 111-126, 10.1002/env.3170050203, 1994.

Pan, C.-J. G., Schmitz, D. A., Cho, A. K., Froines, J., and Fukuto, J. M.: Inherent redox properties of diesel exhaust particles: catalysis of the generation of reactive oxygen species by biological reductants, Toxicol. Sci., 81, 225-232, 10.1093/toxsci/kfh199, 2004.

Pardo, M., Shafer, M. M., Rudich, A., Schauer, J. J., and Rudich, Y.: Single Exposure to near Roadway Particulate Matter Leads to Confined Inflammatory and Defense Responses: Possible Role of Metals, Environ. Sci. Technol., 49, 8777-8785, 10.1021/acs.est.5b01449, 2015.

Paris, R., and Desboeufs, K. V.: Effect of atmospheric organic complexation on iron-bearing dust solubility, Atmos. Chem. Phys., 13, 4895-4905, 10.5194/acp-13-4895-2013, 2013.

Peel, J. L., Tolbert, P. E., Klein, M., Metzger, K. B., Flanders, W. D., Todd, K., Mulholland, J. A., Ryan, P. B., and Frumkin, H.: Ambient air pollution and respiratory emergency department visits, Epidemiology, 16, 164-174, 10.1097/01.ede.0000152905.42113.db, 2005.

Peter, M., and Steffen, L.: Oxidative Damage to DNA and Lipids as Biomarkers of Exposure to Air Pollution, Environmental Health Perspectives, 118, 10.1289/ehp.0901725, 2010.

Peters, A., Wichmann, H., Tuch, T., Heinrich, J., and Heyder, J.: Respiratory effects are associated with the number of ultrafine particles, Am. J. Respir. Crit. Care Med., 155, 1376 - 1383, 1997.

Polissar, A. V., Hopke, P. K., Paatero, P., Malm, W. C., and Sisler, J. F.: Atmospheric aerosol over Alaska: 2. Elemental composition and sources, Journal of Geophysical Research: Atmospheres, 103, 19045-19057, 10.1029/98JD01212, 1998.

Pope, C. A., Thun, M. J., Namboodiri, M. M., Dockery, D. W., Evans, J. S., Speizer, F. E., and Heath, C. W.: Particulate Air Pollution as a Predictor of Mortality in a Prospective Study of U.S. Adults, Am. J. Respir. Crit. Care Med., 151, 669-674, 10.1164/ajrccm/151.3_Pt_1.669, 1995.

Pope, C. A., Burnett, R. T., Thun, M. J., Calle, E. E., Krewski, D., Ito, K., and Thurston, G. D.: Lung cancer, cardiopulmonary mortality, and long-term exposure to fine particulate air pollution, Journal of the American Medical Association, 287, 1132-1141, 10.1001/jama.287.9.1132, 2002.

Pope, C. A., Burnett, R. T., Thurston, G. D., Thun, M. J., Calle, E. E., Krewski, D., and Godleski, J. J.: Cardiovascular mortality and long-term exposure to particulate air pollution: epidemiological evidence of general pathophysiological pathways of disease, Circulation, 109, 71-77, 10.1161/01.CIR.0000108927.80044.7F, 2004.

Pöschl, U., and Shiraiwa, M.: Multiphase Chemistry at the Atmosphere–Biosphere Interface Influencing Climate and Public Health in the Anthropocene, Chemical Reviews, 115, 4440-4475, 10.1021/cr500487s, 2015.

Quiterio, S. L., Sousa da Silva, C. R., Arbilla, G., and Escaleira, V.: Metals in airborne particulate matter in the industrial district of Santa Cruz, Rio de Janeiro, in an annual period, Atmos. Environ., 38, 321-331, http://dx.doi.org/10.1016/j.atmosenv.2003.09.017, 2004.

Radi, R., Cassina, A., Hodara, R., Quijano, C., and Castro, L.: Peroxynitrite reactions and formation in mitochondria, Free Radical Biology and Medicine, 33, 1451-1464, https://doi.org/10.1016/S0891-5849(02)01111-5, 2002.

Raizenne, M., Neas, L. M., Damokosh, A. I., Dockery, D. W., Spengler, J. D., Koutrakis, P., Ware, J. H., and Speizer, F. E.: Health effects of acid aerosols on North American children: pulmonary function, Environmental Health Perspectives, 104, 506-514, 10.2307/3432991, 1996a.

Raizenne, M., Neas, L. M., Damokosh, A. I., Dockery, D. W., Spengler, J. D., Koutrakis, P., Ware, J. H., and Speizer, F. E.: Health effects of acid aerosols on North American children: pulmonary function, Environ. Health Perspect., 104, 506-514, 1996b.

Reuter, S., Gupta, S. C., Chaturvedi, M. M., and Aggarwal, B. B.: Oxidative stress, inflammation, and cancer: How are they linked?, Free radical biology & medicine, 49, 1603-1616, 10.1016/j.freeradbiomed.2010.09.006, 2010.

Richard, A., Gianini, M. F. D., Mohr, C., Furger, M., Bukowiecki, N., Minguillón, M. C., Lienemann, P., Flechsig, U., Appel, K., DeCarlo, P. F., Heringa, M. F., Chirico, R., Baltensperger, U., and Prévôt, A. S. H.: Source apportionment of size and time resolved trace elements and organic aerosols from an urban courtyard site in Switzerland, Atmos. Chem. Phys., 11, 8945-8963, 10.5194/acpd-11-3727-2011, 2011.

Riediker, M., Devlin, R., Griggs, T., Herbst, M., Bromberg, P., Williams, R., and Cascio, W.: Cardiovascular effects in patrol officers are associated with fine particulate matter from brake wear and engine emissions, Particle and Fibre Toxicology, 1, 2, 10.1186/1743-8977-1-2, 2004.

Rodríguez, S., Querol, X., Alastuey, A., Viana, M. a.-M., Alarcón, M., Mantilla, E., and Ruiz, C. R.: Comparative PM10–PM2.5 source contribution study at rural, urban and industrial sites during PM episodes in Eastern Spain, Sci. Total Environ., 328, 95-113, http://dx.doi.org/10.1016/S0048-9697(03)00411-X, 2004.

Roginsky, V. A., Barsukova, T. K., and Stegmann, H. B.: Kinetics of redox interaction between substituted quinones and ascorbate under aerobic conditions, Chem Biol Interact, 121, 177-197, 1999.

Saffari, A., Daher, N., Shafer, M. M., Schauer, J. J., and Sioutas, C.: Seasonal and spatial variation in dithiothreitol (DTT) activity of quasi-ultrafine particles in the Los Angeles Basin and its association with chemical species, J. Environ. Sci. Health, Part A: Toxic/Hazard. Subst. Environ. Eng., 49, 441-451, 10.1080/10934529.2014.854677, 2014a.

Saffari, A., Daher, N., Shafer, M. M., Schauer, J. J., and Sioutas, C.: Global perspective on the oxidative potential of airborne particulate matter: a synthesis of research findings, Environmental Science & Technology, 48, 7576-7583, 10.1021/es500937x, 2014b.

Samet, J. M., Dominici, F., Curriero, F. C., Coursac, I., and Zeger, S. L.: Fine particulate air pollution and mortality in 20 U.S. cities, 1987–1994, N. Engl. J. Med., 343, 1742-1749, doi:10.1056/NEJM200012143432401, 2000.

Sarnat, J. A., Marmur, A., Klein, M., Kim, E., Russell, A. G., Sarnat, S. E., Mulholland, J. A., Hopke, P. K., and Tolbert, P. E.: Fine particle sources and cardiorespiratory morbidity: an application of chemical mass balance and factor analytical source-apportionment methods, Environ. Health Perspect., 116, 459-466, 10.1289/ehp.10873, 2008.

Sauvain, J.-J., Deslarzes, S., and Riediker, M.: Nanoparticle reactivity toward dithiothreitol, Nanotoxicology, 2, 121-129, 10.1080/17435390802245716, 2008.

Sauvain, J.-J., Rossi, M. J., and Riediker, M.: Comparison of three acellular tests for assessing the oxidation potential of nanomaterials, Aerosol Sci. Technol., 47, 218-227, 10.1080/02786826.2012.742951, 2012.

Sauvain, J.-J., Deslarzes, S., Storti, F., and Riediker, M.: Oxidative Potential of Particles in Different Occupational Environments: A Pilot Study, Ann. Occup. Hyg., 59, 882-894, 10.1093/annhyg/mev024, 2015.

Schaumann, F., Borm, P. J. A., Herbrich, A., Knoch, J., Pitz, M., Schins, R. P. F., Luettig, B., Hohlfeld, J. M., Heinrich, J., and Krug, N.: Metal-rich ambientparticles (particulate matter2.5) cause airway inflammation in healthy subjects, American Journal of Respiratory and Critical Care Medicine, 170, 898-903, 10.1164/rccm.200403-423OC, 2004.

Schoonen, M. A. A., Cohn, C. A., Roemer, E., Laffers, R., Simon, S. R., and O'Riordan, T.: Mineral-induced formation of reactive oxygen species, Rev. Mineral. Geochem., 64, 179, 2006.

Schwartz, J., Dockery, D. W., and Neas, L. M.: Is Daily Mortality Associated Specifically with Fine Particles?, J. Air Waste Manage. Assoc., 46, 927-939, 10.1080/10473289.1996.10467528, 1996.

Schwertmann, U.: Solubility and dissolution of iron oxides, Plant Soil, 130, 1-25, 10.1007/BF00011851, 1991.

Seagrave, J., McDonald, J. D., Gigliotti, A. P., Nikula, K. J., Seilkop, S. K., Gurevich, M., and Mauderly, J. L.: Mutagenicity and in vivo toxicity of combined particulate and semivolatile organic fractions of gasoline and diesel engine emissions, Toxicological sciences : an official journal of the Society of Toxicology, 70, 212-226, 10.1093/toxsci/70.2.212, 2002.

Seagrave, J., Gigliotti, A., McDonald, J. D., Seilkop, S. K., Whitney, K. A., Zielinska, B., and Mauderly, J. L.: Composition, toxicity, and mutagenicity of particulate and

semivolatile emissions from heavy-duty compressed natural gas-powered vehicles, Toxicological sciences : an official journal of the Society of Toxicology, 87, 232-241, 10.1093/toxsci/kfi230, 2005.

Seinfeld, J. H., and Pandis, S. N.: Atmospheric Chemistry and Physics - From Air Pollution to Climate Change, John Wiley & Sons, Inc., New York, 2006.

Shakya, K. M., and Peltier, R. E.: Non-sulfate sulfur in fine aerosols across the United States: Insight for organosulfate prevalence, Atmospheric Environment, 100, 159-166, http://dx.doi.org/10.1016/j.atmosenv.2014.10.058, 2015.

Shen, H., and Anastasio, C.: Formation of hydroxyl radical from San Joaquin Valley particles extracted in a cell-free surrogate lung fluid, Atmospheric chemistry and physics 11, 9671-9682, 10.5194/acp-11-9671-2011, 2011.

Shi, T., Schins, R. P., Knaapen, A. M., Kuhlbusch, T., Pitz, M., Heinrich, J., and Borm, P. J.: Hydroxyl radical generation by electron paramagnetic resonance as a new method to monitor ambient particulate matter composition, Journal of environmental monitoring : JEM, 5, 550-556, 10.1039/B303928P, 2003.

Shi, Z., Bonneville, S., Krom, M. D., Carslaw, K. S., Jickells, T. D., Baker, A. R., and Benning, L. G.: Iron dissolution kinetics of mineral dust at low pH during simulated atmospheric processing, Atmos. Chem. Phys., 11, 995-1007, 10.5194/acp-11-995-2011, 2011.

Shiraiwa, M., Sosedova, Y., Rouvière, A., Yang, H., Zhang, Y., Abbatt, J. P. D., Ammann, M., and Pöschl, U.: The role of long-lived reactive oxygen intermediates in the reaction of ozone with aerosol particles, Nat. Chem., 3, 291-295, http://www.nature.com/nchem/journal/v3/n4/abs/nchem.988.html#supplementary-information, 2011.

Shirmohammadi, F., Hasheminassab, S., Wang, D., Saffari, A., Schauer, J. J., Shafer, M. M., Delfino, R. J., and Sioutas, C.: Oxidative potential of coarse particulate matter (PM10-2.5) and its relation to water solubility and sources of trace elements and metals in the Los Angeles Basin, Environ. Sci.: Processes Impacts, 17, 2110-2121, 10.1039/C5EM00364D, 2015.

Shuster-Meiseles, T., Shafer, M. M., Heo, J., Pardo, M., Antkiewicz, D. S., Schauer, J. J., Rudich, A., and Rudich, Y.: ROS-generating/ARE-activating capacity of metals in roadway particulate matter deposited in urban environment, Environ. Res., 146, 252-262, http://dx.doi.org/10.1016/j.envres.2016.01.009, 2016.

Sies, H., Cadenas, E., Symons, M. C. R., and Scott, G.: Oxidative Stress: Damage to Intact Cells and Organs [and Discussion], Philosophical Transactions of the Royal Society of London. B, Biological Sciences, 311, 617, 1985.

Spector, A.: Oxidative stress-induced cataract: mechanism of action, The FASEB Journal, 9, 1173-1182, 1995.

Spengler, J. D., Keeler, G. J., Koutrakis, P., Ryan, P. B., Raizenne, M., and Franklin, C. A.: Exposures to acidic aerosols, Environ. Health Perspect., 79, 43-51, 1989.

Spengler, J. D., Koutrakis, P., Dockery, D. W., Raizenne, M., and Speizer, F. E.: Health effects of acid aerosols on North American children: air pollution exposures, Environ. Health Perspect., 104, 492-499, 1996.

Steenhof, M., Gosens, I., Strak, M., Godri, K. J., Hoek, G., Cassee, F. R., Mudway, I. S., Kelly, F. J., Harrison, R. M., Lebret, E., Brunekreef, B., Janssen, N. A. H., and Pieters, R. H. H.: In vitro toxicity of particulate matter (PM) collected at different sites in the Netherlands is associated with PM composition, size fraction and oxidative potential--the RAPTES project, Part. Fibre Toxicol., 8, 26, 10.1186/1743-8977-8-26, 2011.

Steenhof, M., Mudway, I. S., Gosens, I., Hoek, G., Godri, K. J., Kelly, F. J., Harrison, R. M., Pieters, R. H. H., Cassee, F. R., Lebret, E., Brunekreef, B. A., Strak, M., and Janssen, N. A. H.: Acute nasal pro-inflammatory response to air pollution depends on characteristics other than particle mass concentration or oxidative potential: the RAPTES project, Occup. Environ. Med., 70, 341, 2013.

Stein, T. P.: Space flight and oxidative stress, Nutrition, 18, 867-871, https://doi.org/10.1016/S0899-9007(02)00938-3, 2002.

Sternbeck, J., Sjödin, Å., and Andréasson, K.: Metal emissions from road traffic and the influence of resuspension—results from two tunnel studies, Atmos. Environ., 36, 4735-4744, http://dx.doi.org/10.1016/S1352-2310(02)00561-7, 2002.

Stohs, S. J., and Bagchi, D.: Oxidative mechanisms in the toxicity of metal ions, Free Radicals Biol. Med., 18, 321-336, http://dx.doi.org/10.1016/0891-5849(94)00159-H, 1995.

Strak, M., Janssen, N. A., Godri, K. J., Gosens, I., Mudway, I. S., Cassee, F. R., Lebret, E., Kelly, F. J., Harrison, R. M., Brunekreef, B., Steenhof, M., and Hoek, G.: Respiratory health effects of airborne particulate matter: the role of particle size, composition, and oxidative potential-the RAPTES project, Environ. Health Perspect., 120, 1183-1189, 10.1289/ehp.1104389, 2012.

Strickland, M. J., Darrow, L. A., Klein, M., Flanders, W. D., Sarnat, J. A., Waller, L. A., Sarnat, S. E., Mulholland, J. A., and Tolbert, P. E.: Short-term Associations between Ambient Air Pollutants and Pediatric Asthma Emergency Department Visits, American Journal of Respiratory and Critical Care Medicine, 182, 307-316, 10.1164/rccm.200908-1201OC, 2010.

Sun, Q. H., Hong, X. R., and Wold, L. E.: Cardiovascular effects of ambient particulate air pollution exposure, Circulation, 121, 2755-2765, 10.1161/circulationaha.109.893461, 2010.

Sunyer, J., Esnaola, M., Alvarez-Pedrerol, M., Forns, J., Rivas, I., Lopez-Vicente, M., Suades-Gonzalez, E., Foraster, M., Garcia-Esteban, R., Basagana, X., Viana, M., Cirach,

M., Moreno, T., Alastuey, A., Sebastian-Galles, N., Nieuwenhuijsen, M., and Querol, X.: Association between traffic-related air pollution in schools and cognitive development in primary school children: a prospective cohort study, PLoS Med., 12, e1001792, 10.1371/journal.pmed.1001792, 2015.

Tang, M. J., Whitehead, J., Davidson, N. M., Pope, F. D., Alfarra, M. R., McFiggans, G., and Kalberer, M.: Cloud condensation nucleation activities of calcium carbonate and its atmospheric ageing products, Phys. Chem. Chem. Phys., 17, 32194-32203, 10.1039/C5CP03795F, 2015.

Thurston, G. D., Ito, K., Kinney, P. L., and Lippmann, M.: A multi-year study of air pollution and respiratory hospital admissions in three New York State metropolitan areas: results for 1988 and 1989 summers, J. Exposure Anal. Environ. Epidemiol., 2, 429-450, 1991.

Thurston, G. D., Ito, K., Hayes, C. G., Bates, D. V., and Lippmann, M.: Respiratory Hospital Admissions and Summertime Haze Air Pollution in Toronto, Ontario: Consideration of the Role of Acid Aerosols, Environ. Res., 65, 271-290, http://dx.doi.org/10.1006/enrs.1994.1037, 1994.

Tolocka, M. P., and Turpin, B.: Contribution of organosulfur compounds to organic aerosol mass, Environmental Science & Technology, 46, 7978-7983, 10.1021/es300651v, 2012.

Tong, H., Rappold, A. G., Diaz-Sanchez, D., Steck, S. E., Berntsen, J., Cascio, W. E., Devlin, R. B., and Samet, J. M.: Omega-3 fatty acid supplementation appears to attenuate particulate air pollution-induced cardiac effects and lipid changes in healthy middle-aged adults, Environ Health Perspect, 120, 952-957, 10.1289/ehp.1104472, 2012.

Torre, C., Mattutino, G., Vasino, V., and Robino, C.: Brake linings: a source of non-GSR particles containing lead, barium, and antimony, Journal of forensic sciences, 47, 494-504, 2002.

Tsutsui, H., Kinugawa, S., and Matsushima, S.: Oxidative stress and heart failure, American Journal of Physiology - Heart and Circulatory Physiology, 301, H2181, 2011.

Turn, S. Q., Jenkins, B. M., Chow, J. C., Pritchett, L. C., Campbell, D., Cahill, T., and Whalen, S. A.: Elemental characterization of particulate matter emitted from biomass burning: Wind tunnel derived source profiles for herbaceous and wood fuels, Journal of Geophysical Research: Atmospheres, 102, 3683-3699, 10.1029/96jd02979, 1997.

Turpin, B. J., and Lim, H.-J.: Species contributions to PM2.5 mass concentrations: revisiting common assumptions for estimating organic mass, Aerosol Sci. Technol., 35, 602-610, 10.1080/02786820119445, 2001.

Turrens, J. F.: Mitochondrial formation of reactive oxygen species, The Journal of Physiology, 552, 335-344, 10.1113/jphysiol.2003.049478, 2003.

Valavanidis, A., Salika, A., and Theodoropoulou, A.: Generation of hydroxyl radicals by urban suspended particulate air matter. The role of iron ions, Atmos. Environ., 34, 2379-2386, http://dx.doi.org/10.1016/S1352-2310(99)00435-5, 2000.

Valavanidis, A., Fiotakis, K., Bakeas, E., and Vlahogianni, T.: Electron paramagnetic resonance study of the generation of reactive oxygen species catalysed by transition metals and quinoid redox cycling by inhalable ambient particulate matter, Redox Rep., 10, 37-51, 10.1179/135100005X21606, 2005.

Valavanidis, A., Fiotakis, K., and Vlachogianni, T.: Airborne particulate matter and human health: toxicological assessment and importance of size and composition of particles for oxidative damage and carcinogenic mechanisms, J. Environ. Sci. Health, Part C: Environ. Carcinog. Ecotoxicol. Rev., 26, 339-362, 10.1080/10590500802494538, 2008.

Valko, M., Morris, H., and Cronin, M. T.: Metals, toxicity and oxidative stress, Curr. Med. Chem., 12, 1161-1208, 10.2174/0929867053764635 2005.

Vejerano, E., Lomnicki, S. M., and Dellinger, B.: Formation and Stabilization of Combustion-Generated, Environmentally Persistent Radicals on Ni(II)O Supported on a Silica Surface, Environmental science & technology, 46, 9406-9411, 10.1021/es301136d, 2012.

Vejerano, E. P., Ma, Y., Holder, A. L., Pruden, A., Elankumaran, S., and Marr, L. C.: Toxicity of particulate matter from incineration of nanowaste, Environmental Science: Nano, 2, 143-154, 10.1039/C4EN00182F, 2015.

Velali, E., Papachristou, E., Pantazaki, A., Choli-Papadopoulou, T., Planou, S., Kouras, A., Manoli, E., Besis, A., Voutsa, D., and Samara, C.: Redox activity and in vitro bioactivity of the water-soluble fraction of urban particulate matter in relation to particle size and chemical composition, Environ. Pollut., 208, Part B, 774-786, http://dx.doi.org/10.1016/j.envpol.2015.10.058, 2016.

Venkatachari, P., Hopke, P. K., Grover, B. D., and Eatough, D. J.: Measurement of particle-bound reactive oxygen species in rubidoux aerosols, J. Atmos. Chem., 50, 49-58, 10.1007/s10874-005-1662-z, 2005.

Verma, V., Ning, Z., Cho, A. K., Schauer, J. J., Shafer, M. M., and Sioutas, C.: Redox activity of urban quasi-ultrafine particles from primary and secondary sources, Atmospheric Environment, 43, 6360-6368, 10.1016/j.atmosenv.2009.09.019, 2009a.

Verma, V., Polidori, A., Schauer, J. J., Shafer, M. M., Cassee, F. R., and Sioutas, C.: Physicochemical and toxicological profiles of particulate matter in Los Angeles during the October 2007 southern California wildfires, Environmental Science & Technology, 43, 954-960, 10.1021/es8021667, 2009b.

Verma, V., Shafer, M. M., Schauer, J. J., and Sioutas, C.: Contribution of transition metals in the reactive oxygen species activity of PM emissions from retrofitted heavy-duty

vehicles, Atmospheric Environment, 44, 5165-5173, http://dx.doi.org/10.1016/j.atmosenv.2010.08.052, 2010.

Verma, V., Rico-Martinez, R., Kotra, N., King, L. E., Liu, J., Snell, T. W., and Weber, R. J.: Contribution of water-soluble and insoluble components and their hydrophobic/hydrophilic subfractions to the reactive oxygen species-generating potential of fine ambient aerosols, Environmental Science & Technology, 46, 11384-11392, 10.1021/es302484r, 2012.

Verma, V., Fang, T., Guo, H., King, L. E., Bates, J. T., Peltier, R. E., Edgerton, E. S., Russell, A. G., and Weber, R. J.: Reactive oxygen species associated with water-soluble PM2.5 in the southeastern United States: spatiotemporal trends and source apportionment, Atmos. Chem. Phys., 14, 12915-12930, 10.5194/acp-14-12915-2014, 2014.

Verma, V., Fang, T., Xu, L., Peltier, R. E., Russell, A. G., Ng, N. L., and Weber, R. J.: Organic aerosols associated with the generation of Reactive Oxygen Species (ROS) by water-soluble PM2.5, Environ. Sci. Technol., 49, 4646-4656, 10.1021/es505577w, 2015a.

Verma, V., Wang, Y., El-Afifi, R., Fang, T., Rowland, J., Russell, A. G., and Weber, R. J.: Fractionating ambient humic-like substances (HULIS) for their reactive oxygen species activity – Assessing the importance of quinones and atmospheric aging, Atmos. Environ., 120, 351-359, 10.1016/j.atmosenv.2015.09.010, 2015b.

Waldman, J. M., Lioy, P. J., Thurston, G. D., and Lippmann, M.: Spatial and temporal patterns in summertime sulfate aerosol acidity and neutralization within a metropolitan area, Atmos. Environ., Part B, 24, 115-126, http://dx.doi.org/10.1016/0957-1272(90)90017-O, 1990.

Walsh, G. M.: Targeting Airway Inflammation: Novel Therapies for the Treatment of Asthma, Current medicinal chemistry, 13, 3105-3111, 10.2174/092986706778521779, 2006.

Weber, R. J., Guo, H., Russell, A. G., and Nenes, A.: High aerosol acidity despite declining atmospheric sulfate concentrations over the past 15 years, Nat. Geosci., 9, 282-285, 10.1038/ngeo2665

http://www.nature.com/ngeo/journal/v9/n4/abs/ngeo2665.html#supplementary-information, 2016.

Weichenthal, S., Crouse, D. L., Pinault, L., Godri-Pollitt, K., Lavigne, E., Evans, G., van Donkelaar, A., Martin, R. V., and Burnett, R. T.: Oxidative burden of fine particulate air pollution and risk of cause-specific mortality in the Canadian Census Health and Environment Cohort (CanCHEC), Environ. Res., 146, 92-99, http://dx.doi.org/10.1016/j.envres.2015.12.013, 2016a.

Weichenthal, S., Lavigne, E., Evans, G., Pollitt, K., and Burnett, R. T.: Ambient PM(2.5) and risk of emergency room visits for myocardial infarction: impact of regional PM(2.5)

oxidative potential: a case-crossover study, Environ. Health, 15, 46, 10.1186/s12940-016-0129-9, 2016b.

Weinbruch, S., Worringen, A., Ebert, M., Scheuvens, D., Kandler, K., Pfeffer, U., and Bruckmann, P.: A quantitative estimation of the exhaust, abrasion and resuspension components of particulate traffic emissions using electron microscopy, Atmos. Environ., 99, 175-182, https://doi.org/10.1016/j.atmosenv.2014.09.075, 2014.

Willeke, K., and Whitby, K. T.: Atmospheric Aerosols: Size Distribution Interpretation, J. Air Pollut. Control Assoc., 25, 529-534, 10.1080/00022470.1975.10470110, 1975.

Wilson, J. G., Kingham, S., Pearce, J., and Sturman, A. P.: A review of intraurban variations in particulate air pollution: Implications for epidemiological research, Atmospheric Environment, 39, 6444-6462, http://dx.doi.org/10.1016/j.atmosenv.2005.07.030, 2005.

Winquist, A., Schauer, J. J., Turner, J. R., Klein, M., and Sarnat, S. E.: Impact of ambient fine particulate matter carbon measurement methods on observed associations with acute cardiorespiratory morbidity, J Expos Sci Environ Epidemiol, 25, 215-221, 10.1038/jes.2014.55, 2015.

Xia, T., Kovochich, M., Brant, J., Hotze, M., Sempf, J., Oberley, T., Sioutas, C., Yeh, J. I., Wiesner, M. R., and Nel, A. E.: Comparison of the abilities of ambient and manufactured nanoparticles to induce cellular toxicity according to an oxidative stress paradigm, Nano Lett., 6, 1794-1807, 10.1021/nl061025k, 2006.

Xu, N., and Gao, Y.: Characterization of hematite dissolution affected by oxalate coating, kinetics and pH, Appl. Geochem., 23, 783-793, http://dx.doi.org/10.1016/j.apgeochem.2007.12.026, 2008.

Yang, A., Jedynska, A., Hellack, B., Kooter, I., Hoek, G., Brunekreef, B., Kuhlbusch, T. A. J., Cassee, F. R., and Janssen, N. A. H.: Measurement of the oxidative potential of PM2.5 and its constituents: The effect of extraction solvent and filter type, Atmos. Environ., 83, 35-42, http://dx.doi.org/10.1016/j.atmosenv.2013.10.049, 2014.

Yang, A., Janssen, N. A., Brunekreef, B., Cassee, F. R., Hoek, G., and Gehring, U.: Children's respiratory health and oxidative potential of PM2.5: the PIAMA birth cohort study, Occup. Environ. Med., 73, 154-160, 10.1136/oemed-2015-103175, 2016.

Zanobetti, A., Coull, B. A., Gryparis, A., Kloog, I., Sparrow, D., Vokonas, P. S., Wright, R. O., Gold, D. R., and Schwartz, J.: Associations between arrhythmia episodes and temporally and spatially resolved black carbon and particulate matter in elderly patients, Occupational & Environmental Medicine, 71, 201-207, 2014.

Zhang, X., Hecobian, A., Zheng, M., Frank, N. H., and Weber, R. J.: Biomass burning impact on PM 2.5 over the southeastern US during 2007: integrating chemically speciated FRM filter measurements, MODIS fire counts and PMF analysis, Atmos. Chem. Phys., 10, 6839-6853, 10.5194/acp-10-6839-2010, 2010.

Zhang, Y., Schauer, J. J., Shafer, M. M., Hannigan, M. P., and Dutton, S. J.: Source apportionment of in vitro Reactive Oxygen Species bioassay activity from atmospheric particulate matter, Environmental Science & Technology, 42, 7502-7509, 10.1021/es800126y, 2008.

Zhao, Y., Chen, Z., Shen, X., and Huang, D.: Heterogeneous reactions of gaseous hydrogen peroxide on pristine and acidic gas-processed calcium carbonate particles: Effects of relative humidity and surface coverage of coating, Atmos. Environ., 67, 63-72, https://doi.org/10.1016/j.atmosenv.2012.10.055, 2013.

Zielinski, H., Mudway, I. S., Berube, K. A., Murphy, S., Richards, R., and Kelly, F. J.: Modeling the interactions of particulates with epithelial lining fluid antioxidants, Am. J. Physiol.: Lung Cell. Mol. Physiol., 277, L719-L726, 1999.

Zomer, B., Collé, L., Jedyńska, A., Pasterkamp, G., Kooter, I., and Bloemen, H.: Chemiluminescent reductive acridinium triggering (CRAT)—mechanism and applications, Anal Bioanal Chem, 401, 2945-2954, 10.1007/s00216-011-5342-3, 2011.